2026 FMC

XXVII Fluid Mechanics Conference

23–26 June 2026 in Lodz

Book of Abstracts

Lodz University of Technology

XXVII
Fluid Mechanics Conference

23–26 June 2026 in Lodz

Book of Abstracts

Lodz University of Technology

Editors:

dr hab. inż. Krzysztof Sobczak, prof. PŁ, mgr inż. Ewa Kłys, mgr Anna Słota

Linguistic editing: Joanna Pawliczak, Tomasz Krakowiak

Technical editing and typesetting: Aleksandra Gajderowicz

Cover design: Aleksandra Gajderowicz

ISBN: 978-83-67934-99-2

DOI: 10.34658/9788367934992

Lodz University of Technology Press

93–005 Lodz, 223 Wólczańska St.

Phone: 42-631-20-87, 42-631-29-52

E-mail: zamowienia@info.p.lodz.pl

www.wydawnictwo.p.lodz.pl

Lodz University of Technology Conference Proceedings, No 2597

Circulation 200 copies

Printing and bookbinding: Quick-Druk

90–562 Lodz, 11 Łąkowa St

INTERNATIONAL SCIENTIFIC COMMITTEE

Prof. Janusz Badur	Institute of Fluid-Flow Machinery, PAS, Gdańsk, Poland
Prof. Tomas Bodnar	CTU Prague, Czech Republic
Prof. Andrzej Bogusławski	Częstochowa University of Technology, Poland
Prof. Paul Cizmas	Texas A&M University, USA
Prof. Piotr Doerffer	Institute of Fluid-Flow Machinery, PAS, Gdańsk, Poland
Prof. Sławomir Dykas	Silesian University of Technology, Gliwice, Poland
Prof. Maria Ekiel-Jeżewska	Institute of Fundamental Technological Research, PAS, Warsaw, Poland
Prof. Witold Elsner	Częstochowa University of Technology, Poland
Prof. Krzysztof Fidkowski	University of Michigan, USA
Prof. Paweł Flaszyński	Institute of Fluid-Flow Machinery PAS, Gdańsk, Poland
Prof. Jerzy Maciej Floryan	University of Western Ontario, Canada
Prof. Krzysztof Jóźwik	Łódź University of Technology, Poland
Prof. Genta Kawahara	Osaka University, Japan
Prof. Tomasz Kowalewski	Institute of Fundamental Technological Research PAS, Warsaw, Poland
Prof. Sławomir Kubacki	Warsaw University of Technology, Poland
Prof. Anna Kucaba-Piętal	Rzeszów University of Technology, Poland
Prof. Henryk Kudela	Wrocław University of Technology, Poland
Prof. Lech Łobocki	Warsaw University of Technology, Poland
Prof. Jacek Pozorski - chairman	Institute of Fluid-Flow Machinery PAS, Gdańsk, Poland
Prof. Bartosz Protas	McMaster University, Hamilton, Canada
Prof. Spencer Sherwin	Imperial College London, UK
Prof. Alfredo Soldati	TU Wien, Austria
Prof. Janusz Szmyd	AGH University, Kraków
Prof. Jacek Szumbarski	Warsaw University of Technology, Poland
Prof. Andrzej Teodorczyk	Warsaw University of Technology, Poland
Prof. Krzysztof Tesch	Gdańsk University of Technology, Poland
Prof. Ewa Tuliszka-Sznitko	Poznań University of Technology, Poland
Prof. Artur Tyliszczak	Częstochowa University of Technology, Poland
Prof. Markus Uhlmann	KIT Karlsruhe, Germany
Prof. Luc Vervisch	INSA Rouen, France
Prof. Włodzimierz Wróblewski	Silesian University of Technology, Gliwice, Poland

ORGANIZING COMMITTEE

Krzysztof Jóźwik	Conference Chair
Krzysztof Sobczak	Conference Vice-Chair
Ewa Kłys	Conference Manager
Anna Słota	Conference Secretary
Michał Błaszczyk	Member
Anna Frąckiewicz	Member

BOARD OF REVIEWERS

CONFERENCE SCIENTIFIC TOPICS

- Aerodynamics
- AI and machine learning in fluid mechanics
- Biological flows
- Combustion and reactive flows
- Computational fluid dynamics
- Environmental fluid mechanics
- Experimental methods in fluid mechanics
- Flow machinery
- Flow control and optimization
- Fluid-structure interaction
- General fluid dynamics
- Micro- and nanofluidics
- Multiphase flows and complex fluids
- Thermal-fluid problems
- Turbulence and transition

The project is financed from the state budget funds granted
by the Minister of Science and Higher Education
under the Vectors of Science Programme,
pursuant to Agreement No. WNK/SP/0246/2025/01, entitled
"International Conference XXVII Fluid Mechanics Conference
(FMC 2026)".

Minister of Science and Higher Education
Republic of Poland

Minister Nauki
i Szkolnictwa Wyższego

WEKTORY
NAUKI

Funding provided by the Ministry of Science and Higher Education:
PLN 165,220.00.

Total project value: PLN 256,120.00.

Projekt finansowany ze środków budżetu państwa, przyznanych przez
Ministra Nauki i Szkolnictwa Wyższego w ramach Programu Wektory Nauki

HONORARY PATRONAGE

Marcin Kulasek
Minister of Science and Higher Education
Republic of Poland

PAN
POLISH ACADEMY OF SCIENCES
Committee
for Mechanics

ERCOFTAC
European Research Community On
Flow, Turbulence And Combustion

ptmts
Rok zał. 1958

MAYOR OF THE CITY OF LODZ
HANNA ZDANOWSKA

Lodz University
of Technology

SPONSORS

Eurotek International

DANTEC DYNAMICS

MESCO

AMECAM

AMECAM IS THE OFFICIAL PARTNER OF LAVISION IN POLAND

LAVISION

FOCUS ON IMAGING

VEOLIA

PREFACE

This Book of Abstracts contains the abstracts of presentations delivered at the XXVII Fluid Mechanics Conference (FMC 2026), held from 23rd to 26th June 2026 in Łódź. The FMC series (formerly Krajowa Konferencja Mechaniki Płynów) has been held biennially since 1974 at various locations across Poland, under the auspices of the Committee for Mechanics of Polish Academy of Sciences.

The FMC 2026 edition is organized by Lodz University of Technology which is proud to host this edition of the Conference for the third time. Previous editions organized by the University were held in 1980 and 2000.

The Fluid Mechanics Conference series is a leading regional event dedicated to presenting and discussing advances in fluid mechanics research, development and applications. The FMC brings together researchers from both academia and industry, providing a forum for the exchange and discussion of ideas across the diverse fluid mechanics community.

The Conference covers a broad spectrum of contemporary fluid flow problems, including fundamental and applied studies, novel experimental and numerical methods, and innovative applications. The presented contributions span the full range of topics defined in the Conference scientific programme.

We are pleased that the Conference has attracted significant interest. All submitted extended abstracts were peer-reviewed by members of the International Scientific Committee and invited experts. Over 100 contributions were selected for presentation at the XXVII Fluid Mechanics Conference. They are presented in plenary and poster sessions, preceded by four plenary and four semiplenary lectures delivered by leading international and Polish experts.

In keeping with the tradition of the Fluid Mechanics Conference, the Competition in Memory of Prof. Janusz W. Elsner for the best scientific work in fluid mechanics is held under the auspices of PTMTS (Polish Society of Theoretical and Applied Mechanics) and the Polish Pilot Centre of ERCOFTAC (European Research Community on Flow, Turbulence and Combustion). The competition aims to promote the research achievements of outstanding young scientists (up to 35 years of age) working in the field of fluid mechanics. Based on 17 extended abstracts submitted to the competition, six contributions were selected by the Competition Jury for the final presentation at the Conference.

We would like to express our sincere gratitude to the Minister of Science and Higher Education of the Republic of Poland, Dr Marcin Kulasek, for his honorary patronage. We are equally grateful for the patronage of the Committee for Mechanics of the Polish Academy of Sciences, the European Research Community on Flow, Turbulence and Combustion, the Polish Society of Theoretical and Applied Mechanics, the Mayor of the City of Łódź, Hanna Zdanowska and Lodz University of Technology.

We gratefully acknowledge the support of all members of the fluid mechanics community, especially the members of the International Scientific Committee and other reviewers, for their contribution to the review and improvement of the submitted abstracts. We would like to express our special thanks to Prof. Jacek Pozorski, Chairman of the International Scientific Committee, for his invaluable support in coordinating the review process, advising on the session structure, and contributing to the overall organization and execution of the Conference.

We also appreciate the broad participation of scientists representing numerous research centres, whose involvement underscores the relevance of the Conference and enriches its scientific programme.

On behalf of the XXVII Fluid Mechanics Conference Committees,

Prof. Krzysztof Jóźwik

INVITED LECTURERS

Prof. Colm-cille P. Caulfield
University of Cambridge

Colm-cille P. Caulfield is Professor of Environmental and Industrial Fluid Dynamics in the Department of Applied Mathematics and Theoretical Physics (DAMTP) at the University of Cambridge and a faculty member of the Institute for Energy and Environmental Flows (IEEF). He is also a Professorial Fellow in Mathematics at Churchill College, Cambridge. He is the co-chair of the Cambridge Centre for Data-Driven Discovery, the University's Inter-disciplinary Research Centre (IRC) which brings together researchers and expertise from across the academic departments and industry to drive research into the analysis, understanding and use of data science and AI. He is also Co-Director (Science) of the University's Institute of Computing for Climate Science (ICCS), which studies and supports the role of software engineering, computer science, AI and data science within climate science.

Prof. Caulfield's personal research interests include instability, turbulence transition and turbulent mixing processes in stratified flows, with particular focus on understanding and improving the modelling of heat transport in the world's oceans. Following postdoctoral training in the Department of Physics at the University of Toronto, Canada and the Department of Engineering Science at Hokkaido University, Japan, he was a lecturer in the School of Mathematics at the University of Bristol, UK. Prof. Caulfield subsequently joined the faculty of the Department of Mechanical and Aerospace Engineering at the University of California, San Diego. Following tenure at UCSD, Prof. Caulfield joined the BP Institute (now IEEF) and DAMTP. Prof. Caulfield has served as the Head of DAMTP from January 2020 to September 2025, as the Editor-in-Chief of the Journal of Fluid Mechanics since January 2022, and as the Chair of the Euromech Turbulence Conference Committee from January 2020 to December 2025. He was elected a Fellow of the American Physical Society (Division of Fluid Dynamics) in 2014.

Stratified Turbulence: Climate's Mysterious Mixer

Statically stable density stratification is ubiquitous in geophysical flows, with the atmosphere, lakes and oceans all typically having an average density distribution that decreases upwards in a gravitational field. Due to the associated stabilising effect of the buoyancy force, it would seem intuitive that such statically stable density distributions should suppress vertical motions, relative to horizontal motions. Such inevitable anisotropy complicates even further developing an understanding of turbulence in density-stratified fluids. Stratified turbulence is not just a fascinating (and inherently complicated) research challenge in classical physics, but also a key component of the global climate system, as stratified turbulence has a leading order effect on the transport of heat and other scalars such as carbon dioxide, pollutants etc in the world's oceans and atmosphere. Indeed, how stratified turbulence can actually be 'born' and then 'survive' for a significant period, hence irreversibly mixing significant scalar quantities, are open questions, associated with ongoing controversy in the global research community. In this talk, I will review some recent studies by my collaborators that have advanced our understanding of various key properties of stratified turbulence and mixing, while also demonstrating that there is still much more to learn about this fascinating and vitally important class of fluid flows.

Prof. Paul G. A. Cizmas
Texas A&M University

Paul G. A. Cizmas is a Professor of Aerospace Engineering at Texas A&M University. Over the past 30 years he has performed research on numerical simulation of transport phenomena for aerospace applications, covering a large range of topics, including reduced-order modeling, aerothermoelasticity, combustion and computational fluid dynamics.

Prior to joining Texas A&M in 1998, Paul held positions at the Westinghouse Science and Technology Center and Duke University, from which he received his Ph.D. He is a Fellow of American Society of Mechanical Engineers and an Associate Fellow of the American Institute of Aeronautics and Astronautics.

Paul pioneered the use of the time-linearization method for prediction of stall flutter in turbomachinery. For this contribution he received the ASME Liquid Propulsion 1995 Best Paper Award. He was among the first to use parallel processing for numerical simulation of unsteady flows in turbomachinery. For this contribution he received the Westinghouse Science and Technology 1997 Technical Publication Award. For his work on the prediction of aeroacoustic resonance in cavities of hole-pattern stator seals, Paul received the ASME Structures & Dynamics Committee Best Paper Award in 2011. For his contribution to reducing sonic boom, Paul received the Boeing Research and Technology Performance and Innovation Award in 2018.

Reduced-order Models and Machine Learning of Unsteady Flows

Unsteady flows, and especially reacting unsteady flows, require large computational times. To decrease the computational cost, several reduced-order models based on novel proper orthogonal decomposition (POD) methods are explored. The dynamic POD model is illustrated for unsteady flows with moving boundaries. This method is applied to vibrating turbomachinery blades. To further decrease the computational time, the zeta-POD model is introduced so that the time coefficients of the system of ordinary differential equations obtained after the Galerkin projection can be precomputed. Finally, a methodology is presented that uses machine learning to calculate the time coefficients of the POD method. This method is applied for modeling two-phase flows in chemical reactors.

Manuel García-Villalba is professor with the chair of computational fluid dynamics at TU Wien, Vienna, Austria. Previously he worked at Universidad Carlos III de Madrid, Spain and at the Karlsruhe Institute of Technology, Germany. He is an expert in aerodynamics, fluid-structure interaction, cardiac flows and high-performance computing. He has co-authored more than 50 journal articles and co-supervised 8 PhD theses, with 2 PhD students more underway. He is currently Associate Editor of the journal European Journal of Mechanics B/Fluids.

Prof. Manuel García-Villalba
TU Wien

Computational modelling of flow and transport phenomena in the left atrium

The left atrium is a thin-walled chamber that receives blood from the pulmonary veins and drives it into the left ventricle. Atrial fibrillation, the most common cardiac arrhythmia, disrupts its wall motion and is a leading cause of ischemic stroke. The associated thromboembolic risk is largely attributed to clot formation in the left atrial appendage, a small pouch where impaired kinematics promote blood stasis. Computational fluid dynamics provides a framework for analyzing the resulting flow and transport phenomena in patient-specific geometries reconstructed from CT imaging. This lecture presents advances in this modeling approach, illustrated with examples from recent and ongoing work. Accurate prescription of wall kinematics is shown to be essential for reliable hemodynamic predictions. Blood residence time, computed via passive scalar transport, serves as the primary metric to quantify local stasis. Furthermore, transport models for biochemical species allow coagulation risk to be assessed more directly. Results are evaluated against clinical outcomes from cohorts of patients with and without confirmed thrombus. Together, these studies illustrate how classical fluid mechanics tools can address a problem of significant clinical relevance.

Prof. Ramis Örlü
OsloMet – Oslo Metropolitan University

Ramis Örlü is a Professor of Fluid Mechanics at OsloMet – Oslo Metropolitan University. He earned a Diplom-Ingenieur (Dipl.-Ing.) degree in Mechanical Engineering from Ruhr University Bochum in 2003, followed by a Ph.D. in Engineering Mechanics, specializing in Experimental Fluid Dynamics and Turbulence, from KTH Royal Institute of Technology in 2009. In 2015, he was appointed docent in Experimental Fluid Physics at KTH, where he has been a researcher since 2009 and continues to contribute on a part-time basis. Since 2017, he has also held an adjunct professorship at the University of Bologna.
In 2023, he joined OsloMet as an Associate Professor of Fluid Mechanics and was promoted to Full Professor in 2024. Over the years, he has held fellowships and guest professorships in Germany, Italy, and Turkey.

His research focuses on the fundamental aspects of turbulent flows, with particular emphasis on skin-friction and drag reduction through passive and active flow-control techniques. He employs large-scale wind tunnel facilities and integrates high-fidelity simulations to cross-validate experimental and computational results. In addition to his research, he is the Editor-in-Chief of Experimental Thermal and Fluid Science, serves on the Editorial Advisory Boards of Flow, Turbulence and Combustion and Advances in Aerodynamics, and has co-edited the Progress in Turbulence series. He is also the recipient of the FLUCOME Nakayama Award (2025) and the Friedrich Wilhelm Bessel Research Award from the Alexander von Humboldt Foundation (2026).

High-Resolution or High-Illusion? Revisiting the Role of Hot-Wire Anemometry in Wall-Bounded Turbulence

For nearly a century, hot-wire anemometry has played a central role in shaping our understanding of turbulence, particularly in wall-bounded flows. Its reputation for exceptional temporal response and fine spatial resolution has made it a cornerstone of experimental turbulence research. Yet this status also masks important limitations. Hot-wire measurements continue to underpin many classical and modern studies of near-wall turbulence, including debates in which differences between proposed scaling laws often fall within the uncertainties of the measurements themselves. Over time, numerous corrections and best practices addressing spatial and temporal resolution, near-wall interference, blockage, filtering effects and probe attenuation have become deeply embedded in experimental methodology. Many of these procedures are now treated as standard practice despite growing questions about their validity in the context of increasingly demanding measurements and interpretations. This keynote revisits the historical legacy and current role of hot-wire anemometry in wall-bounded turbulence research, examining both its major contributions and inherent limitations. The central question is whether hot-wire anemometry still offers the highest-resolution view of turbulence or whether part of that resolution has become an experimental illusion.

Prof. Paweł Flaszyński
Polish Academy of Sciences

Prof. Paweł Flaszyński is the Head of the Department of Aerodynamics at the Institute of Fluid-Flow Machinery of the Polish Academy of Sciences. For 25 years, he has been involved in numerical simulations for turbomachinery flows and aerospace aerodynamics. His research mainly focuses on the subsonic and transonic flow structure analysis, flow control methods in turbomachinery, on aircraft wings and in wind energy applications, as well as aeroacoustics. The research has been conducted as part of numerous European and national projects. He coordinated the european project TFAST – Transition Location Effect on Shock Wave Boundary Layer Interaction and the H2020 MSCA-ITN project TEAMAero – Towards Effective Flow Control and Mitigation of Shock Effects in Aeronautical Applications.

He was awarded the 2018 team prize by the Minister of Science and Higher Education for outstanding scientific or technological achievements in the category 'research for economic development', recognizing his work on the development of flow control methods in aerodynamics.
Prof. Paweł Flaszyński is a member of the European Turbomachinery Society, an Alternate Representative in the International Society for Air Breathing Engines and a member of the Steering Committee of ERCOFTAC SIG 10 (Transition Modelling).

Shock wave boundary layer interactions in compressor configurations

The future sustainable growth of the aviation industry relies on continued improvements in efficiency, leading to reduced fuel consumption and increased payload capacity. Research efforts therefore focus on enhancing aerodynamic performance while reducing structural weight. This inherently requires higher-performing wings, control surfaces and turbomachinery blades, particularly in applications where transonic flow is common and shock-wave formation poses a significant aerodynamic challenge.
The interaction of shock waves with boundary layers is particularly important, as it represents one of the main performance-limiting and safety-critical flow phenomena across these flow regimes. The flow within a transonic compressor cascade is intrinsically unsteady because of shock-wave/boundary-layer interactions (SBLI) occurring on the blade surfaces. Despite extensive research over several decades, the underlying mechanisms responsible for this behaviour are still not fully understood.
At cruise altitude, the reduced Reynolds number causes the boundary layer on the suction side of a transonic fan blade to remain laminar up to the SBLI region. In transitional SBLI cases with pronounced shock-induced separation, a self-sustained shock oscillation mechanism can develop, driven by the cyclic growth and subsequent suppression of the upstream laminar portion of the separation bubble. Low-Reynolds number effects are also challenging for highly loaded transonic stator configurations, even when located downstream of the rotor and operating under high inflow turbulence levels.
For this reason, promoting a controlled laminar-to-turbulent transition upstream of the shock interaction is considered a promising strategy for improving compressor performance and stability. One possible approach is the deliberate modification of blade surface characteristics, such as roughness patches, surface roughness resulting from machining, or flow-control techniques.
The presentation will focus on SBLI in two configurations: a transonic fan profile and a highly loaded transonic stator configuration.

Prof. Maciej Marek
Czestochowa University
of Technology

Maciej Marek is an Associate Professor at Faculty of Mechanical Engineering, Częstochowa University of Technology (CUT), Poland. He earned his master's degree in electronics and telecommunications from AGH University of Technology (2002) and Ph.D. degree in mechanical engineering from CUT (2006). In his doctoral thesis he introduced a new computational technique based on cellular automata for numerical modelling of alloy solidifcation at the scale of single grains. Habilitated at CUT in 2019 on the basis of series of publications concerning numerical modelling of moving boundary problems. Member of the Section of Fluid Mechanics of the Committee on Mechanics of the Polish Academy of Sciences. Editor of the ERCOFTAC Bulletin.

At CUT, Prof. Maciej Marek teaches numerical methods, optimisation in engineering and computational fluid dynamics. His recent works focus on the modelling of random packing of particles and fluid flow simulations in porous media.

Fluid flow through randomly packed particles

In cylindrical random packed beds, the ordered near-wall layering of particles creates preferential flow channels that cause severe maldistribution even under a uniform inlet flow. This study investigates how a regular, periodic corrugation of the container wall can disrupt this particle ordering and improve the uniformity of the flow field. The packing structure is generated using a validated sequential algorithm that captures the radial void-fraction oscillations characteristic of near-wall layering. Gas flow in the low Reynolds number regime is then computed via an immersed boundary method on a Cartesian grid, with the solver validated against experimental MRI velocity profiles. Simulation results demonstrate that wall corrugation significantly suppresses the strong oscillations in the averaged radial velocity profiles that are otherwise induced by particle layering. Remarkably, the characteristic high-velocity peak near the wall is diminished, even though a large void-fraction peak persists in the corrugation troughs. Detailed inspection reveals that flow penetration into these troughs is limited, so the added voidage does not act as a preferential path. The uniformity of the velocity field is quantified using a Shannon entropy measure which yields higher entropy (i.e. a more uniform distribution) for the corrugated configuration relative to a flat-wall reference. Conversely, when the corrugation parameters promote geometric resonance and increased ordering, entropy decreases for both the packing structure and the flow field. These results highlight that wall corrugation is an effective passive flow-control strategy for mitigating near-wall channelling in packed beds, with direct relevance to the fluid dynamics of fixed-bed chemical reactors.

Dr Tomasz Bobiński
Warsaw University
of Technology

Tomasz Bobiński is an Assistant Professor in the Department of Aerodynamics at the Faculty of Power and Aeronautical Engineering, Warsaw University of Technology. He earned his Ph.D. in fluid mechanics from Université Pierre et Marie Curie in Paris in 2016. His academic excellence has been recognised with the START scholarship from the Foundation for Polish Science (FNP) and a distinction for outstanding young scientists awarded by the Minister of Science and Higher Education. Dr. Bobiński's research lies in the field of experimental fluid dynamics, with a particular focus on surface water waves, wettability and anti-icing applications of ultra-low surface energy materials. His recent work centers on the development of novel cloaking devices designed to render objects invisible to incident waves, contributing to the emerging field of transformation hydrodynamics.

Nature-Inspired Cloaking Technology in Water Waveguide Systems

Metamaterials and transformation-optics methods have opened new avenues for controlling wave propagation in acoustics, electromagnetism, and surface water waves. For water waves, transformation-based cloaks are typically implemented as engineered bathymetries, however, standard coordinate transformations yield anisotropic depth profiles that violate the small-gradient assumptions of depth-averaged wave models. Conformal mapping offers a strictly isotropic alternative, but when applied to compact obstacles it produces depth gradients so steep that the long-wave approximation breaks down. We circumvent these limitations by applying conformal mapping to waveguide systems rather than isolated obstacles. In the first approach, a spatially varying bathymetry is designed to suppress scattering induced by wall irregularities of a meandering waveguide, yielding a smooth, isotropic depth profile free of singularities. Numerical simulations using both shallow-water and mild-slope equations confirm robust cloaking performance even in the dispersive regime, validated experimentally with 3D-printed waveguides. Extending this approach to waveguides with parallel walls, we achieve invisibility of a surface-piercing circular cylinder through local deformations of the waveguide walls, with the optimal shape determined by numerical optimization. Our method yields a reflection coefficient at least 20 times lower than in the unperturbed waveguide over a broad frequency range. Experimental results confirm the high efficiency of this approach, with backscattered energy reduced by a factor of 100 to 5,000 compared to the reference case. The method is directly applicable to any Helmholtz-governed waveguide system, including acoustics and electromagnetism.

Dr Michał Lipian
Lodz University
of Technology

Researcher in applied aerodynamics and aeroacoustics, experienced in experimental and numerical flow analysis. PhD in Mechanical Engineering at Lodz University of Technology and Power Engineering at Arts et Metiers ParisTech. Project manager in wind turbines development and propeller design and optimisation. Science animator and tutor in Renewable Energy Sources and Aerodynamics. Key research directions: rotor aerodynamics for wind turbines and propellers.

Surrogate modelling in the GPU era: Rethinking the role of low-fidelity aerodynamic models

Surrogate or hybrid modelling plays a pivotal role in aerodynamic analysis by providing computationally efficient approximations of complex physical phenomena. Hybrid models are capable of capturing key aerodynamic behaviours across a wide range of applications, including performance prediction, sensitivity analysis and design optimisation. Traditionally, surrogate models have been indispensable in scenarios where high-fidelity simulations were prohibitively expensive, such as in the aerodynamic modelling of airscrews using Blade Element Theory (BET).

With the advent of GPU-accelerated computing, the feasibility of running large-scale CFD simulations in practical timeframes has significantly improved, challenging the dominance of low-fidelity models for quick assessment and optimisation. Nonetheless, the presented research argues that surrogate modelling remains essential for rapid design iteration, particularly when integration of additional functionalities such as aeroacoustics and control-oriented modelling is performed. Through the lens of hybrid BET-CFD frameworks for airscrew analysis, the research demonstrates how surrogate models are evolving to incorporate richer physics while maintaining computational efficiency. This evolution underscores their continued relevance in the design and optimisation of next-generation aerodynamic systems.

Prof. Szymon Malinowski
University of Warsaw

Born, 1957
1982 MSc in physics – University of Warsaw,
1988 PhD in geophysics – Institute of Geophysics, Polish Academy of Sciences.
Since 1987 employed at the University of Warsaw, faculty of Physics, Institute of Geophysics, since 2002 as professor.
Posts, sabbaticals, long-term scientific visits: 1990–92 post doc at the University of Quebec in Montreal (Canada), 1993-2020 multiple posts at the National Center of Atmospheric Research, Boulder, USA, post and programs at DLR (Oberpfaffenhofen, Germany), Meteo-France (Toulouse, France), University of California (Santa Barbara, USA), visiting professor at universities in Mainz (Germany) and Toulouse (France). Since 2020 corresponding member of the Polish Academy of Sciences.

Co-author of over 100 peer reviewed publications and 3 textbooks, PI and leader of over 20 national and international scientific projects.
Scientific interests: atmospheric physics, in particular cloud physics, atmospheric turbulence, airborne measurements, numerical modelling.
Science popularization: co-founder of naukaoklimacie.pl (Climate Science) website and Climate Education Foundation (https://fundacjaedukacjiklimatycznej.pl/).
Laureate of the Foundation for Polish Science Prof. Maciej W. Grabski Distinction (2022) for individuals who actively advance public understanding of science and of Polish Minister of Science and Education and Polish Press Agency prize Populariser of Science 2017 in category 'Team' for web portal naukaoklimacie.pl.

Fluid dynamics of Earth's climate

Atmosphere and ocean are fluids. Fluids flow and carry heat, momentum, tracers. Their motion on rotating planet is governed by differences in absorption of solar energy in the form of shortwave electromagnetic radiation and emission of Earth's energy to space in form of infrared radiation. These are physical principles of weather and climate.
In the lecture, I will show simple, yet barely known physical foundations of climate science explaining recent anthropogenic climate change and climate projections for future.

INDUSTRY SESSION PRESENTATIONS

Dantec Dynamics systems in Macro and Micro Experimental Fluid Dynamics

A. Antonowicz[1], **K. Dörner**[2]

[1] Eurotek International Sp. z o.o.

[2] Dantec Dynamics A/S

E-mail: aantonowicz@eurotek.com.pl

Scientists and Engineers in fluid dynamics and solid mechanics rely on measurements to make breakthroughs in applied research, technology development and quality assurance. Eurotek implements commercial fluid dynamics measurement systems, develops their functionality extensions and sells integrated measurement systems for diagnostics and research into fluid mechanics, solid mechanics, microfluidics, spray analysis and combustion technology. We deliver turnkey and customized solutions built on high-end laser optics, imaging and sensor technologies. Our user-friendly software performs advanced data analysis and produces real-time results. Furthermore, we pride ourselves in providing our clients superior technical application long-time support. You gain accurate measurement results easily and quickly which help you accelerate the pace of discovery, innovation and quality control. Our distinct competence and experience in integrating measurement methods and technologies into the right solution for you, is unique. Partnering with Eurotek and Dantec Dynamics helps you gain crucial knowledge from any test or measurement campaign. Dantec Dynamics – Turn Measurements into Knowledge.

Adaptive surrogate-based exploration of parametric CFD design spaces

J. Tumidajski

MESco Sp. z o.o.

E-mail: jtumidajski@mesco.com.pl

Parametric studies based on high-fidelity CFD simulations are widely used in aerodynamic design and optimisation. However, exploring complex design spaces typically requires a large number of computationally expensive simulations. Surrogate models provide an efficient alternative by approximating the relationship between design parameters and aerodynamic responses, enabling rapid evaluation of design variants.

In this work, an adaptive surrogate-based workflow for efficient exploration of parametric CFD design spaces is presented. The proposed approach combines automated CFD simulations, design of experiments and surrogate modelling with adaptive sampling to iteratively improve model accuracy in selected regions of the design space. Particular attention is given to the influence of model parameterization and strategies for improving the robustness and predictive capability of surrogate models.

The methodology is demonstrated on a parametric aerodynamic configuration of a fixed-wing unmanned aerial vehicle. The presented framework aims to support efficient exploration of CFD design spaces and to provide insights into practical strategies for improving surrogate-based modelling in aerodynamic applications.

SPIS TREŚCI

International Scientific Committee 3

Organizing Committee 4

Board of Reviewers 5

Conference Scientific Topics 6

Honorary Patronage 9

Sponsors 11

Preface 13

Invited Lecturers 15

Industry Session Presentations 27

Abstracts of the Conference Presentations 35

A. Ababaei, B. Rosa, M. Manna The Effect of Charge Magnitude on the Collision Efficiency Between Two Settling Cloud Droplets 37

A. Alavi, K. Urbanowicz 1D, 2D Axis-Symmetric and 3D Numerical Simulation of Valve Induced Water Hammer 39

B. Allweyer, S. Grün, D. Hübner, F. Rückert Experimental Assessment of Efficiency Increase on UAV Propellers Using Microstructures 41

B. Allweyer, S. Grün, D. Hübner, F. Rückert Determination of Optimal Locations of River Turbines Based on Simulations 43

M. Amiri, A. Tyliszczak NO_x Emissions in NH_3/H_2 Co-Combustion Under O_2-Enrichment and Steam Dilution Conditions 45

R. Ayats, L. Klotz, B. Hof From Directed Percolation to Patterned Turbulence 47

A. Banerjee Rheological and Thermal Influences on Secondary Flow in Polygonal Duct Manifolds 49

A. Bartosik, **B. Jaworska-Jóźwiak**, **M. Sadowski, M. Pasiarski** Experiments on Human Blood Shear Stress and Viscosity at Low and Moderate Haematocrit 51

St. Biegowski, M. Paprota Shoaling of Gravity-Capillary Waves 53

M. Błaszczyk Dynamics of Emulsion Droplet Transport in Cross-Capillary Microstructures 55

A. Bogusławski , A. Tyliszczak, B.J. Geurts Global Stability Analysis of Multi-Step Time-Integration Methods Applied to the Fourier-Discretised Linear Convection-Diffusion Equation 57

K. Bukowski, T. De Maria, S. Ahizi , M.A. Mendez Data-Driven Modeling and State Estimation of Sloshing Dynamics from Sparse Measurements: an Experimental and Numerical Study 59

C. Burns, M. Kulak, K. Sobczak Low-Fidelity Geometric Shape Optimization of a Counter-Rotating Open Rotor 61

L. Caban, A. Wawrzak, A. Tyliszczak From Passive to Active Control of Flame Dynamics Using Bluff Body Stabilization and Oxidizer Flow Excitation 63

L.H. Carnevale, K.L. Ng, P. Deuar, Z. Che, M. Klamka, T. Bobiński, P.E. Theodorakis Many-Body Dissipative Particle Dynamics of Micro and Nano Scale Flows 65

Ł. Ciorga, T. Banaszkiewicz Design of a Nitrous Oxide Filling System for Sounding Rocket Propellant Tanks 67

M. Czarnecki, K. Wójciak, J. Kopania, P. Gaj Acoustic Properties of Silencers with Micro Perforated Panels of Multiple Perforation Sizes in Airflow 69

N.F. Dimitrieva Complex Flows in a Ventilated Cavity 71

A. Dróżdż, M. Romańczyk, W. Elsner Passive Control of the Turbulent Separation Induced by the Convex Geometry of NACA4412 73

J. Dziuba, K. Smołka Comparison of Traditional Methods of Industrial Fan Calculations with Modern Tools 75

J. Fabisiak, S. Gepner Algorithm for Extracting Advection-Diffusion Operator Eigenvalue as Mixing Measure in Double Gyre Flow 77

P. Gaj, I. Czajka, J.M. Kopania Laboratory Investigation of Aeroacoustic Phenomena Occurring During High-Pressure Gas Ejection 79

J. Gałecki, J. Szumbarski A Consistent Splitting Scheme for Unsteady Incompressible Flows with Exact Incompressibility Enforcement 81

S. Gepner, G. Kawahara From Square to Circle: Discovering Steady Localised Travelling Waves in Pipe Flow Through Geometric Homotopy 83

S. Grün, B. Allweyer, D. Hübner, F. Rückert Surveying River Beds with Flow Simulation for Optimal Positioning of River Turbines 85

P. Hercel, D. Kardaś Simulation of Thermal–Fluid Phenomena During Single Wood Particle Pyrolysis with Shrinkage Effects 87

A. Hokpunna Performance of Very Higher-Order Multi-Moment Method in the Nonlinear Convection-Diffusion Equations 89

K.K. Jani, A. Giesecke, T. Gundrum, F. Stefani Identification of Flow States for the Dresdyn Precession Experiment Using Ultrasound Doppler Velocimetry 91

J.A. Jankiewicz Numerical Analysis of the Effect of Gothic Vortex Generator Chordwise Location on the Aerodynamic Characteristics of the NACA 4415 Airfoil 93

B. Jóźwiak Thermal and Rheological Behavior of Fly Ash–Based Deep Eutectic Solvent Dispersions 95

A. Kajzer Revisiting the 2nd-Order Semi-Discrete Finite Volume Schemes for Hyperbolic Conservation Laws On Cartesian Grids 97

P. Kamiński, A. Tyliszczak Mixing Enhancement Via Shape Altering of Bluff Body Flame Stabilizers 99

M. Klamka, T. Bobiński Shaking Things Up: Dynamic Contact Angle Hysteresis Measurement Using a Harmonically Oscillated Substrate 101

J. Knight, H. Medina, C. Ellis, S. Ambrose, H. Fadhila, C. Eastwick Neural Network Inlet Condition for Simulating Boundary Layer Natural Transition 103

A. Kocoń, R. Gnatowska Transitional Flow Regimes in Tandem Configurations of Triangular Cylinders 105

A. Kołata, K. Zawadzki, W. Tomecki, M. Dorenda, K. Rozbicki, J. Klepacz, K. Juszczak, G. Widerska, J. Maciejewski, M. Lipian, M. Kulak, K. Olasek Development of Aerodynamic Components in a Small Wind Turbine by the GUST Team 107

J.M. Kopania Impact of Orientation Angle on Vortex Shedding and Noise Generation of a Square Cylinder in Low-Velocity Airflows 109

T.A. Kowalewski Flow of DNA Chains in Molecular and Microfluidic Systems 111

T. Krakowski, W. Stankiewicz Active Flow Control for Drag Reduction – Machine Learning Strategies Comparison 113

A. Kraszewska, J. Donizak Validation of a Numerical Model for Thermomagnetic Convection of a Paramagnetic Fluid in Strong Magnetic Fields 115

S. Król, M. Wacławczyk Scaling of Turbulence Kinetic Energy Dissipation and Temperature Variance Destruction Rates in Dry Convection and in Marine Boundary Layers 117

S. Kubacki, K. Kurec, A. Jaworski, M. Wielgosz Numerical Study of Surface Thermal Load on a Mars Entry Capsule 119

D. Kumar Blockage Effect on Linearly Unstable Modes in Flow Past Elliptic Cylinders 121

Ł. Łaniewski-Wołłk, C. Leonardi Improving of Proppant Screen-Out Modelling for Rough Fractures 123

Y. Li, B.r. Noack Jet-Mixing Control Landscapes Revealed by Bayesian Optimization 125

E. Lo Pinto, M. Katz, S. Clément, S. Gaillot, Y. Weiss Evaluation of Flow Entrainment Ratio of a Jet-Pump Based System Intended for JHR Experimental Devices 127

M. Majkut, S. Dykas, K. Smołka, A. Bogusławski, K. Skoczylas Influence of Humidity on Self-Excited Shock Wave Oscillations in Transonic Planar Nozzles 129

M. Manna, B. Rosa, A. Ababaei The Effect of Electric Field on the Collision Efficiency Between Two Uncharged Settling Cloud Droplets 131

P. Marczak, M. Jaszczur CFD Simulations of Multiphase Flow and Radiometric Probe Response 133

M. Marek, P. Niegodajew Fluid Flow Through Randomly Packed Particles 135

A. Merdjani, W. Olszewski, N. Kizilova Fractal Flow-Based Cooling Systems for Single Fuel Cells and Fuel Cell Stacks 137

J. Muller, S. Rozborski, D. Boldo Time Dependent Transition on Vertical Heating Plate 139

S. Naqvi , N. Kizilova Fractal Biomimetic Fins for Optimal Flow-Based Systems for Internal/External Cooling/Heating 141

M.A. Nasr, B.Y.J. Wong, C.M.J. Tay Deep-Learning-Based Design Optimization and Aerodynamic Performance Validation of a Natural Laminar Flow Airfoil 143

P. Niegodajew, M. Wilczyński, A. Durajski, M. Marek Effect of Column Wall Corrugation on Liquid Transport in Random Packed Beds of Spherical Particles 145

B. Okonokhua, M. Pahlavanzadeh, K. Rusin, W. Wróblewski Porous Media Layer Model to Account for Roughness in the Mini-Channel Flows 147

A. Olczyk, K. Sobczak, K. Kantyka, G. Liśkiewicz, B. Miller, M. Tomecka, P. Rusinow Numerical and Experimental Analysis of Flow Uniformity in a Star-Type Manifold 149

A. Olszewska, Z. Peter Numerical and Experimental Analysis of Drag Coefficient of a Disc-Gap-Band Parachute 151

M. Pilecki, J. Płuziński Active Suppression of Vortex-Induced Vibrations: Comparative Study Between PID and SMC Controllers 153

M. Piotrowicz, M. Kurowski, A. Hanfy, P. Doerffer, M. Śleszyński, P. Flaszyński Effect of Inflow Conditions on Shock-Induced Separation on a Compressor Stator Profile 155

M. Pisula, M. Poćwierz, J. Szumbarski Pedestrian Comfort and Ventilation - Numerical Analysis of Airflow in a Building Quarter 157

B. Potęga, E. Cieślikowski, K. Walicki, M. Remer Understanding of the Flow Complexity of Motorcycle While Cornering 159

B. Potęga, J. Lepiarz, K. Skalska, M. Remer Aerodynamic Characteristics of a Leaning Racing Motorcycle Under Combined Slip and Lean Angles: Experimental Study 161

M. Rajek , J. Pozorski High-Fidelity Pseudo-Spectral Simulation of Single-Phase and Dispersed Two-Phase Isotropic Turbulence 163

R. Ramadas, S. Advaith Effect of Chevron-Induced Jet Mixing on Entrainment Characteristics of a Supersonic Ejector 165

M. Remer, T. Bobiński Mesoscopic Oscillations of Triple Line in Capillary Flows 167

M.P. Rezaei, G. Kudra, K. Witkowski, J. Awrejcewicz Pre-, Near-, And Post-Resonance Regimes of Shear-Thickening Fluids: Distinct Dynamic Responses 169

M. Romańczyk, A. Dróżdż, W. Elsner Experimental Study of Left-Tilted Wavy Wall for Turbulent Separation Control 171

A Rożek, **S Rulik** Multiphase Modelling of Vacuum Insulated TES Charging Process 173

F. U. Rückert, **D. Hübner, S Grün, B. Allweyer, C. Sassen** Influence of Turbulence on the Flow Behavior of Propeller Blade Geometries 175

N. Rupasinghe, S. Michel, A. Baumann, S. Gülde, D. Biermann, P. Eberhard Investigation of Fluid Flow in the Ejector Nozzle During Ejector Deep Hole Drilling Using Mesh-Free Methods 177

K. Rusin , **W. Wróblewski** Semi-Analytical Flow Model of Low-Boiling Medium in Tesla Turbine 179

H. Saini, K. Gyoten, P. Friend, T. Pruett, J. Sushil Rao, J. Tithof Pre-Clinically Validated Lumped Parameter Liver Model to Guide Pre-Operative Resection 181

S. Sengupta Critical Assessment of the Buoyant Flow Dynamics for Enhancing the Performance of a Solar Updraft Tower 183

Ch. Shekhar, H.N. Mirajkar, P. Zdybel, Y. Melikhov, M.I. Ekiel-Jeżewska Hydrodynamic Orienting of Rigid Particles Settling Under Gravity in a Viscous Fluid at Low Reynolds Number 185

A.B. Şimşek, B. Erdoğan, N.B. Üner Multiphysics Modeling and Experimental Characterization of a Commercial High-Pressure Reciprocating Compressor 187

A.B. Şimşek, B. Erdoğan, N.B. Üner Numerical and Experimental Study of External Heat Loss on the Piston-Barrel Assembly of a High-Pressure Reciprocating Compressor 189

K. Sindera Experimental and Numerical Study of the Biomimetic Catalytic Carrier Based on Fish Gills 191

K. Skoczylas, A. Bogusławski, S. Dykas, M. Majkut, K. Smołka Numerical and Experimental Studies of Low-Frequency Unsteadiness in Shock Wave Boundary Layer Interaction 193

E.Smyk On the use of Entropy Generation to Quantify Flow Conditioning 195

J. Spała, M. Wacławczyk, J-I. Yano Multiscale Analysis of Turbulent Fluxes for Reynolds Averaging in Atmospheric Flows 197

W. Stankiewicz, T. Krakowski A Comparative Study of Physics-Based, Sparse, and Black-Box Reduced Order Models of Tandem Cylinder Wake Dynamics 199

W. Stryczniewicz Application of Helium Filled Soap Bubbles for 3D PIV Investigations of Large Scale Passive Flow Control Devices 201

T. Suresh, N. Maynard, J.A. Khalil, R. El Akoury, M. Braza, **O. Szulc, P. Flaszyński** Aeroacoustic Investigation of Travelling Wave as Flow Control for Airfoil Drag Reduction 203

O. Szulc, T. Suresh, A. Sieradzki , P. Flaszyński High-Fidelity Analysis of Low-Noise UAV Rotor Designs 205

J. Szumbarski Flow Instability in a Channel with Obliquely Corrugated Walls 207

J. Szumbarski, J. Gałecki Simulation of Unsteady Internal Flows with Novel Dissipative Inlet/Outlet Conditions 209

M. Szydłowski, G. Górecki A. Gutkowski Experimental Investigation of a 3D-Printed Heat Pipe with Mathematically Determined Operating Limits 211

S. Telyma Some Aspects of Modelling the Process of Organic Wastewaters Removal in Bioreactors and Influence of Oxygen Regime on Efficiency of Purification 213

F.D. Tomczak Explicit Algebraic Reynolds Stress Model Validation Based on Shock Wave-Boundary Layer Interaction Experiment 215

E. Tuliszka-Sznitko Subcritical Transition to Turbulence in the Flow Between Counter-Rotating Cylinders 217

I.P. Ungureanu, M. Boni, I.R. Andrei, A. Staicu Control of Interface Oscillations in Hanging Droplets Via Long-Range Interactions 219

T. Wacławczyk Numerical Study of a Twin-Foil System for Diode Laser Hygrometer 221

D. Walisiak , J.M. Kopania, P. Gaj, K. Wójciak Identification of Noise Sources in Hvac end Elements Using Acoustic Camera in an Anechoic Environment 223

I. Wardach-Święcicka XDEM for Modelling Thermal Conversion Processes in Granular Media 225

F. Wasilczuk, P. Flaszyńki, M. Piotrowicz, K. Gnebner, Y. Govers, B. Zima, M. Wojcik Analysis of Aerodynamic Damping of a Wind Turbine Blade Oscillating in a Cold Chamber 227

A. Wawrzak Dynamics of Lifted Flame Base Influenced by Global Instability 229

K. Wawrzak Influence of Diffusion Models on LES/DNS of Hydrogen Flames 231

J. Wiśniewski, J. Szumbarski VAWT Load-Limiting Optimization Using Height-Variable Blade Skew 233

K. Wójciak, I. Czajka, J. Kopania Real-World Aerodynamic and Acoustic Performance of Multi-Disk Radial Fans 235

J-I. Yano Analysis of a Thermal Vortex Ring Generated in the Laboratory: Vortex Dynamics 237

P.J. Ziółkowski, M. Bryk, T. Ochrymiuk, J. Badur Critical Strouhal Velocity During Flow Over Semi-Fixed Industrial Steel Chimney 239

D. Żyła-Jabłońska, T. Bobiński Towards Perfect Cloaking - Combining Cloaks for Enhanced Invisibility in Water Waveguide Systems 241

INDEX OF AUTHORS 243

ABSTRACTS OF THE CONFERENCE PRESENTATIONS

THE EFFECT OF CHARGE MAGNITUDE ON THE COLLISION EFFICIENCY BETWEEN TWO SETTLING CLOUD DROPLETS

A. Ababaei[1], **B. Rosa**[1,2], **M. Manna**[1]

[1] *Institute of Meteorology and Water Management – National Research Institute, Podleśna 61, 01–673 Warsaw, Poland*

[2] *Department of Applied Mathematics, Warsaw University of Life Sciences (SGGW), Nowoursynowska 166, 02–776 Warsaw, Poland*

E-mail: bogdan_rosa@sggw.edu.pl

Abstract. The collision efficiency of charged, micron-sized, inertial cloud droplets settling in still air is quantified using analytical models that incorporate charge-induced polarization and capture short-range interactions which are commonly omitted in earlier studies. Numerical simulations were performed for uncharged droplet pairs as well as for like-charged, oppositely charged and charged-uncharged pairs. The results demonstrate that electrostatic interaction significantly modifies collision efficiency. Under certain conditions, collisions of like-charged droplets are found to be more efficient than those of uncharged droplets.

Keywords: Atmospheric Science, Collision efficiency, Charged cloud droplets.

1. Introduction

Collisions between cloud droplets are fundamental to coalescence, droplet growth and the onset of precipitation. While the collision efficiency of uncharged droplets has been studied extensively, far less is known about collisions involving charged droplets, particularly at micron scales. Small cloud droplets (≈1–10 μm) interact over short timescales, during which electrostatic forces, charge polarization and hydrodynamic lubrication can strongly modify collision dynamics, yet these effects are often neglected or treated using oversimplified models. Experimental data for charged droplet collisions are scarce due to technical limitations, making numerical simulations essential for exploring the wide parameter space of droplet size, charge magnitude and charge configuration. Understanding the role of electrostatic interactions is therefore crucial for improving microphysical representations of cloud processes.

Most existing numerical studies rely on approximate hydrodynamics, consider only a single charge configuration (e.g., like-charged [1]) or employ a point-charge approach based on Coulomb's law. This study addresses these limitations by evaluating the collision efficiency of non-deformable spherical droplet pairs settling in quiescent air over a wide range of charge magnitudes. The larger droplet (collector) settles faster than the smaller (collected) and collision efficiency is defined as $E_{12} = y_c^2 / (a_1 + a_2)^2$, where y_c is the maximum horizontal offset leading to collision. Various charge configurations are examined, with electrostatic interaction forces computed using analytically derived models in the Stokes regime [2]. These results are relevant for future large-scale simulations involving many interacting droplets, where both physical accuracy and computational efficiency are critical.

2. Results and discussion

The results presented in Fig. 1 demonstrate the influence of charge magnitude on the collision efficiency for various pair charge configurations, marked by different colors. Interestingly, for like-charged pairs, collision efficiency initially increases with q/e due to short-range attraction, but after reaching a peak it drops sharply once repulsion dominates, yielding E_{12} values far below those of uncharged droplets. These results are consistent with the conclusion of Patra et al. [1] that E_{12} for like-charged droplets can be much higher than that of uncharged ones.

In the left panel, the like-charged E_{12} (red) is larger than collector-charged (blue) one at low to moderate charge magnitudes. This is because like-charged pairs experience a stronger short-range polarization-induced attraction than collector-charged pairs, whose attraction appears only at very short gaps. However, once the repulsive regime is reached, the red curve drops sharply below all others, reflecting the strong suppression of collisions by long-range electrostatic repulsion. The remaining cases, i.e., unlike-charged and charged–uncharged pairs, display a monotonic increase in E_{12} with charge magnitude. The enhancement is strongest for unlike-charged pairs, followed by collected-charged and then collector-charged ones.

These results not only show the importance of the size of collected droplet, a_2, but also identify the minimum charge magnitude required for EI effects to influence the collision efficiency. For smaller radius ratios (3 μm and 10 μm pairs), the like-charged, unlike-charged and collected-charged pairs begin to exhibit noticeable EI effects at nearly the same value of q/e, whereas collector-charged pairs require larger charge magnitudes. These trends do not agree well with the estimates proposed by Beard and Pruppacher [3], e.g. E_{12} is not impacted by like-charged EI if $q < 0.4a_1^2$ in E.S.U. with radius in cm. Since the patterns reported here may change when $q_1 \neq q_2$, any general criterion for the charge range over which electrostatic interactions can be safely neglected remains premature and would benefit from further investigation.

References

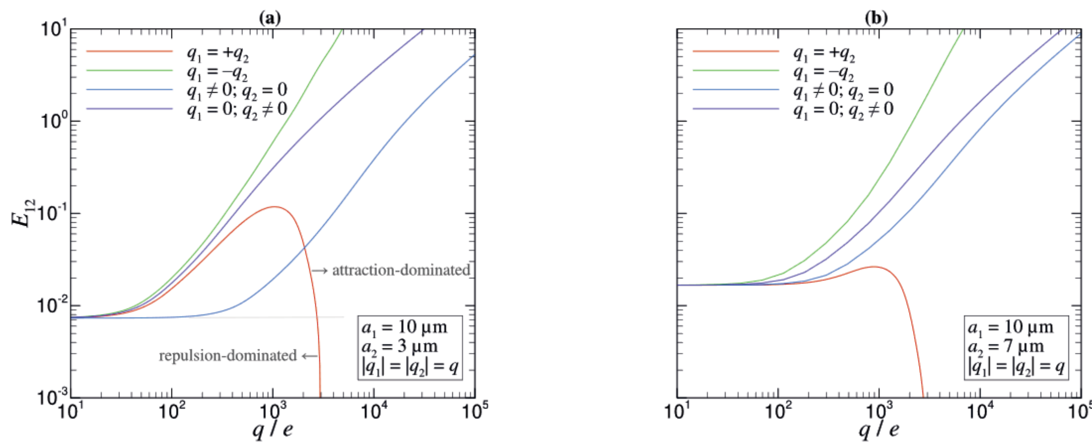

Figure 1. E_{12} as a function of the number of elementary charges for droplets that are like-charged (red), unlike-charged (green), collector-charged (blue), and collected-charged (purple) with 10-μm collectors and **(a)** 3-μm as well as **(b)** 7-μm collected droplets

[1] Davis M.H., *Two charged spherical conductors in a uniform electric field: forces and field strength*, 'The Quarterly Journal of Mechanics and Applied Mathematics' 1964, vol. 17, no. 4, pp. 499–511.

[2] Patra P., Koch D.L., Roy A., *Collision efficiency of like-charged spheres settling in a quiescent environment*, 'Journal of Fluid Mechanics' 2023, vol. 968.

[3] Beard K.V., Pruppacher H.R., *An experimental test of theoretically calculated collision efficiencies of cloud drops*, 'Journal of Geophysical Research' 1968, vol. 73, no. 20, pp. 6407–6414.

1D, 2D AXIS-SYMMETRIC AND 3D NUMERICAL SIMULATION OF VALVE INDUCED WATER HAMMER

A. Alavi, K. Urbanowicz

West Pomeranian University of Technology, Faculty of Mechanical Engineering and Mechatronics, Al. Piastów 19, 70–310 Szczecin, Poland

E-mail: as61302@zut.edu.pl, kamil.urbanowicz@zut.edu.pl

Abstract. A numerical investigation of water hammer induced by rapid valve closure in a pipe system is performed. Three modeling approaches with increasing spatial fidelity are applied: 1D with convolution-based friction, 2D and 3D models implemented in OpenFOAM and ANSYS Fluent. Predicted pressure responses at the valve section are validated against experimental data. The models are compared in terms of accuracy versus computational cost, and numerical dissipation, and dispersion are analyzed with respect to mesh resolution, CFL number, turbulence modeling and numerical schemes.

Keywords: Computational Fluid Dynamics, Water hammer, Unsteady friction, Turbulence.

1. Introduction

Water hammer (WH) is an unwanted phenomenon resulting from an abrupt change in fluid velocity in a hydraulic system. WH generates pressure waves within the pipeline, traveling back and forth at the pressure wave speed in the fluid until they are fully damped due to friction. This phenomenon has been the subject of intensive research using various methods, including analytical, experimental and numerical approaches, as it typically affects hydraulic systems negatively.

Experimental investigations have been reported in the literature [1], focusing on valve-induced WH. Numerical studies are also of significant interest, particularly for capturing unsteady friction (UF) effects. Mandair et al. [2] developed both 1D Method of Characteristics (MOC) and 3D CFD numerical models, comparing different UF modeling approaches with 3D CFD and experimental results. Martin and Wahba [3] investigated this effect by comparing 2D quasi-steady axisymmetric CFD with full 3D CFD simulations. The effect of valve closure modeling was examined by Kalantar et al. [4], including dynamic mesh, sliding mesh and immersed solid methods. Bergant et al. [5] compared 1D analytical and MOC models with 3D CFD simulations, highlighting the influence of UF modeling and turbulence treatment on pressure wave attenuation and waveform shape.

In this study, a systematic comparison between 1D, 2D and 3D modeling approaches is performed under rapid valve closure boundary conditions. Particular emphasis is placed on the influence of computational grid resolution and time-step selection, as well as their interdependence through the CFL number. In addition, the effect of turbulence modeling in 3D CFD simulations on UF behavior is examined.

2. Analysis and Methodology

1D, 2D and 3D models are employed in the present study to investigate the differences between them in WH representation. A convolution-based method is used for modeling UF in 1D model as it has been shown to provide more realistic results compared to other methods. The main challenges associated with 2D and 3D CFD solutions include appropriate setting of computational grid, time step selection, boundary condition specification and using a suitable turbulent model.

In this study, the computational domain consists of a pipe with constant radius, discretized in the radial, circumferential and axial directions with refinement near the wall region. For a selected simulation, the number of divisions in the axial, radial and circumferential directions is 1000, 16 and 40 for the laminar case, and 500, 39 and 60 for the turbulent case respectively. The chosen time step is 0.00001 s, and the Reynolds-averaged k-ω SST model is used for turbulence treatment.

Figure 1 presents a comparison between experimental measurements, 1D solution, 2D axis-symmetric and 3D results for the cases: a) laminar, b) turbulent. The amplitude of the first pressure wave (Fig 1a) is slightly overestimated in 3D simulation. However, agreement with laminar flow experimental data improves in subsequent cycles compared to the 1D results whereas the 2D axis-symmetric solution is closely correlated with 1D results. In addition, the Ansys 3D simulation more accurately represents the rounded pressure waveform compared to OpenFOAM.

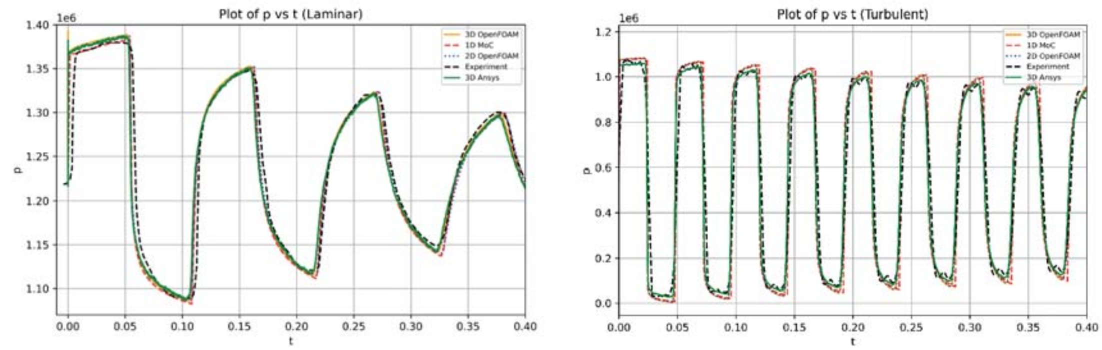

Figure 1: 1D MOC, 2D axis-symmetric and 3D CFD results compared to experimental results

Figure 1b illustrates the exemplary results of 1D and 3D in comparison to turbulent flow experimental measurements. Compared to 1D, the 3D simulation significantly improved the accuracy in terms of wave amplitude and roundedness in peaks.

3. Conclusion

This preliminary study provides a systematic comparison between 1D MOC, 2D axis-symmetric and 3D CFD approaches for simulating WH phenomenon under rapid valve-closure conditions. The results demonstrate that 3D CFD simulations offer improved accuracy in capturing pressure wave attenuation and waveform roundedness, particularly in turbulent flow regimes, compared to the 1D MOC and 2D axis-symmetric model. The analysis highlights the critical role of mesh resolution, time-step selection and turbulence modelling in accurately representing UF effects. These findings establish a foundation for future investigations of more complex hydraulic systems, including networked pipelines and fluid–structure interaction effects.

References

[1] Soares A.K., Martins N.M., Covas D.I., *Transient vaporous cavitation in a horizontal copper pipe*, 'Journal of Hydraulic Research' 2017, vol. 55, no. 5, p. 731–736.

[2] Mandair S., Magnan R., Morissette J.F. Karney, B., *Energy-based evaluation of 1D unsteady friction models for classic laminar water hammer with comparison to CFD*, 'Journal of Hydraulic Engineering' 2020, vol. 146, no. 3.

[3] Martins N.M.C, Wahba E.M., *On the Hierarchy of Models for Pipe Transients: From Quasi-2D Water Hammer Models to Full 3D CFD Models*, 'Journal of Pressure Vessel Technology' 2021, vol. 144, no. 2.

[4] Neyestanaki M.K., Dunca G., Jonsson P., Cervantes M.J., *A comparison of different methods for modelling water hammer valve closure with cfd*, 'Water' 2023, vol. 15, no. 8.

[5] Bergant A., Rek Z., Urbanowicz K., *Analytical, numerical 1D and 3D water hammer investigations in a simple pipeline apparatus*, 'Strojniški vestnik – Journal of Mechanical Engineering' 2025, vol. 71, no. 5–6.

EXPERIMENTAL ASSESSMENT OF EFFICIENCY INCREASE ON UAV PROPELLERS USING MICROSTRUCTURES

B. Allweyer, S. Grün, D. Hübner, F. Rückert[1]

[1] *Hochschule für Technik und Wirtschaft des Saarlandes (htw saar), Faculty of economics, including industrial engineering, 66123 Saarbrücken, Waldhausweg 14*

E-mail: benjamin.allweyer@htwsaar.de, sebastian.gruen@htwsaar.de, dirk.huebner@htwsaar.de, frank.rueckert@htwsaar.de

Abstract. Drag and turbulence are mainly influenced by the boundary layer. Usually, the surface of bodies, like UAV propellers, aim to be smooth. Contradictorily, non-smooth surfaces can be observed as being better suited to various conditions. Sharks have developed riblets that reduce drag. This raises the question, if smooth surfaces in technical appliances are best suited. It is studied, whether similar effects can be translated to UAV propellers. So, commercially available UAV propellers with riblets are tested at various RPM speeds. The effect on drag and lift are studied.

Keywords: Experimental Fluid Mechanics, Aerodynamics, Microflows, Microstructures, Flow Machinery, Propellers, Drones, Unmanned Aerial Vehicles (UAV).

1. Introduction

The importance of Unmanned Aerial Vehicles (UAV) in modern day applications is rapidly increasing. The success and acceptance of UAV usage is mainly influenced by its physical properties, such as noise emissions, load capacity, operating range or overall efficiency. A main influence in this is the propulsion system (propellers) in which the necessary thrust and lift are generated. In order to increase overall UAV efficiency, this work aims to improve propeller efficiency by applying riblet like surface structures.

Often, flow related appliances aim to have as smooth surfaces as possible. This is also the case for UAV propeller. Contradictorily, there are occurrences, where non smooth surfaces tend to improve aero- and hydrodynamic properties. The golf-ball for instance is manufactured with its iconic dimples that reduce drag and thus increase airtime. Further, sharks have developed riblet on their scales that also seem to decrease drag and thus give them an evolutionary advantage.

The performance increasing effect of riblet structures on flat surfaces is already subject to research. In [1], Grüneberger and Hage have manufactured test plates with trapezoidal riblet groves. The data they present suggests a 7.6% maximum drag reduction in relation to a smooth surface. Analog to this, Sasamori, Mamori, Iwamato and Murata [2] translated a theoretically optimal two-dimensional riblet structure into a real, three dimensional application. They observe a maximum drag reduction of 11.7%. Furthermore [3], Bechert, Bruse and Hage have equipped test plates with riblets ('fins') in a three-dimensional pattern. They conclude an overall drag reduction, even compared to two-dimensional riblet structures.

This raises the question whether the physical properties of UAV propellers can be increased by applying riblets to their surface.

2. Methodology

In order to explore the effect of riblets on the propeller blade, a commercially available UAV propeller is fitted with a variety of riblet geometries.

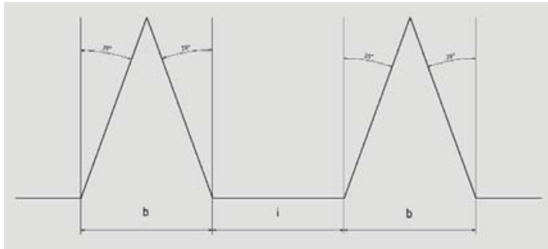

Figure 1. Basic riblet geometry

The riblets are defined by their base dimension (base – b) as well as the distance to the next riblet (increment – i). The base dimension varies from 0.1 mm to 1 mm, as well as the i parameter. The exterior angles of the isosceles triangle remain fixed at 20°. This results in a total of 100 possible combinations which are physically tested on a test rig.

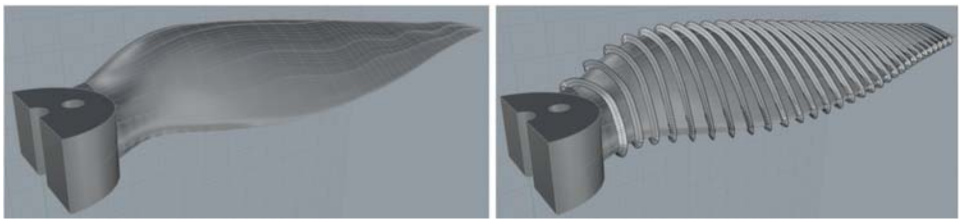

Figure 2. plain blade (left), blade fitted with riblets (right)

It is important to note, that propellers are axially symmetrical. The applied surface structures need to be adapted to this. Then, the propellers are tested at different RPM speeds and the effect on drag, lift and necessary shaft power are observed.

The work aims to find optimized surface patterns in comparison to the plain blade. Potential optimizations are measured in a increase in efficiency, notably in an increased lift to shaft power ratio.

Previous experiments conducted at *htw saar* indicate an possible increase in propeller efficiency for certain types of surface structures [4]. A propeller has been fitted with different kind of random surface structures of which a riblet like structure was the most promising. In this work, the basic riblet structure on propellers is subject of further investigation in order to find better geometries.

References

[1] Grüneberger R., Hage W., *Drag characteristics of longitudinal and transverse riblets at low dimensionless spacings*, 'Experiments in Fluids' 2010, vol. 50, p. 363–373.

[2] Sasamori M., Mamori H., Iwamoto K., Murata A., *Experimental study on drag-reduction effect due to sinusoidal riblets in turbulent channel flow*, 'Experiments in Fluids' 2014, vol. 55, no. 10.

[3] Bechert D.W., Bruse M., Hage W., *Experiments with Three-Dimensional Riblets as an Idealized Model of Shark Skin*, 'Experiments in Fluids' 2000, vol. 28, pp. 403–412.

[4] Allweyer B., Gruen S., DiBenedetto F., Bulduk G., Huebner D., Rueckert F., *Advances in Computational Heat and Mass Transfer II*, Springer, 2026.

DETERMINATION OF OPTIMAL LOCATIONS OF RIVER TURBINES BASED ON SIMULATIONS

B. Allweyer, S. Grün, D. Hübner, F. Rückert[1]

[1] *Saarbrücken University of Applied Sciences, Waldhausweg 14, 66123 Saarbrücken, Germany*

E-mail: benjamin.allweyer@htwsaar.de, sebastian.gruen@htwsaar.de, dirk.huebner@htwsaar.de, frank.rueckert@htwsaar.de

Abstract. This article presents the results of a numerical flow-field simulation for a section of the Rhine near St. Goar (Ehrenthaler Werth), with the aim of identifying optimal locations for river turbines[1]. For this purpose, the flow field is computed in a riverbed model generated using an AI-supported modelling approach. The simulation results are evaluated through comparison with measured local near-surface flow velocities. Subsequently, the river level is varied to analyse its influence on discharge and flow velocity. This enables the effects on the flow field and on the previously identified potential turbine locations to be assessed and the site selection to be adjusted accordingly. The proposed method incorporates flow-field characteristics directly into the site-selection process, an aspect that has so far only been considered in a rudimentary manner.

Keywords: Environmental fluid mechanics, AI and machine learning in fluid mechanics, Computational Fluid Dynamics, Experimental Fluid Mechanics, Power Buoys.

1. Introduction

The variability of most renewable energy sources has increased the demand for alternatives capable of providing base-load power, such as run-of-river hydropower plants. However, the potential for conventional run-of-river hydropower in Germany is considered to be largely exhausted[2]. Consequently, attention is increasingly shifting towards decentralized systems based on power buoys (river turbines), as the kinetic energy of river flow is regarded as a highly predictable and largely weather-independent energy source[3]. Identifying suitable locations for individual power buoys or clusters is therefore a key challenge.

2. Description of the procedure

The developed workflow consists of the following steps:

- Riverbed modelling based on measurement data;
- CFD simulation of the flow field, including identification of potential turbine locations;
- Variation of water levels to analyze their impact on the identified potential locations.

2.1. Riverbed Modelling

Accurate modelling of the riverbed is essential for the calculation of flow fields. To achieve this, the riverbed was surveyed using a specially developed measurement system (Fig. 1, left). The acquired data were processed with an AI-supported application which interpolates missing points to generate a complete mesh. This results in a surface-based riverbed model suitable for CFD simulations (Fig. 1, right).

Figure 1. Measurement system (left) and model of the measured riverbed (right)

2.2. CFD calculation, Validation and Site Identification

The riverbed model is assigned appropriate boundary conditions and the flow field is computed (Fig. 2, left). The simulated near-surface flow velocities are compared with measured values and if sufficient agreement is achieved, potential turbine locations are identified from the simulation results.

2.3. Variation of Water Levels and Site Adjustment

Simulations are then repeated for varying water levels to analyze their effect on the flow field (Fig. 2, right). This approach allows for the adjustment of potential turbine locations and enables estimation of the approximate annual energy yield based on seasonal water-level variations.

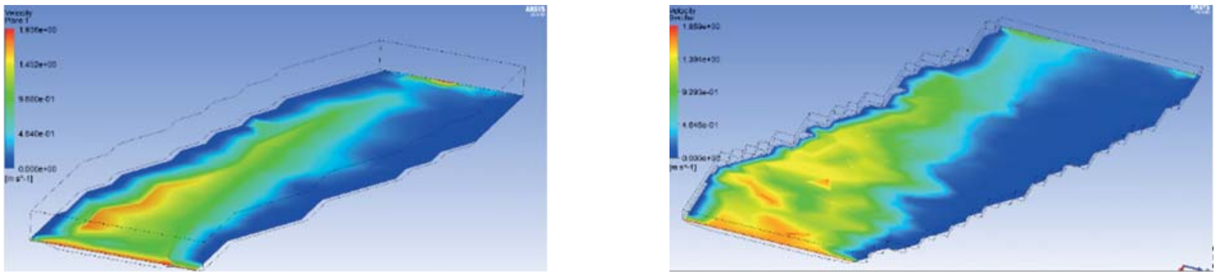

Figure 2. flow field at average water level (left) and low water level (right)

3. Summary and outlook

This article presents a method for determining suitable locations for power buoys. The approach can be further extended to consider clusters of turbines (interactions between units) and based on these findings, it would be worthwhile to develop an AI-based tool capable of identifying optimal locations solely from the riverbed model or from 2D representations of the river course.

Acknowledgements

We gratefully acknowledge the Federal Ministry BMUV of the Federal Republic of Germany for funding the project ‘FluKIT’.

References

[1] Umweltbundesamt Deutschland (German Environment Agency), *Nutzung der Wasserkraft*, https://www.umweltbundesamt.de/themen/wasser/fluesse/nutzung-belastungen/nutzung-von-fluessen-wasserkraft#stromproduktion-aus-wasserkraft-in-deutschland (access: 18.09.2019).

[2] Fräger C.,*Energieertrag von Flussturbinen – Abschätzung des Energieertrags von Turbinen ohne Staustufen am Oberrhein, der Weser, der Werra und der Unterelbe*, https://serwiss.bib.hs-hannover.de/files/398/Energieertrag_Flussturbinen_2013-11-02a.pdf, 2014 (access: 1.01.2023).

[3] Küffner G., *Propellerräder unter Wasser liefern Strom*, https://www.faz.net/aktuell/technik-motor/technik/flussturbine-propellerraeder-unter-wasser-liefern-strom-1579186.html (access: 10.10.2010).

NO_X EMISSIONS IN NH_3/H_2 CO-COMBUSTION UNDER O_2-ENRICHMENT AND STEAM DILUTION CONDITIONS

M. Amiri, A. Tyliszczak

Faculty of Mechanical Engineering, Czestochowa University of Technology, Armii Krajowej 21, 42–201 Czestochowa, Poland

E-mail: milad.amiri@pcz.pl, artur.tyliszczak@pcz.pl

Abstract. Combustion under oxygen-enriched conditions enhances flame stability and reactivity in NH_3/H_2 co-combustion but increases NO_x via thermal and fuel-bound pathways. To address this issue, steam dilution (10–40%) reduces flame temperature and partially suppresses NO_x. Using Cantera simulations, the effects of O_2 enrichment (23–45%), hydrogen fraction and steam dilution on ignition, flame temperature, and NO_x formation are analysed. The optimum values of H_2, O_2, and steam identified within the investigated ranges are then applied in CFD simulation performed using the ANSYS Fluent code to obtain combustion characteristics under practical combustion conditions.

Keywords: Combustion, NO_x emissions, Ignition behaviour, Cantera, Oxygen-enrichment, Combustion stability, Steam dilution.

1. Introduction

The increasing global demand for clean and sustainable energy has driven significant interest in carbon-free fuels, among which NH_3 has emerged as a promising candidate due to its zero-carbon content, high H2 density and established production infrastructure [1]. When co-fired with H_2, NH_3 combustion can achieve improved flame stability, higher reactivity and faster ignition characteristics, overcoming some of the limitations of pure NH_3, such as low flammability and slow kinetics.

Despite these advantages, NO_x emissions remain a major challenge in NH_3-H_2 co-combustion [2], particularly under O_2-enriched conditions. Elevated O_2 levels in the oxidizer improve flame temperature and ignition rates but simultaneously intensify thermal NO formation and the oxidation of fuel-bound nitrogen intermediates, resulting in higher NO_x levels [3]. Effective strategies to control NO_x emissions are crucial.

Several approaches have been explored to mitigate NO_x in NH3 combustion. Fuel staging [4], H2 fraction optimization [5] and moderate O2 enrichment [6] have been proposed to reduce thermal NO formation while maintaining stable ignition. Steam or N2 dilution has also been recognized as an effective flame temperature control mechanism [7] which suppresses thermal NO formation and modifies radical pool dynamics. Previous studies have demonstrated that combining H2 addition with controlled oxidizer composition can influence NH_3 decomposition pathways, reducing NO_x through enhanced radical-mediated reduction mechanisms. However, most existing investigations have focused on either pure NH3 or H2-enriched fuels under atmospheric conditions and the combined effects of O_2 enrichment, H2 addition and steam dilution on NO_x formation in NH_3/H_2 co-combustion remain insufficiently understood.

To address this gap, the present study systematically investigates NH_3/H_2 co-combustion under O_2-enriched conditions, focusing on NO_x formation, ignition characteristics and combustion performance. Detailed chemical kinetics simulations are initially performed using Cantera and validated against available experimental data, after which the identified optimum values are applied as known conditions in CFD simulations performed using the ANSYS Fluent code for modelling stabilized flame in non-premixed regimes. The study examines the effects of oxidizer oxygen concentration (23–45%), hydrogen fraction and steam dilution (10–40%) on flame temperature, radical pool dynamics and NO_x emissions. The findings provide fundamental insights into the mechanisms of NO_x formation and reduction in ammonia-hydrogen systems, offering guidance for the development of low-emission, high-performance ammonia-based combustion strategies suitable for industrial and power-generation applications.

2. Results

Figure 1a shows the results of simulations performed using the Cantera software employing chemical mechanism of 21 species and 64 reactions. It presents variability of an ignition delay time (IDT) in mixture fraction space for different mixture composition (NH_3 with/without H_2 and oxidizer with/without steam) at the initial temperature 1200 K. It can be seen adding small amount of H_2 (5% by mass) significantly reduces IDT (approx. two orders of magnitude), indicating enhanced mixture reactivity, while steam dilution delays ignition due to thermal and chemical effects. Mass fraction of NO at ignition onset and after 0.1s is demonstrated in Figs.1b, c, respectively. It can be seen that initially the maximum NO value is higher when the steam is present, but in a regime of developed flame, it effectively reduces NO peak, approximately four times. The reason for that is a high heat capacity of the steam which causes lowering the flame temperature and thus the thermal NO production. During the conference, the conditions similar to the present one will be used in 3D CFD simulations.

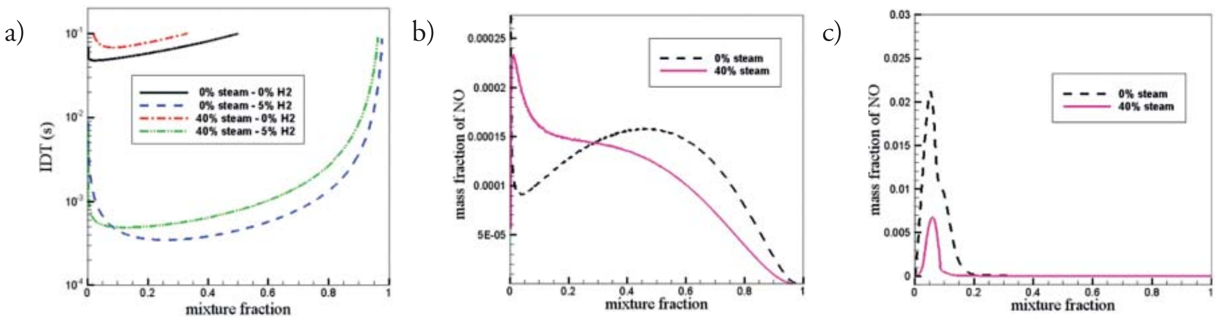

Figure 1. a) Variation of IDT at different steam and H2 mass fraction, b) NO mass fraction in mixture fraction at the ignition instant and c) after a residence time (0.1s) for the case with initial temperature of 1200K, H2 = 5%; NH3 = 95% at constant pressure (1 atm)

Acknowledgements

This work was supported by the National Science Centre (NCN) under Grant No. 2024/53/B/ST8/02908.

References

[1] Zhang Y., Hao Q., Huang M., Liu Z., Li Q., Yu Z., Du J., Zhang X., Xiong Z., Zhang Q., *Numerical investigation on the influence of temperature on combustion and emission characteristics of NH3/H2/CH4 mixtures under gas turbine conditions*, '*Fuel*' 2026, vol. 405, art. no. 136609.

[2] Deng K., Lin Q., He A., Zhu J., Ye S., Lin W., Zhu J., Dai F., Wang S., Liang Z., *Plasma-assisted combustion of CH4/NH3/H2 ternary fuel for NOX formation mechanisms analysis*, 'International Journal of Heat and Mass Transfer' 2026, vol. 256, art. no. 128029.

[3] Wei Z., Zhang X., Liu L., Huang G., Zhen H., *Lower NO emission conditions of NH3–H2 mixtures under the oxygen-enriched premixed combustion mode*, 'International Journal of Hydrogen Energy*'* 2024, vol. 89, pp. 570–582.

[4] Mubashir M., Shen D., Kraiem H., Flah A., Alshammari N.F. Hanif M.M., *Machine learning assisted CFD optimization of fuel-staging natural gas burners*, 'Scientific Reports' 2025, vol. 15, art no. 23547.

[5] Seo C.K., *Effect on NO_x and CO Reduction Performance According to the Support and the Precious Metals Used When NH_3 is Supplied toH_2-SCR*, 'International Journal of Automotive Technology' 2025, vol. 26, pp. 1177–1184.

[6] Zhang H., Cui B., Du J., Yu Z., Liang X., Cheng Y.B. Wang Y., *Combining staged combustion and oxygen enrichment for stable and low-NOx porous media combustion of ammonia*,*'Fuel'* 2026, vol. 410, art. no. 137894.

[7] Sadkin I.S., Shadrin E.Y., Kopyev E.P., *Investigation of steam-jet liquid fuel combustion as low NO_x and CO emission approach in high-pressure combustion chambers*, '*Energy*' 2025, vol. 336, art. no. 138409.

FROM DIRECTED PERCOLATION TO PATTERNED TURBULENCE

R. Ayats[1,3], L. Klotz[2], B. Hof[1]

[1] *Institute of Science and Technology Austria, 3400, Klosterneuburg, Austria*

[2] *Institute of Aeronautics and Applied Mechanics, Warsaw Universty of Technology, 00–665, Warsaw, Poland*

[3] *Universitat Politècnica de Catalunya, Departament de Física (FIS), 08034 Barcelona, Spain*

E-mail: lukasz.klotz@pw.edu.pl

Abstract. Directed percolation (DP) has recently emerged as a possible solution to the century old puzzle surrounding the transition to turbulence. We show that the complex dynamics encountered at the onset of turbulence can be fully rationalized within the framework of statistical mechanics. In addition, we also demonstrate that patterns self-assemble with increasing distance from critical point. Our study exemplifies that macroscopic patterns can arise solely from local stochastic rules, in the absence of wavelength selection typically associated with pattern formation.

Keywords: Experimental Fluid Mechanics / General Fluid Dynamics / Hydromechanics, Transition to turbulence, Directed percolation.

1. Introduction

Multiple model studies reported DP exponents, however, experimental evidence is limited since the largest possible observation times are orders of magnitude shorter than the flows' characteristic timescales. An exception is cylindrical Couette flow, where the limit is not temporal, but rather the realizable system size. Approaching the critical point to within less than 0.1% we determine five critical exponents, describing dependence of turbulent fraction on control parameter, distribution of laminar gaps in space and in time, as well as dependence of characteristic length and time scales on control parameter. All of these exponents were shown to be in excellent agreement with the DP universality class which describes the behaviour of turbulent flow (i.e. active phase). Next, we demonstrate that starting from the corresponding directed percolation (DP) critical point, regular patterns are established within the scaling range of the DP transition. Likewise, the patterns' expansion rates are set by the DP critical exponents, attesting that all underlying processes are stochastic. This apparent contradiction between the inherent stochasticity and the displayed order is resolved by abandoning the common perception of laminar and turbulence as opposing states.

Most of the presented work consists of experimental results measured in a Couette setup of unprecedented azimuthal and axial aspect ratios. Specifically, experiments were performed in the narrow gap of 2h = 240 μm, spanning between two high-precision concentric cylinders. This forms the test section with very large azimuthal and axial aspect ratios of $L_\theta/h = 3927$ and $L_z/h = 1500$, respectively. The outer cylinder was made of glass that rotated at the rotation speed exceeding 1000 RPMs. Frictionless air-bearings were applied in order to increase the precision of the motion, as well as to decrease heat production and temperature variations. The inner cylinder remained stationary. In Fig. 1, we illustrate the experimental configuration of large-aspect-ratio Taylor-Couette flow, featuring turbulent bands along the entire test section. In Fig. 2, we present flow visualisations with increasing Reynolds number from left to right.

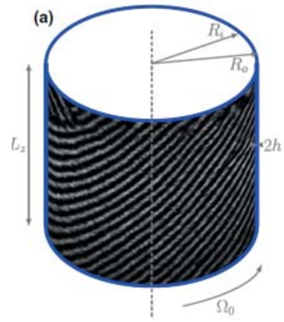

Figure 1. Schematical representation of experimental set-up. Taken from [5]

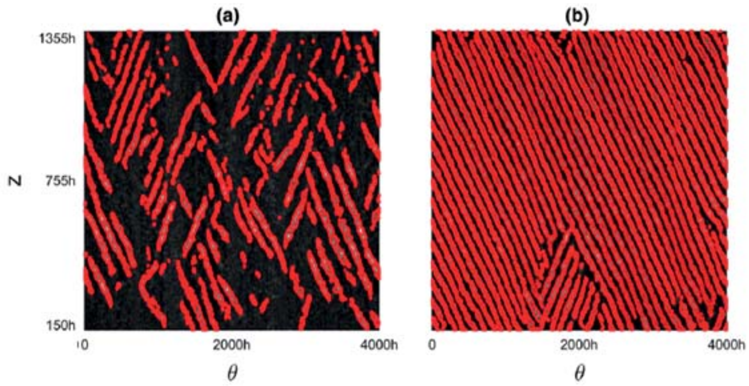

Figure 2. Illustration of macroscopic patterns arising solely from local stochastic rules of directed percolation. Taken from [5]

Acknowledgements

We thank Gökhan Yalnız for contributing with initial simulations and fruitful discussions. R.A. was supported by the European Union's Horizon 2020 research and innovation program under the Marie Skłodowska-Curie Grant Agreement No. 101034413 and by the Austrian Science Fund (FWF) 10.55776/ESP1481224. L.K. was supported by the European Union's Horizon 2020 research and innovation program under the Marie Skłodowska-Curie Grant Agreement No. 754411 and by the National Science Center (Poland) within OPUS-21 project (2021/41/B/ST8/03142).

References

[1] Avila M., Barkley D., Hof B., *Transition to turbulence in pipe flow*, 'Annual Review of Fluid Mechanics' 2023, vol. 55, no. 1, pp. 575–602.

[2] Hof B., *Directed percolation and the transition to turbulence*, 'Nature Reviews Physics' 2023, vol. 5, no. 1, pp. 62–72.

[3] Tuckerman L.S., Chantry M., Barkley D., *Patterns in wall-bounded shear flows*, 'Annual Review of Fluid Mechanics' 2020, vol. 52, no. 1, pp. 343–367.

[4] Lemoult G., Shi L., Avila K., Jalikop S.V., Avila M., Hof B., *Directed percolation phase transition to sustained turbulence in Couette flow*, 'Nature Physics' 2016, vol. 12, no. 3, pp. 254–258.

[5] Klotz L., Lemoult G., Avila K., Hof B., *Phase Transition to Turbulence in Spatially Extended Shear Flows*, 'Physical Review Letters' 2022, vol. 128, art. no. 014502.

[6] Ayats R., Klotz. L., Hof. B., *From directed percolation to patterned turbulence*, under review in 'Nature Reviews Physics', https://arxiv.org/pdf/2501.08014.

RHEOLOGICAL AND THERMAL INFLUENCES ON SECONDARY FLOW IN POLYGONAL DUCT MANIFOLDS

A. Banerjee

Department of Mechanical Engineering, NIT Durgapur, Durgapur-713209, West Bengal, India

E-mail: ab.19me1504@phd.nitdgp.ac.in, contactarkaban@gmail.com

Abstract. The following paper examines Prandtl's second kind secondary flows in regular polygonal ducts for Newtonian and power-law fluids in laminar flow regime under isothermal and non-isothermal conditions. Novel geometrical parameters correlate duct anisotropy with entry length, friction factor, and peak-to-bulk velocity ratio. Entry length rises with lower number of sides and higher flow behavior index; friction factor drops with fewer sides. Secondary flow intensifies in dilatant fluids and varies thermally, enabling optimized designs for compact heat exchangers and fluid transport systems.

Keywords: Interdisciplinary Areas in Heat and Fluid Flow, Secondary Flows, Non-Newtonian Fluids, Computational Fluid Dynamics.

1. Introduction

The study of secondary flow in ducts remains a relevant topic of research for engineering and biomedical applications, as it plays a crucial role in redistributing mass & energy and incurring additional losses. The present study numerically investigates the laminar (Reynolds number, *Re* ranging 50–500) and turbulent (*Re* ranging 10^4 – 10^5 regimes, illustrating the evolution of different types of secondary flow within various in-plane double bends (Prandtl's first kind) and polygonal ducts (Prandtl's second kind) for Ostwald-de Waele power-law fluids. Contextually, the development of a third kind arising due to obstructions or imperfections in biological ducts is also examined. Special attention is paid to the influence of side-count (m, ranging from 3 to 10) and flow behavior index (n, ranging from 0.6 to 1.4) on isothermal and non-isothermal flow through polygonal ducts. Duct corner anisotropy [1] manifests counter-rotating vortex pairs, typically characterized by convex primary velocity isotachs [2]. A pair of geometrical parameters [3-4] is introduced, namely the Factor of approach and the Integrity index, to correlate this geometrical anisotropy with gross parameters, including entry length, friction factor and the fully developed peak-to-bulk velocity ratio.

2. Methodology

Simulations with 3-D computational geometries employing fully structured meshes and adopting pertinent inlet profile assumptions are performed. A pressure-based finite volume solver (ANSYS Fluent) is employed to solve the conservation equations. A broad spectrum of rheological fluids including pseudoplastic ($n < 1$, Newtonian ($n = 1$ and dilatant $n > 1$ (is considered. Second-order discretization schemes are adopted and the convergence criterion is set to 10^{-6}. Numerical results are validated with benchmark experimental data [5].

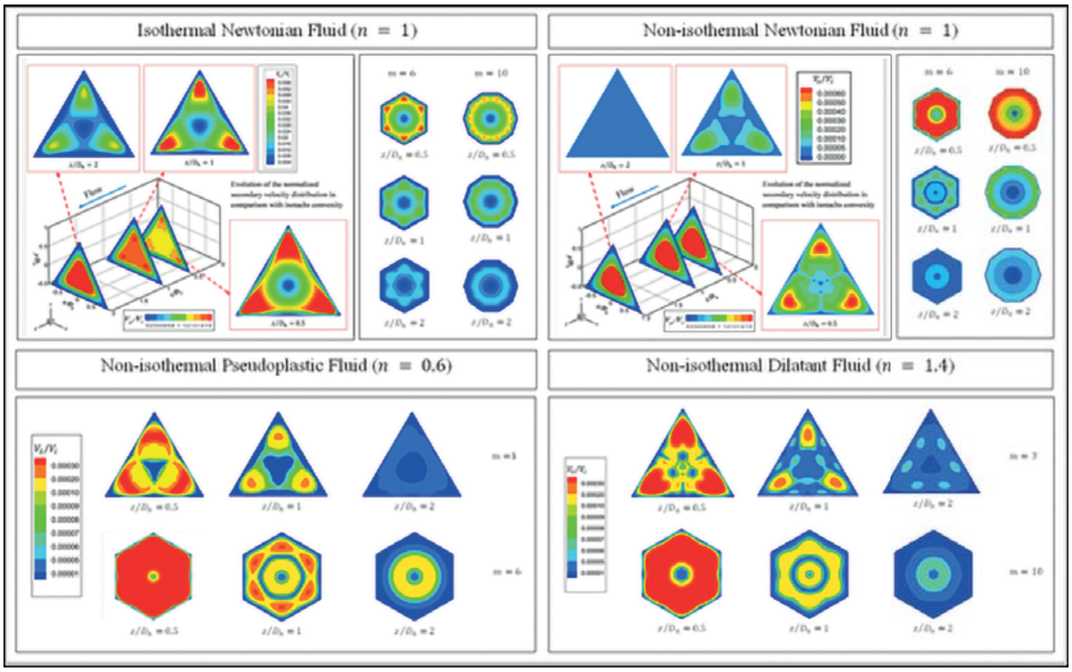

Figure 1. Morphology of various rheological secondary flows in polygonal duct geometries

3. Conclusion

Several important conclusions from the numerical study are drawn. An enhancement ratio to gauge the velocity rise across a bend is introduced. The study of polygonal ducts reveals the disproportionate changes of the friction factor and entry length with m. The fully developed value peak-to-bulk velocity ratio is nearly 2.25 in Newtonian fluids, for a triangular duct ($m = 3$) and this approaches the asymptotic value 2 as m rises to infinity (circular duct). The entry length increases as n increases. The initial strength and persistence of the secondary flow are greater for lower m , and decrease continuously under isothermal flow. In a non-isothermal flow with constant wall temperature, the secondary flow magnitude is significantly weaker: it first increases as m varies from 3 to 6, then decreases as m increases further. Dilatant fluids exhibit more localized and intense secondary motion than Newtonian and pseudoplastic fluids. Future work will extend the analysis to non-isothermal rheological flows in biologically relevant geometries.

Acknowledgements

The author is grateful to his PhD supervisor Dr. Sayantan Sengupta.

References

[1] [1] Madabhushi R.K,Vanka S.P., *Large eddy simulation of turbulence-driven secondary flow in a square duct*, 'Physics of Fluids A: Fluid Dynamics' 1991, vol. 3, p. 2734–2745.

[2] [2] Nikitin N.V, Popelenskaya N.V., Stroh A., *Prandtl's Secondary Flows of the Second Kind. Problems of Description, Prediction, and Simulation*, 'Fluid Dynamics' 2021, vol. 56, p. 513–538.

[3] [3] Sengupta S., Banerjee A., Pramanik S., *Morphology of laminar rheological flow in polygonal ducts*, 'Physics of Fluids' 2024, vol. 36, art. no. 083627.

[4] [4] Banerjee A., Sengupta S., Pramanik S., *Unified numerical study of turbulent rheological flows in regular polygonal ducts: secondary flow mechanisms and design correlations*, 'Proceedings of the Institution of Mechanical Engineers, Part C: Journal of Mechanical Engineering Science' 2026, vol. 240, no. 2, pp. 329–350.

[5] [5] Mohanty A.K, Asthana S.B.L., *Laminar flow in the entrance region of a smooth pipe*, 'Journal of Fluid Mechanics' 1979, vol. 90, pp. 433–447.

EXPERIMENTS ON HUMAN BLOOD SHEAR STRESS AND VISCOSITY AT LOW AND MODERATE HAEMATOCRIT

A. Bartosik[1], B. Jaworska-Jóźwiak[1], M. Sadowski[2], M. Pasiarski[3]

[1] *Kielce University of Technology, Department of Production Engineering, 7 Tysiaclecia Ave., 25–314 Kielce, Poland*

[2] *Jan Kochanowski University of Kielce, Faculty of Medicine, 19A IX Wiekow Kielc Ave., 25–516 Kielce, Poland*

[3] *Holy Cross Cancer Center, Department of Haematology, 3 Artwinskiego St., 25–734 Kielce, Poland*

E-mail: beataj@tu.kielce.pl

Abstract. The study presents results of measurements of human blood rheology using the Anton Paar rheometer. Measurements of the dependence of the shear stress on the shear rate were made in the range of the shear rate of 1 s^{-1} to 200 s^{-1} and for three blood samples with different haematocrit. The purpose of this study is to experimentally determine the dependence of the shear stress on the shear rate at low and moderate haematocrits of human blood. Based on the measurements, blood viscosity was determined, yield stress was estimated and compared with data from the literature and a suitable rheological model was proposed and discussed. The results of the measurements are presented in the form of graphs and conclusions.

Keywords: Experimental Fluid Mechanics, Bio-fluid, Human Blood Rheology, Blood Yield Stress.

1. Introduction

Blood is a suspension with unique structure and physical properties. It has no equivalent among industrial suspensions and, so far, it is not possible to produce a synthetic blood. Most solid components suspended in whole blood are red blood cells (RBC) which contribute to about 99% of all cells. The rest of solid components belongs mainly to white blood cells and platelets. Carrier liquid, named as plasma, is responsible for transportation of all solid components and contribute to about 55% by volume, while the rest of volume belongs to all solid components. Plasma is a Newtonian liquid which contains about 90% of water therefore its density and viscosity are like water [1]. The blood is non-Newtonian suspension. This is because it can form rouleaux at a low shear rate, causing a significant increase in yield stress and viscosity [2,3]. With increasing shear rate, the erythrocyte rouleaux become progressively disassociated. The term 'rouleaux' (singular: rouleau) indicates clotting or aggregation of RBC [4].

Blood rheology is one of the most neglected areas in the clinical literature and diagnosis. Experiments on blood rheology still pose a significant challenge and require special preparations, including protection against blood clotting. Several rheological models are available to consider human blood flow, e.g. Bingham, Ostwald-de Waele, Carreau, Casson or Herschel-Bulkley. The Bingham model is too simple because it includes constant viscosity. Two- and three-parameter models, such as the Casson or Herschel-Bulkley models, describe the dependence of shear stress on the shear rate with greater precision. Comprehensive measurements of blood rheology were performed by Wells and Merrill [5]. The authors used radially symmetric coaxial cylinders (Couette) and made measurements of shear stress versus shear rate in the range of shear rate of 10 to 125 s^{-1} [5]. The yield stress was determined, although the estimation of the yield shear stress is a complex issue [6].

Despite recent achievements in blood rheology [7], the effect of non-Newtonian blood viscosity and yield shear stress on the hydrodynamics of blood flow is not yet well understood. The purpose of this study is to experimentally determine the dependence of the shear stress on the shear rate at low and moderate haematocrit in human blood. Based on the measurements, blood viscosity was determined, yield stress was estimated and compared with data from the literature and a suitable rheological model was proposed and discussed.

2. Experiments and Results

The recommendation of Baskurt et al. [8] indicates that a human blood viscosity rheometer should operate in a wide range of shear rate from 1 s^{-1} to at least 200 s^{-1}, with an upper range of 300–400 s^{-1}, so that blood reaches its steady apparent viscosity. For routine clinical investigations, two measurements of the apparent viscosity of the sample are recommended [8].

Using Anton Paar equipment [9] which includes coaxial cylinder and rotor, shear stress versus shear rate measurements were performed for three values of haematocrit. The shear rate changed from 1 s^{-1} to 200 s^{-1} for three blood samples with haematocrit between 22% and 40% by volume. On the base of the shear stress measurements, the blood apparent viscosity was determined for three blood samples demonstrating substantial dependence on Haematocrit. Research has clearly shown that blood is a shear-thinning suspension with yield stress, which depends on haematocrit, which determines concentration of RBC.

The results of the measurements are presented as graphs. Based on the measurements, a suitable rheological model is proposed. For all haematocrit values, the yield shear stress was estimated and the results demonstrating compliance with the data in the literature. The results of the experiments are summarised and the conclusions drowned in, and further research was indicated.

Acknowledgements

The research was carried out based on Agreement No. UH/2022/03/0022 between Kielce University of Technology and Jan Kochanowski University of Kielce signed by Rectors on March 8, 2022.

References

[1] Alexander D.E., *Nature's Machines. An Introduction to organismal biomechanics*, Academic Press, Elsevier, London 2017, p. 425.

[2] Abbasi M., Farutin A., Ez-Zahraouy H., Benyoussef A., Misbah C., *Erythrocyte – erythrocyte aggregation dynamics under shear flow*, 'Physical Review Fluids' 2021, vol. 6.

[3] Wu Y., Hsu P., Tsai C., Pan P., Chen Y., *Significantly increased low shear rate viscosity, blood elastic modulus, and RBC aggregation in adults following cardiac surgery*, 'Scientific Reports' 2018, vol. 8, pp. 1–10.

[4] Lee C.A., Paeng D.G., *Numerical simulation of spatiotemporal red blood cel aggregation under sinusoidal pulsatile flow*, 'Scientific Reports' 2021, vol. 11.

[5] Wells R.E., Merrill E., *Influence of flow properties of blood upon viscosity – Hematocrit relationship*, 'The Journal of Clinical Investigation' 1962, vol. 41, no. 8, pp. 1591–1598.

[6] Beris A., Horner J., Jariwala S., Armstrong M., Wagner N., *Recent advances in blood rheology: A review*, 'Soft Matter' 2021, vol. 47, pp. 1–23.

[7] Esmaeel F., Naser K., Hossein F., *A review on rheology of non-Newtonian properties of blood*, 'IIUM Engineering Journal' 2018, vol. 19, no. 1, pp. 237–250.

[8] Baskurt O.K., Boynard M., Cokelet G.C., Connes P., Cooke B.M., Forconi S., Liao F., Hardeman M.R., Jung F., Meiselman H.J., Nash G., Nemeth N., Neu B., Sandhagen B., Shin S., Thurston G., Wautier J.L, *New guidelines for hemorheological laboratory techniques*, 'Clinical Hemorheology and Microcirculation' 2009, vol. 42, no. 2, pp. 75–97.

SHOALING OF GRAVITY-CAPILLARY WAVES

S. Biegowski, M. Paprota*

Institute of Hydro-Engineering, Polish Academy of Sciences, 7 Kościerska St., 80–328 Gdańsk, Poland

*E-mail: mapap@ibwpan.gda.pl

Abstract. We consider the problem of linear gravity-capillary wave shoaling. We provide basic formulas for the shoaling coefficient derived under potential flow assumptions. The diagrammed results give an insight into the effect of surface tension on wave amplitude growth for a range of deepwater wavelengths. In general, capillary forces work against gravity and contribute to reduction of height of waves propagating towards the shore.

Keywords: Hydromechanics, Water Waves, Surface Tension, Wave Shoaling.

1. Introduction

When surface gravity waves approach the shore, they become more steep in shallower waters. An increase in height H of shoaling waves is accompanied with a decrease in wavelength L. In the absence of wave energy dissipation and reflection, the rate of energy transmission (flux) along the direction of wave propagation as well as wave frequency ω remain constant [1]. This allows for expressing the change in height of water waves climbing up a slope in a form of a shoaling diagram which presents the dependence of a shoaling coefficient C_S as a function of reference deepwater wave number ($k_0 = 2\pi/L_0$) multiplied by a local water depth d. For linear waves, this dependence was first reported in the work of Green [2] and is thus called the Green's law. For steeper waves, a useful information on nonlinear shoaling was provided by Rienecker and Fenton [3], who developed a Fourier Approximation Method and used it to calculate C_S for a range of increasing wave heights. It was noticed that for higher initial waves, an increasing steepness results in faster wave growth.

Till now, a reasonable assumption of neglecting surface tension in the shoaling problem was made. This is because the length of waves shoaling at typical natural slopes counts in meters, while gravity and capillary dispersive effects become comparable for wavelengths of the order of centimetres. Since experimental studies on marine hydrodynamics involve decreasing the size of waves to lengths corresponding to the size of laboratory tanks, in some parts of laboratory testing, this may require including capillary forces in the analysis. In this work, we provide some useful information on properties of shoaling within the framework of linear wave theory when the surface tension is taken into account.

2. Shoaling diagram

We consider small-amplitude regular gravity-capillary waves propagating in water of slowly decreasing depth. The linear dispersion relation is [4]
while the total energy is proportional to the square of wave height [5]

$$\omega^2 = \left(gk + \frac{\gamma}{\rho}k^3\right)\tanh(kd) \tag{1}$$

In (1) and (2), g is gravitational acceleration, γ denotes surface tension, and ρ is water density.

$$E = \frac{1}{8}H^2(\rho g + \gamma k^2) \tag{2}$$

By differentiating (1) with respect to k, we get a following formula for group velocity

$$c_g = \frac{1}{2\omega}\left[\left(g + 3\frac{\gamma}{\rho}k^2\right)\tanh(kd) + \left(gk + \frac{\gamma}{\rho}k^3\right) d\,\mathrm{sech}^2(kd)\right] \tag{3}$$

Energy flux remains constant at any distance from deep water to the shore $c_{g0}E_0 = c_g E$, so

$$C_S = \frac{H}{H_0} = \left(\frac{c_{g0}(\rho g + \gamma k_0^2)}{c_g(\rho g + \gamma k^2)}\right)^{\frac{1}{2}} \tag{4}$$

In Fig. 1, we present calculations of the shoaling coefficient C_S using formulas (3) and (4) as a function of a relative local depth $k_0 d$.

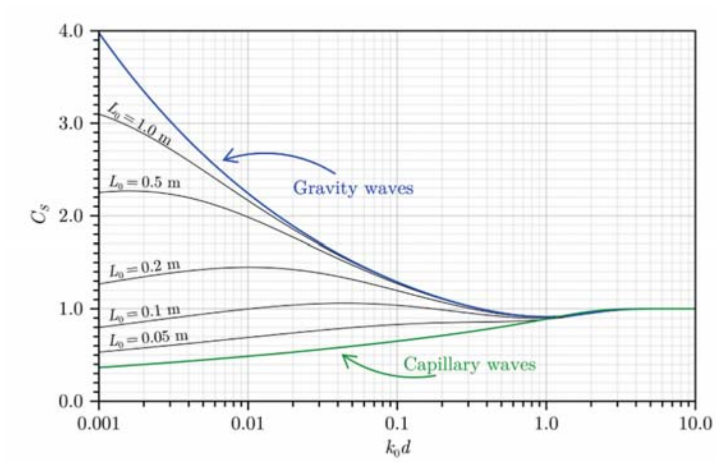

Figure 1. Shoaling diagram for linear gravity-capillary waves (γ = 0.074 N/m)

3. Conclusions

For incident deepwater waves of one meter length, the effect of surface tension is generally weak becoming noticeable at depths as low as one centimetre. Though, it eventually may affect experiments at smaller scales, where capillary forces work against gravity decreasing the heights of waves travelling towards shore. The presented analysis neglects higher-order effects, which generally contribute to faster wave growth. The ongoing research extends the study to nonlinear gravity-capillary wave shoaling to get more exact results for higher waves.

References

[1] Eagelson P.S., *Properties of shoaling waves by theory and experiment*, 'Transactions, American Geophysical Union' 1956, vol. 37, no. 5, pp. 565–572.

[1] Green G., *On the motion of waves in a variable canal of small depth and width*, 'Transactions of the Cambridge Philosophical Society' 1838, vol. 6, pp. 457–462.

[2] Rienecker M.M., Fenton J.D., *A Fourier approximation method for steady water waves*, 'Journal of Fluid Mechanics' 1981, vol. 104, pp. 119–137.

[3] Dean R.G., Dalrymple R.A., *Advanced Series on Ocean Engineering – Volume 2. Water Wave Mechanics for Engineers and Scientists*, Liu PL-F (ed.), World Scientific, Singapore–New Jersey–London–Hong Kong 1991.

[4] Lamb H., *Hydrodynamics*, Dover Publications, New York 1932.

DYNAMICS OF EMULSION DROPLET TRANSPORT IN CROSS-CAPILLARY MICROSTRUCTURES

M. Błaszczyk

Lodz University of Technology, Faculty of Process and Environmental Engineering, Wolczanska 213 Str., 93–005 Lodz, Poland

E-mail: mariola.blaszczyk@p.lodz.pl

Abstract. The transport of oil droplets in an oil-water system in cross-junction capillary microstructures of various diameters was investigated. Generation and flow parameters were analyzed, including formation time, number of droplets, velocity, shape and the effect of surfactant. The dependence of velocity on the length of the droplet ellipse and its position in the channel was demonstrated, and the addition of surfactant increased the frequency of generation.

Keywords: Micro-, Nano- and Bio-flows, Experimental Fluid Mechanics, Droplet Microfluidics, Cross-junction, Emulsion transport, Surfactant.

1. Introduction

Two-phase microflows are a key area in microfluidics, enabling precise droplet generation and transport in channels of tens to hundreds of micrometers. Stable, repeatable droplet production is essential for applications such as emulsion preparation, microreactors and accurate dosing [1]. Droplet size, formation frequency and motion dynamics directly affect process outcomes and dispersion uniformity.

Cross-junction geometries are widely used due to their simplicity and reliable droplet generation. Droplet breakup results from competition between shear/viscous forces (promoting detachment) and interfacial tension (resisting deformation). Flow conditions and channel geometry therefore determine the formation regime, droplet shape and subsequent transport [2,3].

Surfactants significantly modify the process by reducing interfacial tension and enhancing emulsion stability, influencing droplet formation rate, deformation and flow resistance in the channel [4]. Understanding surfactant effects is critical for designing stable, controlled multiphase microfluidic systems.

This study examined droplet generation and transport in oil-water systems within cross-capillary structures with hydraulic diameters of 75, 100 and 200 μm. The effects of continuous-to-dispersed phase flow rate ratio and surfactant addition were analyzed, focusing on droplet formation time, generation frequency, velocity and deformation degree. The findings provide guidance for optimizing geometry and operating conditions in microfluidic systems for controlled emulsion production.

2. Experimental setup and methods

The experimental setup (Fig. 1a) consisted of syringe pumps for flow rate control, a cross-shaped capillary junction with channel diameters of 75, 100 and 200 μm, and a vision system (digital microscope and camera) to record droplet motion. Cross-junction configurations with various oil and water phase inlets were tested (Fig. 1b). Water (with or without surfactant) served as the continuous phase and naphtha as the dispersed phase. Video sequences were analyzed to determine droplet formation time, number, velocity (from center displacement over time) and geometry (approximated as an ellipse) during transport, as well as key generation parameters: T_k – time between successive droplets, T_p – time for a droplet to pass through a channel section, and T_c – time of elongation of the 'front' of the liquid until the droplet detaches.

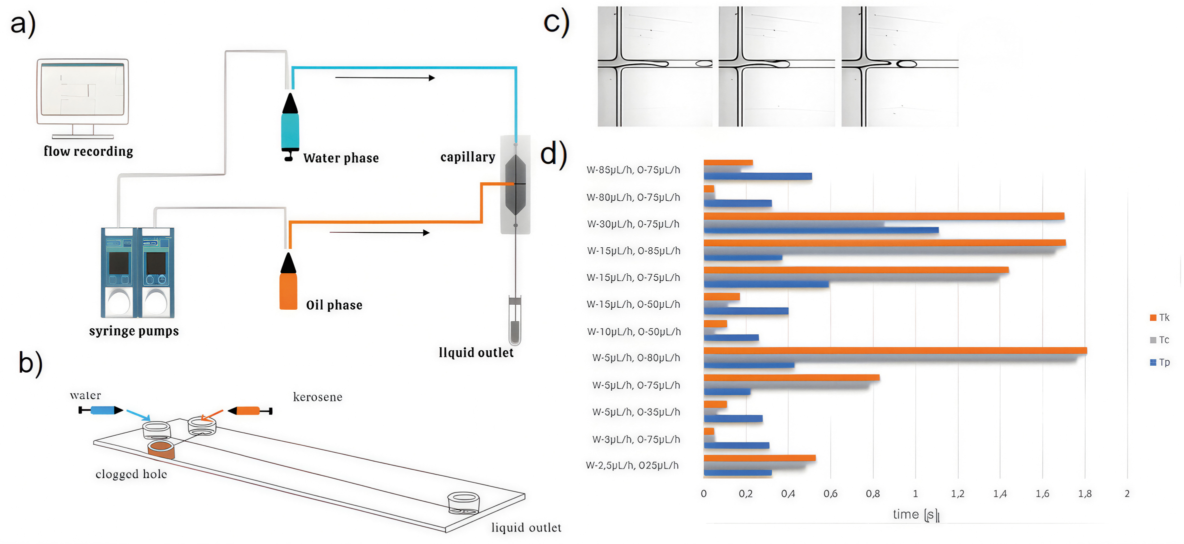

Figure 1. Generation of droplets in a capillary system: a) diagram of the test setup, b) the idea of liquid flow into a cross-shaped capillary, c) drop formation in a cross-shaped capillary, d) changes in drop formation parameters (T_k, T_c, T_p) at different water (W)/oil (O) flow rates for a capillary with a diameter of 75 μm

3. Results and discussion

Droplet generation parameters depended on microchannel geometry and flow conditions. Stable droplet formation occurred for the tested capillary diameters, with flow rates influencing generation time and droplet frequency. Adding surfactant reduced generation time and improved emulsion repeatability. Hydrodynamic conditions affected both droplet detachment at the junction and their subsequent transport. Droplet velocity and deformation varied with flow rate, channel diameter and position in the cross-section, highlighting the role of local flow effects and resistance.

4. Conclusions

The results demonstrate that flow rates and microstructure diameter can be adjusted to control generation time, droplet frequency and transport stability. These findings provide a foundation for optimizing microfluidic systems aimed at producing repeatable oil-water emulsions with predictable droplet properties.

References

[1] Cai Y., Sun R., Ren Y., Gou Y., *Development of droplet-based microfluidics in generation, manipulation and biomedical application*, 'Microchemical Journal' 2025, vol. 211.

[2] Li Z.., Li X., Zhu Y., Zhang J., Wang J., Jia H., Gao K., Li Q., Li J., *Recent advances in droplet microfluidic technology and its applications in food*, 'Trends in Food Science & Technology' 2025, vol. 163.

[3] Guo S., Zhao X., Xu B., Chen Z., Wang X., *Recent progress in droplet dynamics on advanced micro/nano-structured surfaces: Theory, experiments and applications*, 'Desalination' 2026, vol. 617.

[4] Zhou J., Guo X., Liu R., *Innovative applications and challenges of droplet microfluidic technology in energetic materials*, 'Chemical Engineering Science' 2026, vol. 321.

GLOBAL STABILITY ANALYSIS OF MULTI-STEP TIME-INTEGRATION METHODS APPLIED TO THE FOURIER-DISCRETISED LINEAR CONVECTION-DIFFUSION EQUATION

A. Bogusławski[1] , A. Tyliszczak[1], B.J. Geurts[2]

[1] *Częstochowa University of Technology, Department of Thermal Machinery, Al. Armii Krajowej 21, 42 - 2001 Częstochowa, Poland*

[2] *University of Twente, Mathematics of Multiscale Modeling and Simulation, Faculty EEMCS, P.O. Box 217, Enschede, The Netherlands*

E-mail: andrzej.boguslawski@pcz.pl

Abstract. Global Stability Analysis (GSA) of multi-step integration methods is performed for spectrally discretized convection-diffusion dynamics. Stability conditions are obtained and further quantified concerning the presence of physical and spurious modes. The Adams-Bashforth and Adams-Moulton methods provide specific examples for which GSA yields explicit conditions on the Peclet and CFL numbers that need to be respected to achieve simulations free of spurious modes. Stability is investigated for start-up as well as asymptotic simulation conditions.

Keywords: Computational Fluid Dynamics, Global Stability Analysis, Fourier spectral discretization, multistep methods.

1. Introduction

The global spectral analysis (GSA) of numerical methods developed by Sengupta [1] is a valuable tool to quantify a method's characteristics, such as stability, numerical phase speed, group velocity and numerical diffusion coefficient. An extensive study of a variety of spatial discretizations, e.g., finite and compact differences, combined with a one-time-level Runge-Kutta method for time integration, was conducted by Suman et al. [2,3]. For the development of higher-order accuracy while effectively keeping the number of evaluations of the spatial discretization low, multi-level methods offer clear prospects. Important examples include the Adams-Bashforth and Adams-Moulton integration methods. Spectral Fourier discretization is of special interest in turbulence simulations, where high resolution of the small scales is crucial to predict large-scale flow dynamics. However, it turns out that GSA for the Fourier spectral method combined with multi-step time integration approaches has not been developed yet. This is the focus of the current paper. In the performed analysis, we consider under what stability conditions multi-step methods may yield stable simulations without any spurious modes across the entire spectrum of resolved scales.

2. Sample GSA – results

The amplification factor characterizing the multi-step methods is described by two different components: the factor corresponding to the physical mode which for the time step tending to 0 approaches the exact solution, and the factor corresponding to the spurious mode that disappears at such limit conditions. For the time step greater than 0, the spurious mode contaminates the solution, especially in the range of the small scales. The calculations with multi-step methods must be initiated with the use of the one-step methods, such as a Runge-Kutta method. Hence, the amplification factor evolves through integration, approaching a certain converged state after several time steps. This converged state is crucial for the overall stability of the numerical scheme. Figure 1 shows the results for the converged total amplification factor for the second-order Adams-Bashforth method $|G_{tot}^{AB2}|$, with its physical and spurious modes, for Peclet number $Pe = \nu\Delta t/h^2 = 0.05$ (ν-diffusion coefficient, Δt – time step, h- mesh size). The red line denotes the converged stability border $|G_{tot}^{AB2}| = 1$, while the blue line is the same condition but established at the second time step with the first step integrated with the Runge -Kutta method of the 4th – order. The amplification factor is presented in the $N_c - kh$ plane ($N_c = c\Delta t/h - CFL$ number, c – convection velocity, k– wave number). It is seen that the solution within the stability region is dominated by the physical mode, however, a particular region of the small scales is contaminated by the spurious mode, indicated by the red arrow in Fig.1c. The detailed analysis performed for the explicit Adams-Bashforth and implicit Adams-Moulton methods shows that there is a critical Peclet number below which only the physical mode is present. Beyond this critical Pe, there is a range of Peclet numbers in which both physical and spurious modes are present, but spurious mode contamination can be eliminated for a sufficiently low CFL number. Finally, a second critical Peclet number can also be identified above which the spurious mode is always present and the numerical solution is of little value. The detailed analysis of the total stability plane will be presented during the XXVII FMC.

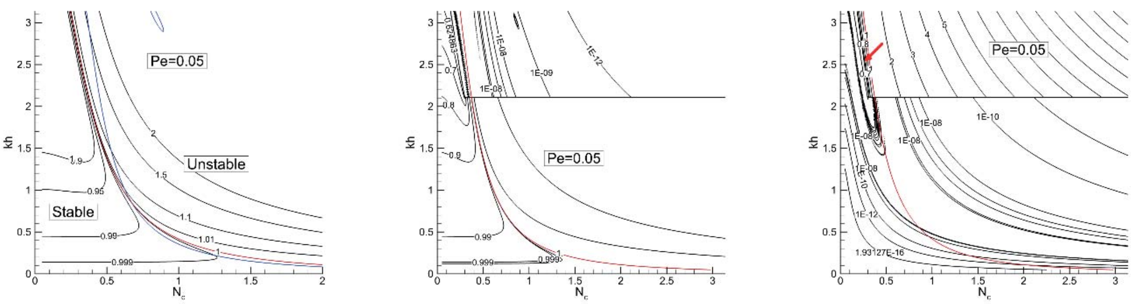

Figure 1. Isolines of asymptotically converged modes (a) the total amplification factor, and the amplification factors of the (b) physical mode, and the (c) spurious mode, at Pe=0.05

Acknowledgements

This research was funded by the National Science Centre, Poland, under project No. 2023/49/B/ST8/00773 and statutory research funds from the Częstochowa University of Technology (BS/PB 1-100-301/2025/P).

References

[1] Sengupta T.K., *High Accuracy Computing Methods: Fluid Flows and Wave Phenomena*, Cambridge University Press, New York 2013.

[2] Suman V.K., Sengupta T.K., Jyothi Durga Prasad C., Surya Mohan K., Sanwalia D., *Spectral analysis of finite difference schemes for convection diffusion equation*, 'Computers & Fluids' 2017, vol. 150, pp. 95–114.

[3] Sagaut P., Suman V.K., Sundaram P., Rajpoot M.K., Bhumkar Y.G., Sengupta S., Sengupta A., Sengupta T.K., *Global spectral analysis: Review of numerical methods*, 'Computers & Fluids' 2023, vol. 261, pp. 105915-87.

DATA-DRIVEN MODELING AND STATE ESTIMATION OF SLOSHING DYNAMICS FROM SPARSE MEASUREMENTS: AN EXPERIMENTAL AND NUMERICAL STUDY

K. Bukowski*, T. De Maria, S. Ahizi , M.A. Mendez

von Karman Institute for Fluid Dynamics, Department of Environmental and Applied Fluid Dynamics, Waterloosesteenweg 72, 1640 Sint-Genesius-Rode, Belgium

E-mail: karol.bukowski@vki.ac.be

Abstract. This work develops a data-driven methodology for real-time reconstruction of the sloshing state from sparse free-surface measurements. A reduced-order basis is obtained from Smoothed Particle Hydrodynamics (SPH) simulations using Proper Orthogonal Decomposition (POD). Optimal sensor locations are identified and sparse experimental elevation-gauge measurements are used to estimate the modal amplitudes, from which the full free surface is reconstructed. The methodology is validated against camera-based free-surface tracking, showing accurate reconstruction with only a limited number of sensors.

Keywords: Experimental Fluid Mechanics, Sloshing, SPH, POD, Free-surface Measurement, Sparse Sensor Placement, System identification, Data assimilation.

1. Introduction

Sloshing is the oscillatory motion of a liquid free surface in a partially filled container under external excitation. In many engineering systems, such as spacecraft fuel tanks, marine vessels and transport containers, sloshing generates large forces on tank walls and induces centre-of-mass displacements, affecting vehicle stability and structural integrity, especially when excitation triggers resonance. Sloshing mitigation strategies can be classified as passive or active. Passive control uses internal baffles to increase energy dissipation and modify the system's natural frequencies, whereas active control applies control actions through actuated baffles or controlled tank motion to counteract the sloshing response based on the estimated system state. In active control, performance strongly depends on reliable real-time state estimation used as input to the control law. This has been demonstrated for both model-based approaches by Konopka et al. [1] and machine-learning-based strategies by Ye et al. [2]. However, real-time free-surface measurements provide only sparse, localised data from elevation gauges and do not fully describe the free-surface state. This limitation motivates the development of methods that reconstruct the complete free surface from limited measurements in real time.

2. Methodology

The present work adopts the framework described by Manohar et al. [3] for reconstructing high-dimensional fields from sparse measurements using low-rank bases obtained from data-driven modal decomposition. The free-surface elevation field $\eta(\mathbf{x}, t)$ is represented using Proper Orthogonal Decomposition (POD), which separates spatial modes $\Phi(\mathbf{x})$ from their temporal coefficients $A(t)$:

$$\eta(\mathbf{x}, t) = \Phi(\mathbf{x})\, A(t)$$

By retaining only the first r dominant modes, a low-rank approximation of the field is obtained:

$$\eta(\mathbf{x}, t) \approx \Phi_{\mathrm{r}}(\mathbf{x})\, A_r(t)$$

This approximation captures the dominant sloshing dynamics while significantly reducing the system dimension. To identify a limited number of sensor locations such that the collected signals are maximally informative, QR factorisation with column pivoting is applied to the truncated spatial POD modes $\Phi_r(x)$. This procedure selects optimal sampling locations tailored to the considered sloshing conditions and the measurements are collected only at these locations. The temporal coefficients are then estimated from the sparse measurements using a least-squares projection onto the same modal basis. Finally, the full free-surface field is reconstructed in real time by combining the truncated spatial modes with their estimated temporal coefficients $\widehat{A}_r(t)$:

$$\eta(x,t) \approx \Phi_r(x)\,\widehat{A_r}(t)$$

This approach allows real-time reconstruction of the full free surface from a small number of sensors.

2.1. Numerical Simulations

Three-dimensional sloshing simulations are performed using the SPH solver DualSPHysics developed by Domínguez et al. [4]. The free surface is extracted from the simulations and used as training data which is decomposed using POD to obtain a reduced-order basis that captures the dominant dynamics.

2.2. Experimental Setup

A rectangular tank (30 × 45 × 50 cm) was mounted on the VKI Shakespeare 3-DOF sloshing table, with a max acceleration of 1g at 10 Hz. Sparse free-surface measurements are obtained using wave gauges placed at numerically identified optimal locations and are fed to model to reconstruct the free-surface. Simultaneously, the full free surface is captured by a high-speed camera and interface tracking. The accuracy of the reconstructed free surface is assessed by comparison with free-surface tracking results.

3. Expected outcome

For a rectangular tank, the sloshing motion can be described using only a few modes, allowing accurate reconstruction with a small number of sensors. When internal baffles are added, the flow becomes more complex, requiring more modes and sensors to keep accuracy. This work aims to evaluate reconstruction accuracy, identify the minimum number of sensors and study the advantage of optimal sensor placement. The results are expected to show that real-time, data-driven reconstruction of sloshing dynamics is possible for more complex geometries with internal baffles. The methodology will be integrated into the Reinforcement Twinning framework by Schena et al. [5] for control applications.

Acknowledgements

This project is supported by the European Research Council (ERC) under the Horizon Europe programme (Starting Grant No. 101165479, RE-TWIST).

References

[1] Konopka M., De Rose F., Strauch H., Jetzschmann C., Darkow N., Gerstmann J., *Active slosh control and damping – Simulation and experiment*, 'Acta Astronautica' 2019, vol. 158, no. 89.

[2] Ye M., Ren Y., Zhang S., Ma H., Hu X., Haidn O.J., *Sloshing suppression with a controlled elastic baffle via deep reinforcement learning and SPH simulation*, 'Fluid Dynamics' 2025.

[3] Manohar K., Brunton B.W., Kutz J.N., Brunton S.L., *Data-Driven Sparse Sensor Placement for Reconstruction: Demonstrating the Benefits of Exploiting Known Patterns*, 'IEEE Control Systems' 2018, vol. 38, no. 63.

[4] Domínguez J.M., Fourtakas G., Altomare C., Canelas R.B., Tafuni A., García-Feal O., Martínez I., Mokos A., Vacondio R., Crespo A.J.C., Rogers B.D., Stansby P.K., Gómez-Gesteira M., *State-of-the-art SPH solver DualSPHysics: from fluid dynamics to multiphysics problems*, 'Fluid Dynamics' 2021.

[5] Schena L., Marques P.A., Poletti R., Ahizi S., Van Den Berghe J., Mendez M.A., *Reinforcement Twinning: From digital twins to model-based reinforcement learning*, 'Journal of Computational Science' 2024, vol. 82.

LOW-FIDELITY GEOMETRIC SHAPE OPTIMIZATION OF A COUNTER-ROTATING OPEN ROTOR

C. Burns, M. Kulak, K. Sobczak

Lodz University of Technology, Institute of Turbomachinery, 217/221 Wolczanska St., 93–005 Lodz, Poland

E-mail: craig.burns@dokt.p.lodz.pl

Abstract. A low-fidelity framework for geometric shape optimization of counter-rotating open rotors is presented. Chord and twist of the upstream and downstream rotors are treated as separate variables in a sequentially coupled optimization, with the downstream rotor influenced by the upstream rotor. Results show increased total rotor efficiency across design points, with strict minimum thrust constraints. Further work will include conducting CFD simulations of baseline and optimized geometries.

Keywords: Aerodynamics, Geometric Shape Optimization, Counter-rotating Open Rotor (CROR).

1. Introduction

Counter-Rotating Open Rotors (CRORs) are increasingly used in UAVs to enhance thrust while maintaining vehicle footprint. Optimizing CRORs is crucial for maximizing endurance and range, but remains challenging as the downstream rotor operates in the unsteady wake of the upstream rotor. Low-fidelity methods, such as Blade Element Momentum Theory (BEMT), provide reasonable aerodynamic results despite neglecting 3D flow effects, enabling rapid exploration of preliminary design spaces [1]. This work presents a BEMT coupled geometric optimization of the upstream (R1) and downstream (R2) rotors using simplified wake modeling.

2. Methodology and Results

T-Motor G28 × 9.2″ propellers using Archer A18 airfoils (Figure 1) were modeled in pyBEMT with Prandtl tip-loss corrections [2]. Airfoil characteristics at each radial position were obtained for each iteration via cubic spline interpolation of XFOIL-generated polar tables. R2 inflow velocity was modeled based on momentum theory, assuming a fully developed slipstream.

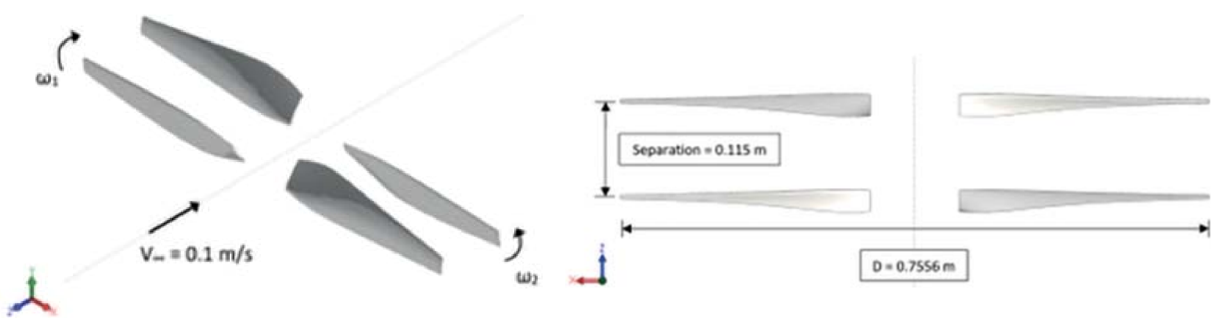

Figure 1. T-Motor G28 CROR 3D model

Multi-point optimization was performed at three points covering the full operational range using Differential Evolution with Latin Hypercube sampling in the SciPy library, followed by L-BFGS-B refinement [3]. Chord and twist distributions were parameterized using quadratic Bézier curves with monotonicity constraints to ensure realistic geometry. R1 was first evaluated at each iteration, followed by R2 using inflow conditions calculated from R1 values, enabling sequentially coupled optimization. The objective function was maximum total rotor efficiency, subject to a minimum thrust equal to baseline configuration across the full operational range.

BEMT simulations were validated against experimental data at hover [2]. Predicted thrust reflected experimental trends across the full operational range (Figure 2). Efficiency deviations were largest for R2 which is consistent with limitations of the simplified wake model used, as reported by Giljarhus et al. [2]. BEMT results indicate that the optimization procedure improved total rotor efficiency by 2.3% averaged across design points, with gains maintained across the full operating range. Thrust for each rotor remained similar to the baseline, with R2 showing the largest efficiency improvement.

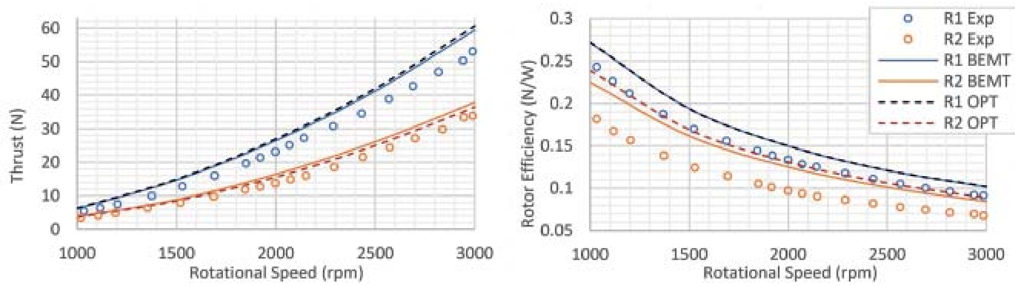

Figure 2. Thrust and efficiency of baseline and optimized rotors with experimental data

Optimized parameters are distinct between rotors (Figure 3), with R2 exhibiting increased twist and smaller, less tapered chord lengths in response to higher inflow velocity. These results highlight the importance of coupled CROR optimization with independent parameters. Future work will incorporate CFD simulations to more accurately assess efficiency gains, which BEMT likely underestimates, and to further develop the optimization procedure.

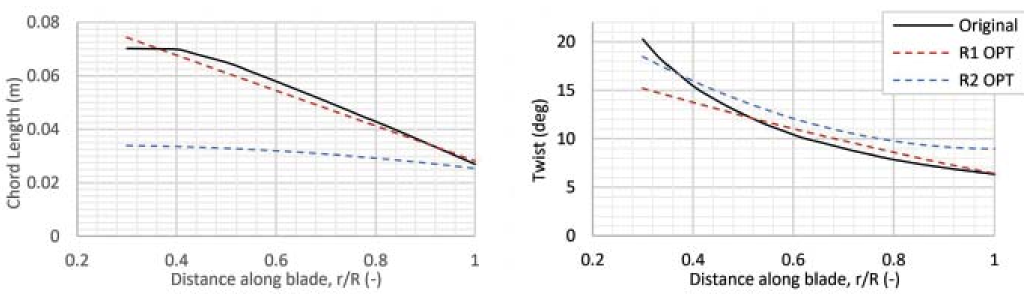

Figure 3. Chord and twist distributions of baseline and optimized rotors

References

[1] Syal M., Leishman J.G., *Aerodynamic optimization study of a coaxial rotor in hovering flight*, 'Journal of the American Helicopter Society', vol. 57, no. 4, pp. 1–15.

[2] Giljarhus K.E.T., Porcarelli A., Apeland J., 2022 *Investigation of rotor efficiency with varying rotor pitch angle for a coaxial drone*, 'Drones' 2012, vol. 6, no. 4.

[3] Virtanen P., Gommers R., Oliphant T.E., Haberland M., Reddy T., Cournapeau D., Burovski E., Peterson P., Weckesser W., Bright J., van der Walt S.J., Brett M., Wilson J., Millman K.J, Mayorov N., Nelson A.R.J., Jones E., Kern R., Larson E., Carey C.J., Polat İ., Feng Y., Moore E.W., VanderPlas J., Laxalde D., Perktold J., Cimrman R., Henriksen I, Quintero E.A., Harris Ch.R., Archibald A.M., Ribeiro A.H., Pedregosa F., van Mulbregt P., *SciPy 1.0: Fundamental algorithms for scientific computing in Python*, 'Nature Methods' 2020, vol. 17, pp. 261–272.

FROM PASSIVE TO ACTIVE CONTROL OF FLAME DYNAMICS USING BLUFF BODY STABILIZATION AND OXIDIZER FLOW EXCITATION

L. Caban, A. Wawrzak, A. Tyliszczak

Department of Thermal Machinery, Czestochowa University of Technology, al. Armii Krajowej 21, 42–201 Czestochowa, Poland

E-mail: lena.caban@pcz.pl

Abstract. The research focuses on the dynamics and stability of a nitrogen-diluted hydrogen flame formed behind cylindrical and star-shaped bluff bodies under the influence of oxidizer mass flow excitation. Large-eddy simulation results indicate that the combined impact of the star-shaped bluff body and excitation disrupts large-scale toroidal vortices, enhances small-scale mixing and lowers the mean flame temperature without increasing fuel consumption, suggesting reduced thermal NOx formation.

Keywords: Computational Fluid Dynamics, Passive and active flow control, Turbulent hydrogen flames.

1. Introduction

Flame control strategies can be broadly divided into passive and active approaches. Passive methods typically involve geometric modifications of the injection system to stabilize the flame by altering the flow field. They offer simplicity and require no external energy input, but lack adaptability to changing flow conditions. Active methods, such as flow excitation, allow for dynamic adjustment of control parameters, including excitation frequency and amplitude, enabling real-time response to variations in the flow. Their combination is therefore expected to increase control efficiency over a wide range of flow regimes. Recently, Wawrzak et al. [1] demonstrated that bluff body shape significantly affects the dynamics and stability of the hydrogen flame. In particular, a star-shaped bluff body was shown to reduce flame temperature without adversely affecting the fuel consumption rate. Furthermore, Kypraiou et al. [2] showed that combining bluff body stabilization with velocity excitation strongly influences flame stability and blow-off mechanism in methane flames. In this study, we perform large-eddy simulations of a nitrogen-diluted hydrogen flame stabilized by a star-shaped bluff body under oxidizer flow excitation and compare the results with those from a conventional cylindrical configuration.

2. Computational configuration and research strategy

Figure 1 illustrates the injection system with a bluff body placed inside the oxidizer duct. Two bluff body geometries are analysed: a cylindrical (C) and a star-shaped (S) configuration, both defined by the same equivalent diameter (D_b). The C configuration corresponds to the experimental setup reported in [2]. In this study, the fuel is a hydrogen-nitrogen mixture ($Y_{H2} = 0.11$, $Y_{N2} = 0.89$) supplied through a central pipe to the combustion chamber, while an excited air stream flows around the bluff body. The simulations employ a two-stage strategy with the computational domain divided into two parts (Fig. 1). In the first stage, ANSYS Fluent is used to simulate the flow around the bluff body, generating time-varying velocity profiles at the oxidizer channel exit. These profiles are then imposed as inlet boundary conditions for the main domain in the second stage, where an in-house high-order SAILOR code [3] is employed.

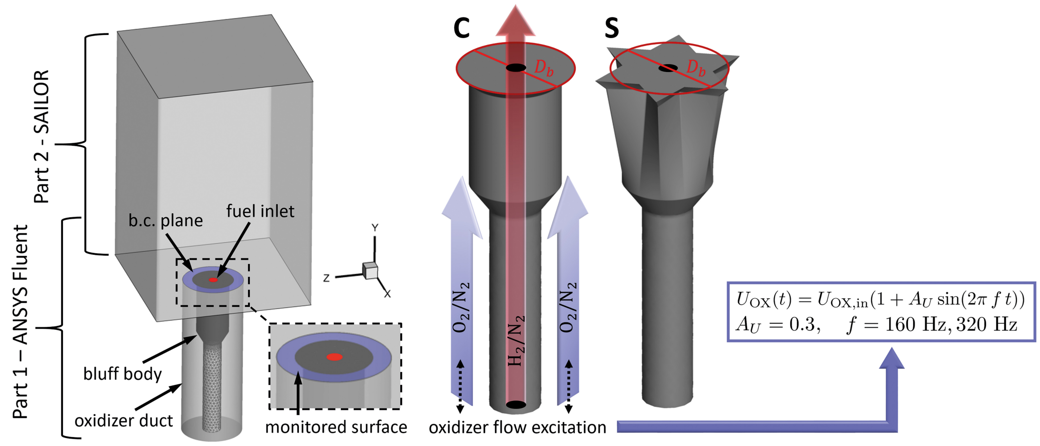

Figure 1. Computational configuration and bluff body geometries: cylindrical (C) and star-shaped (S)

3. Results and main conclusions

Figure 2a shows the contours of the mean temperature and its fluctuations for both the C and S configurations in the case without excitation. Figure 2b presents radial temperature profiles at $y/D_b = 0.5, 1.0$ for different excitation frequencies. The results demonstrate a strong dependence of temperature on the shape of the bluff body and on the oxidizer excitation. The latter results in a significant reduction in temperature, particularly in the recirculation zone above the bluff body and in the fuel-oxidizer mixing zone. This decrease is associated with mixture leaning caused by enhanced mixing and becomes more pronounced at higher excitation frequencies.

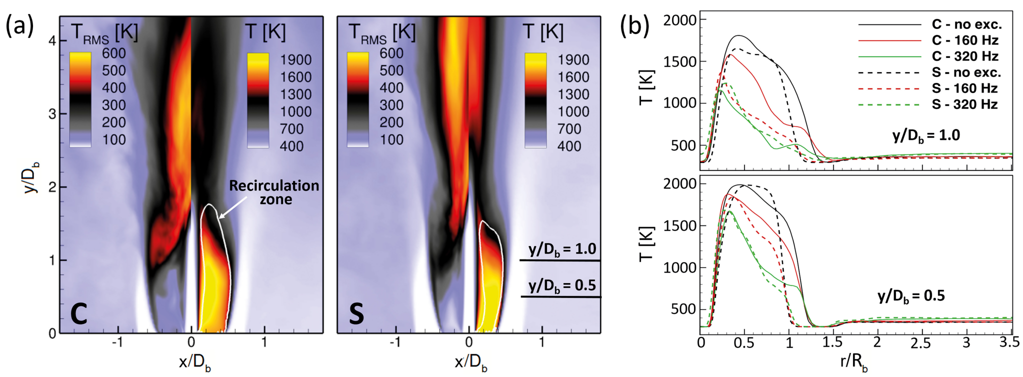

Figure 2. Contours of the mean temperature and its fluctuations for C and S configurations without excitation (a). Radial temperature profiles at $y/D_b = 0.5, 1.0$ for different excitation frequencies (b)

References

[1] Wawrzak A., Caban L., Tyliszczak A., Mastorakos E., *Numerical analysis of turbulent nitrogen-diluted hydrogen flames stabilised by star-shaped bluff bodies*, 'Applied Energy' 2024, vol. 364.

[2] Kypraiou A., Giusti A., Allison P.M. and Mastorakos E., *Dynamics of acoustically forced non-premixed flames close to blow-off*, 'Experimental Thermal and Fluid Science' 2018, vol. 95, pp. 81–87.

[3] Tyliszczak A., *A high-order compact difference algorithm for half-staggered grids for laminar and turbulent incompressible flows*, 'Journal of Computational Physics' 2014, vol. 276, pp. 438–467.

MANY-BODY DISSIPATIVE PARTICLE DYNAMICS OF MICRO AND NANO SCALE FLOWS

L.H. Carnevale[1], K.L. Ng[1], P. Deuar[1], Z. Che[2], M. Klamka[3], T. Bobiński[3], P.E. Theodorakis[1]

[1] *Institute of Physics, Polish Academy of Sciences, Al. Lotników 32/46, 02–668 Warsaw, Poland*

[2] *State Key Laborabory of engines, Tianjin University, 300350 Tianjin, China*

[3] *Institute of Aeronautics and Applied Mechanics, Warsaw University of Technology, Nowowiejska 24, 00–665 Warsaw, Poland*

E-mail: panos@ifpan.edu.pl

Abstract. Many-body dissipative particle dynamics (MDPD) is a suitable particle-based method for investigating with molecular (coarse-grained) resolution various phenomena in soft matter and fluids physics. Here, MDPD was employed to investigate the break-up of liquid threads into droplets as a result of the Plateau–Rayleigh instability and droplet break-up as a result of oscillations due to horizontal vibrations of a substrate. In the first case, the role of fluctuations and surfactants is highlighted, while, in the second case, different break-up phases have been identified and the development of instabilities, and various characteristics are discussed. Moreover, our ongoing work in the Group of Soft Matter and Fluids Physics at the Institute of Physics aims at expanding the MDPD-MARTINI force-field by providing parameters for a wider variety of components following the MARTINI mapping for molecular dynamics. MDPD-Martini is about an order of magnitude faster than MD MARTINI simulations and can also offer better results for certain system properties (e.g. surface tension).

Keywords: Micro-, Nano- and Bio-flows, Many-Body Dissipative Particle Dynamics, Droplet Break-up, Droplet Oscillations, MDPD-MARTINI Force-Field.

1. Introduction

Many-body dissipative particle dynamics (MDPD) is a particle-based method which can be employed for simulating with molecular resolution various multiphase systems, such as fluids [1–6], for example, those having a liquid–air surface in phenomena such as droplet break-up [7,8] or droplet oscillations on vibrating substrates [9,10]. Moreover, MDPD can be used for studying multicomponent systems, for example, fluids laden with surfactant [8]. In such cases, the method offers advantages, such as the possibility of investigating larger systems for longer times which could be prohibitive with molecular dynamics (MD) simulation, even when coarse-grained (CG) models are employed [11]. Hence, developing MDPD CG models that could perform similarly to MD CG models is highly desirable. In this regard, the Group of Soft Matter and Fluids Physics at the Institute of Physics has made steps towards the development of a general purpose MDPD CG force-field (FF) based on the mapping of the MD CG MARTINI FF [11-13], its 'LEGO' approach and other suitable coarse-graining strategies for the parameterization of soft matter and fluids systems [14–16].

2. Presentation content and key results

The presentation will focus on two fluid dynamics phenomena investigated with MDPD. The first refers to the study of the Plateau–Rayleigh instability in liquid threads, where a power law describing the number of satellite droplets as a function of the Ohnesorge and Thermal Capillary numbers has been discovered [7]. The investigation is expanded into systems with sodium dodecyl sulfate (SDS) surfactant, where the role of the latter in the break-up process, both mechanisms and dynamics, is unveiled for surfactant concentration below and above the critical aggregation concentration [8]. In the next part of the presentation, we will focus on a recent study on droplet oscillations caused by a horizontally vibrating substrate [9,10]. In this case, we have identified three different scenarios (phases I, II and III), with phase II and III leading to the droplet break-up. The boundaries between the different phases have been found based on the Capillary and Ohnesorge numbers. Moreover, phase II is particularly interesting, as the growth of instability towards droplet break-up can be characterized by suitable parameters. Finally, the state of the droplet during oscillations has been characterized by measures, such as the number of particle contacts which can reflect the 'energy' of the system in MDPD simulations.

Finally, we will present the current status and examples related to the ongoing development of the MDPD-MARTINI FF [14–16] and future steps in this direction, such as adding more MARTINI beads and integrating methods developed in the frame of previous work, such as the GōMARTINI approach for proteins. The computational efficiency of the MDPD-MARTINI, the inclusion of hydrodynamic interactions, etc., may shift the paradigm from MD to MDPD for simulating for multicomponent soft matter and fluids systems.

Acknowledgements

This research has been supported by the National Science Centre, Poland, under Grant No. 2019/34/E/ST3/00232. We gratefully acknowledge the Polish high-performance computing infrastructure PLGrid (HPC Center: ACK Cyfronet AGH) for providing computer facilities and support within computational Grant No. PLG/2025/018743. T.B. and M.K. acknowledge the support from Warsaw University of Technology within the Excellence Initiative: Research University (IDUB) program.

References

[1] Pagonabarrage I., Frenkel D., *Dissipative particle dynamics for interacting systems*, 'The Journal of Chemical Physics' 2001, vol. 115, no. 11, pp. 5015–5026.

[2] Warren P.B., *Vapor-liquid coexistence in many-body dissipative particle dynamics*, 'Physical Review E' 2003, vol. 68.

[3] Zhao J., Chen S., Phan-Thien N., *Viscometric flow for a many-body dissipative particle dynamics (MDPD) fluid with Lees–Edwards boundary condition*, 'Molecular Simulation' 2017, vol. 44, no. 3.

[4] Zhao C., Zhao J., Si T., Chen S., *Influence of thermal fluctuations on nanoscale free-surface flows: A many-body dissipative particle dynamics study*, 'Physics of Fluids' 2021, vol. 33, no. 11.

[5] Zhao J., Chen S., Zhang K., and Liu Y., *A review of many-body dissipative particle dynamics (MDPD): Theoretical models and its applications*, 'Physics of Fluids' 2021, vol. 33, no. 11.

[6] Han Y., Jin J., Voth G.A., *Constructing many-body dissipative particle dynamics models of fluids from bottom-up coarse-graining*, 'Journal of Chemical Physics' 2021, vol. 154, no. 8.

[7] Carnevale L.H., Deuar P., Che Z., Theodorakis P.E., *Liquid thread breakup and the formation of satellite droplets*, 'Physics of Fluids' 2023, vol. 35, no. 7.

[8] Carnevale L.H., Deuar P., Che Z., Theodorakis P.E., *Surfactant-laden liquid thread breakup driven by thermal fluctuations*, 'Physics of Fluids' 2024, vol. 36, no. 3.

[9] Ng K.L., Carnevale L.H., Klamka M., Deuar P., Bobiński T., Theodorakis P.E., *Oscillations of a water droplet on a horizontally vibrating substrate*, 'Physics of Fluids' 2025, vol. 37, no. 1.

[10] Ng K.L., Carnevale L.H., Klamka M., Deuar P., Bobiński T., Theodorakis P.E., *Phase transitions of oscillating droplets on horizontally vibrating substrates*, 'Physics of Fluids' 2025, vol. 37, no. 10.

[11] Souza P.C.T., Alessandri R., Barnoud J., Thallmair S., Faustino I., Grünewald F., Patmanidis I., Abdizadeh H., Bruininks B.M.H, Wassenaar T.A., Kroon P.C., Melcr J., Nieto V., Corradi V., Khan H.M., Domański J., Javanainen M., Martinez-Seara H., Reuter N., Best R.B., Vattulainen I., Monticelli L., Periole X., Tieleman D.P., de Vries A.H., *Marrink S.J, Martini 3: A general purpose force field for coarse-grained molecular dynamics*, 'Nature Methods' 2021, vol. 18, no. 4, pp. 382–388.

[12] Marrink S.J., de Vries A.H., Mark A.E., *Coarse Grained Model for Semiquantitative Lipid Simulations*, 'The Journal of Physical Chemistry B' 2004, vol. 108, pp. 750–760.

[13] Marrink S.J., Risselada H.J., Yefimov S., Tieleman D.P., de Vries A.H., 'The Journal of Physical Chemistry B' 2007, vol. 111, pp. 7812–7824.

[14] Carnevale L.H.,Theodorakis P.E., *Many-body dissipative particle dynamics with the MARTINI "Lego" approach*, 'The European Physical Journal Plus' 2024, vol. 139.

[15] Kramarz N., Carnevale L.H., and Theodorakis P.E., *Many-body dissipative particle dynamics simulations of lipid bilayers with the MDPD-MARTINI force-field*, 'The European Physical Journal Plus' 2024, vol. 140.

[16] Carnevale L.H., Niechwiadowicz G., and Theodorakis P.E., *Coarse-Grained Model of the Sodium Dodecyl Sulfate Anionic Surfactant Based on the MDPD–Martini Force Field*, 'Langmuir' 2026 (in print).

[17] Poma A.B., Cieplak M., Theodorakis P.E., *Combining the MARTINI and Structure-Based Coarse-Grained Approaches for the Molecular Dynamics Studies of Conformational Transitions in Proteins*, 'Journal of Chemical Theory and Computation' 2017, vol. 13, no. 3, pp. 1366–1374.

DESIGN OF A NITROUS OXIDE FILLING SYSTEM FOR SOUNDING ROCKET PROPELLANT TANKS

Ł. Ciorga, T. Banaszkiewicz

Wroclaw University of Science and Technology, 27 Wybrzeże Stanisława Wyspiańskiego st. 50–370 Wrocław, Poland

E-mail: lukasz.ciorga@gmail.com, tomasz.banaszkiewicz@pwr.edu.pl

Abstract. This paper presents the design and validation of a remote liquid nitrous oxide filling system for the R7 Together sounding rocket. The system utilizes passive subcooling via a high-fin heat exchanger to ensure single-phase liquid flow without pumps. Analytical models verified thermal and hydraulic performance, confirming a flow rate of 0.1 kg/s. The system was successfully deployed during the EuRoC competition, meeting all ECSS safety standards.

Keywords: Experimental Fluid Mechanics, Multi-phase Flows, Measurement Techniques, Nitrous Oxide, Sounding Rocket, Subcooling.

1. Introduction

The rapid development of student-developed sounding rockets (SRAD) necessitates the transition from solid to liquid propulsion systems. This shift introduces significant challenges in Ground Support Equipment (GSE) design, particularly regarding the handling of nitrous oxide (N_2O). As a self-pressurizing oxidizer with a critical temperature of 309.5 K, N_2O is prone to phase transitions (flashing) within transfer lines, leading to two-phase flow instabilities and inefficient tank filling.

This work addresses the design and validation of a remote filling system for the *R7 Together* rocket. The primary objective was to achieve a high-density liquid oxidizer transfer driven solely by pressure differential, eliminating the need for complex cryogenic pumps while complying with ECSS safety standards.

2. System Architecture and Design

The designed system is a modular electro-pneumatic skid. The core innovation lies in the thermal management strategy. To prevent cavitation and ensure liquid ingestion into the flight tank, the oxidizer is subcooled below its saturation temperature.

The fluidic path incorporates a passive heat exchanger submerged in an ice-water bath. Analytical trade-off studies compared natural convection, forced convection and extended surface geometries. A high-fin copper tubing configuration was selected, offering a surface area ratio (AR) of approximately 14.7. This allowed for effective passive cooling without the reliability risks associated with active circulation pumps.

The system architecture also features a custom capacitive level sensor for real-time mass monitoring, based on the permittivity difference between liquid ($\varepsilon_r \approx 1.55$) and gaseous ($\varepsilon_r \approx 1.0$) nitrous oxide. The operational principle of the level sensor relies on the non-polar dielectric nature of nitrous oxide. The relationship between the fluid density p and relative permittivity ε_r was modeled using the Clausius-Mossotti equation:

$$\frac{\epsilon_r - 1}{\epsilon_r + 2} = \frac{N_A \alpha}{3M} \rho \tag{1}$$

This theoretical basis allowed for the conversion of measured capacitance directly into propellant mass, compensating for density variations caused by temperature fluctuations in the tank.

3. Mathematical Verification

Mathematical modelling was conducted to verify the system's hydraulic and thermal performance. The total pressure drop was calculated as the sum of hydrostatic lift, frictional losses (Darcy-Weisbach) and local component losses.

For the subcooling process, the required heat exchanger length (L) was determined using the Logarithmic Mean Temperature Difference (LMTD) method:

$$L = \frac{Q}{U_l \cdot \Delta T_{LMTD}} \tag{2}$$

Where Q represents the total heat load required to subcool 6 kg of oxidizer by 15 K, and U_l is the linear heat transfer coefficient accounting for the high-fin efficiency ($\eta_f \approx 0.87$). The calculations confirmed that a coil length of 3.4 m is sufficient to maintain the target outflow temperature of 278.15 K.

4. Results and Validation

The system underwent rigorous testing, culminating in a field deployment at the *European Rocketry Challenge (EuRoC)* in Portugal.

The analytical flow model predicted a pressure drop of 3.8 bar. This left sufficient differential pressure from the 50 bar supply tanks to maintain the target mass flow rate of 0.1 kg/s.

Field data confirmed the stability of the process. The passive subcooling successfully prevented line flashing, enabling the transfer of 6 kg of propellant in under 60 seconds. The capacitive sensor provide a measurable signal delta of approx. 56 pF, allowing for precise fill-level termination.

5. Conclusions

The developed filling system successfully bridges the gap between theoretical thermodynamics and practical field engineering. The use of high-fin passive subcooling proved to be a robust solution for managing nitrous oxide phase changes in a mobile, pump-less configuration. The successful operation at *EuRoC* validates the design as a reliable platform for future sounding rocket campaigns.

References

[1] ECSS Secretariat, *Space engineering: Liquid propulsion* (ECSS-E-ST-35-10C), https://everyspec.com/ESA/ECSS-E-ST-35-03C_48210/ (access: 2.04.2026).

[2] Lemmon E.W., Span R., *Short Fundamental Equations of State for 20 Industrial Fluids*, 'Journal of Chemical & Engineering Data' 2006, vol. 51, pp. 785–850.

[3] Sutton G.P., Biblarz O., *Rocket Propulsion Elements*, John Wiley & Sons, Hoboken 2017.

ACOUSTIC PROPERTIES OF SILENCERS WITH MICRO PERFORATED PANELS OF MULTIPLE PERFORATION SIZES IN AIRFLOW

M. Czarnecki, K. Wójciak, J. Kopania, P. Gaj

Institute of Power Engineering - National Research Institute, Mory 8, 01–330 Warsaw, Poland

E-mail: marcel.czarnecki@itc.edu.pl

Abstract. The main objective of this paper is to determine the aeroacoustic properties of prototype silencers with micro perforated panels of multiple perforation sizes and compare them to the properties of a reference silencer. The measurements have been carried out according to ISO 7235 standard. In terms of insertion loss, the silencers were proven more efficient than the reference one, although they exhibited a higher flow noise.

Keywords: Aerodynamics, Acoustics, Silencers, Insertion loss, Flow Noise.

1. Introduction

Micro perforated panels (MPPs) are a type of sound absorbers, originally introduced by Maa [1]. Typical MPP can be described as a thin metal sheet with evenly spaced perforations with a diameter smaller than 1 mm. Basic principles of MPP absorbers have been described in the impedance model proposed by Maa [1]. MPP's specific acoustic impedance (Z_{MPP}) is composed of a real part ($Z_{resistance}$) and an imaginary part ($Z_{reactance}$), as given by the equation:

$$Z_{MMP} = Z_{resistance} + Z_{reactance} = r + j\omega m \tag{1}$$

$$r = \frac{32\eta t}{\sigma\rho_0 c d^2}\left[\left(1+\frac{k^2}{32}\right)^{1/2} + \frac{\sqrt{2}}{32}k\frac{d}{t}\right] \tag{2}$$

$$\omega m = \frac{\omega t}{\sigma c}\left[1+\left(1+\frac{k^2}{2}\right)^{-1/2} + 0.85\frac{d}{t}\right] \tag{3}$$

where r and ωm are respectively the acoustic resistance and reactance of the perforations, η is the viscosity coefficient of the air, ρ_0 is the density of the air, c is the speed of sound in air, ω is the angular frequency, d is the orifice diameter, σ is the porosity, and t is the thickness of the panel [1]. The perforation constant k is defined as the ratio of the orifice diameter to the viscous boundary layer thickness of the air in the orifice, according to:

$$k = d\sqrt{\omega\rho_0/4\eta} \tag{4}$$

According to Wu [2], reducing the diameter of the perforations can result in a wider attenuation peak. Esraa et al. achieved better performance, compared to conventional MPPs, using MPP-based absorbers with irregular hole distribution and varying hole diameters [3].

The main objective of this paper is to determine the acoustic performance of silencers with micro perforated panels with multiple perforations diameters, when measured under airflow. Measurements of insertion loss and flow noise were in accordance with ISO7235 Standard [4].

2. Test objects

The test objects consisted of three circular silencers with micro perforated panels, each with perforations with a diameter of 1 mm, combined with perforations of diameters of 0.4, 0.6 and 5 mm respectively. A standard silencer with perforations of 5 mm diameter was used as a reference. All the silencers had an internal diameter of 200 mm and length of 900 mm.

3. Experiment

The measurements were carried out on a test rig consisting of a centrifugal fan, three absorption silencers, a sound source and an outlet located inside the reverberation chamber. The test stand has been constructed in accordance with ISO7235 Standard [4]. The reverberation chamber used for measurements has a volume of 237 m^3 and an area of 231.5 m^2 and consists of nonparallel reflecting walls. A schematic of the test rig is presented in Figure 1.

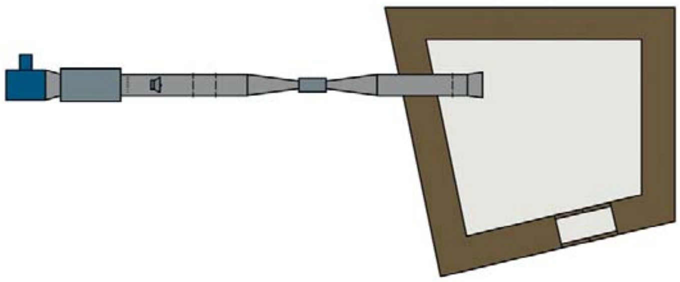

Figure 1. Test stand with reverberation room scheme

The tests involved measuring the sound pressure level with and without the pink noise source for flow velocities of 4, 8 and 12 m/s. The measurements were in accordance with the ISO3741 Standard [5], at 1/3 octave steps in 50–10,000 Hz frequency range.

4. Conclusions

All of the measured silencers yielded similar insertion loss results and proved to be more efficient than the reference 5 mm silencer, especially in low and high frequency ranges. The 1-0.4 mm silencer had slightly better insertion loss in the low frequency range, compared to the other silencers, whereas in higher frequency range, the 1–5 mm silencer had the biggest insertion loss.

The self noise of the tested silencers was higher than of the reference one under all the set air velocities, the difference being the most apparent in the low frequency range. Under the air velocities of 4 m/s and 12 m/s, the self-noise of the 1–0.4 mm silencer was the highest, with noticeable peaks at 200 Hz. Under the 8 m/s velocity, the self-noise of all three silencers were comparable.

References

[1] Maa D-Y., *Potential of microperforated panel absorber*, 'The Journal of the Acoustical Society of America', 1998, vol. 104, no. 5, pp. 2861–2866.

[2] Wu M., *Micro-perforated panels for duct silencing*, 'Noise Control Engineering Journal' 1997, vol. 45 no. 2, pp. 69.

[3] Esraa A-A., Putra A., Dan R.M, Mosa A.I. (2020). *Sound absorption coefficient of MPP with irregular holes distribution*, 'International Journal Of Advanced Research In Engineering & Technology', vol. 11, pp. 638–648.

[4] ISO 7235:2003. Acoustics – Laboratory measurement procedures for ducted silencers and air-terminal units – Insertion loss, flow noise and total pressure loss, 2003.

[5] ISO 3741:2010. Acoustics – Determination of sound power levels and sound energy levels of noise sources using sound pressure – Precision methods for reverberation test rooms, 2010.

COMPLEX FLOWS IN A VENTILATED CAVITY

N.F. Dimitrieva

Institute of Hydromechanics of National Academy of Sciences of Ukraine, 8/4 Marii Kapnist St., 03–057 Kyiv, Ukraine

E-mail: Dimitrieva@nas.gov.ua

Abstract. This study examines complex vortex flows within a cavity and the influence of ventilation parameters on vortex reorganization. A technique for numerical calculations of two-phase flows using the open-source software OpenFoam is proposed. The 3D unstructured mesh with a predominance of hexahedral elements takes into account small-scale flow structures in the phase transition zone and near the streamlined body. The influence of geometric and dynamic parameters on the formation and development of an air cavity, its size, shape and stability has been investigated.

Keywords: Computational Fluid Dynamics, Two-Phase Flow, Cavity, Vortex, Volume of Fluid.

1. Introduction

The problem of supercavitation as a method of flow control has been known since the middle of the 20th century [1]. Supercavitation is essentially the process of formation of a single gas bubble (cavity) behind a streamlined object. To create and maintain a stable cavity, air is injected into the vapor-containing cavity.

This study is devoted to the study of complex vortex flows inside the cavity and the influence of injection parameters on the restructuring of the vortex structure. At a low flow velocity, the evaporation effect can be neglected.

2. Mathematical Modelling

A two-phase immiscible medium water-air is studied.

Volume of Fluid (VOF) method is used to solve the two-phase flow problem [2]. The two immiscible media are considered one effective fluid all over the domain. Mathematical modelling of the problem is based on the equation set of incompressible fluid mechanics which includes equations of continuity, Navier-Stokes, diffusion of phase volume fraction:

$$\frac{\partial u_j}{\partial x_j} = 0 \tag{1}$$

$$\frac{\partial(u_i)}{\partial t} + u_j \frac{\partial(u_i)}{\partial x_j} = -\frac{1}{\rho}\frac{\partial p}{\partial x_i} + \upsilon \frac{\partial^2 u_i}{\partial x_j^2} + \sigma\kappa \frac{\partial \alpha}{\partial x_i} \tag{2}$$

$$\frac{\partial \alpha}{\partial t} + u_j \frac{\partial \alpha}{\partial x_j} = 0 \tag{3}$$

Here $i, j = 1, 2, 3$, u_i is component of the velocity field, ρ is the pressure, α is the phase fraction, υ is the kinematic viscosity coefficient, t is time, density ρ is calculated as weighted averages based on the fraction distribution of the fluid, σ is the surface tension constant, κ is the curvature.

3. Computations

The computations are performed using the OpenFoam software. The interFoam model is used for two incompressible isothermal media without phase transition. The mesh is constructed by the stepwise cell refinement method using the snappyHexMesh utility. The calculation results were presented in the open software ParaView.

Numerical experiments showed that a stable air cavity is formed in the wake of the body. Good qualitative agreement with experimental data was obtained [3, 4].

The developed cavity of high elongation can be conditionally divided into three zones (Fig.1).

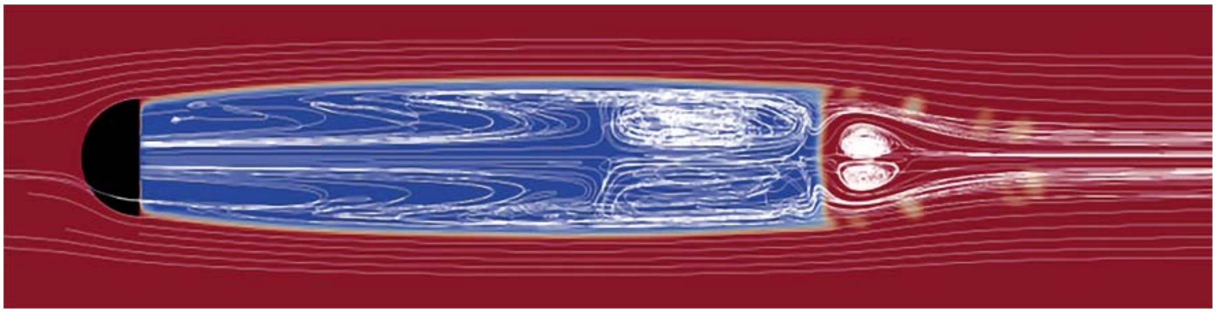

Figure. 1. Central section: the cavitator is in black; air is in blue; water is in red; streamlines are in white

The first zone is characterized by a constant pressure and is quite accurately determined by the boundary of the molecular layer of the air-water interface. The second zone is characterized by the thickness of the layer, which is filled with small drops of water due to viscous diffusion, as well as blowing air into the cavity to maintain a constant pressure. The third zone is characterized by a two-phase mixing layer, which forms the wake of the cavity. The calculation results are in qualitative agreement with the theoretical ones in [5].

The dimensions of the cavity parts depend on the velocity of the main fluid flow and the flow rate of the injected gas.

4. Conclusions

Based on the open-source software OpenFOAM the numerical model of two-phase flows is proposed. Calculations of an air cavity in a moving fluid were performed. The thickness of the air cavity depends on the diameter of the cavitator and does not depend on the diameter of the blowing hole. A complex vortex structure inside a ventilated cavity is described. Three zones are distinguished: constant pressure, viscous diffusion and a two-phase mixing layer. The dimensions of the cavity regions depend on the velocity of the main fluid flow and the injected gas flow rate. Good agreement between theoretical and experimental data is achieved.

References

[1] Tulin M.P., *Supercavitating flows, small perturbation* theory, 'Journal of Ship Research' 1964, vol. 8.

[2] Hirt C.W., Nichols B.D., *Volume of fluid (VOF) method for the dynamics of free* boundaries, 'Journal of Computational Physics' 1981, vol. 39, no. 1.

[3] Savchenko Y.N. Savchenko G.Y., *Gas Flows in Ventilated Supercavities*, [in:] I. Nesteruk (ed.) *Supercavitation: Advances and Perspectives A collection dedicated to the 70th jubilee of Yu.N. Savchenko*, Springer-Verlag, Berlin-Heidelberg 2012, pp. 115–126.

[4] Voropaiev G.O., Korobov V.I. Dimitrieva N.F., *Modeling of a ventilated cavity behind a streamlined body*, 'Journal of Numerical and Applied Mathematics' 2021, vol. 135, no. 1.

[5] Voropaiev G.O., *Viscous entrainment of gas in a ventilated cavity of a given shape*, 'Applied Hydromechanics' 2013, vol. 15, no 1.

PASSIVE CONTROL OF THE TURBULENT SEPARATION INDUCED BY THE CONVEX GEOMETRY OF NACA4412

A. Dróżdż, M. Romańczyk, W. Elsner

Czestochowa University of Technology, Department of Thermal Machinery, Armii Krajowej 21, 42–2200 Czestochowa, Poland

E-mail: artur.drozdz@pcz.pl

Abstract. In this paper, the first experimental study of the novel wavy-wall-based method proposed in Dróżdż et al. 2021 (Exp Therm Fluid Sci 2021;121:110291) of flow separation control of turbulent boundary layer on the convex geometry is carried out at a single Reynolds number $Re_\tau \approx 3100$. The skin friction coefficient increases by 42% downstream of the wavy wall. Results also show a decreasing by 5% the boundary layer thickness when using wavy wall which suggests a thinning of the wake of the airfoil which can potentially improve the lift-to-drag ratio by 10%.

Keywords: Aerodynamics, Flow control, Separation, Turbulent flow.

1. Introduction

Most passive flow-control strategies for airfoils aim to reduce skin friction by attenuating large-scale streak [5]. To mitigate skin friction reduction which acts as a laminar-to-turbulent transition postponer, active methods are employed to counteract its detrimental effect on lift by delaying separation.

A promising passive alternative is the utilisation of a streamwise wavy wall (WW) which yields a more than 35% increase in the skin friction coefficient ($C_f = 2\left(\frac{u_\tau}{U_e}\right)^2$) at high Reynolds numbers [1]. The WW design must be carefully tailored to local flow conditions. The undulations should maintain a viscous scaled amplitude of $A^+ = 170$, and a period adjusted so that the flow troughs are on the verge of separation (effective slope around 0.15). The recent work of [2] aimed to test the single WW geometry selected in [1] across a range of Reynolds numbers ($Re_\tau \approx 2600$, 4000 and 4500) and under varying pressure gradient conditions. The overall effectiveness of the increase in C_f was 23% across the tested pressure ranges and Reynolds number variation remains high.

The results in this paper document the performance of the wavy wall, designed with the knowledge gained during previous studies, applied to a convex curved surface similar to the surface of a wind turbine blade at a single Reynolds number $Re_\tau \approx 3100$.

2. Experimental setup

The experiment was carried out in a modular wind tunnel explicitly designed for studying wind turbine blades' surfaces under real atmospheric conditions, located at Czestochowa University of Technology, where the canonical turbulent boundary layer (TBL) can develop up to a 7500 mm long flat plate without tripping. The Reynolds number based on developing distance is $Re_x = 10^7$. Downstream the inlet channel, a curved surface section corresponds to the part of the NACA4412 profile suction side at the angle of attack (AoA) equal to 5° was installed (see Fig. 1a). The mean velocity and its fluctuation profiles were measured with a free-from-spatial-averaging hot-wire probe. To estimate skin friction the method by [4] was used.

3. Results

In Figure 1b, the skin friction coefficient C_f for the wavy surface (open symbols) is compared to the C_f unmodified wing surface (dark symbols), where a second-order polynomial extrapolated the distribution to predict the separation point.

The streamwise distance x was reduced by the boundary layer thickness at the inlet δ_{in}. The selected corrugation geometry produces 42.3% increase of C_f within the integration area. In Figure 1c, the distributions of Θ as a function of x/δ_{in} for the wavy surface (open symbols) are compared with the unmodified wing surface (dark symbols). The results show the increase or maintenance of the momentum at the same level downstream of WW. As the momentum-loss thickness is unchanged (see Fig. 1b), there is no additional drag penalty.

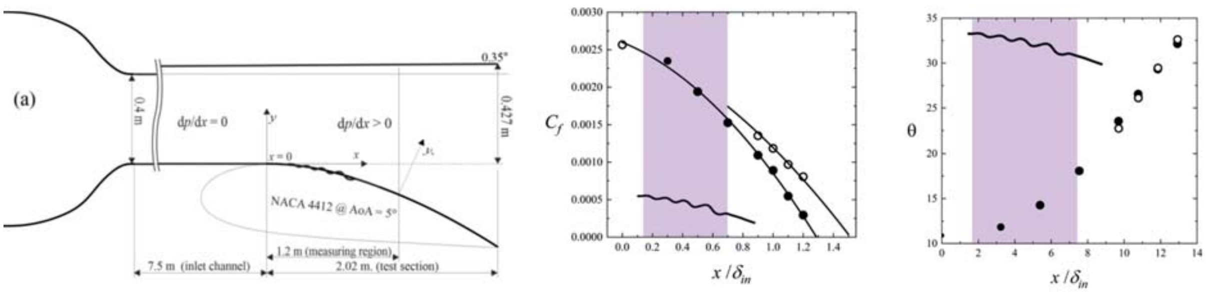

Figure 1. Schematic of the test section (a) comparison of skin-friction coefficient distributions (b) and momentum loss thickness distributions (c). The open symbol corresponds to the wavy wall, while the dark symbols correspond to the unmodified wing surface

Although the increase in the lift coefficient C_L remains undetermined, a tangential shift in the flow separation point quantified as $\frac{\Delta x_t}{c} = 8.3\%$, where $c = 2.5$ m is the chord of the applied wing section, can be associated at this Reynolds number with a roughly 5% increase in lift. Moreover, the boundary layer thickness decreases by 5% (not shown here), making the method a potential candidate for application.

In the full paper, the streamwise Reynolds stresses and premultiplied streamwise energy spectra will be presented to discuss the changes in the contributions from small and large scales downstream of the wavy wall.

Acknowledgements

The investigation was supported by National Science Centre under Grant No. DEC-2020/39/B/ST8/01449.

References

[1] Dróżdż A., Niegodajew P., Romańczyk M., Sokolenko V. Elsner W., *Effective use of the streamwise waviness in the control of turbulent separation*, 'Experimental Thermal and Fluid Science' 2021, vol. 121.

[2] Dróżdż A., Sokolenko V. Elsner W., *Performance analysis of novel wavy-wall-based flow control method for wind turbine blade*, 'Experimental Thermal and Fluid Science' 2025, vol. 169.

[3] Niegodajew P, Dróżdż A, Elsner W., *A new approach for estimation of the skin friction in turbulent boundary layer under the adverse pressure gradient conditions*, 'International Journal of Heat and Fluid Flow' 2019, vol. 79.

COMPARISON OF TRADITIONAL METHODS OF INDUSTRIAL FAN CALCULATIONS WITH MODERN TOOLS

J. Dziuba, K. Smołka

Silesian University of Technology, Department of Power Engineering and Turbomachinery, 2A Akademicka St., 44–100 Gliwice, Poland

E-mail:jaroslaw.dziuba@polsl.pl, krystian.smolka@polsl.pl

Abstract. This paper compares traditional industrial fan design methods, developed in recent years at the Department of Power Engineering and Turbomachinery, with modern approaches based on CFD analysis. Using a centrifugal fan currently operating in industry and originally designed at the Department as a reference case, a comparative analysis of geometry and flow characteristics is carried out. The study discusses differences in the design workflow, reports the observed deviations in geometry and predicted performance between the reconstructed and CFturbo-generated fans and identifies the main sources of discrepancy between traditional and CFturbo-assisted methods.

Keywords: Radial Fan, CFturbo, Computational Fluid Dynamics.

1. Introduction

Radial fans are key components in industrial ventilation, process engineering and HVAC systems, where they handle large volume flows, contaminated gases and significant pressure rises under demanding operating conditions. Meeting these requirements efficiently and reliably depends on the quality of the aerodynamic and structural design of the impeller, volute and associated flow passages. The design practice at the Department has traditionally relied on correlation-based methods for determining main dimensions, blade angles and volute geometry of industrial fans. These procedures are transparent and well suited for engineering education but they require considerable manual effort when multiple design variants or operating points must be analysed [1]. CFturbo represents a modern conceptual design tool that integrates classical turbomachinery theory with parametric geometry generation and direct CAD/CFD export, guiding the designer from duty-point specification through main-dimension selection, meridional contour design, blade definition and volute generation, and enabling rapid modification of 3D-ready geometries with straightforward CFD coupling.

The comparison is based on a single-stage centrifugal fan currently employed in industrial service and originally designed at the Department using the traditional method, operating with air at near-ambient conditions and characterized by a prescribed volume flow rate, total pressure rise and rotational speed typical for industrial ventilation applications. The as-built geometry of the impeller and volute is identified from drawings and measurements, defining the main dimensions and serving as the reference configuration for both the traditional calculation scheme and the CFturbo model. In the traditional route, similarity parameters and empirical correlations are used to determine the main dimensions, blade angles and volute area law, while performance is estimated using one-dimensional loss models and the resulting geometry, and predicted characteristic serve as a benchmark for the historically used method.

In the CFturbo-assisted route, a new fan project is created with the same fluid, duty point and rotational speed; main-dimension and meridional-contour steps are adjusted to match measured diameters and widths, while the blade-design and volute modules are used to generate a new configuration consistent with the reference casing. For both routes, the resulting 3D geometries are exported to a CFD environment, where steady simulations are carried out under identical boundary conditions with the same turbulence model, mesh strategy and convergence criteria so that differences in predicted performance and flow structure can be attributed primarily to the design methodology and geometric details.

2. Comparative analysis

The comparison method treats the industrial radial (centrifugal) fan as a reference object (Fig. 1) and evaluates how well the different design approaches reproduce its geometry and performance under realistic operating conditions. The procedure consists of four main steps: (1) defining the reference fan and available measurements, (2) building numerical and modern-tool-based models, (3) comparing geometry, integral characteristics and detailed flow fields, and (4) quantifying discrepancies and identifying their sources. On the geometric level, main dimensions, blade angles, volute area progression and clearances obtained from the traditional procedure and from CFturbo are compared with the measured data and the resulting relative deviations are used to indicate which features are most sensitive to the chosen design route.

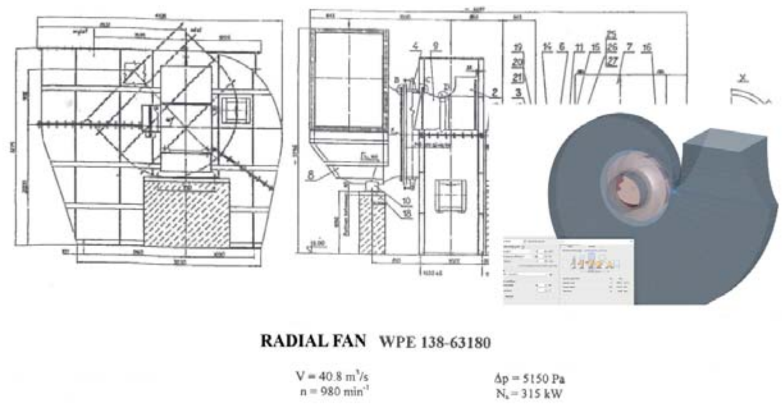

Figure.1. Radial fan subjected to comparative analysis

3. Results and discussion

We reconstruct the original machine using traditional methods and create a new configuration in CFturbo, keeping the same duty point and dimensions. This results in differences in blade shape, blade angle distribution, and volute area progression. Preliminary CFD simulations confirm that these geometric changes translate into measurable differences in pressure rise, efficiency and internal flow structure between the two variants. These geometric variations were analyzed through computational fluid dynamics (CFD) simulations, comparing key performance indicators such as pressure rise, shaft power and efficiency, alongside internal flow structures. The paper will detail the comparisons between the traditional design and the CFturbo variant, highlighting the trends already identified in the preliminary analysis and the benefits of a modern CAD-CFD approach in industrial fan design.

Acknowledgment

This work was supported by statutory research funds.

References

[1] Otte J., *Wybrane zagadnienia projektowania i konstrukcji wentylatorów przemysłowych i energetycznych*, „Zeszyty Naukowe Politechniki Śląskiej Seria: Energetyka Z" 1996, vol. 127.

ALGORITHM FOR EXTRACTING ADVECTION-DIFFUSION OPERATOR EIGENVALUE AS MIXING MEASURE IN DOUBLE GYRE FLOW

J. Fabisiak, S. Gepner

Warsaw University of Technology, Institute of Aeronautics and Applied Mechanics, Nowowiejska 24, 00–665 Warsaw, Poland

E-mail: jakub.fabisiak.dokt@pw.edu.pl

Abstract. We developed an iterative algorithm for extracting eigenvalues and eigenmodes of Advection-Diffusion (AD) operator. Such eigenvalues can be seen as an upper bound of mixing efficiency and used as a mixing measure independent of mixed scalar initial distribution. The authors perform parametric analysis on benchmark double gyre flow case to test algorithm's performance and validate its convergence to same value from different initial scalar distributions.

Keywords: Computational Fluid Dynamics, Mixing Measure, Advection-Diffusion Operator, Double Gyre.

1. Introduction

Mixing in laminar periodic velocity fields is known to result in persistent spatial patterns known as 'strange eigenmodes'. After initial, transient phase of mixing, the advected scalar settles into patterns with repeating spatial shape and exponentially decaying amplitude [1]. Such shapes are defined by the Advection-Diffusion operator – the advection velocity field and diffusivity coefficient. Mixed scalar field can be decomposed into sum of modes with corresponding decay rates. As homogenization progresses, the fast-decaying modes contribution diminishes quickly, and they do not manifest in the asymptotic state of the process. Consequently, this leads to mixing being governed by the slowest decaying, dominant mode that can be associated with the upper bound on mixing efficiency.

$$c(\boldsymbol{x},t) = \sum_{k=0}^{N-1} e^{-\lambda_k t}\varphi_k(\boldsymbol{x},t) \approx e^{-\lambda_d t}\varphi_d(\boldsymbol{x},t) \tag{1}$$

In practical mixing cases, such dominant mode will be the same for given kinematics and diffusivity regardless of initial scalar distribution [2].

In their previous works, the authors developed an iterative algorithm for fast computation of dominant eigenvalues and eigenmodes. The idea behind this algorithm uses similarity between AD equation and eigenproblem [3] and is based on power method. Arbitrary initial field is chosen, and then iterative process consists of application of AD operator (using previously generated and approximated velocity field snapshots; only advection-diffusion is solved) and renormalization of results. Process is repeated until convergence – stabilization of eigenvalue (tracked by exponential decay rate of scalar field variance). Such method can measure the whole mixing protocol by assigning it a single numerical value (computed eigenvalue), thus, can be further used as a simple, yet efficient optimization tool.

2. Problem statement

This work outlines the use of algorithm to measure mixing rate in double gyre flow (both stationary and periodically expanding and contracting). The parametric study is performed to show process change and algorithm performance with diffusivity ranging from 10^{-2} to 10^{-4} for both stationary and periodic cases. For periodic case the change in oscillation frequency and amplitude is also considered.

Three different initial conditions are considered, all with mean value of 0 – first with two peaks of value 1 and -1 in opposite corners of domain and two cases with domain separated in halves with values 1 and -1 with vertical and horizontal separation lines (Fig 1). All cases are repeated using all different initial distributions to show convergence path and its change with change of the flow kinematics and diffusivity.

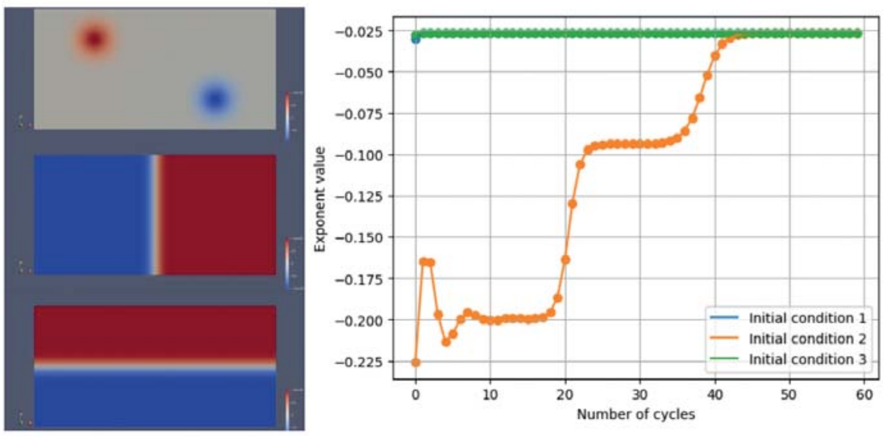

Figure 1. Exemplary case of algorithm convergence from different initial conditions to the same resulting exponential decay rate

3. Conclusions

The authors present the algorithm for fast computation of AD operator eigenvalue as a mixing measure and show its independence on the initial condition of mixed scalar field. A parametric analysis on double gyre flow to show algorithm's application and performance is performed. Usage of the algorithm as an optimization tool is discussed.

References

[1] Pierrehumbert R.T., *Tracer microstructure in the large-eddy dominated regime*, 'Chaos, Solitons & Fractals' 1994, vol. 4, no. 6, pp. 1091–1110.

[2] Liu W., Haller G., *Strange eigenmodes and decay of variance in the mixing of diffusive tracers*, 'Physica D' 2004, vol. 188, pp. 1–39.

[3] Singh M.K., Speetjens M.F.M., Anderson P.D., *Eigenmode analysis of scalar transport in distributive mixing*, 'Physics of Fluids' 2009, vol. 21, no. 9.

LABORATORY INVESTIGATION OF AEROACOUSTIC PHENOMENA OCCURRING DURING HIGH-PRESSURE GAS EJECTION

P. Gaj[1], **I. Czajka**[2], **J.M. Kopania**[1]

[1] *Institute of Power Engineering, Institute of Turbomachinery, Mory Street 8., 01–330 Warsaw, Poland*

[2] *AGH University of Science and Technology, Department of Power Systems and Environmental Protection Facilities, 30 Mickiewicza Av., 30–059 Kraków, Poland*

E-mail: patryk.gaj@itc.edu.pl

Abstract. In this article, the feasibility of measuring acoustic phenomena during high-pressure air discharges under laboratory conditions was examined. The research involved the development, construction and testing of a test stand capable of producing controlled air discharges while simultaneously determining aerodynamic and acoustic parameters. The tests were conducted for two configurations of the test stand: one with an undisturbed outlet and another with a gas expander installed. The obtained results confirmed the feasibility of using the developed test stand to determine the acoustic parameters of high-pressure air discharges.

Keywords: Experimental Fluid Mechanics, Jet Dynamics, Aeroacoustics.

1. Introduction

Currently, people are becoming more aware of and understanding the impact of noise on human health. Currently, noise nuisance is considered by the World Health Organisation (WHO) one of the greatest environmental threats to public health in Europe, as it leads to serious health consequences. Especially, high levels of low-frequency noise (LFN) have a significant detrimental influence on multiple aspects of human health. Symptoms such as annoyance, agitation, cognitive alterations, an increase in cardiovascular diseases, sleep disorders and a degrading influence on dental wear were recorded [1]. Low frequencies often can coincide with the resonant frequencies of walls, windows and entire buildings, leading to noticeable vibrations and 'rattling'. Low-frequency noise (LFN) is also difficult to mask because conventional acoustic screens and absorbent materials are much less effective at suppressing these sounds. Moreover, LFN is poorly dampened in the air and can propagate over large areas [2].

Low-frequency noise sources of industrial origin are particularly important. In the energy sector, large, slow-rotating fans, turbine blades, combustion chambers and exhaust systems (chimneys) generate strong mechanical vibrations and flow instabilities that resonate in the low-frequency range. Some aspects of this noise are still not described sufficiently. Steam discharge to air is still a common occurrence in thermal power plants; however, due to technical difficulties, the aeroacoustics of that are very often determined theoretically or studied using Computational Fluid Dynamics [4, 5] which is still a difficult issue. To validate the computational model, tests under experimental conditions are required. The aim of this work was to develop a measurement methodology for high-pressure air exhausts that can simulate steam exhaust. A test bench was designed, constructed and tested to enable testing of the aerodynamic and acoustic parameters of steam exhaust silencers.

2. Test procedure

The research station was constructed in the Acoustic Laboratory of the Institute of Power Engineering. For safety reasons, compressed air was used as a substitute for steam. The outlet of the test stand was led out into the reverberation chamber (Fig. 1) which makes it possible to determine the sound pressure level at the outlet of the station. The gas pressure, temperature, velocity of ejected gas andsound pressure level present in the chamber during the discharge were recorded. The test was performed for four values of gas pressure and two installation setups: with an open outlet and a simple one-stage gas expander installed on the outlet. Acoustic tests were conducted in accordance with the ISO3741 standard, utilising a high-pressure microphone and the microphone-array with 64 microphones for the measurements. The microphone and microphone-array were set up 1.5 meters away from the outlet of the research station at the 45° angle. The test was performed in a reverberation chamber in which there is a diffuse acoustic field, reducing the influence of the distance between the microphone and the sound source.

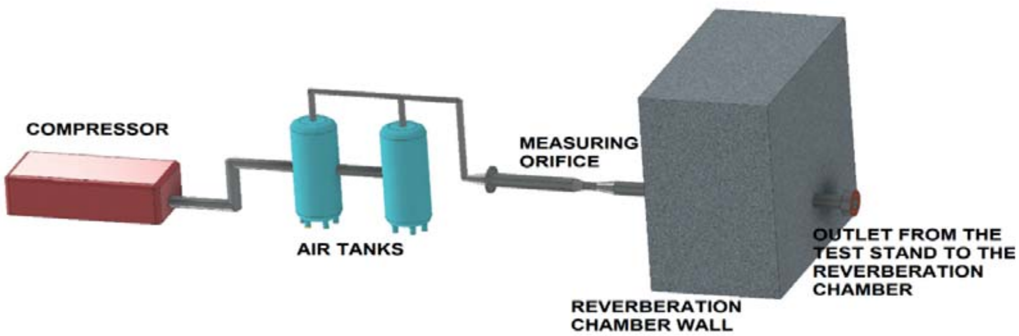

Figure 1. Simplified model of the research station

3. Conclusions

This work allowed for the experimental reproduction of aerodynamic and acoustic phenomena occurring during steam discharge in thermal power plants. The sound pressure level present during the gas discharge from the research station exceeded 130 dB. The design used, along with the study of its parameters (pressure, temperature, outlet velocity and sound pressure level), became the basis for verifying the measurement range and capabilities of the test stand. Tests of the expander at the outlet of the stand, together with the evaluation of the obtained results, also allowed for the validation of simulations performed in previous research works.

References

[1] Araújo-Alves J., Neto Paiva F., Torres Silva L., Remoaldo P., *Low-Frequency Noise and Its Main Effects on Human Health A Review of the Literature between 2016 and 2019*, 'Applied Science' 2020, vol. 10, art no. 5205.

[2] Vincent P., Larsonnier F., Rodrigues D., Durand S., *Analytical modelling and characterisation of an infrasound generator in the air*, 'Applied Acoustics' 2019, vol. 148, pp. 476–483.

[3] Gaj P., Sobczak K., Kopania J., Wójciak K, *Influence of shell shape on flow and acoustic parameters of a steam silencer*, 'Archives of Thermodynamics' 2021, vol. 42, no. 4, pp. 141–154.

[4] Rajgopal, Kiran K., Ashtagi Y., *An Investigation on Shape Optimization of Pressurized Inlet Diffuser in Steam Vent Silencer By Using Computational Fluid Dynamics*, 'Journal of Engineering Research and Applications' 2014, vol. 4, no. 12. pp. 103–109.

[5] ISO 3741:2010. Acoustics. Determination of sound power levels and sound energy levels of noise sources using sound pressure – Precision methods for reverberation test rooms.

A CONSISTENT SPLITTING SCHEME FOR UNSTEADY INCOMPRESSIBLE FLOWS WITH EXACT INCOMPRESSIBILITY ENFORCEMENT

J. Gałecki, J. Szumbarski

Warsaw University of Technology, Faculty of Power and Aeronautical Engineering, ul. Nowowiejska 24, 00–665 Warszawa, Poland

E-mail: jakub.galecki@pw.edu.pl

Abstract. The talk discusses a consistent splitting scheme for the incompressible Navier-Stokes equations which explicitly enforces the continuity constraint. Convergence studies are presented, along with a representative simulation of a three-dimensional flow.

Keywords: Computational Fluid Dynamics, Incompressible Flow, Open Boundary Conditions, Projection Methods, Least-Squares Finite Element Method.

1. Introduction

A major difficulty in the solution of the incompressible Navier-Stokes equations using the finite element method (FEM) lies in the proper coupling of the velocity and pressure via the continuity equation. To overcome this obstacle, projection methods [1] have been developed which split the coupled Navier-Stokes system at each time step into multiple smaller problems for the individual solution components. The present work focuses on the consistent splitting scheme originally proposed by Pontaza [2] which involves an intermediate correction step for the velocity.

2. Splitting scheme description

The splitting scheme consists of the following three steps. First, an advection-diffusion type problem is solved to find the intermediate velocity $\hat{\mathbf{u}}$:

$$\frac{\partial \hat{\mathbf{u}}^{n+1}}{\partial t} + (\mathbf{u}_*^{n+1} \cdot \nabla)\hat{\mathbf{u}}^{n+1} - \nu \Delta \hat{\mathbf{u}}^{n+1} = -\nabla p_*^{n+1} + \mathbf{f}^{n+1} \tag{1}$$

where the index $(\cdot)^{n+1}$ indicates the time step, the time derivative is discretized using an implicit formula, and $(\cdot)_*$ denotes a quantity which is extrapolated in time. The next step can be viewed as a projection of $\hat{\mathbf{u}}$ onto a divergence-free space, yielding the solenoidal velocity u:

$$\begin{cases} \nabla \times \mathbf{u}^{n+1} = \nabla \times \hat{\mathbf{u}}^{n+1} \\ \quad \nabla \times \mathbf{u}^{n+1} = 0 \end{cases} \tag{2}$$

Finally, the last step consists of the pressure Poisson problem:

$$\Delta p^{n+1} = \nabla \cdot \mathbf{f}^{n+1} - \nabla^T \mathbf{u}^{n+1} \colon \nabla \mathbf{u}^{n+1} \tag{3}$$

Note that all equations are subject to the appropriate boundary conditions.

The authors' novel contribution consists of incorporating open boundary conditions into the scheme described above. Additionally, different types of FEM formulations were tested for each of the steps, including the classical Galerkin method and the least-squares formulation [3]. The computations were performed using the L3STER framework [4].

$$-p\mathbf{n} + \nu\mathbf{n} \cdot \nabla\mathbf{u} = 0 \tag{4}$$

3. Results and conclusions

Convergence studies of the approach are discussed, exhibiting a convergence rate of $\mathcal{O}(\Delta t^{2.8})$, exceeding the scheme's formal order of 2. To demonstrate its applicability to real-world fluid dynamics problems, the proposed approach is used to simulate a three-dimensional flow with complex dynamics, shown in Figure 1.

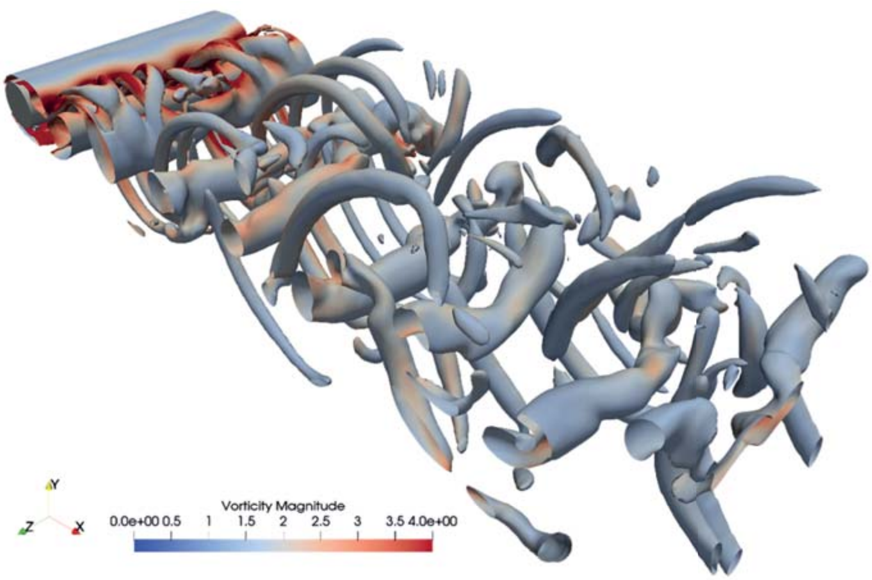

Figure 1. Flow past a cylinder at Re = 400, Q-criterion isocontours

Acknowledgements

Computations were partially carried out at the Interdisciplinary Center for Mathematical and Computational Modeling of the Warsaw University, under grant g101-2387.

References

[1] Guermond J.L., Minev P., Shen J., *An overview of projection methods for incompressible flows*, 'Computer Methods in Applied Mechanics and Engineering' 2006, vol. 195, no. 44/47, pp. 6011–6045.

[2] Pontaza J.P., *A new consistent splitting scheme for incompressible Navier–Stokes flows: A least-squares spectral element implementation*, 'Journal of Computational Physics' 2007, vol. 225, no. 2, pp. 1590–1602.

[3] Gunzburger M.D., Bochev P.B., Least-Squares Finite Element Methods, [in:] *Applied Mathematical Sciences*, Springer, New York 2009.

[4] Gałecki J., *L3STER*, https://github.com/kubagalecki/L3STER, (access: 31.03.2026).

FROM SQUARE TO CIRCLE: DISCOVERING STEADY LOCALISED TRAVELLING WAVES IN PIPE FLOW THROUGH GEOMETRIC HOMOTOPY

S. Gepner[1], **G. Kawahara**[2]

[1] *Warsaw University of Technology, Faculty of Power and Aeronautical Engineering, ul. Nowowiejska 24, 00–665 Warszawa, Poland*

[2] *Graduate School of Engineering Science, Osaka University,1–3 Machikaneyama, Toyonaka, Osaka 560–8531, Japan*

E-mail: stanislaw.gepner@pw.edu.pl

Abstract. Streamwise-localised exact coherent structures are rare in circular pipe flow. Using geometric homotopy, we morph a discretely symmetric square-duct geometry into an axisymmetric circular pipe, continuing invariant solutions from the square duct to obtain a steady, streamwise-localised travelling-wave solution of the pipe flow. To our knowledge, this is the first simple streamwise-localised travelling wave identified in a circular pipe.

Keywords: Transition to turbulence, exact coherent structures, pipe flow, travelling waves, homotopy continuation.

1. Introduction

Invariant solutions of the Navier-Stokes equations – travelling waves (TW), periodic or relative periodic orbits (RPO) – provide a geometric framework for understanding transitional turbulence [1], acting as organising centres whose stable manifolds form the skeleton of the turbulent attractor [2]. Spatially localised exact coherent structures (ECS) are particularly relevant for understanding localised turbulence such as puffs in pipe flow.

Despite extensive cataloguing efforts, streamwise-localised solutions remain scarce in circular pipe flow. Avila et al. [3] and Chantry et al. [4] reported streamwise-localised RPO solutions appearing near transition onset and emerging from globally periodic TW through modulational instabilities. However, no simple steady TW has been reported, despite the observation that *there now seems no reason why a steady modulational instability might not give rise to a steady streamwise-localized traveling wave* [4], motivating the present work.

2. Geometric homotopy approach

We introduce a geometric homotopy method transitioning from discrete to continuous symmetries.Discrete symmetries regularise the search by collapsing the continuous neutral manifold of azimuthal rotations into finite discrete transformations, making localised edge states accessible through standard bisection and Newton-Krylov methods. These solutions are then traced continuously as the geometry deforms toward the circular pipe.

Our implementation leverages the spectral element method (SEM) via Nektar++ [5], whose geometric flexibility enables domain morphing – a capability unavailable to the customarily employed dedicated global spectral solvers. This geometric continuation strategy differs fundamentally from earlier approaches that generated localisation through modulational symmetry-breaking bifurcations within a fixed circular geometry [4].

2.1. Seed solution in square duct

We initiate from a turbulent snapshot of square duct flow at Re = 4000 (duct half-width, laminar centreline velocity) with streamwise period $L_z = 8h$. Edge-tracking bisection [6,7] followed by Newton-Krylov iteration converges to an exact streamwise-localised steady TW. Arnoldi analysis confirms asingle unstable eigenvalue, verifying edge-state status. Discrete symmetry is crucial – direct edge tracking in circular pipe fails due to continuous azimuthal invariance, with the edge state hypothesised to be chaotic [8].

2.2. Continuation to circular pipe

With the square-duct edge state as seed, homotopy parameter $\varepsilon \in [0,1]$ controls cross-sectional shape ($\varepsilon = 0$: square; $\varepsilon = 1$: circular). At each $\Delta\varepsilon$, we project the solution onto the deformed mesh and reconverge via Newton-Krylov iteration. SEM's geometric flexibility enables direct point-to-point mesh correspondence, avoiding interpolation errors. Continuation to $\varepsilon = 1$ yields a fully converged steady streamwise-localised TW of circular pipe flow.

3. Results and significance

Geometric homotopy successfully yields a steady streamwise-localised TW in circular pipe flow at Re = 4000 (pipe diameter, mean flow velocity, $L_z = 8h$). The solution exhibits near-wall streak-roll-wave organisation confined to a streamwise-localised region spanning 4–5 pipe radii. Crucially, this is a simple steady TW rather than an RPO – to our knowledge, the first such streamwise-localised solution in circular pipe flow without imposed symmetry constraints.

This directly addresses the gap identified by Chantry et al. [4] and establishes geometric homotopy as a systematic route to discover localised ECS by exploiting discrete symmetries as regularisation toward continuous symmetries. Simple steady TWs offer minimal building blocks for understanding state-space structure in extended domains, complementing known localised RPO solutions [3,4].

Acknowledgements

The authors acknowledge financial support from JSPS postdoctoral fellowship PE20715 and the National Science Centre, Poland (Sonata grant 2019/35/D/ST8/00090). Computational resources were provided by ICM, University of Warsaw.

References

[1] Kawahara G., Uhlmann M., van Veen L., *The significance of simple invariant solutions in turbulent flows*, 'Annual Review of Fluid Mechanics' 2012, vol. 44, pp. 203–225.

[2] Hof B., van Doorne C.W.H., Westerweel J., Nieuwstadt F.T.M., Faisst H., Eckhardt B., Wedin H., Kerswell R.R., Waleffe F., *Experimental observation of nonlinear traveling waves in turbulent pipe flow*, 'Science' 2004, vol. 305, no. 5690, pp. 1594–1598.

[3] Avila M., Mellibovsky F., Roland N., Hof B., *Streamwise-localized solutions at the onset of turbulence in pipe flow*, 'Physical Review Letters' 2013, vol. 110, no. 22, art. no. 224502.

[4] Chantry M., Willis A.P., Kerswell R.R., *Genesis of streamwise-localized solutions from globally periodic traveling waves in pipe flow*, 'Physical Review Letters' 2014, vol. 112, no. 16, art. no. 164501.

[5] Cantwell C.D., Moxey D., Comerford A., Bolis A., Rocco G., Mengaldo G., De Grazia D., Yakovlev S., Lombard J.E., Ekelschot D., Jordi B., Xu H., Mohamied Y., Eskilsson C., Nelson B., Vos P., Biotto C., Kirby R.M., Sherwin S.J., *An open-source spectral/hp element framework*, 'Computer Physics Communications' 2015, vol. 192, pp. 205–219.

[6] Itano T., Toh S., *The dynamics of bursting process in wall turbulence*, 'Journal of the Physical Society of Japan' 2001, vol. 70, no. 3, pp. 703–716.

[7] Skufca J.D., Yorke J.A., Eckhardt B., *Edge of chaos in a parallel shear flow*, 'Physical Review Letters' 2006, vol. 96, no. 17, art. no. 174101.

[8] Budanur N.B., Hof B., *Heteroclinic path to spatially localized chaos in pipe flow*, 'Journal of Fluid Mechanics' 2017, vol. 827, p. R1.

SURVEYING RIVER BEDS WITH FLOW SIMULATION FOR OPTIMAL POSITIONING OF RIVER TURBINES

S. Grün, B. Allweyer, D. Hübner, F. Rückert

Saarbrücken, University of Applied Science, Business Faculty, Waldhausweg 14, 66123 Saarbrücken, Germany

E-mail: sebastian.gruen@htwsaar.de, benjaminallweyer@htwsaar.de, dirk.huebner@htwsaar.de, frank.rueckert@htwsaar.de

Abstract. This work presents a method for the optimal placement of river turbines used in hydrokinetic energy generation. Accurate flow profile simulations are essential for site selection and require detailed riverbed data. A purpose-built measuring system acquires this data with minimal measurement effort. Custom software converts the measurements into a river profile used for simulation. The simulation results further indicate how many measurement points are necessary to produce a sufficiently accurate model.

Keywords: Computational Fluid Dynamics, Environmental fluid mechanics, Experimental Fluid Mechanics, AI and machine learning in fluid mechanics, Power Buoys.

1. Introduction

The European Union has committed to becoming climate neutral by 2050. With the help of the European Climate Law, all participating countries are obliged to achieve this goal. This necessitates the large-scale expansion of climate-neutral energy production. In the European Union, almost half of the electricity fed into the grid will come from renewable sources by 2025. In Germany, which says it wants to be climate neutral by 2045, the share was 55.9 percent. Wind power accounts for the largest share of electricity generation from renewable energies at 31.8%, followed by photovoltaic systems at 16.8%. In contrast, only 4.2% of electricity was generated using water. [1]

River turbines harness the untapped energy potential of flowing water. To maximize their energy output, optimal positioning within the watercourse is critical, as higher flow velocities directly translate to greater power generation. Furthermore, positioning should ensure the greatest possible independence from fluctuating water levels. This work presents the development and application of a process for the optimal placement of river turbines.

Site selection requires a simulation of the watercourse's flow behavior which, in turn, depends on an accurate river cross-section profile. A custom-built measuring system is introduced, capable of capturing the necessary data points in as few survey passes as possible. To determine the optimal number and placement of measurement points, dedicated software was developed that employs AI to generate a mesh compatible with Ansys CFX. By comparing simulations of varying models, the minimum number of measurement points required for a reliable simulation can be established.

2. Determination of the Required Measurement Point Density

While the measurement system reliably captures riverbed data, boat surveys carry significant operational costs. A key advantage of the proposed approach is the scale of data produced: conventional multibeam echo sounder surveys generate datasets of several gigabytes, whereas this system produces only a few kilobytes – a reduction of several orders of magnitude. This smaller dataset directly translates to reduced mesh size, lowering computational time and hardware requirements. However, this raises the question of whether such reduced data still captures essential riverbed geometry with sufficient accuracy. To evaluate this, simulation results from reduced datasets are compared against a high-resolution reference model using established metrics, with the goal of identifying the minimum dataset size that still yields comparable results.

The developed software is capable of constructing a three-dimensional body from the recorded riverbed measurement points which serves as the geometric foundation for the mesh used in the subsequent flow simulation. To evaluate how many measurement points are necessary to achieve reliable results, a series of flow simulations was conducted using Ansys CFX.

These simulations are based on multiple geometries generated by the software, each differing in the number of input measurement points and the resulting surface resolution. By analyzing the simulated velocity profiles and comparing them against one another, conclusions can be drawn regarding the accuracy with which each model reflects real-world flow conditions. This allows for an informed trade-off between survey effort and simulation fidelity.

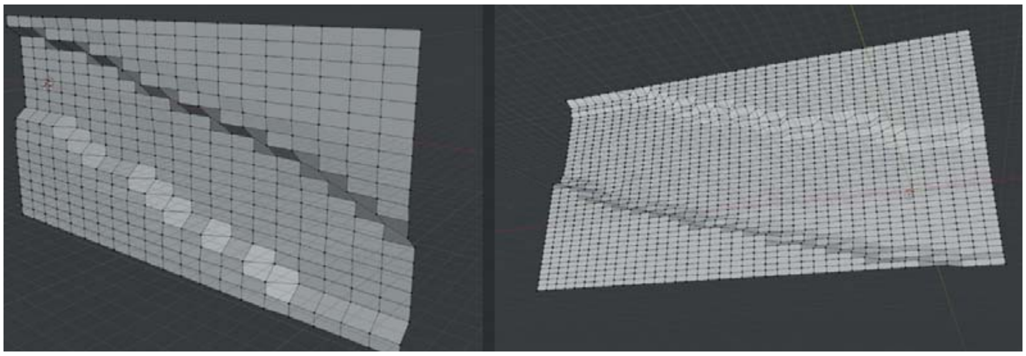

Figure 1. Mesh resolution comparison: low resolution (left) vs. high resolution (right)

To evaluate the minimum number of data points required and assess the influence of mesh resolution on simulation accuracy, existing measurement data from the Rhine near the town of St. Goar was utilized. Initially, a geometry was constructed using the complete set of available measurement points. Based on this geometry, a high-resolution, computationally intensive mesh was generated to simulate the flow under well-defined boundary conditions. Before this model can serve as a reference for subsequent data reduction studies, its ability to accurately represent real-world flow conditions must first be validated. Only if the reference simulation sufficiently reflects reality can the results be used as a benchmark against which models derived from reduced datasets are compared, ultimately allowing conclusions to be drawn regarding the minimum data requirements for generating a sufficiently accurate simulation model.

References

[1] Fraunhofer ISE, *Öffentliche Stromerzeugung 2025: Wind und Solar erstmals als Doppelspitze*, https://www.ise.fraunhofer.de/de/presse-und-medien/presseinformationen/2026/oeffentliche-stromerzeugung-2025-wind-und-solar-erstmals-als-doppelspitze.html (access: 2.04.2026).

SIMULATION OF THERMAL–FLUID PHENOMENA DURING SINGLE WOOD PARTICLE PYROLYSIS WITH SHRINKAGE EFFECTS

P. Hercel, D. Kardaś

Institute of Fluid-Flow Machinery, Polish Academy of Sciences, Fiszera 14, 80–231 Gdańsk, Poland

E-mail: phercel@imp.gda.pl

Abstract. The study presents a 2D transient model of a single wood particle pyrolysis. It couples mass and energy conservation to predict temperature, mass loss, moisture evaporation, gas pressure and velocity, and particle shrinkage. The governing equations are solved using explicit and control-volume methods on a dynamically adapting mesh. The model has been validated against experimental data. It offers a computationally efficient tool for complex thermochemical simulations of pyrolysis.

Keywords: Interdisciplinary Areas in Heat and Fluid Flow, Pyrolysis, Thermal-Fluid Modelling.

1. Introduction

Thermal conversion of biomass, including pyrolysis, gasification and combustion, plays a key role in renewable energy production and sustainable fuel generation. These processes are governed by strongly coupled heat transfer, mass transport and fluid flow phenomena occurring within individual biomass particles. During pyrolysis, solid mass decomposition generates volatile gases that build up internal pressure and induce flow through the porous wooden structure.

Accurate modeling of a single shrinking particle is essential for improving predictive capabilities of larger-scale simulations of packed or fluidized beds, where particle–gas interactions dominate reactor performance. However, many existing models primarily focus on heat transfer and reaction kinetics, while internal particle gas pressure and velocity fields are often ignored. The present model resolves a set of coupled physical parameters, while maintaining low computational cost through an efficient numerical approach.

2. Methodology

The computational domain represents a two-dimensional wooden sample initially shaped as a rectangle of dimensions 20 × 5 mm. The domain is discretized using a structured Cartesian grid composed of square control volumes. As pyrolysis progresses, non-uniform material degradation leads to deformations. To capture this effect, a dynamically adapting, non-orthogonal mesh is implemented. New node positions are updated based on locally computed displacements.

The model includes mass balance equations for solid mass ($\alpha = m_s/m_{s,0}$) and moisture:

$$\frac{\partial m_s}{\partial t} = -k\left(\alpha - \bar{\alpha}(T)\right) m_{s,0}, \qquad \frac{\partial m_w}{\partial t} = -j_w A_i \tag{1}$$

energy balance including conduction and mass transfer effects:

$$\frac{1}{V}\frac{\partial}{\partial t}(m_s u_s + m_w u_w) = -\nabla\cdot\vec{q} + \frac{h_g}{V}\frac{\partial m_s}{\partial t} + \frac{h_{wv}}{V}\frac{\partial m_w}{\partial t} \tag{2}$$

and gas pressure equation for pyrolysis gases and velocity components [1]:

$$\frac{\partial p_g}{\partial t} = \left(\nabla(\rho_g \cdot \vec{v}) + S_g\right)\frac{1}{C_f \varphi}\ , \qquad u = -\frac{K}{\mu}\left(\frac{\partial p_g}{\partial x}\right), \qquad v = -\frac{K}{\mu}\left(\frac{\partial p_g}{\partial y}\right) \tag{3}$$

where $C_f = \partial\rho_g/\partial p_g$ is a constant value determined using data from thermodynamic tables. Shrinking is modeled with a proposed equation integrating deformations with mass loss effects:

$$\rho\frac{\partial^2 \mathrm{u}}{\partial t^2} = -\,\mathrm{K}_\alpha \nabla\alpha \tag{4}$$

where u is deformation (m) and is calculated for both direction in each point (u_x, u_y), and K_α is an empirically fitted deformation coefficient.

The governing equations are solved using an in-house code written in Modern Fortran. An explicit forward Euler scheme is employed for mass, energy and pressure equations to ensure computational efficiency for transient simulations. Finite-volume approach is used to maintain local conservation of mass and energy.

3. Results

The model has been validated with experimental data and shows good fit in terms of temperature field and mass loss. Current results focus on the evolution of temperature, mass, gas pressure and velocity inside the particle. The simulations reveal a clear sequence of coupled phenomena. First, heat conduction raises the local temperature, then pyrolysis reactions occur. This leads to localized mass loss, generation of volatile gases and local pressure increase (Fig 1).

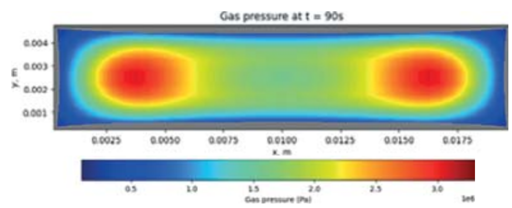

Figure 1. Pyrolysis gas pressure field during the decomposition process

As devolatilization intensifies, an increase in gas pressure develops locally. The resulting pressure gradients drive gas flow through the porous structure, producing internal velocity fields that redistribute gases towards the lower pressure zones and then – particle boundaries.

4. Conclusions

A coupled thermal–fluid model of single wood particle pyrolysis has been developed. The numerical framework captures the strong interdependence between heat transfer, mass loss, gas generation and fluid flow in porous biomass. Its computational efficiency make it suitable not only for single particle studies but also for a base for simulations of particle beds in reactors. Presented simulation required approximately 30 min to complete, while comparable simulations found in the literature often require computation times as high as a couple of hours [2].

Acknowledgements

This work was supported by the Horizon Europe research and innovation programme under the project ResMe2E, grant agreement No. 101172988.

References

[1] Hercel P., Orhon A., Jóźwik M., Kardaś D., *2D Model of a Biomass Single Particle Pyrolysis—Analysis of the Influence of Fiber Orientation on the Thermal Decomposition Process*, 'Sustainability' 2025, vol. 17, no. 1, p. 279.

[2] Hoang N., Vanierschot M., Croymans T., Pittoors R., Van Caneghem J., *Simulation of Moving Grate Waste Incinerators Using the Continuous Porous Medium Approach: a Comparison Between the Conventional Fixed Bed Method and a New Feeding Method*, *Proccedings of 12th European Conference on Industrial Furnaces and Boilers*, Porto 2021.

PERFORMANCE OF VERY HIGHER-ORDER MULTI-MOMENT METHOD IN THE NONLINEAR CONVECTION-DIFFUSION EQUATIONS

A. Hokpunna

Departmnt of Mechanical Engineering, Faculty of Engineering, Chiang Mai University, 239 Huaykaew Rd., Suteph, Muang, Chaing Mai, Thailand

E-mail: arpiruk.hok@eng.cmu.ac.th

Abstract. This presentation introduces a novel, very high-order multi-moment method that leverages all geometric entities defining the volumetric cells in the computational domain. The method simultaneously solves multiple discrete equations and employs cross-data-type approximation to achieve resolving power beyond the Nyquist limit of a single grid. Its accuracy and theoretical performance are demonstrated through 1D convection tests involving sinusoidal waves and Runge's function. The method's ability to capture sharp features is showcased using the viscous Burgers' equation. Finally, its performance in the frontogenesis problem is evaluated and compared to higher-order finite difference schemes.

Keywords: Computational Fluid Dynamics, multi-moment method, higher order scheme, finite surface method.

1. Introduction

The convection-diffusion equation (CDE) serves as a mathematical cornerstone for modeling heat and mass transfer, with applications ranging from chemical mixing to aerosol transport. In convection-dominant regimes, resolving complex sub-grid structures can be challenging. For example, scalar transport at high Schmidt numbers and heat transfer at low Prandtl numbers pose a significant numerical challenge due to the scale differences between the base flow and the scalar structures. Standard approaches often rely on local mesh refinement which can lead to high computational costs and difficulties in maintaining mass conservation across hierarchical grid levels. To address these limitations, this talk presents a very high-order multi-moment method that resolves structures beyond the natural Nyquist limit of a single grid without requiring mesh refinement.

The proposed framework evolves multiple data types simultaneously according to their respective governing equations. This hierarchy of geometric entities includes volumetric cells, planar faces, boundary edges and nodal points. Consequently, each variable can be solved by the corresponding method. The cell-average is solved by the finite volume method (FVM) [1], the surface and the edge-averages are solved by the finite surface method (FSM) [2] and the pointwise data are solved by the classical finite difference method (FDM) [3]. In this presentation, the author presents the basic formulation of the method, followed by the treatment of nonlinearity and boundary closure. Then the accuracy in comparison to higher-order finite difference and discontinuous Galerkin methods. Finally, the author presents the conclusion and the outlook of the research.

2. Formulation of the multi-moment method

The multi-moment method simultaneously solves multiple data types. In principle, the data or the degree of freedom, can be anything. Our current approach is to define the data for the geometric entities that made up the computational cell as shown in Figure 1. This setting enables each data type to leverage the presence of other data types and improve approximation accuracy. The most striking feature is that the availability of the line-average data at the edge of the cell area. This means the net flux over the cell can be computed directly from these line-average bypassing the usual interpolation procedure needed in the finite volume method. The low cost of the flux computation is key to the method's performance and the staggered arrangement allows the approximation scheme to capture the wave finer than its natural Nyquist limit.

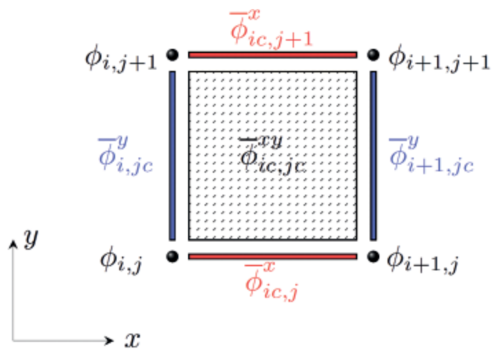

Figure 1. Figure with short caption (caption centred)

3. Analysis and Numerical Examples

The author presents a new coupled Fourier Analysis which described the energy transfer among the variables, then the application of the method in one and two dimensions are discussed. The boundary closures and the nonlinearity treatment are addressed. Finally, the method is applied to a 2D nonlinear convection-diffusion equation for the frontogenesis problem. It is demonstrated the lower requirement in the treatment of the nonlinearity and the performance of the proposed method in comparison with the higher order finite difference scheme. The results indicate that, the method can be much faster than the classical second-order scheme. In comparison to other higher-order schemes, the method can deliver the same result while using 1.5 to 3 times lower numerical operations in linear problems. In nonlinear problem, the method remains competitive with the finite difference method.

References

[1] Hokpunna A., Manhart M., *Compact fourth-order finite volume method for numerical solutions of navier–stokes equations on staggered grids*, 'Journal of Computational Physics', 2010, vol. 229, no. 20, 7545–7570.

[2] Hokpunna A., Misaka T., Obayashi S., Wongwises S., Manhart M., *Finite surface discretization for incompressible Navier-Stokes equations and coupled conservation laws*, 'Journal of Computational Physics' 2020, vol. 423.

[3] Lele S., *Compact Finite Difference Schemes with Spectral-like Resolution*, 'Journal of Computational Physics' 1992, vol. 103, pp. 16–42.

[4] Imai Y., Aoki T., Takizawa K., *Conservative form of interpolated differential operator scheme for compressible and incompressible fluid dynamics*, 'Journal of Computational Physics' 2008, vol. 227, no. 4, pp. 2263–2285.

IDENTIFICATION OF FLOW STATES FOR THE DRESDYN PRECESSION EXPERIMENT USING ULTRASOUND DOPPLER VELOCIMETRY

K.K. Jani, A. Giesecke, T. Gundrum, F. Stefani

Magnetohydrodynamics in Geophysics and Astrophysics, Institute of Fluid Dynamics, Helmholtz-Zentrum Dresden–Rossendorf, Germany

E-mail: k.jani@hzdr.de

Abstract. The precession-driven flow in a rapidly rotating cylinder undergoes abrupt, hysteretic transitions in inertial modes. Using a 1:6 downscaled water model of the DREsden Sodium DYNamo (DRESDYN) precession experiment, thresholds are identified for the appearance of an axisymmetric double-roll circulation in the transition regime. Velocity, pressure and power diagnostics are correlated to better understand the instabilities caused by precession.

Keywords: Experimental Fluid Mechanics, Axial Precession, Inertial Modes, Ultrasound Doppler Velocimetry (UDV), Hysteresis.

1. Introduction

Precession-driven flows in rapidly rotating cylinders are promising drivers of laboratory dynamos. However, the flow transitions that precede magnetic field generation are highly sensitive to control parameters and difficult to detect in real time. The present work focuses on the identification of flow states for the DREsden Sodium DYNamo (DRESDYN) precession experiment, with a preliminary focus on using a distributed network of Ultrasound Doppler Velocimetry (UDV) transducers deployed in a 1:6 downscaled water model (radius $R = 163$ *mm*, height $H = 326$ *mm*).

2. Experimental Layout

Figure 1 shows the layout of this experiment, where Ω_p and Ω_c denote the axis of precession and rotation, respectively, and α is the angle of nutation between them. The identification of the flow states is done using UDV with ultrasound transducer that are located at various radial positions on one end cap of the cylinder. Measurements are performed sequentially, with only one transducer active at a time. The red arrows (the cones schematically show the exaggerated widening of the beam) in Figure 1 show how the axial velocity field is obtained using the ultrasound transducer at a particular radial location.

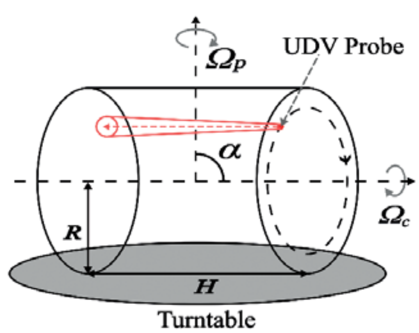

Figure 1. Schematic of the 1:6 downscaled water model

3. Objectives

Building on prior characterisations [1,2] of inertial modes and their dependence on the Poincaré number (precession ratio = Ω_p/Ω_c) and Reynolds number ($Re = 2\pi R^2\Omega_c/\nu$, ν being the kinematic viscosity),this work targets the transition regimes, associated hysteresis and the emergence of large-scale structures. Particular focus is given to the axisymmetric double-roll mode (azimuthal wave number $m = 0$, and axial wave number $k = 2$), which can be linked to the onset of dynamo action [3]. The upper and lower transition thresholds in Poincaré number for different Reynolds numbers remained insufficiently constrained in previous investigations, yet are essential for the forthcoming DRESDYN experiment.

A key aim of this study is therefore to establish these thresholds accurately and to identify the most effective strategy for reliably accessing and sustaining the double-roll mode flow state, achieved by approaching the transition regime using multiple complementary methodologies. These methodologies include systematic upward and downward sweeps of the Poincaré number using step sizes of varying magnitude, as well as sustained measurements at fixed Poincaré numbers over extended durations to obtain statistically converged axial velocity profiles.

Additional simultaneous data acquisition from pressure transducers on the end caps and power measurements also help in qualitatively identifying the flow transitions by correlation with the UDV data. This method will be particularly valuable at higher Reynolds numbers where UDV data alone becomes less reliable for flow state characterisation.

Acknowledgements

This project has received funding from Deutsche Forschungsgemeinschaft (DFG) under the research project 532905681 'Real-time identification of flow states in the DRESDYN precession experiment using distributed ultrasound sensors'.

References

[1] Giesecke A., Vogt T., Pizzi F., Kumar V., García G., Gundrum T., Stefani F., *The global flow state in a precessing cylinder*, 'Journal of Fluid Mechanics' 2024, vol. 998.

[2] Kumar V., Pizzi F., Giesecke A., Šimkanin J., Gundrum T., Ratajczak M., Stefani F., *The effect of nutation angle on the flow inside a precessing cylinder and its dynamo action*, 'Physics of Fluids' 2023, vol. 35, 014114.

[3] Giesecke A., Vogt T., Gundrum T., Stefani F., *Nonlinear Large Scale Flow in a Precessing Cylinder and Its Ability To Drive Dynamo Actio*, 'Physical Review Letters' 2018, vol. 120.

NUMERICAL ANALYSIS OF THE EFFECT OF GOTHIC VORTEX GENERATOR CHORDWISE LOCATION ON THE AERODYNAMIC CHARACTERISTICS OF THE NACA 4415 AIRFOIL

J.A. Jankiewicz

Wrocław University of Science and Technology, Faculty of Mechanical and Power engineering, PWr in Space, Wybrzeże Stanisława Wyspiańskiego 27, 50–370 Wrocław, Poland

E-mail: jjankiewicz5@gmail.com

Abstract. This numerical study analyzes the chordwise placement of gothic vortex generators (VGs) at Re = 3×10^6 using the SST Gamma ReTheta model. Validating and calibrating the eddy viscosity limiter a_1 proved essential to accurately predict flow separation. Results reveal that tested VGs delay separation and vorticity analysis shows boundary layer eruption phenomenon. VGs placed at 20% chord yielded the highest max lift coefficient (+35%), with them placed at 30% yielding +30% but allowing a higher *L/D*.

Keywords: Aerodynamics, Computational Fluid Dynamics, Vortex Generators, Boundary Layer, Transition Modelling.

1. Introduction

Flow separation control is a fundamental challenge in the aerodynamic design of aircraft wings and wind turbine blades. Passive vortex generators (VGs) are a standard solution due to their simplicity and effectiveness. While rectangular and triangular VGs have been extensively studied [1,2], the gothic geometry (characterized by a curved leading edge) offers a potential reduction in drag penalty [3]. Existing literature focuses predominantly on low Reynolds numbers (Re < 5×10^5) [4,5]. This study addresses a significant gap in literature regarding the chordwise placement of Gothic VGs in the high Reynolds number regime (Re ≈ 3×10^6). This regime is typical for General Aviation aircraft and wind turbine blades.

2. Methodology

The analysis employed steady-state *Reynolds-Averaged Navier-Stokes* (RANS), the Shear Stress Transport (SST) k-ω turbulence model coupled with the γ-Re_θ transition model [6,7]. Numerical simulations were conducted using *Ansys Fluent 2025 R1* on a 3D wing section with periodic boundary conditions. The domain was discretized using a polyhedral mesh with high near-wall resolution ($y^+_{avg} = 0.48$) to resolve the viscous sublayer.

2.1. Validation and model calibration

Preliminary validation against experimental data [8,9] for the clean airfoil revealed that the standard SST model constants ($a_1 = 0.31$) significantly over-predicted the maximum lift and delayed stall. To correct this, the eddy viscosity limiter was calibrated by reducing to $a_1 = 0.272$ [see Fig. 1.]. This modification reduced the over-production of eddy viscosity in regions of strong adverse pressure gradients, yielding decent agreement with experimental lift and drag polars. Although the experimental references date back to 1945 and 1982, they remain the primary sources for validation as, to the author's best knowledge, more recent experimental data for this Reynolds number is limited.

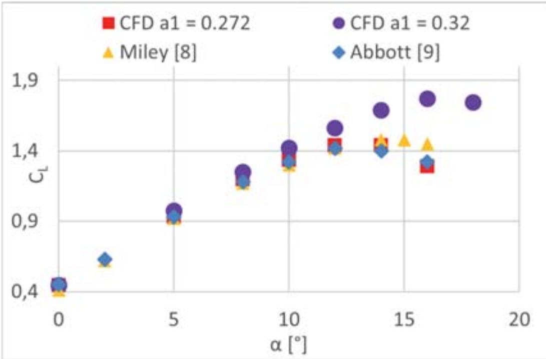

Figure 1. Model validation

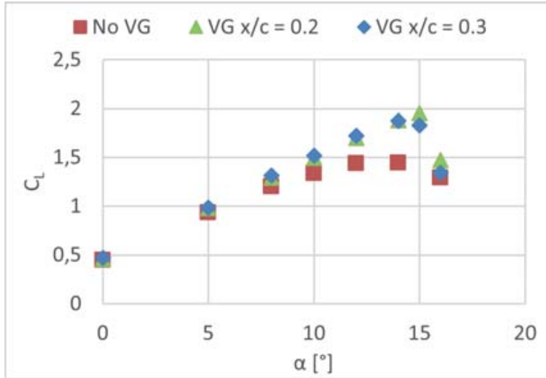

Figure 2. Comparison of lift coefficient (C_L) vs. angle of attack (α) for clean airfoil and wing sections with gothic VGs at x/c = 0.2 and x/c = 0.3

3. Results

Two chordwise locations for VGs were analysed: $x/c = 0.2$ and $x/c = 0.3$. The $x/c = 0.2$ configuration resulted in the highest maximum lift coefficient (C_{Lmax}), showing a 35% improvement over the clean baseline. The $x/c = 0.3$ configuration yielded a 30% increase (see Fig. 2). However, the configuration with VGs placed further downstream demonstrated lower drag and a higher C_L/C_D as well as higher endurance factor$(E = C_L^3/C_D^2)$.

Visualisations of the vorticity field show the occurrence of the boundary layer eruption phenomenon [10,11] downstream of the VGs.

References

[1] Jayanarasimhan K., Balasubramanian N.K., *An overview of flow control in aerodynamic surfaces using vortex generators*, 'Physics of Fluids' 2025, vol. 37.

[2] Moon H., Jeong J., Park S., Ha K., Jeong J.-H., *Numerical and experimental validation of vortex generator effect on power performance improvement in MW-class wind turbine blade*, 'Renewable Energy' 2023, vol. 212, no. 22, pp. 443–454.

[3] Sen W., Rahman K., Tanim I., *Experimental anf CFD Analysis On Car With Several Types of Vortex Generators*, [in:] Proceedings of the International Conference on Mechanical Engineering and Renewable Energy 2019, Chittagong 2019.

[4] Solnay D.Á., Molnár J., Lakatos I., *Effects of Location and Height of Vortex Generators on Aerodynamic Performance of NACA 4412 Airfoil*, 'Periodica Polytechnica Transportation Engineering' 2025, vol. 53, no. 3, pp. 267–276.

[5] James E., Zhang L., Lu K., *Numerical Study of Drag Reduction by Conventional and Micro Vortex Generators*, [in:] AIAA AVIATION 2021 FORUM, 2021.

[6] Menter F., *Two-equation eddy-viscosity turbulence models for engineering applications*, 'AIAA Journal' 1994, vol. 32, no. 8.

[7] Langtry R., Menter F., *Correlation-Based Transition Modeling for Unstructured Parallelized Computational Fluid Dynamics Codes*, 'AIAA Journal' 2009, vol. 47, no. 12, pp. 2894–2906.

[8] Miley S.J., *Catalog of low-Reynolds-number airfoil data for wind-turbine applications*, Office of Scientific and Technical Information (OSTI), Collego Station, Texas 1982.

[9] Abbott I., Von Doenhoff A.S.L., *Summary of Airfoil Data*, National Advisory Committee for Aeronautics, Langley Field 1945.

[10] Kudela H., Malecha Z., *Eruption of a boundary layer induced by a 2D vortex patch*, 'Fluid Dynamics Research' 2009, vol. 41, no. 5.

[11] Kudela H., Malecha Z., *Investigation of unsteady vorticity layer eruption induced by vortex patch using vortex particles method*, 'Journal of Theoretical and Applied Mechanics' 2007, vol. 45, no. 4, pp. 785–800.

THERMAL AND RHEOLOGICAL BEHAVIOR OF FLY ASH–BASED DEEP EUTECTIC SOLVENT DISPERSIONS

B. Jóźwiak

Lodz University of Technology, Faculty of Process and Environmental Engineering, 213 Wolczanska St., 93–005 Lodz, Poland

E-mail: bertrand.jozwiak@p.lodz.pl

Abstract. This study investigates the thermal conductivity and rheological properties of deep eutectic solvent (ChCl–EG 1:5 and 1:10) dispersions containing fly ash (2–20 wt%) as an alternative to conventional oxide fillers. Thermal conductivity increased nearly linearly with particle loading, reaching enhancements of up to 19%. All samples exhibited Newtonian behavior and moderate viscosity over the investigated range, indicating their suitability as heat transfer media.

Keywords: Interdisciplinary Areas in Heat and Fluid Flow, Rheology, Deep Eutectic Solvent Dispersion, Fly Ash.

1. Introduction

Deep eutectic solvents (DESs) are a new class of 'green' solvents which, due to their properties such as low toxicity and volatility, non-flammability, high thermal stability, tunable physicochemical properties, low cost and simple synthesis, have gained increasing attention in various industrial fields, including chemistry and biotechnology [1]. A typical DES is formed by mixing at least two components in an appropriate molar ratio, where one acts as a hydrogen bond donor (e.g., urea, glucose, ethylene glycol, glycerol) and the other as a hydrogen bond acceptor (e.g., choline chloride). By introducing a third component in the form of solid particles, DES-based dispersions can be obtained. The use of oxides is particularly advantageous due to their high chemical and thermal stability, biocompatibility, ease of production and tunable morphology [2]. An alternative to conventional oxide fillers may be fly ash – an inorganic waste generated during the combustion of hard coal, lignite, as well as municipal and industrial waste, produced globally in hundreds of millions of tons annually [3]. Owing to its abundance and wide availability, fly ash represents an attractive secondary raw material. Its use as a dispersed phase in deep eutectic solvents may not only enhance their functional properties (e.g., thermal conductivity), but also enable the valorization of a significant industrial waste stream, reducing its landfilling and environmental impact.

This study analyzes the effect of fly ash at different concentrations on the thermal conductivity and rheological properties of deep eutectic solvent dispersions with various molar ratios of the hydrogen bond acceptor to the hydrogen bond donor.

2. Materials and methods

The dispersed phase consisted of fly ash (dominated by Ca- and Cl-rich phases, with minor contributions of Na, K and S) obtained from Ekospalarnia Kraków (Figure 1, left). The base fluids were low-viscosity DESs (< 25 mPa·s at 25°C) composed of choline chloride (ChCl) and ethylene glycol (EG) at molar ratios of 1:5 and 1:10 [4]. Dispersions with particle concentrations of 2–20 wt% were prepared by ultrasonication using a VCX 750 homogenizer (Sonics & Materials, USA), operated in continuous mode for 10 min at 70% amplitude. Thermal conductivity was measured at 25°C using a KD2 Pro analyzer with a KS-1 sensor (Decagon Devices, USA). The rheological properties were determined at 25°C over a shear rate range of 1–100 s^{-1} by means of a Physica MCR 301 rheometer (Anton Paar, Austria) equipped with a concentric cylinder geometry.

3. Results and discussion

An increase in fly ash concentration led to a nearly linear enhancement of thermal conductivity for both ChCl–EG systems (Figure 1, right). For all investigated loadings, ChCl–EG (1:10) dispersions exhibited higher thermal conductivity than ChCl–EG (1:5). At the highest particle concentration (20 wt%), the enhancement reached approximately 19% for ChCl–EG (1:10), while only about 13% was observed for ChCl–EG (1:5). The lower thermal conductivity observed for the ChCl–EG (1:5) system may be attributed to its higher viscosity and stronger hydrogen-bonding interactions at elevated ChCl content. Increased ionic character likely leads to a more rigid and viscous supramolecular network, limiting molecular mobility and heat transport efficiency [5]. All samples remained Newtonian, liquid-like and non-gelled. Their viscosity increased with ChCl and fly ash concentrations, ranging from 21.4 mPa·s for pure ChCl–EG (1:5) to 91.1 mPa·s at 20 wt% particles. Slight sedimentation was observed after one day of storage, particularly at elevated fly ash loadings, possibly due to particle agglomeration. However, higher ChCl content improved dispersion stability, limiting phase separation.

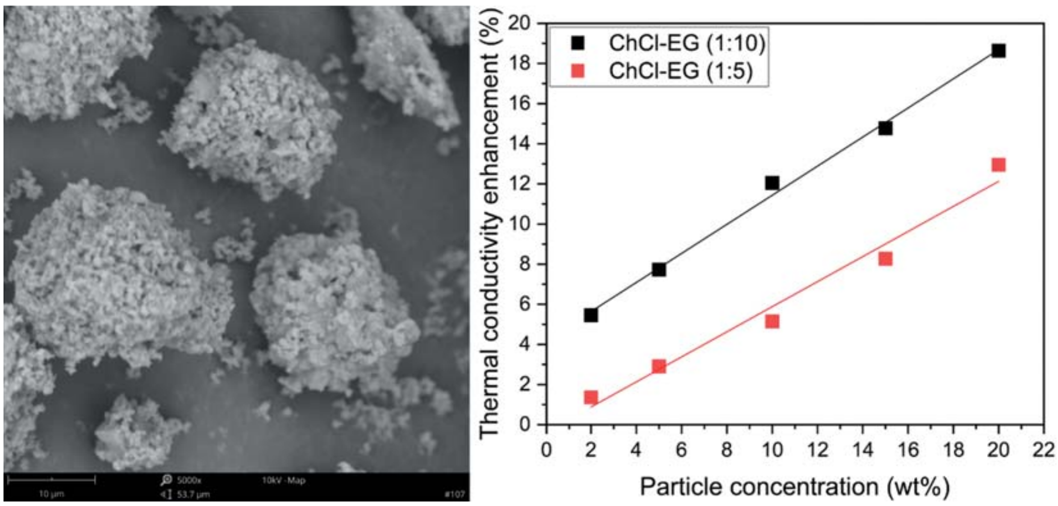

Figure 1. SEM micrograph of raw fly ash (left) and thermal conductivity enhancement of ChCl–EG dispersions containing fly ash (right)

References

[1] Płotka-Wasylka J., de la Guardia M., Andruch V., Vilková M., *Deep eutectic solvents vs ionic liquids: Similarities and differences*, 'Microchemical Journal' 2020, vol. 159.

[2] Nikolova M., Chavali M., *Metal Oxide Nanoparticles as Biomedical Materials*, 'Biomimetics' 2020, vol. 5, no. 2.

[3] Kępys W., Wisła-Walsh E., Matusik J., *Chemical Examination of Fly Ash and Bottom Ash Derived from Incineration of Hazardous Waste*, 'Inżynieria Mineralna' 2018, vol. 1, no. 1, pp. 221–234.

[4] Jóźwiak B., Dzido G., *Oxide nanoadditives as an effective route to thermal refinement of deep eutectic solvents*, 'International Journal of Thermal Sciences' 2025, vol. 215.

[5] Atilhan M., Aparicio S., A review on the thermal conductivity of deep eutectic solvents, 'Journal of Thermal Analysis and Calorimetry' 2023, vol. 148, pp. 8765–8776.

REVISITING THE 2ND-ORDER SEMI-DISCRETE FINITE VOLUME SCHEMES FOR HYPERBOLIC CONSERVATION LAWS ON CARTESIAN GRIDS

A. Kajzer

Institute of Fluid Flow Machinery, Polish Academy of Sciences, ul. Fiszera 14, 80–231 Gdańsk, Poland

E-mail: akajzer@imp.gda.pl

Abstract. The explicit time integration methods and the 2nd-order spatial schemes in the context of the finite volume method are of interest. A novel 2nd-order smooth slope limiter and its proper implementation is proposed. This new limiter, together with the reduction of the disparity between the physical and numerical domains of dependence by fixing the spatial gradients for all stages of the 2nd-order Runge-Kutta type methods, significantly improves the quality and accuracy of the solutions.

Keywords: Computational Fluid Dynamics, Finite Volume Method, Semi-discrete methods, MUSCL schemes.

1. Introduction

The semi-discrete [1] schemes for hyperbolic conservation laws on Cartesian grids are revisited. For the spatial discretisation the 2nd-order slope limited MUSCL schemes are used [1,2]. The author focuses on the explicit Runge-Kutta (RK) type methods of order two and three for the temporal discretisation, including those possessing the strong stability preserving (SSP) property. The reduction of the spatial stencils size by freezing the MUSCL slopes for the entire time step is shown to significantly improve the stability and accuray of the 2nd-order RK methods: SSPRK22 and mid-point rule (MIP) method. The MIP method with frozen slopes (FS), which can be interpreted as a semi-discrete, unstaggered variant of the MUSCL-Hancock (MH) scheme, can be used beyond the hyperbolic problems and is shown to be attractive alternative to SSPRK methods. Importantly, this holds for a wide range of the Courant numbers (Cr), including values close to the stability limit, while at low Cr the performance is very similar to SSPRK-based schemes.

Next, the author proposes a new one-parameter family of continuously differentiable 2nd-order total variation diminishing slope limiters which allows to control the required level of numerical diffusion to reduce (or eliminate) the spurious oscillations. The well-known harmonic limiter of van Leer is a special case of the new limiter. The proposed techniques provide stable simulations of fluid flows involving strong shocks. When a very low Mach number flow is considered, the MIPFS method together with the new slope limiter provide convergence while no convergence is obtained with the SSPRK methods and traditional limiters. Importantly, this improvement is obtained when simple and universal numerical flux is applied: approximate Riemann solver of HLL-type [1] with low-Mach corrected diffusive part [3].

2. Chosen examples

In Fig. 1 we present the solution of the 1D advection equation with constant velocity and discontinuous initial condition. Clearly, for larger Courant numbers the MIPFS method preserves the geometrical symmetry of the advected shape (i.e. the invariance w.r.t. the velocity direction) much better than SSPRK methods (with or without FS technique).

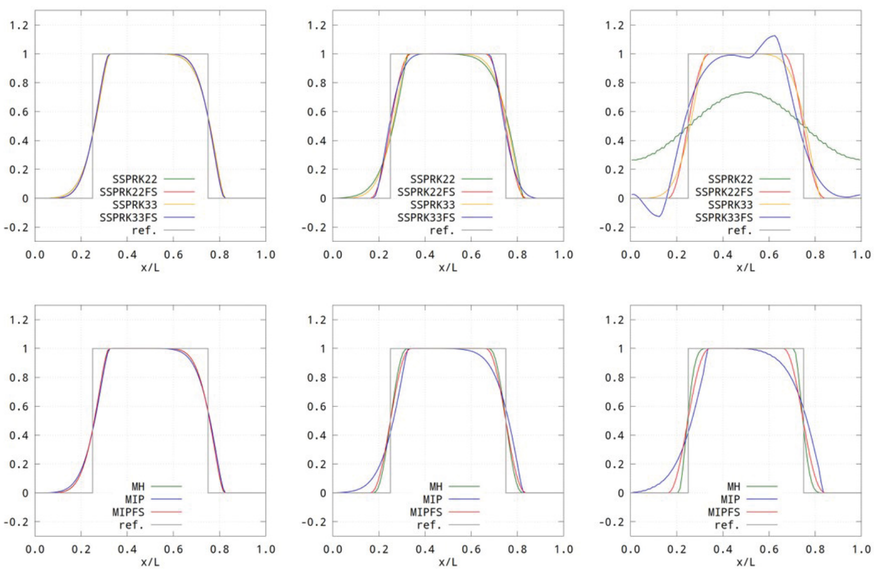

Figure 1. Numerical solution of the advection equation obained with different approaches; from left to right Cr = 0.1, 0.45 and 0.9

Figure 2 presents the results of a 2D inviscid flow simulation. The case of the stationary isentropic vortex is considered at Mach number 10^{-3}. The difficulty stems here from low variations of the density and the large disparity between the speed of sound and the convective velocity scale. The MIPFS with the new limiter outperforms the traditional approach.

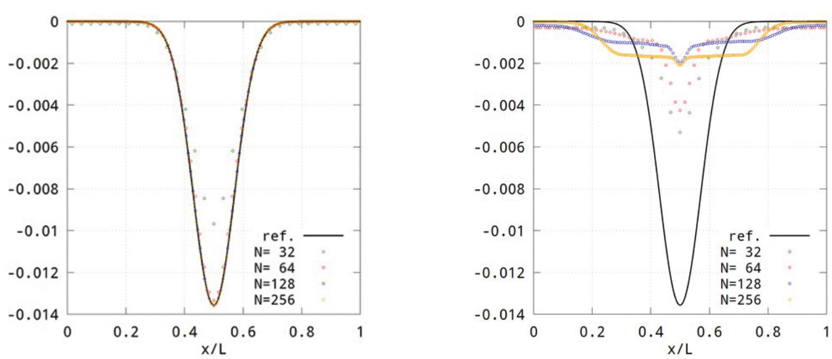

Figure 2. The density profiles in the case of the isentropic vortex after one revolution; MIPFS with new slope limiter and SSPRK22 with traditional van Leer limiter are shown in the left and right panels respectively

References

[1] Toro E.F., *Riemann Solvers and Numerical Methods for Fluid Dynamics*, Springer, Berlin–Heidelberg 2009.

[2] Berger M., Aftosmis M.J, Murman S.M., *Characterization of Space Shuttle Ascent Debris Using CFD Methods*, AIAA 43rd Aerospace Sciences Meeting, Reno 2005.

[3] Chen S.S ., Chao Y., Xiang X.H., 'Computers and Mathematics with Applications' 2022, vol. 75, pp. 3737–3755.

MIXING ENHANCEMENT VIA SHAPE ALTERING OF BLUFF BODY FLAME STABILIZERS

P. Kamiński, A. Tyliszczak

Department of Thermal Machinery, Czestochowa University of Technology, al. Armii Krajowej 21, 42-201 Częstochowa, Poland

E-mail: piotr.kaminski@pcz.pl

Abstract. This paper investigates mixing enhancement by altering the cross-sectional shape of a bluff body (BB) flame stabilizer. Large-eddy simulations are performed for four BB shapes: circular, star, triangle and square. An incompressible, isothermal air flow at $Re \approx 5000$ is assumed. The results show that the BB shape strongly influences the downstream region by modifying the size of the recirculation zone and the intensity, and spatial distribution of velocity fluctuations. In particular, shapes with sharper edges (most prominently the triangle and star) promote locally elevated turbulent kinetic energy in the shear-layer regions, thereby enhancing mixing.

Keywords: Computational Fluid Dynamics, Passive flow control, Mixing enhancement, Turbulent flame.

1. Introduction

Enhancing mixing within a turbulent flame is critical in combustion processes, where a uniform mixture of fuel and oxidizer ensures high combustion efficiency. This can be achieved via flow control techniques, which are commonly classified as passive or active. In this work, we focus on the passive approach, which relies on surface alterations and does not require an external energy input. Specifically, we consider bluff bodies (BBs) which have received considerable attention [1] and are widely employed as flame stabilizers. BBs redirect the gas flowing around them and form a recirculation zone which facilitates a more uniform air-fuel mixture. However, altering their shape can modify the characteristics of the surrounding flow, in particular its structure and dynamics [2] which in turn affects pollutant emissions [3]. In the present work, we employ large-eddy simulations (LES) to investigate the impact of various BB shapes on the recirculation zone and their potential for improving the combustion process.

2. Problem statement

Four BB shapes, shown schematically in Fig. 1a are considered and arranged in the direction of the flow. They are labeled as Crc, Str, Sqr, Tri and each of them is designed such that its cross-sectional area S at $y = 0$ is constant and identical between cases, e.g., $S_{circ} = S_{star}$. We assume an incompressible and isothermal air flow at $Re = DU_{in}/\nu \approx 5000$, where D denotes the diameter of the circular BB, U_{in} the inlet flow velocity and ν the kinematic viscosity. LES is performed using a two-stage approach (see Fig. 1b) in which the flow developing along BB is simulated with ANSYS Fluent, whereas the high-order in-house SAILOR code is used to model the flow above BBs, including the recirculation and downstream regions. This approach, described in detail in [4], ensures high accuracy and accelerates the simulation process.

a) b)

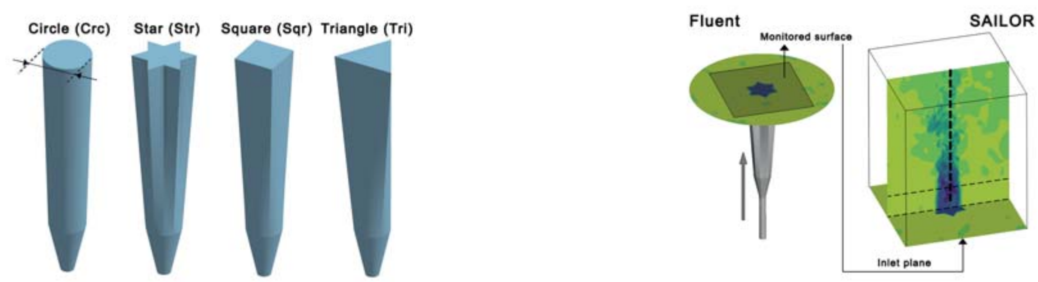

Figure 1. Bluff body shapes (a); numerical setup (b)

3. Preliminary results

The preliminary results indicate that the BB shape influences the downstream flow field, as evident from Fig. 2a which shows axial profiles of the mean axial velocity (black) and its RMS values (red), normalised by U_{in}. Specifically, variations in the recirculation zone length (intersection of the profiles with $U/U_{in} = 0$, indicated by the grey dashed line) are observed. The longest recirculation zone is found for Str, whereas the shortest is for the Crc case. This is accompanied by notable changes in velocity fluctuations which at $y/D < 1$ are reduced for Str, Tri, and Sqr. More modifications in the turbulence field are seen in Fig. 2b, which presents contour maps of u'/U_{in}^2 . Worth noting is that the distribution of u'/U_{in}^2 closely follows the BB shape, and a pronounced increase in u'/U_{in}^2 is observed inregions associated with BB edges, i.e., where the shear layer forms, contributing to enhanced mixing.

a) b)

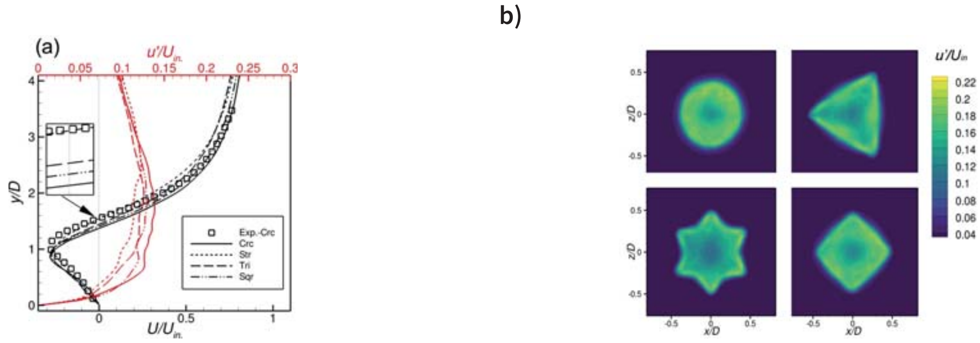

Figure 2. Axial profiles of the mean axial velocity (black) and its RMS values (red) in (a); contour maps of u'/U_{in}^2 extracted at $y/D = 1$ in (b)

Acknowledgments

This work is supported by the National Science Center in Poland (Grant 2020/39/B/ST8/02802) and PLGrid ACK Cyfronet AGH (Grants PLG/2024/017751 and PLG/2025/018864).

References

[1] Docquier N., Candel S., *Combustion control and sensors: a review* , 'Progress in Energy and Combustion Science' 2002, vol. 28, no. 2, pp. 107–150.

[2] Wei J., Xie Q., Zhang J., Ren Z., *Flow, mixing, and flame stabilization in bluff-body burner with decreased central jet velocity*, 'Physics of Fluids' 2021, vol. 33, no. 6.

[3] Nahvi M., Mazaheri K., Targhi M.Z., Eskandari F., *Experimental investigation of bluff body geometry effects on nitrogen oxides emissions from Cambridge stratified burner*, 'Scientific Reports' 2025, vol. 15, no. 1.

[4] Wawrzak A., Caban L., Tyliszczak A., Mastorakos E., *Numerical analysis of turbulent nitrogen-diluted hydrogen flames stabilised by star-shaped bluff bodies*, 'Applied Energy' 2024, vol. 364.

SHAKING THINGS UP: DYNAMIC CONTACT ANGLE HYSTERESIS MEASUREMENT USING A HARMONICALLY OSCILLATED SUBSTRATE

M. Klamka, T. Bobiński

Warsaw University of Technology, Institute of Aeronautics and Applied Mechanics, 24 Nowowiejska St., 00–665 Warsaw, Poland

E-mail: michal.klamka@pw.edu.pl, tomasz.bobinski@pw.edu.pl

Abstract. This work introduces an experimental method for measuring contact angle hysteresis using a harmonically oscillated substrate. The proposed approach reduces the uncertainty typical of conventional techniques, particularly at very high macroscopic contact angles and avoids the liquid modification required by novel techniques. We present a comparison of contact angle hysteresis measurement results obtained using our method and a classic tilted plane method.

Keywords: Experimental Fluid Mechanics, Measurement Techniques, Droplet, Wetting.

1. Introduction

Liquid-surface adhesion plays a crucial role in both nature and industry. Precise description of wettability is key to numerous industrial processes, from surface coating, through spray cooling, to the design of self-cleaning or hydrophobic surfaces. The adhesion force between a droplet and a surface is described by means of contact angle hysteresis which is the difference between the advancing and receding contact angles. Contact angle hysteresis directly corresponds to the force required to remove the droplet from the surface. Accurate measurement of contact angle is essential for a complete description of a droplet-substrate interaction. Conventional methods for contact angle hysteresis measurement, such as the sessile droplet method and the inclined surface method, suffer from increasing measurement uncertainty with superhydrophobic surfaces, exceeding 5 degrees at contact angles of 160° [1]. Recent advances [2] employing ferrofluid-doped water droplets exposed to magnetic fields show improved accuracy, but require liquid modification that may alter surface energy, which impacts the contact angle.

2. Controlled substrate motion contact angle hysteresis measurements

To circumvent these limitations, we developed an alternative approach in which oscillatory motion is applied directly to the substrate rather than to the droplet. A computer-controlled linear motor drives a carriage with a polished silicon wafer substrate, capable of generating accelerations up to 9 times the gravitational acceleration at a constant frequency of 10 Hz. The substrate is coated with Glaco Zero superhydrophobic surface treatment. High-speed camera documentation enables detailed analysis of droplet dynamics across a wide range of motion amplitudes and, consequently, accelerations.

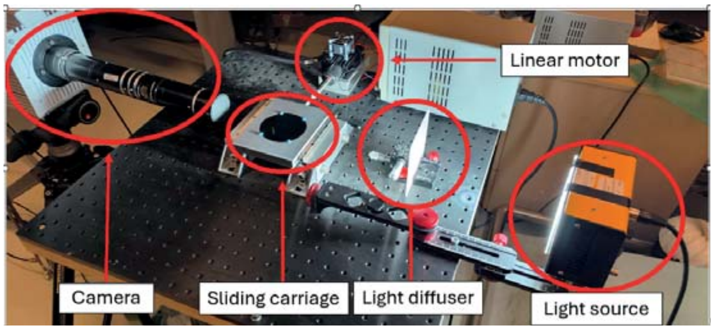

Figure 1. Experimental setup

3. Contact angle extraction

Edge extraction and corner detection algorithms process high-speed footage to determine contact angles. The image processing pipeline converts frames to luminosity matrices, calculates luminosity gradient magnitude for edge detection and employs polynomial fitting to the discrete set of edge points in the image to extract contact angle values. The algorithm provides comprehensive uncertainty quantification, including sensitivity to fitting coefficients and camera tilt.

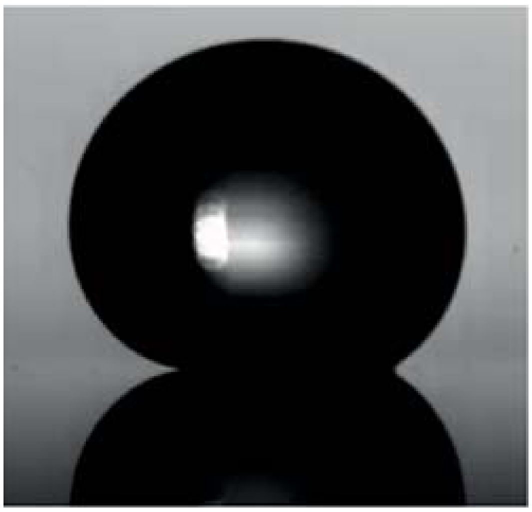

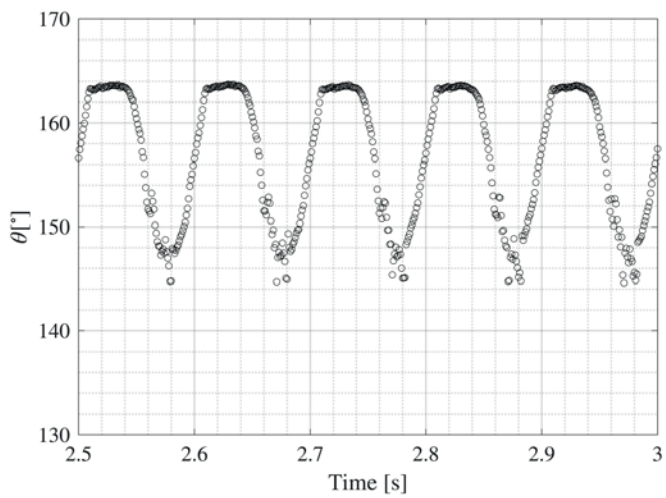

Figure 2. Footage (left) and extracted contact angle history $\theta(t)$ on the advancing side (right)

4. Conclusions

The oscillating-substrate methodology provides contact angle measurements with higher accuracy than conventional methods, without altering liquid properties. It also facilitates exploration of contact line velocity, dynamic contact angle measurement and demonstration of distinct droplet behaviour: adhesion-dominated sticking at low accelerations and rolling at higher accelerations.

References

[1] Liu K., Vuckovac M., Latikka M., Huhtamäki T., Ras R.H.A., *Improving surface-wetting characterization*, 'Science' 2019, vol. 363, no. 6432, pp. 1147–1148.

[2] Muhammad J., Nurmi H.A., Latikka M., Vuckovac M., RasR.H.A., *Oscillating droplet tribometer for sensitive and reliable wetting characterization of superhydrophobic surfaces*, 'Droplet' 2022, vol. 1, no. 1, pp. 38–47.

NEURAL NETWORK INLET CONDITION FOR SIMULATING BOUNDARY LAYER NATURAL TRANSITION

J. Knight, H. Medina, C. Ellis, S. Ambrose, H. Fadhila, C. Eastwick

University of Nottingham, Department of Mechanical, Materials and Manufacturing Engineering, University Park Campus, Nottingham, NG7

E-mail: egyjk5@nottingham.ac.uk

Abstract. Natural transition is simulated using a machine learning generated inlet condition trained on eigenvalue solutions to the Orr-Sommerfeld equation. The methodology removes the need for per-case linear stability solves, simplifying the process of modelling natural transition and removing the need for a forcing strip downstream to inject disturbances, enabling a reduction in overall computational domain by 15%. Predicted amplification factors of Tollmien-Schlichting (TS) waves from 2D simulations are found to reproduce stable/unstable behavior in agreement with experimental data.

Keywords: Computational Fluid Dynamics, Transition, Linear Stability, Machine Learning.

1. Introduction

The accurate prediction of boundary layer transition is of key importance for many sectors such as aerospace, automotive and wind energy, since transition location strongly influences drag performance and heat transfer. In low-disturbance environments, natural transition on a zero-pressure gradient flat plate is characterized by the amplification of two-dimensional Tollmien-Schlichting (TS) instability waves which are well described by classical linear stability theory.

CFD simulation of natural transition using linear stability theory has been shown to be feasible using localized forcing downstream of the inlet to inject disturbances [1] which mimic the effect of the vibrating ribbon often used in TS wave experiments. While this method is effective and accurate, it requires a longer development region upstream of the transition, increasing the computational cost. The aim of the present work is to replace the forcing strip used to trigger transition with a machine-learning generated inlet condition that reproduces the correct TS-wave disturbance directly at the inlet, across varying wave amplitudes within the T-S driven natural transition regime. This allows for the inlet to be positioned closer to the region of interest and therefore the overall computational domain can be shortened.

2. Neural Network

To produce inlet disturbances, a dataset of temporal stability eigenvalue solutions to the Orr-Sommerfeld equation with a parallel Blasius flow was generated. This dataset was used to train a fully connected feedforward neural network using supervised learning to predict the fluctuating velocity profiles required to trigger a TS wave. The network acts as a surrogate model, mapping the Reynolds number, non-dimensional frequency (defined as $F = (2\pi f \nu / U_\infty^2) \times 10^6$ with freestream velocity U_∞) and wall normal coordinate (Re_x, F, y) to the wall-normal distributions of fluctuating profiles (u', v'), avoiding repeated stability solves and enabling consistent inlet injection without using a forcing strip. The dataset covered a range of non-dimensional frequencies $1 < F < 226$ and Reynolds numbers $4 \times 10^4 < Re_x < 4 \times 10^6$. The network comprises of three hidden layers with 32 neurons, tanh activation and achieves a mean relative L_2 profile error of 3.8×10^{-5} on a validation set.

3. Preliminary 2D Results

The growth and decay of Tollmien-Schlichting (TS) waves on a zero-pressure-gradient flat plate are investigated numerically on the open-source finite-volume based CFD library XCALibre.jl [2], using the laminar solver. Two cases are shown, one with a decaying TS wave with non-dimensional inlet frequency $F = 162$ and one amplifying case at $F = 100$. The fluctuating profiles generated by the neural network are used as a sinusoidal, time varying inlet disturbance, on a Blasius mean profile and a disturbance amplitude of 0.001 m/s is used for both cases. The discretization of the domain in the streamwise direction was selected to ensure 128 cells per wavelength to fully resolve the TS wave, resulting in a two-dimensional quadrilateral mesh with 372,000 cells for the decaying case and 722,000 cells for the amplifying case. Second order discretization schemes were used in both space and time.

The amplification factor $N = \ln(A/A_0)$, where A is the root mean square of the streamwise velocity fluctuation at a given streamwise location (averaged over 10 flow-throughs), and A_0 is the amplitude at the location where the wave starts to amplify, quantifies the growth/decay of the TS wave. The numerical results are compared with experiments by Klingmann et al. [3] who investigated natural transition on a zero-pressure-gradient flat plate in a wind tunnel, using a vibrating ribbon to generate disturbances at a range of non-dimensional frequencies. Fig 1. shows that the simulations reproduce the expected behavior: growth of TS wave amplitude in the unstable region and then decay in the stable region which are consistent with the neutral stability curve in the Blasius boundary layer. Compared to the downstream forcing approach of [1], the domain length is reduced by at least 15% for both cases. Since the inlet disturbance can be imposed at arbitrary streamwise locations provided they lie within the linear amplification region, larger reductions are feasible. With the initial validation completed for 2D cases, work is underway to apply the methodology in 3D to investigate secondary instability and TS wave breakdown on the route to transition, with potential scope for applying the methodology to pressure gradient Falkner-Skan cases, by retraining on the appropriate stability eigenfunctions.

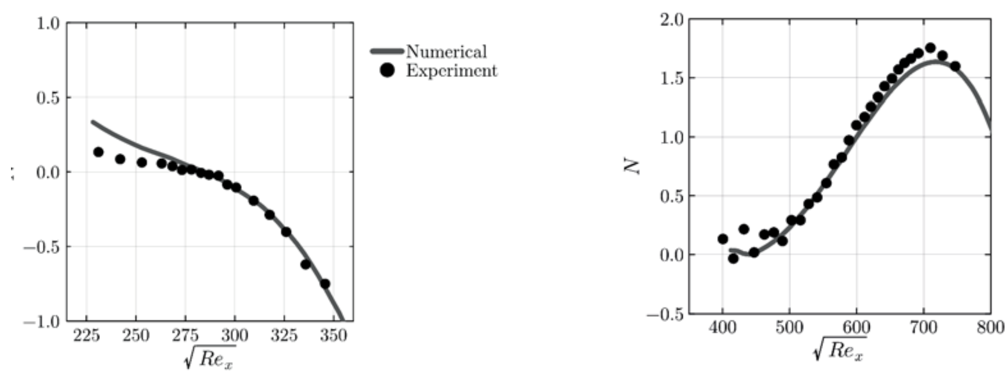

Figure 1. Amplification factor N versus square root of Reynolds number, Re_x, compared against experiment [3] for a decaying case (left) at $F = 162$, and an amplifying case (right) at $F = 100$

References

[1] Jee S., Joo J. Lin R.S., *Toward cost-effective boundary layer transition computations with large-eddy simulation*, 'Journal of Fluids Engineering' 2018, Vol. 140, no. 11, art. no. 111201.

[2] Medina H., Ellis C.D., Mazin T., Osborn O., Ward T., Ambrose S., Aleksandrova S., Rothwell B., Eastwick C., *XCALibre.jl: a Julia XPU unstructured finite volume computational fluid dynamics library*, 'The Journal of Open Source Software' 2025, vol. 10, no. 107, p. 7441.

[3] Klingmann B.G.B, Boiko A.V., Westin K.J.A., Kozlov V.V., Alfredsson P.H., *Experiments on the stability of Tollmien–Schlichting waves*, 'European Journal of Mechanics B-fluids' 1993,vol. 12, no. 4, pp. 493–514.

TRANSITIONAL FLOW REGIMES IN TANDEM CONFIGURATIONS OF TRIANGULAR CYLINDERS

A. Kocoń, R. Gnatowska

Czestochowa University of Technology, Department of Thermal Machinery, 21 Armii Krajowej Ave., 42–200 Czestochowa, Poland

E-mail: agnieszka.kocon@pcz.pl

Abstract. Flow regimes of tandem triangular cylinders were studied using PIV at Re = 10^4 with a fixed spacing of 6D, representing the transitional regime between reattachment and co-shedding flows. Apex and rotational angles were examined for triangular and square downstream bodies. Triangular cylinders may produce up to 2 times longer wakes; apex angle affects wake stability, while rotational angle governs wake symmetry.

Keywords: Experimental Fluid Mechanics, Triangular Cylinders, Apex Angle, PIV.

1. Introduction

Previous studies have shown that triangular cylinders can strongly alter flow characteristics [1-3]. In tandem configurations, the upstream body shape influences wake structures, with sharp triangular leading edges delaying flow regime transitions compared to square cylinders [2]. Small angular variations in triangular arrangements affect flow symmetry, vortex distribution, and turbulence intensity [4]. These findings motivate a systematic investigation of apex and rotational angle effects and the classification of flow regimes at a fixed spacing of 6D, corresponding to the transitional regime between reattachment and co-shedding flows [2,5].

2. Methodology

The experiments were conducted in a closed-loop wind tunnel with a square cross-section of 0.3 × 0.3 m and a length of 2 m. Two tandem configurations were considered: TT and TS, comprising an upstream triangular cylinder and a downstream triangular (TT) or square (TS) cylinder of equal dimension (D = 0.02 m, base edge length). Three upstream apex angles (60°, 45° and 30°) and three orientations relative to the flow (0°, 90° and 180°), denoted as T60–T30 and A0–A180 were examined respectively. A fixed spacing of 6D and a single Reynolds number of Re=10^4 were examined. Velocity fields were measured using PIV at a sampling frequency of 600 Hz over a total acquisition of 10 s.

3. Results

Figure 1 shows the dimensionless streamwise velocity fields for case T30 A90, while Figure 2 presents the dimensionless wake length behind the upstream cylinder for different upstream orientations in the TS and TT configurations.

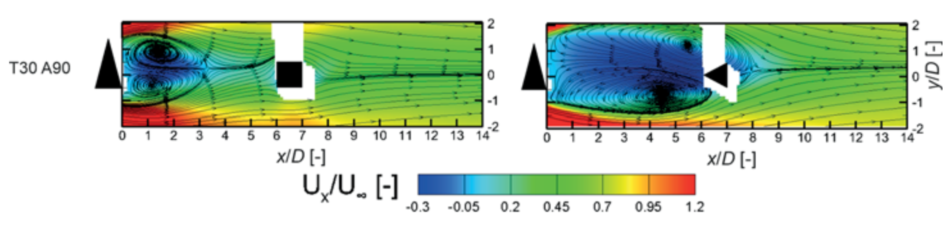

Figure 1. Dimensionless streamwise velocity field

The representative case T30 A90 (Fig. 1) highlights the differences observed between the TS and TT configurations. TT arrangement exhibits longer recirculation zones, lower turbulence levels and more organised vorticity patterns, whereas the TS configuration produces shorter wakes, higher turbulence, an earlier velocity recovery.

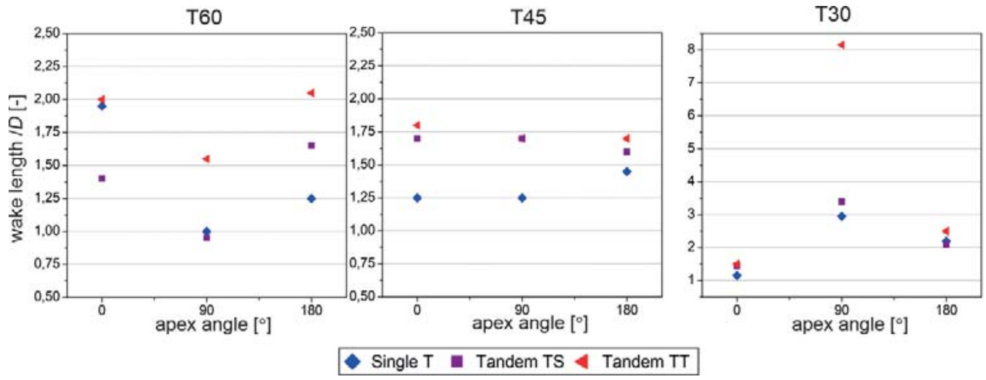

Figure 2. Dimensionless wake length behind upstream cylinder

These trends are further illustrated in Fig. 2 which shows that TT configurations generate longer wakes behind the upstream body. Overall, these observations indicate that the shape and orientation of the upstream body strongly influence wake development.

4. Conclusions

The results show that TT configurations promote wakes with higher coherence of vortical structures and more organized patterns than TS configurations. Wake dynamics are strongly influenced by the upstream cylinder orientation which alters the effective frontal area and shear-layer alignment. Larger apex angles (T60) enhance wake symmetry and smoother reattachment, whereas smaller angles (T30) increase instability and orientation sensitivity. In summary, these findings indicate that triangular cylinders offer an effective passive method for bluff-body wake control, with wake characteristics tunable via apex angle and orientation.

Acknowledgements

This work was supported by the Polish National Science Centre under grant UMO-20204/5339/B/ST8/02908802 and the Statutory Funds of Czestochowa University of Technology BS/PB-100-301/2025/P.

References

[1] Agrwal N., Dutta S., Gandhi B.K., *Experimental investigation of flow field behind triangular prisms at intermediate Reynolds number with different apex angles*, 'Experimental Thermal and Fluid Science' 2016, vol. 72, pp. 97–111.

[2] Niegodajew P., Gajewska K., Elsner W., Gnatowska R., *Experimental investigation of flow characteristics around tandem arrangement of triangular and square cylinders*, 'Journal of Fluids and Structures' 2024, vol. 124, no. 6.

[3] Hamid A.H.A., Noh M.H.M., *Laminar Flows Over Equilateral Triangular Cylinders in tandem arrangement*, 'Journal of Mechanical Engineering' 2020, vol. SI9, no. 1, pp. 137–152.

[4] Gnatowska R., Kocoń A., Gajewska K., *Experimental investigation of flow characteristics around triangular cylinders in various angular orientations in a tandem configuration*, 'Ocean Engineering' 2025, vol. 331.

[5] Martinuzzi R.J., Havel B., *Turbulent Flow Around Two Interfering Surface-Mounted Cubic Obstacles in Tandem Arrangement*, 'Journal of Fluids Engineering' 2000, vol. 122, no. 1, pp. 24–31.

DEVELOPMENT OF AERODYNAMIC COMPONENTS IN A SMALL WIND TURBINE BY THE GUST TEAM

A. Kołata, K. Zawadzki, W. Tomecki, M. Dorenda, K. Rozbicki, J. Klepacz, K. Juszczak, G. Widerska, J. Maciejewski, M. Lipian, M. Kulak, K. Olasek

Lodz University of Technology, Institute of Turbomachinery, 217/221 Wolczanska St., 93-005 Lodz, Poland

E-mail: gustproject.imp@gmail.com

Abstract. Over the years, GUST team has taken the following small wind turbine blade properties into account to optimize its performance: amount, airfoil, pitch angle, chord length, overall span and mounting. Every year, the team conducted tests in a wind tunnel at the International Small Wind Turbine Contest to check performance of their design. Due to aerodynamic improvements implemented between 2016 and 2024, the maximum efficiency of the turbine increased from 0.31 to 0.41. High efficiency and better adaptation to wind conditions enabled an increase in annual energy production of up to 80%.

Keywords: Aerodynamics, Small Wind Turbines, Flow Machinery, Wind Tunnel.

1. Introduction

The GUST Project (Generative Urban Small Turbine), developed within the Power Engineering Students Association at Lodz University of Technology, has been designing a Small Wind Turbine (SWT) for individual users since 2015. The turbine is limited to a rotor area of $A \leq 2$ m², corresponding to a 1.6 m diameter Horizontal Axis Wind Turbine (HAWT). The maximum power of the turbine is approximately 1-1.5 kW. This article summarizes the development of the turbine from 2016 to 2026, focusing on the evolution of design concepts and aerodynamic solutions. The project's goal is to continuously improve performance by increasing power output, efficiency and annual energy production (AEP). Annual wind-tunnel testing at TU Delft during the International Small Wind Turbine Contest has guided these improvements and supported steady aerodynamic and structural optimization.

2. Optimization of aerodynamic properties

Wind turbine aerodynamics and power curves are primarily shaped by rotor diameter and the use of a Variable Pitch Mechanism (VPM) which optimizes the angle of attack for higher output and low-wind self-starting. While large-scale turbines standardize three blades to balance efficiency against material and transport costs, SWTs often justify a higher blade count for specific performance needs.

Furthermore, rotational speed is limited by noise regulations, directly influencing the blade twist distribution and the Reynolds number critical for laminar-turbulent flow [1]. Subsequently, the airfoil shape, chord length and twist determine the lift-to-drag ratios and structural properties. For household SWT, maximizing year-round self-consumption through a low cut-in speed is prioritized over the total energy volume produced.

3. Performance of the GUST wind turbine

From the beginning of the GUST project, the aerodynamic design of the turbine has been constantly modified to achieve the best possible performance in both power generation and Annual Energy Production, two key parameters of SWT. Figure 1 shows the historical evolution of the GUST wind turbine aerodynamic design. Every year novel solutions are presented, with their positive outcomes reflected in the curves of Power and AEP, based on the wind tunnel tests.

Figure 1 GUST wind turbine results obtained through wind tunnel testing at TU Delft

From 2015 to 2017, at the beginning of the blade design process, a decision was made that rotor geometry would not be changed via pitch adjustment under operation and only a fixed-pitch rotor configuration would be considered. Initially the design focuses on a three-bladed, fixed-pitch rotor optimized for a 3–12 m/s wind speed range which accounts for 98% of total energy production. The geometry utilizes S834 and S826 airfoils. In 2018 new research has showed that maximum power is obtained at TSR ≈ 3.75, where Cp = 0.307. In 2019 studies showed that the highest decremental AEP values occur at wind speeds of 6–7m/s.

From 2021 to 2022, the focus shifted from optimizing S826 chord lengths and solidity to introducing the SG6043 airfoil for better low-Reynolds number performance. QBlade [2] simulations of six configurations revealed that 4-bladed rotors excel at low TSR, while 3-bladed SG6043 rotors offer higher efficiency at elevated TSR. In 2024, refinements to the SG6043 design – including a smaller hub, a 1 cm length extension and the introduction of pitch control – resulted in a higher Cp for TSR > 4. By 2025, adaptations moved back to the S826 airfoil with a variable pitch hub, featuring a 15 mm tip extension and a converging section to further boost aerodynamic adaptability and power generation.

4. Conclusions

After almost a decade of intensive research into the design of our wind turbine, the authors investigated key parameters. This work was conducted both independently and in international collaboration and supported by advanced computer simulations as well as practical testing in wind tunnels. The authors achieved maximum turbine efficiency of 0.41 and an increase in annual energy production of approximately 80%. The above research has demonstrated that in-depth analysis of blade design is a critical factor in determining the efficiency of a wind turbine.

References

[1] Kądrowski D., Kulak M., Lipian M., Stępień M., Baszczyński P., Zawadzki K., Karczewski M., *Challenging low Reynolds – SWT blade aerodynamics*, MATEC Web of Conferences. EDP Sciences, 2018, https://www.matec-conferences.org/articles/matecconf/pdf/2018/93/matecconf_bultrans2018_01004.pdf (access: 02.04.2026).

[2] Marten D.-I.D., *QBlade – Next Generation Wind Turbine Simulation*, QBlade.org, 2026, https://qblade.org/ (access: 02.04.2026).

IMPACT OF ORIENTATION ANGLE ON VORTEX SHEDDING AND NOISE GENERATION OF A SQUARE CYLINDER IN LOW-VELOCITY AIRFLOWS

J.M. Kopania

Lodz University of Technology, Żeromskiego 116, 90–924 Lodz, Poland

E-mail: joanna.kopania@p.lodz.pl

Abstract. This study presents an aeroacoustic and aerodynamic investigation of a square cylinder at low Reynolds numbers, focusing on the impact of airflow velocity and orientation angle on noise generation and wake dynamics. Experimental measurements conducted in an anechoic chamber reveal that increasing inflow velocity shifts acoustic peak frequencies upward, while the cylinder's rotation angle significantly alters the spectral composition and the velocity field distribution. The results provide a physical interpretation of vortex shedding and acoustic shadowing, offering valuable data for optimising ventilation system components and validating numerical flow models.

Keywords: Experimental Fluid Mechanics, Measurement Techniques, Aeroacoustics.

1. Introduction

Aeolian tones generated by air flowing over structural objects are a critical focus of engineering research, essential for understanding fluid dynamics and validating numerical models. The study of circular and rectangular cylinders emphasizes complex wake dynamics [1, 2, 3, 4, 5]. For rectangular geometries, the length-to-width (L/D) ratio remains a decisive factor in determining both the nature and frequency of these acoustic events [6]. This study examines the acoustic and aerodynamic characteristics of a square cylinder at low Reynolds numbers, typical for ventilation systems. The experimental methodology allowed the determination of one-third-octave spectral analysis at different angle positions of the studied square rod from multiple microphone positions. Additionally, the velocity field before and after the rod was determined. These integrated datasets provide a detailed physical interpretation of the correlation vortex evolution and aeroacoustics emissions of the studied object.

Test procedure

The measurements were performed on a specially constructed open-end test stand (with the outlet for the anechoic room) at the Institute of Power Energy in Lodz, similar to an open jet anechoic wind tunnel at the Institute of Sound and Vibration Research, University of Southampton [7]. Airflow was induced by a fan mounted on the inlet of the stand and regulated by the power inverter. An acoustically lined three-muffler was positioned between the fan and anechoic chamber to reduce fan-induced noise at the test section further. The anechoic test chamber is cubic, approximately 350 m³ in volume, and has walls that are acoustically treated with foam wedges, providing a reflection-free environment. In these studies, acoustic and aerodynamic measurements were performed on a single square cylinder (17 × 17 mm). The cylinder was supported by two vertical side plates that were mounted to the short sides of the nozzle. The four angles of square position in relation to air flow were studied: 0°, 15°, 30° and 45°.

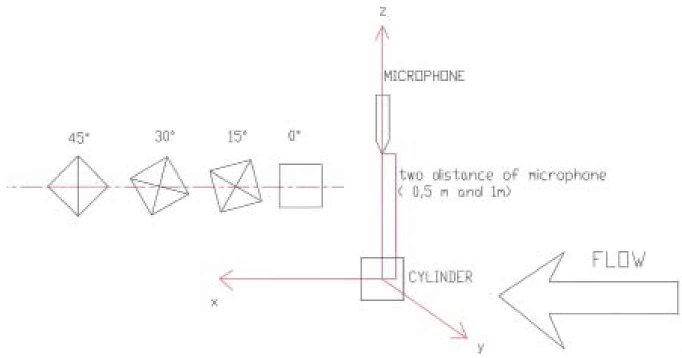

Figure 1. Scheme of studied square cylinder in the anechoic chamber

The noise measurements were done in low air-flow velocities – 1 m/s, 2.5 m/s, 5 m/s, 7 m/s, 10 m/s and 12 m/s – which can be referenced to the flow in the ventilation system (elements like grills, diffusers and slats). The measurements of 1/3-octave SPL spectrums were recorded using the Nor 140 measuring set with the Nor850 software with filter Lin and a fast detector in two distances (0.5 m and 1 m). Data were obtained for 10 s measurement time with a sampling rate of 48 kHz and an RMS detector of 0.1 dB. The mean velocity in the outlet of the stand test (before and after the rod) was measured by using a wing anemometer connected with an HD 2103.2 instrument and calculated by using the logarithmic Chebyshev method. Additionally, detailed flow measurements every 5 mm in the cross-section of the airflow field at the outlet of the channel in front of and behind the rod have been performed using the thermo-anemometer measurement technique to know the velocity distribution.

2. Conclusions

In this work, the 1/3 SPL spectrum and Strouhal number depended on the air inflow velocity and angle position of the studied square rod. The Strouhal number generally falls in the range of 0.12 to 0.16 for the primary vortex shedding frequency, as it was reported in literature. But results also show that increasing inflow velocity causes the primary SPL peak to shift toward higher frequencies, and the cylinder's orientation significantly impacts noise intensity and spectral composition. For example, a rod with the 0° angle produces a single peak, while the 45° angle causes the peak to split into two lower-intensity components. Additionally, velocity field mapping revealed distinct areas of acoustic shadowing and local velocity increases that vary according to the rod's position. Notably, the velocity shadowing region was found to be significantly larger at a 45° angle compared to the 0° configuration.

References

[1] Williamson C.H.K., *Vortex Dynamics in the Cylinder Wake*, 'Annual Review of Fluid Mechanics' 1996, vol. 28, no. 1, pp. 477–539.

[2] Zdravkovich M.M., Bearman P.W., *Flow Around Circular Cylinders Volume 1: Fundamentals*, 'Journal of Fluids Engineering' 1998, vol. 120, no. 1, p. 216.

[3] Matsumoto M., *Vortex shedding of bluff bodies: a review*, 'Journal of Fluids and Structures' 1999, vol. 13, no. 7–8, pp. 791–811.

[4] Joubert E.C., Harms T.M. and Venter G., *Computational simulation of the turbulent flow around a surface mounted rectangular prism*, 'Journal of Wind Engineering and Industrial Aerodynamics' 2015, vol. 142, pp. 173–187.

[5] Deniz S., Staubli T., *Oscillating rectangular and octagonal profiles: interaction of leading- and trailing-edge vortex formation*, 'Journal of Fluids and Structures' 1997, vol. 11, no. 1, pp. 3–31.

[6] Morgenthal G., *Fluid Structure Interaction Bluff-body Aerodynamics and Long-span Brige Design: Phenoma en Methods*, University of Cambrige, Department of Engineering, 2000.

[7] Fujita H., Sha W., Furutani H., Suzuki H., *Experimental investigations and prediction of aerodynamic sound generated from square cylinders*, 4th AiAA/CEAS Aeroacoustics Conference, Tolouse (France) 1998.

FLOW OF DNA CHAINS IN MOLECULAR AND MICROFLUIDIC SYSTEMS

T.A. Kowalewski

Institute of Fundamental Technological Research PAN, 5B Pawinskiego St., 02–106 Warsaw, Poland

E-mail: tkowale@ippt.pan.pl

Abstract. The flow of DNA chains can be interpreted both as the transmission of genetic information and as the physical transport of long biopolymers in driven environments. This contribution summarizes the molecular basis of DNA information flow – replication, transcription and translation – and connects it to recent advances in the controlled motion, stretching and manipulation of DNA in micro- and nanofluidic systems. Bridging molecular biology with soft-matter physics enables new approaches to single-molecule analysis, genome mapping and lab-on-chip technologies. Particular emphasis is placed on the nonequilibrium dynamics of DNA under confinement and external forcing, as well as on the limitations of current theoretical models.

Keywords: Micro-, Nano- and Bio-flows.

1. Introduction

DNA is the fundamental carrier of genetic information in all living organisms. The classical central dogma describes the unidirectional flow of information from DNA to RNA to protein. Beyond this informational perspective, DNA is also a semi-flexible polymer whose transport, deformation and alignment under flow are of increasing importance in biophysics and biotechnology. Understanding both aspects of DNA flow is essential for modern genomics, synthetic biology and microfluidic diagnostics. In recent years, micro- and nanofluidic technologies have enabled direct visualization and manipulation of single DNA molecules. This has opened a new research field at the interface of molecular biology, polymer physics and microfluid mechanics, where DNA is treated as an active material subject to hydrodynamic forces, electrostatic interactions and geometrical confinement.

2. Molecular Information Flow in DNA

DNA replication is a semi-conservative process ensuring accurate genome duplication prior to cell division [1]. The coordinated action of helicases, polymerases and ligases yields extremely low error rates, on the order of 10^{-9} per base pair after proofreading [2]. Transcription converts genetic information into RNA via RNA polymerase-driven synthesis, followed in eukaryotes by splicing, capping and polyadenylation. Translation at the ribosome decodes mRNA into proteins, with ribosomal RNA catalyzing peptide bond formation. Translation rates typically range from 5 to 20 amino acids per second and depend on codon usage and ribosomal kinetics [3].

While DNA → RNA → protein is the dominant pathway, important extensions exist. Reverse transcription enables RNA-to-DNA information transfer in retroviruses and RNA-dependent RNA polymerases replicate RNA genomes in RNA viruses. Epigenetic regulation, including DNA methylation and histone modification, modulates gene expression without altering nucleotide sequences [4]. These mechanisms illustrate that information flow in biological systems is more flexible and adaptive than the classical linear scheme suggests.

3. Physical Transport and Deformation of DNA

From a physical standpoint, DNA behaves as a charged, semi-flexible polymer with a persistence length of approximately 50 nm. Under confinement and external forcing, DNA exhibits stretching, coiling-stretch transitions, anisotropic diffusion and strong hydrodynamic coupling to surrounding fluid. Recent experiments in micro- and nanofluidic systems demonstrate precise control of DNA motion using pressure-driven flow, electric fields and geometrical confinement [5]. In particular, the work reported in [6] shows that long DNA molecules can be reproducibly stretched to more than 80–90% of their contour length in engineered microchannels. These results provide quantitative insight into DNA rheology, polymer–wall interactions and nonequilibrium conformational dynamics.

Such experiments confirm that DNA dynamics cannot be described solely by equilibrium polymer statistics. Instead, strong coupling between hydrodynamic forces, thermal fluctuations and molecular elasticity must be taken into account. This is especially important in lab-on-chip devices, where confinement scales are comparable to the persistence length of DNA.

4. Critical Perspective on Recent Modeling Approaches

A recent theoretical study by Słowicka et al. [7] proposes a continuum framework for DNA transport in microfluidic environments. While the model provides an analytically tractable description of polymer migration under external forcing, it relies on several strong assumptions that limit its physical relevance. In particular, DNA is treated as an effectively homogeneous viscoelastic continuum, neglecting its discrete molecular structure, long-range hydrodynamic interactions and stochastic conformational fluctuations. As a result, important phenomena observed experimentally – such as coil–stretch transitions, intermittent trapping near channel walls and large molecule-to-molecule variability – cannot be captured by the proposed formulation.

Moreover, the model in [7] does not account for electrostatic effects and counterion dynamics which are known to play a dominant role in DNA mobility and stretching in realistic microfluidic conditions. Consequently, while the approach may be useful for qualitative scaling arguments, it should not be interpreted as a predictive theory for single-molecule DNA transport.

This highlights a broader issue in current literature: overly simplified continuum models may obscure the fundamentally stochastic and multiscale nature of DNA flow and should be carefully validated against single-molecule experiments.

5. Conclusions

The concept of DNA flow unifies genetic information transfer with polymer transport physics. Classical molecular biology establishes how information is replicated and expressed, while modern microfluidics enables direct control of DNA as a flowing chain.

Future research should integrate single-molecule experiments, mesoscale simulations and refined theoretical models that explicitly account for molecular discreteness, hydrodynamic interactions and electrostatic effects. Such an approach is essential for reliable prediction and control of DNA behavior in micro- and nanoscale devices, with direct implications for diagnostics, genome mapping and synthetic biology.

References

[1] [Meselson M., Stahl F.W., The replication of DNA in Escherichia coli, '*Proceedings of the National Academy of Sciences of the United States of America*' 1958, vol. 44, no. 7, pp. 671–682.

[2] Kornberg A., Baker T.A., *DNA Replication*, 2nd ed., University Science Books, Sausalito 2005.

[3] Rodnina M.V., Wintermeyer W., '*Current Opinion in Cell Biology*' 2009, vol. 21, no. 3, pp. 435–443.

[4] Jaenisch R., Bird A., Epigenetic Regulation of Gene Expression: How the Genome Integrates Intrinsic and Environmental Signals, '*Nature Genetics*' 2003, vol. 33, pp. 245–254.

[5] Zembrzycki K., Pawłowska S., Pierini F., Kowalewski T.A., Brownian Motion in Optical Tweezers, a Comparison between MD Simulations and Experimental Data in the Ballistic Regime, '*Polymers*' 2023, vol. 15, no. 3.

[6] Pawłowska S., Kowalewski T.A., Pierini F., Fibrous polymer nanomaterials for biomedical applications and their transport by fluids: an overview, '*Soft Matter*' 2018, vol. 14, pp. 8421–8444.

[7] Słowicka A.M., Xue N., Liu L., Nunes J.K., Sznajder P., Stone H.A., Ekiel-Jeżewska M.L., Highly elastic fibers in a shear flow can form double helices, '*New Journal of Physics*' 2024, vol. 26.

ACTIVE FLOW CONTROL FOR DRAG REDUCTION – MACHINE LEARNING STRATEGIES COMPARISON

T. Krakowski[1], **W. Stankiewicz**[2]

[1, 2] *Poznan University of Technology, Institute of Applied Mechanics, ul. Jacka Rychlewskiego 1, 61–131 Poznan, Poland*

E-mail: tomasz.krakowski@put.poznan.pl

Abstract. This study investigates active flow control for drag reduction using waste heat converted into electrical energy. A rotating cylinder was tested with a 3D model and wind tunnel validation (Re 8798–70388). The PPO-based DRL controller reduced drag by ~6% with robust performance, the PID controller achieved ~5% with lower adaptability and open-loop control gave ~3% with oscillations.

Keywords: Computational Fluid Dynamics, Active Flow Control, Deep Machine Learning, Drag Reduction.

1. Introduction

One of the biggest concerns in engineering is how to transport people and goods efficiently, which requires increasingly faster and more energy-efficient vehicles. However, power demands continue to grow, while fossil fuel reserves and electrical energy resources remain limited.

In road vehicles, nearly 50% of the chemical energy from fuel is lost as waste heat in the engine. At a constant speed of 80 km/h, approximately 50% of the non-thermal losses are attributed to aerodynamic drag, while drivetrain and rolling resistance account for around 38% [1]. The implementation of thermoelectric systems for recovering engine waste heat can generate up to 1 kW of electrical power from a diesel truck engine [2]. This recovered energy can be used to power active aerodynamic actuators like fans or rotating components of vehicle body. Compared to passive aerodynamic devices, active systems have been shown to reduce aerodynamic drag more effectively.

The control system developed for this task must be robust and versatile. The utilization of deep machine learning offers the potential to reduce the complexity associated with model development and tuning. As a test case, a rotating cylinder was selected for numerical investigations. The present study extends the concept introduced in previous work [3] by transitioning from a two-dimensional numerical framework to a fully three-dimensional configuration and by complementing the simulations with wind tunnel experiments. This approach enables a more realistic representation of flow structures and provides experimental validation of the control strategy under practical operating conditions. The added comparison baseline is a PID regulator with tabulated coefficients and open-loop regulation. Active flow control training environments need to be prepared carefully and have a high level of fidelity, while also employing dimension reduction to ensure the model can provide reasonable response times during the training process. This can be achieved using tailored (designed for faster convergence and validated against the k-omega SST) turbulence models which were applied in the control part of the study.

2. Test and numerical setup

The test set consists of a rotating cylinder assembly, with pressure-sensing orifices installed on the cylinder surface in eight sections (input to the controller). The cylinder is mounted on a rotational table which allows the angular velocity to be set. The coarse computational mesh cross-section is shown in Figure 1. The mesh is designed to obtain high-fidelity flow data in the test section of a small wind tunnel (Armfield C30).

The computational domain consists of a velocity inlet (maximum 4 m/s which corresponds to 40 m/s in the test section) and a pressure outlet. The mesh contains 4.5 million hexahedral elements. The boundary layer sizing aims to achieve $y^{+} \sim 1$ for both the cylinder walls and the tunnel test section. The Reynolds numbers for the studied flow cases are 8798 (5 m/s), 35194 (20 m/s) and 70388 (40 m/s). The cylinder diameter (25 mm) is used as the characteristic length and the upstream flow velocity defines the flow condition.

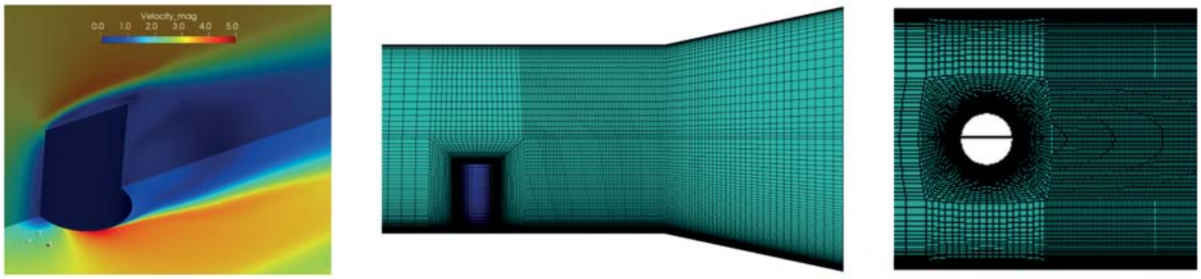

Figure 1. Flow field (velocity at Re = 8798) and computational mesh used in studies

Numerical simulations were performed using Ansys Fluent 2025R2, utilizing GPU acceleration to achieve transient solutions with the k-omega SST-SBES model. Preliminary calculations for the initialization of transient studies were performed using RANS (Reynolds-Averaged Navier-Stokes) and the two-equation k-omega SST turbulence model.

3. Control Strategies

Closed-loop control is implemented using the Proximal Policy Optimization (PPO) algorithm within a deep reinforcement learning (DRL) framework. In this approach, system feedback is incorporated through a cost function, referred to in reinforcement learning terminology as the reward function. The reward is formulated based on key aerodynamic and actuation parameters, including drag, lift and the cylinder's rotational velocity.

For comparison, a conventional tabular PID controller and an open-loop control strategy withpredefined actuation were also implemented. The PPO-based DRL controller achieved a drag reduction of approximately 6%, representing the highest performance among the tested methods. The open-loop strategy resulted in a 3% drag reduction but exhibited significant oscillatory behaviour. The PID controller achieved about a 5% drag reduction, however, its performance was less robust under varying flow conditions compared to the PPO-based approach.

Acknowledgements

The studies are supported by science grant 0612/SBAD/3640 from the Ministry of Science and Higher Education.

References

[1] Woodrooffe J., *Reducing Truck Fuel Use and Emissions: Tires, Aerodynamics, Engine Efficiency, and Size and Weight Regulations*, The University of Michigan, Transport Research Institute, Michigan 2014, p. 41.

[2] Bass J.C., Elsner N.B., Leavitt F.A., *Performance of the 1 kW Thermoelectric Generator for Diesel Engines*, 'AIP Conference Proceedings' 1994, vol. 316, no. 1, pp. 295–298.

[3] Gabriel F., *Active flow control of the flow past a cylinder under varying Reynolds number using deep reinforcement learning; the study uses a DRL agent to control cylinder rotation to reduce forces in the wake of a 2D cylinder flow*, https://zenodo.org/records/5634050 (access: 2.04.2026).

VALIDATION OF A NUMERICAL MODEL FOR THERMOMAGNETIC CONVECTION OF A PARAMAGNETIC FLUID IN STRONG MAGNETIC FIELDS

A. Kraszewska, J. Donizak

AGH University of Krakow, Faculty of Energy and Fuels, al. A. Mickiewicza 30, 30–059 Krakow, Poland

E-mail: anna.kraszewska@agh.edu.pl

Abstract. Thermo-magnetic convection in a paramagnetic fluid was investigated experimentally and numerically in a shallow Rayleigh–Bénard (RB) enclosure. Experiments for various magnetic field strengths and temperature differences were compared with quasi-DNS simulations accounting for gravitational and magnetic buoyancy. Global heat transfer, quantified by the Nusselt number was validated using uncertainty-aware error metrics and trend analysis with respect to the magnetic field. Strong agreement was observed, with regression slopes near unity, small statistically insignificant intercepts and high correlation coefficients, confirming the numerical model accurately reproduces the evolution of thermo-magnetic convection and its global heat transfer.

Keywords: Computational Fluid Dynamics, Experimental Fluid Mechanics, Thermo-magnetic Convection, Heat Transfer.

1. Introduction

Thermo-magnetic convection results from the interaction between temperature-dependent magnetic susceptibility and applied magnetic field gradients, enabling active control of buoyancy-driven heat transfer in weakly magnetic fluids. Advances in high-intensity superconducting magnets have enabled experimental and numerical studies demonstrating significant enhancement or suppression of convective heat transfer. However, most previous studies have limited validation to qualitative visual comparisons, without detailed statistical assessment of global heat transfer.

This study validates a numerical model of thermo-magnetic convection in a shallow enclosure through direct comparison with experimental data, focusing on global heat transfer. Uncertainty-aware error metrics account for experimental uncertainties, while trend analysis with respect to magnetic induction assesses the model's ability to reproduce the observed heat transfer evolution. This approach provides a solid, physically meaningful framework for validation and supports predictive reliability in magnetically controlled heat transfer applications.

2. Numerical model

Thermo-magnetic convection was simulated by coupling the equations of non-isothermal incompressible flow with a stationary magnetic field. The magnetic field was computed in the magnetostatic limit using a finite-element formulation of Ampère's law, and the resulting magnetic induction and its gradients were introduced as body forces in the flow solver. The flow was modeled using the Boussinesq approximation, considering both gravitational and magnetic buoyancy. The magnetic force was formulated using Curie's law. A quasi–DNS approach without a turbulence model was adopted. Simulations were performed in a 3D domain corresponding to the experimental geometry, using second-order accurate finite-element discretization in space and an implicit second-order time-integration scheme. The simulations were initialized from a purely conductive temperature field and advanced until statistically steady conditions were reached. Global heat transfer was quantified by the time-averaged Nusselt number at the heated wall and compared with experimental data.

3. Results

In Figure 1, the correlation between the Nusselt number determined numerically (Nu_{num}) and experimentally (Nu_{exp}) is presented. The relationship between these quantities was described using a linear regression model:

$$Nu_{num} = -0.14 + 1.01 \cdot Nu_{\exp} \tag{1}$$

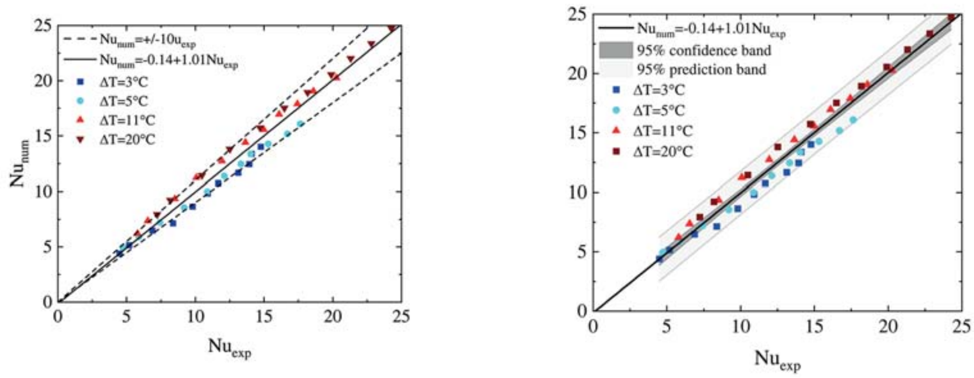

Figure 1. Correlation between numerical and experimental Nusselt number results

The obtained slope is very close to unity and the intercept is small and statistically insignificant ($p_{value} = 0.69$) indicating the absence of a systematic error between the results. In Figure 1a most of the measurement points are located within ±10% of the ideal agreement line ($Nu_{num} = Nu_{exp}$), demonstrating very good model–experiment consistency. This indicates a high quality of the numerical model predictions, regardless of the Nu values. The second plot (Fig.1b) confirms this observation from the regression statistics perspective. The narrow 95% confidence and prediction bands indicate a small data scatter and a good ability of the model to predict experimental values. High Pearson and Spearman correlation coefficients ($r_P = 0.986$, $r_S = 0.9821$) and determination coefficient ($R^2 = 0.972$) validate a strong linear relationship between the numerical and experimental results. The p_{value} ($p < 10^{32}$) for both correlations further confirms the statistical significance of the relationship between results, while the analysis of confidence and prediction intervals indicates a good predictive capability of the model for Nu values.

The conducted statistical analysis clearly shows a good agreement between numerical and experimental Nusselt numbers. The numerical model reliably reproduces the global heat transfer and the observed differences fall within the range considered a high-quality fit. Consequently, the obtained results confirm both the accuracy and the usefulness of the numerical model for analysing global heat transfer. The fact that the adequacy of the numerical model has been demonstrated authorizes the use of simulation results for an objective and precise determination of the ranges of laminar, transitional and turbulent flows in thermo-magnetic RB convection, based on the turbulence intensity criterion.

Acknowledgements

This work was supported by the Polish National Agency for Academic Exchange (NAWA), within the Strategic Partnerships Programme, Project No. BPI/PST/2024/1/00046 and also partially supported by AGH University of Krakow (Grant AGH No. 500.00-210000-10000).

SCALING OF TURBULENCE KINETIC ENERGY DISSIPATION AND TEMPERATURE VARIANCE DESTRUCTION RATES IN DRY CONVECTION AND IN MARINE BOUNDARY LAYERS

St. Król[1], M. Wacławczyk[2]

[1] *Insititute of Geophysics, Polish Academy of Sciences;*

[2] *Institute of Geophysics, Faculty of Physics, University of Warsaw*

E-mail: stanislaw.krol@igf.edu.pl

Abstract. We derive a functional relation between scalar-equivalent Taylor constant $C_{\varepsilon\theta}$ and Taylor microscale-based Reynolds number Re_λ. We then test the formula against two datasets: one collected during Methane-to-go experiment (MtG), representing cloudless atmosphere over land, and one collected during MAGPIE project, which represents cloudy atmosphere over subtropical ocean. We investigate the vertical distribution of the quantities characterising turbulence, and notice the expected surface effect. Various numerical effects and their influence on results were also tested, highlighting the robustness of the analysis.

Keywords: Atmospheric Science, Turbulence, Non-Stationarity.

1. Introduction

Turbulence is an inherent property of atmospheric flows. Its better representation in numerical weather and climate models is key to their better accuracy. For example, clouds are associated with the biggest uncertainty in models, and turbulence in clouds plays a crucial role in their dynamics and microphysics. In equilibrium turbulence, it is assumed that the energy production rate at the largest scales is equal to the energy dissipation rate at the smallest scales. Then, in non-equilibrium turbulence, this balance is disturbed. Such disturbance may come from sudden physical processes, e.g. sudden decrease of forcing [1, 2, 5]. An analysis of non-equilibrium turbulence has been performed in the past for the velocity spectrum, however no such analysis has been performed for scalar (temperature) spectrum. In this project, we have derived the formula stemming from the assumption of non-equilibrium of the scalar spectrum and tested it against measurement data.

2. Data and Methods

The data used to verify the approach comes from two measurement campaigns: one conducted in Silesia region in southern Poland during Methane-to-go Poland measurements [3] and the second one conducted near Barbados in 2023 as part of Moisture and Aerosol Gradients / Physics of Inversion Evolution (MAGPIE) project. In both of these measurements an Ultra Fast Thermometer [4] was installed on top of a measurement platform (helicopter platform or research aircraft) and data was collected along the flight path, consisting of horizontal segments and profiles. From the obtained data, we have obtained profiles of quantities characterising turbulence, as well as the quantities needed to verify the derived formula. The TKE dissipation rate was obtained using the power spectral density method.

3. Results

We have derived an expression connecting the Taylor microscale-based Reynolds number and the Taylor law coefficient for scalar variance destruction $C_{\varepsilon\theta}$ of the form:

$$C_{\varepsilon\theta} \sim \mathrm{Re}_\lambda^{\ a} \tag{1}$$

where a is a function of the inverse of timescales: $\frac{\varepsilon}{\dot{\varepsilon}}$ and $\frac{\varepsilon_\theta}{\dot{\varepsilon_\theta}}$. The above formula was tested against measurement data from MtG and MAGPIE research campaigns, and the results are plotted in figure (1):

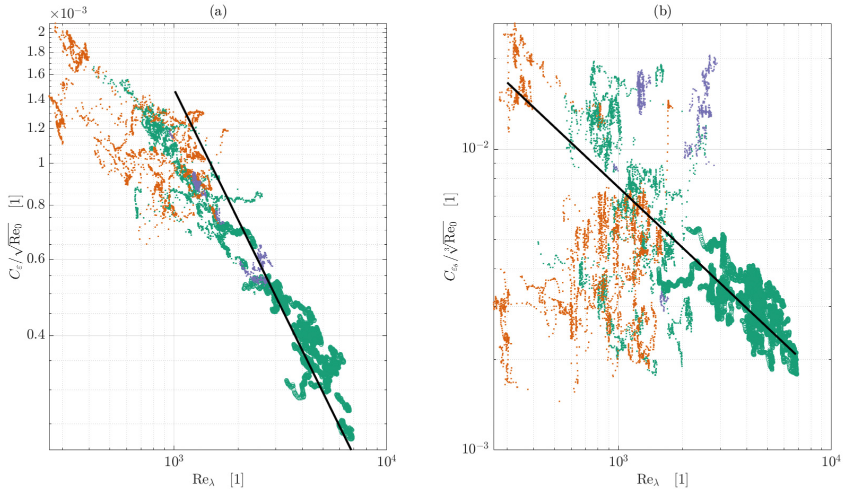

Figure 1: In panel (a), we test the formula derived for velocity spectrum [1], and as we can see, it agrees quite well. In panel (b), we test the derived formula for scalar spectrum. It agrees in some cases (dry convection - green dots) but disagrees in other (clouds - orange points; measurements near the surface - blue points). The results, their robustness and implications will be discussed during the talk

References

[1] Bos W.J.T., *Unsteady and inhomogeneous turbulent fluctuations around isotropic equilibrium*, 'Atmosphere' 2024, vol. 15, no. 5.

[2] Vassilicos J.C., *Dissipation in turbulent flows*, 'Annual Review of Fluid Mechanics' 2015, vol. 47, pp. 95–114.

[3] Pätzold F., Bretschneider L., Nowak S., Brandt B., Schlerf A., Asmussen M.O., Bollmann S., Bärfuss K., Harm-Altstädter B., Hecker P., Wehner B., van der Wall B.G., Sachs T., Huntrieser H., Roiger A., Lampert A., *HELiPOD – Revolution and evolution of a helicopter-borne measurement system for multidisciplinary research in demanding environments*, 'Elementa: Science of the Anthropocene' 2023, vol. 11, no. 1.

[4] Kumala W., Haman K.E., Kopec M.K., Khelif D., Malinowski S.P., *Modified ultrafast thermometer UFT-M and temperature measurements during Physics of Stratocumulus Top (POST)*, 'Atmospheric Measurement Techniques' 2013, vol. 6, no. 8, pp. 2043–2054.

[5] Wacławczyk M., Nowak J.L., Siebert H., Malinowski S.P., *Detecting nonequilibrium states in atmospheric turbulence*, 'Journal of the Atmospheric Sciences' 2022, vol. 79, no. 10, pp. 2757–2772.

NUMERICAL STUDY OF SURFACE THERMAL LOAD ON A MARS ENTRY CAPSULE

S. Kubacki[1], K. Kurec[2], A. Jaworski[3], M. Wielgosz[3]

[1] *Warsaw University of Technology, Institute of Aeronautics and Applied Mechanics, Nowowiejska 24, 00–665, Poland*

[2] *Warsaw University of Technology, Institute of Micromechanics and Photonics, Sw. A. Boboli 8, 02–525 Warsaw, Poland*

[3] *CIM-mes Projekt Sp. z o.o., Aleje Jerozolimskie 125/127, 02–017, Warsaw, Poland*

E-mail: slawomir.kubacki@pw.edu.pl

Abstract. This study evaluates experimental correlation and a RANS-based transition model for predicting surface heat fluxes on the Mars 2020 aeroshell. Numerical results for various flow regimes are validated against flight data. Results demonstrate that incorporating the Kato–Launder limiter is essential for the reduction of turbulence production at the bow shock on the aeroshell forebody. Both the correlation and the standard γ–Re_θ model produce heat-transfer rates that match the flight data.

Keywords: Computational Fluid Dynamics, Mars Reentry Capsule, Thermal Protection Systems, Hypersonic Flow, Correlations, Reynolds-Averaged Navier-Stokes.

1. Introduction

The Mars entry, descent, and landing process may be divided into several distinct phases, each subject to strongly varied flow and thermal conditions. In the initial approach phase, the spacecraft is directed into the entry corridor by the spacecraft's propulsion system. After the initial cruise stage separation, the lander capsule enters the Mars atmosphere. During this drop, the body of the capsule experiences peak heating as well as maximal pressure which typically occurs 70–90 seconds after entry for large blunt-body type aeroshells (cone-like shape). High thermal loads are observed during peak heating, reaching 50–100W/cm^2. A laminar-to-turbulent transition may occur on the surface of the capsule due to rapid changes in Reynolds number, bow-shock-induced disturbances, surface roughness due to ablation and strongly varying thermal conditions, making the prediction of surface heat transfer particularly challenging. Accurate assessment of the resulting thermal loads, however, remains crucial for designing the Thermal Protection System (TPS) and the overall feasibility of the mission.

This study investigates the applicability of the Edquist [1] correlation and the γ–Re_θ model by Menter et al. [2] in predicting transitional flow behaviour and thermal loads on the smooth surface of the capsule at selected trajectory points of the Mars 2020 mission [3]. The predicted heat fluxes are assessed using reconstructed heat-shield data inferred from surface thermocouple measurements acquired during Mars entry and landing.

2. Numerical approach

For predicting the flow and heat transfer characteristics over an aeroshell (Fig. 1a), the density-based solver of Ansys Fluent has been employed. The time-averaged reacting Navier–Stokes equations, together with the turbulence or transition model equations, were solved for a Mars-representative environment. Chemical non-equilibrium was modelled using the Mars5speciesMcKenzie mixture which includes CO, O_2, C, O and CO_2, along with the McKenzie chemical mechanisms. N_2 was added to the mixture, but it did not participate in any reactions. It was added exclusively to establish the mass fraction composition of the Martian atmosphere in the free stream as 97% CO_2 and 3%N_2. The mixture's density was modelled as an ideal gas, with specific heat based on the NASA9 piecewise polynomial function, thermal conductivity derived from kinetic theory, and molecular viscosity calculated using Sutherland's law. The surface of the capsule was treated as supercatalytic. Thermal radiation was not included, as it has a minor impact on the capsule forebody [3].

3. Results

Figure 1a shows contours of velocity magnitude with superimposed velocity vectors, along with the static pressure distribution on the aeroshell surface, for a freestream Mach number of $Ma = 23.35$ and an inlet flow angle of $\alpha = 16°$ (diameter = 4.5m). The bow shock wave is clearly visible in the front part of the capsule. Figure 1b shows a comparison of flight-measured and computed heat-transfer rates at the symmetry plane of the front-cone surface using the Wilcox k–ω model with the Edquist correlation [1], and the γ–Re_θ model. Two levels of freestream turbulence were assumed, one corresponding to a laboratory experiment ($Tu = 0.5\%$) and one to flight conditions (0.1%). Good correspondence is reported, proving the credibility of the numerical techniques. The paper will discuss other flow conditions and provide a summary of the results and conclusions obtained.

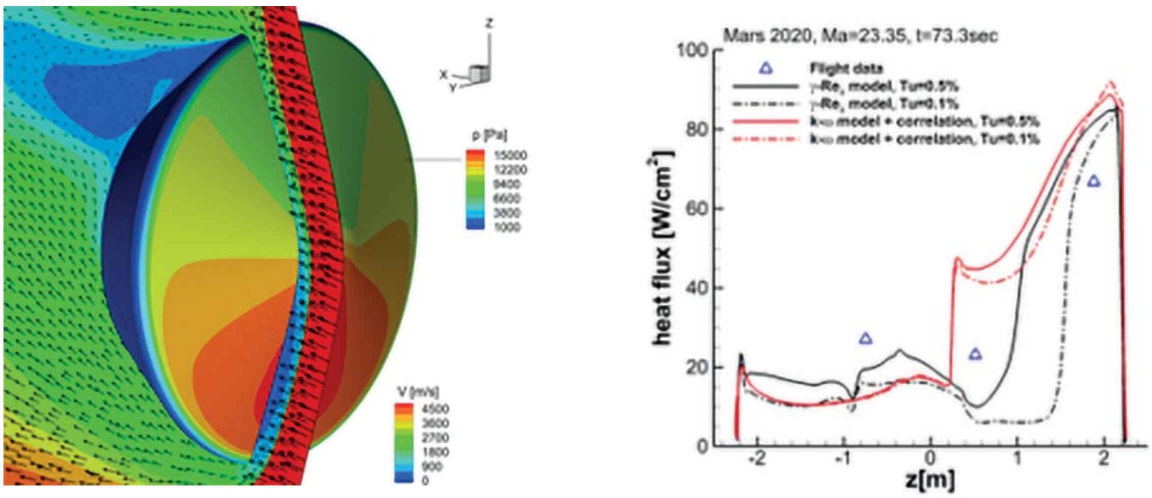

Figure 1. The flow and heat transfer results for trajectory point $t = 73.3$ sec (peak heating)

Acknowledgement

The authors acknowledge the financial support from the ESA project *Martian Re-Entry Flows over Aerodynamically Rough Surfaces* (Contract No. 4000146370/24/NL/RK).

References

[1] Edquist K.T., Liechty D.S., Hollis B.R., Alter S.J., Loomis M.P., *Aeroheating Environments for a Mars Smart Lander*, 'Journal of Spacecraft and Rockets' 2006, vol. 43, no. 2.

[2] Menter F.R., Langtry R.B., Likki S.R., Suzen Y.B., Huang P.G., Volker S., *A correlation-based transition model using local variables – Part I: Model formulation*, ASME Turbo Expo: Power for Land, Sea, and Air, American Society of Mechanical Engineers Digital Collection, 2008, pp. 57–67.

[3] Edquist K.T., West T.K., Mahzari M., Alpert H.S., *Analysis of Mars 2020 entry vehicle aerothermal flight data*, 'Journal of Spacecraft and Rockets' 2023, vol. 60, no. 4, pp. 1201–1219.

BLOCKAGE EFFECT ON LINEARLY UNSTABLE MODES IN FLOW PAST ELLIPTIC CYLINDERS

D. Kumar

Department of Mechanical Engineering, National Institute of Technology Durgapur, Durgapur-713209, India

E-mail: dkumar.me@nitdgp.ac.in

Abstract. This study performs a linear stability analysis of steady flow past elliptic cylinders with varying aspect ratio (*Ar*). The analysis focuses on examined the blockage effect on recently reported linearly unstable modes [1] in the wake of elliptic cylinders. A change in blockage significantly affect the critical Reynolds number (Re_c) and Strouhal number (St_c) for all three modes.

Keywords: Computational Fluid Dynamics, Linear Stability Analysis, Blockage effect, critical Reynolds number.

1. Introduction

Linear stability of bluff body flows, particularly flow past circular and elliptic cylinders, has been extensively studied, with several works [1-4] reporting their stability characteristics. Previous studies show that changes in the cross-stream width of the domain, known as the blockage effect [2-3], significantly affect critical parameters such as the Reynolds numbers and Strouhal numbers. This study focuses on investigating the effect of blockage on recently reported unstable modes [1]: primary wake mode (PWM), secondary wake mode (SWM) and tertiary wake mode (TWM) in the wake of elliptic cylinder.

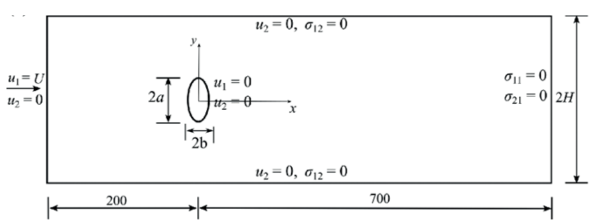

Figure 1. Computational domain and boundary conditions: H is the half cross-stream width. The cylinder centre is at the origin of the Cartesian coordinate system. The semi-major axis of the ellipse is used as the characteristic length scale

2. Numerical Method and Flow-Setup

The equations governing the flow are the incompressible form of the Navier-Stokes equations. The author utilizes the stabilized finite element formulation for computing the steady flow and for solving the linear stability equations. The flow setup and the computational domain are shown in figure 1. The semi-major axis is used as the length scale; the minor axis is $2b$, and the aspect ratio is $Ar = b/a$. In this study, the boundaries of the domain are positioned far enough from the cylinder to minimize any substantial impact on the overall flow field. To investigate the impact of blockage, the author had considered five different lateral widths (H = 100, 50, 30, 20, and 10). The linear stability analysis is performed using the same finite element mesh as in our recent publication [5]. For steady flow computation, the boundary conditions are shown in figure 1. For linear stability analysis, the same boundary conditions are applied, except at the inflow boundary where the velocity components are set to zero.

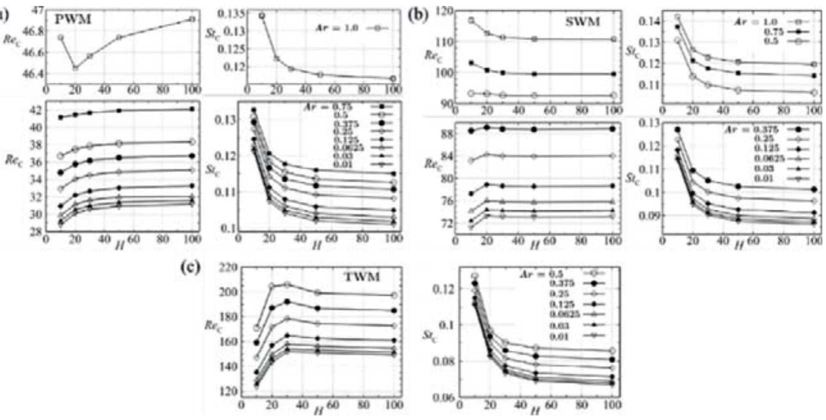

Figure 2: Effect of blockage on Re_c and St_c for (a) PWM, (b) SWM and (c) TWM for aspect ratio ($0.01 \leq Ar \leq 1$) and domain size ($10 \leq H \leq 100$)

3. Results and Discussion

The author determined the critical parameters for PWM, SWM, and TWM corresponding to their zero-growth rates. From figure 2, it can be observed that Ar has a significant effect on the variation of Re_c with H. In contrast, St_c variation does not show any qualitative change with Ar. Based on the trend in the Re_c curve, we therefore divide the plots into two categories for PWM and SWM. The top row of figure 2(a) shows the results for $Ar = 1.0$. For this case, Re_c first decreases with blockage and then increases. The non-monotonic variation of Re_c with blockages is similar to that presented by Kumar and Mittal [2]. The second row of figure 2(a) shows the results for other aspect ratios ($0.01 \leq Ar \leq 0.75$). It is observed that the Re_c monotonically decreases as we increase the blockage. This possibly happens because the decrease in the aspect ratio causes the shear layer on either side of the cylinder to become stronger, leading to stronger instability of the wake and a consequent decrease in the critical Re. But the author expects that as we bring the boundary closer to the cylinder, it will make the flow more stable like $Ar = 1.0$ and the critical Re value will increase. At this moment, this is a conjecture which needs a separate study to come up with a definite conclusion. The plot shown in figure 2(b) illustrates how Re_c and St_c change with H for SWM. The top row presents the results for higher aspect ratios ($0.5 \leq Ar \leq 1.0$). Here, Re_c is found to increase with increase in blockage. An exception is $Ar = 0.5$. In this case there is no significant change in Re_c down to $H = 10$. In the second row of figure 2(b), results for lower aspect ratios ($0.01 \leq Ar \leq 0.375$) are shown. The relationship between Re_c and blockage exhibits a non-monotonic pattern. For all Ar, both in the top and bottom row of the figure, Re_c seems to settle beyond $H = 50$. The St_c curve however shows an increase with blockage for all Ar. For TWM (figure 2c), Re_c first increases with blockage, reaches a maximum at $H = 30$, and then decreases. Unlike PWM and SWM, the trend for TWM is same for all Ar. St_c for TWM shows a monotonic increase with blockage for all Ar.

References

[1] Kumar D., Kumar B., *Tertiary wake mode in flows past elliptic cylinders*, 'European Journal of Mechanics-B/Fluids' 2024, vol. 106, pp. 130–136.

[2] Kumar B., Mittal S., *Effect of blockage on critical parameters for flow past a circular cylinder*, 'International Journal for numerical methods in fluids' 2006, vol. 50, no. 8, pp. 987–1001.

[3] Boppana V.B.L., Gajjar J.S.B., *Onset of global instability in the flow past a circular cylinder cascade*, 'Journal of fluid mechanics' 2011, vol. 668, pp. 304–334.

[4] Verma A., Mittal S., *A new unstable mode in the wake of a circular cylinder*, 'Physics of Fluids' 2011, vol. 23, no. 12.

[5] Kumar D., Kumar B., *Steady flow past elliptic cylinders with blockage effects*, 'Physics of Fluids' 2022, vol. 34, no. 5.

IMPROVING OF PROPPANT SCREEN-OUT MODELLING FOR ROUGH FRACTURES

Ł. Łaniewski-Wołłk[1,2], **C. Leonardi**[2]

[1] *Warsaw University of Technology, Faculty of Power and Aeronautical Engineering, ul. Nowowiejska 24, 00–665 Warszawa, Poland*

[2] *University of Queensland, School of Mechanical & Mining Engineering, Mansergh Shaw Building, Queensland 4072, Australia*

E-mail: lukasz.laniewski@pw.edu.pl

Abstract. It is well established that particles in particle laden flows get jammed between walls in sufficiently narrow rock fractures. This jamming, which for proppant particles is called *screen-out*, is assumed to occur abruptly when a certain size-exclusion criterion is matched. In this presentation the authors show the results of numerical simulations done with coupled Lattice Boltzmann Method and Discrete Element Method, that show no such clear cut-off for rough fracture geometries. In such geometries screen-out occurs smoothly across particle concentrations. Finally the influence of particle shape is discussed.

Keywords: Computational Fluid Dynamics, Particle laden flow, Lattice Boltzmann Method, Discrete Element Method.

1. Introduction

Predicting the effective permeability of a fracture to particle laden medium, such as a proppant carrying fluid, is integral for the planning of hydraulic fracturing (HF) for non-conventional gas extraction. This permeability is influenced by factors ranging from fracture width, roughness, connectivity and tortuosity of natural and induced fractures. These geometrical parameters can vary substantially. The size of injected particles can also vary by orders of magnitude. The resulting variabilities, mean that HF treatments are frequently not repeatable which can only be improved with deeper understanding of the transport processes involved.

2. Methodology

This study investigates the relationship between effective permeability and particle solid volume fraction ϕ, via direct numerical simulation. Synthetic rough fracture geometries are generated with parameters based on surface scans of real coal fractures and fluid flow is simulated in periodic cells of such a generated geometry. The lattice Boltzmann method (LBM) is used for the fluid flow and the discrete element method (DEM) is used for the solid phase.

For coupling the LBM, the partially saturated cell method (PSM) is used. The most common approach for such coupling consists of four steps, (i) the particle positions, velocities and radii from the DEM solver are sent to the LBM solver, (ii) the LBM solver uses these to add obstacles in the fluid flow, (iii) the LBM solver then calculates the hydrodynamic reaction forces acting on the obstacles and sends them to the DEM solver, (iv) finally, the forces are added to the other forces acting on the particles and integrated in time by the DEM solver.

In PSM, coverage ratio from zero to one is calculated in every cell of the LBM that is overlapped by a particle and subsequently used to force the velocity of the fluid to be equal to the particle velocity.

3. Results and Conclusions

For wide apertures, the behaviour of permeability follows an adjusted cubic-law with viscosity adjusted to account for particle saturation. Additionally, permeability decreases with increasing fracture roughness. In narrow fractures, however, the permeability is strongly influenced by so-called bridging and localised clogging of the particles. Nevertheless, no clear cut-off for screen-out (complete jamming) is observed (see Fig. 1), in contrast to the screen-out criteria frequently employed by commercial HF simulation software. Such smooth screen-out behaviour suggests different mechanisms, to previously assumed, for the sudden high pressure increases observed in some HF operations.

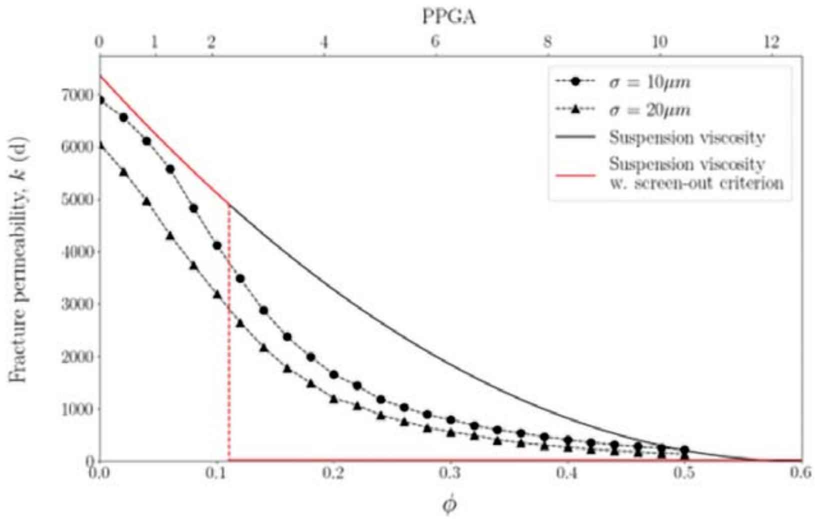

Figure 1. Dependence of fracture permeability on solid volume fraction, Φ, and fracture roughness, σ

Furthermore, the presentation will show dependence of this behaviour on particle shape for non-spherical proppant particles.

Acknowledgements

We would like to acknowledge work done in this study by Nathan Di Vaira. We gratefully acknowledge Polish high-performance computing infrastructure PLGrid (HPC Center: ACK Cyfronet AGH) for providing computer facilities and support within computational grant no. PLG/2025/018466.

References

[1] Noble D.R., Torczynski J.R., *A lattice-Boltzmann method for partially saturated computational cells*, 'International Journal of Modern Physics C' 1998, vol. 9, no. 8, pp. 1189–1201.

[2] Di Vaira N.J., Laniewski-Wollk L., Johnson Jr. R.L., Aminossadati S.M., Leonardi Ch.R. , *Proppant transport at the intersection of coal cleats and hydraulic fractures*, 'Powder Technology' 2026, vol. 469.

JET-MIXING CONTROL LANDSCAPES REVEALED BY BAYESIAN OPTIMIZATION

Y. Li[1], **B.R. Noack**[2,3]

[1] *Department of Mechanical Engineering, University College London, London WC1E 7JE, UK*

[2] *Low-Altitude Economy Science and Technology Research Institute, Harbin Institute of Technology (Shenzhen), Shenzhen 518055, People's Republic of China*

[3] *College of Mechatronics and Control Engineering, Shenzhen University, Canghai campus, Shenzhen 518060, People's Republic of China*

E-mail: yiqing.li@ucl.ac.uk

Abstract. This work presents a machine-learned control landscape for global optimization of jet mixing from large-eddy simulations at a Reynolds number of 3000. The control is implemented via axial and radial periodic forcing at the nozzle exit. The resulting search space is explored efficiently using Bayesian optimization with a deep-learning surrogate. A two-dimensional embedding of the database reveals basins of attraction for effective control, such as a blooming jet and a suboptimal double-helix mode. The resulting axisymmetric-helical radial forcing is further refined and implemented in the experiment.

Keywords: Turbulence, Jet mixing, Active flow control, Machine learning, Data mining.

1. Introduction

Jet mixing plays a pivotal role in both academic research and engineering applications[1]. Previous studies have demonstrated control of entrainment and spreading via external excitation at the nozzle exit[2]. However, global optimization of general actuation strategies remains costly and largely unexplored. To enable systematic exploration of such high-dimensional actuation spaces, the present study considers general periodic forcing in time and space at the jet nozzle exit and investigates its potential using machine learning[3] and data mining[4]. The authors propose a data-efficient Bayesian optimization (BO) combined with topological analysis to identify robust mixing strategies in a high-dimensional control space.

2. Configuration and Methodology

As illustrated in Fig. 1, the actuation imposed at the nozzle exit includes axial u^{α} and radial components u^{β} u^{γ}. The forcing commands are defined to approximate a general periodic function of time and azimuthal angle with up to 22 degrees of freedom, so that the design space can emulate most forcing modes previously studied. The optimization problem is formulated to maximize mixing in response to the actuation input, parameterized by b. To quantify mixing under non-axisymmetric forcing, the authors introduce an equivalent mixing radius, R_{eq}, defined as the normalized streamwise velocity variance at a cross-section $8D$ downstream of the nozzle, where D denotes the nozzle diameter. This high-dimensional optimization is addressed using Bayesian optimization (BO) with a deep operator network (DeepONet) as the surrogate model. To further understand the learning process, the authors also performed a topological data analysis [5] of the resulting database.

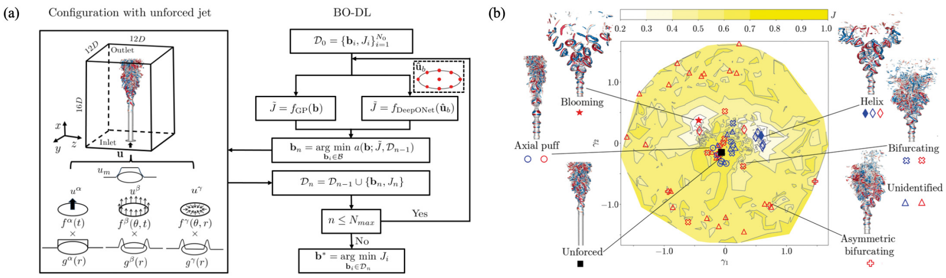

Figure 1. (a) Setup and method (b) Topological interpretation of the control landscape

3. Results

The achieved control landscape features two pronounced minima, a global minimum corresponding to a 7-armed blooming jet, and a suboptimal parameter with a double-helix shape that performs comparably. A state-of-the-art BO (blue samples in Fig. 1b) converges towards this double-helix solution. The learning is accelerated and converges to the global optimum by including the DeepONet (red samples in Fig. 1b). Intriguingly, many of the less persistent minima also correspond to known actuated jet mixing mechanisms.

Compared with the unforced jet, both the helical and the blooming jet shorten the length of the potential core substantially from $7.5D$ to $2D$. The valley of the mean centerline velocity is located around $6D$ in the downwash, corresponding to the peak of the fluctuation profiles. The reversal flow in the blooming jet amplifies the local turbulence intensity and leads to even negative velocity in the centerline. The optimized control laws show that the radial component dominates the non-axisymmetric forcing mode. The optimized forcing for the helical jet is a triple-mode that combines the axisymmetric bulk component, a helical and a flapping mode in the periphery. The 7-armed blooming jet is produced by a dual-mode forcing with only axisymmetric and helical modes.

In the subsequent experimental study [6], radial actuation is applied using eight loudspeakers distributed around the nozzle lip of a turbulent jet at a Reynolds number of 10,000. The forcing command is further refined and again converges to an axisymmetric-helical mode.

This study demonstrates that deep learning-enhanced BO combined with topological analysis enables efficient discovery and effective interpretation of high-dimensional flow-control landscapes.

Acknowledgements

This work is supported by the National Natural Science Foundation of China under grants 12172109 and 12302293, by the Guangdong Basic and Applied Basic Research Foundation under grant 2022A1515011492, and by the Shenzhen Science and Technology Program under grant JCYJ20220531095605012.

References

[1] Crow S.C., Champagne F.H., *Orderly Structure in Jet Turbulence*, 'Journal of Fluid Mechanics' 1971, vol. 48, no. 3, pp. 547–591.

[2] Shaabani-Ardali L., Sipp D., Lesshafft L., *Optimal triggering of jet bifurcation: an example of optimal forcing applied to a time-periodic base flow*, 'Journal of Fluid Mechanics' 2020, vol. 885.

[3] Brunton S.L., Noack B.R., Koumoutsakos P., *Machine Learning for Fluid Mechanics*, 'Annual Review of Fluid Mechanics' 2020, vol. 52, pp. 477–508.

[4] Chazal F., Michel B., *An Introduction to Topological Data Analysis: Fundamental and Practical Aspects for Data Scientists*, 'Frontiers in Artificial Intelligence', 2021, vol. 4.

[5] Wang T., Cornejo Maceda G.Y., Noack B.R., *xPDT: A Toolkit for Persistent Data Topology*, Technische Universität Braunschweig, Braunschweig (Germany) 2023.

[6] Reumschüssel M., Li Y., zur Nedden M., Wang T., Noack B.R., *Paschereit C.O., Experimental jet control with Bayesian optimization and persistent data topology*, 'Physics of Fluids' 2024, vol. 36, no. 9.

EVALUATION OF FLOW ENTRAINMENT RATIO OF A JET-PUMP BASED SYSTEM INTENDED FOR JHR EXPERIMENTAL DEVICES

E. Lo Pinto[1], M. Katz[2], S. Clément[1], S. Gaillot[1], Y. Weiss[3]

[1] *CEA, DES, IRESNE, Department of Nuclear Technology, Cadarache F-13108 Saint-Paul-Lez-Durance, France*

[2] *NRCN, P.O.Box 9001 Beer Sheva, 84190, Israel*

[3] *Mechanical Engineering, Ben-Gurion University, Ben-Gurion Blvd. 1, Beer-Sheva, 84190, Israel*

E-mail: emmanuel.lopinto@cea.fr

Abstract. A flow entrainment module based on single phase water-water injector-diffuser systems (or jet pump) is tested experimentally to investigate how its entrainment ratio varies depending on the injected flowrate. The design allows for a constant entrainment factor over a broad operating range, up to thermal-hydraulic conditions encountered in reactor cores. Measurements are compared with analytical and numerical predictions. They support the use of numerical tools for the design of future jet pump prototypes.

Keywords: General Fluid Dynamics, Jet Pump, Injector-Diffuser, Flow Entrainment.

1. Introduction

Single phase jet-pumps are considered to be used in experimental devices to be integrated in the research reactor Jules Horowitz (JHR). These systems enable passive coolant circulation within the devices thanks to a remote pump, thereby facilitating maintenance. While they are employed in other industries, nuclear applications present a specific challenge regarding compactness. The design of such systems relies mainly on simulations, however, validation data for the targeted operating range and specific geometries are missing, especially for water flow at high pressures and temperatures (up to 330°C). Consequently, experimental campaigns have been carried out on CORAIL loop, an experimental facility located in CEA Cadarache research centre, in parallel to simulations done at NRCN.

2. Experiments

The tested flow entrainment unit included two injector-nozzle systems, arranged in parallel. It was integrated into a simplified version of a JHR experimental device, which was connected to CORAIL water loop. It embarked a full set of sensors to allow measurement of flowrate, pressure and temperature at several points of the circuit and within the device.

The right drawing of Figure 1 illustrates the operating principle and geometry features of a jet pump. Primary flow (1) (supplied to injectors by CORAIL facility) exits from the injector nozzle at high velocity V_n, entraining a fraction of the fluid (secondary flow (2)) circulating within the device, while the rest of it is drawn out to be re-injected as primary flow. Primary and secondary flows are mixed together through the throat of the diffuser and then circulate in the device, only to be separated again at the secondary inlet (2) of the jet pump. The operating point of investigated jet pump is defined by a momentum balance of the head gained in the jet pump and the pressure loss in the device.

For the considered experimental campaigns, more than 50 sets of operating conditions were tested, from reactor start-up conditions (30 bar - 50°C) to Pressurized Water Reactor (PWR) core conditions (155 bar - 330°C). Water total mass flow rate supplied to the injectors was varied from 15 g/s to 45 g/s.

3. Modelling

3.1 Analytical model

An analytical model of a jet pump system based on balances of mass, momentum and energy [1] was used to predict the entrainment factor M, defined as the ratio of secondary volumetric flowrate over primary volumetric flowrate (Q_2/Q_1). To that purpose, it was combined with a hydraulic model of the device circuit, built from correlations for minor and major pressure losses taken in reference [2].

3.2. 2D CFD model

Due to the lack of experimental data on miniature jet-pumps, a benchmark work was done on an existing case from the literature [3], selected from dimensional ratios. The comparison of results from several RANS models (k-ε realizable, k-ω SST, RSM) and wall treatments has led to the choice of the k-ω SST model with linear law for the final set of simulations. Eventually, a mesh sensitivity study was done.

The findings of this benchmark were used to estimate the performance of the flow entrainment module to be tested on CORAIL loop. A CFD model of the jet pumps was built and associated to boundary conditions (pressure drop correlation) to take into account the rest of the test section.

4. Results

The results are summed up on the graph on the left side of Figure 1 (M as a function of Reynolds number Re_n in the injector nozzle). Experimentally, M is found to be nearly constant around 3.9 over the whole operating range. Repeatability of measurements was verified. Modelling results match with the values and behaviour identified experimentally, giving confidence in the use of modelling to support the design of alternative jet pump prototypes for the different experimental devices of JHR reactor.

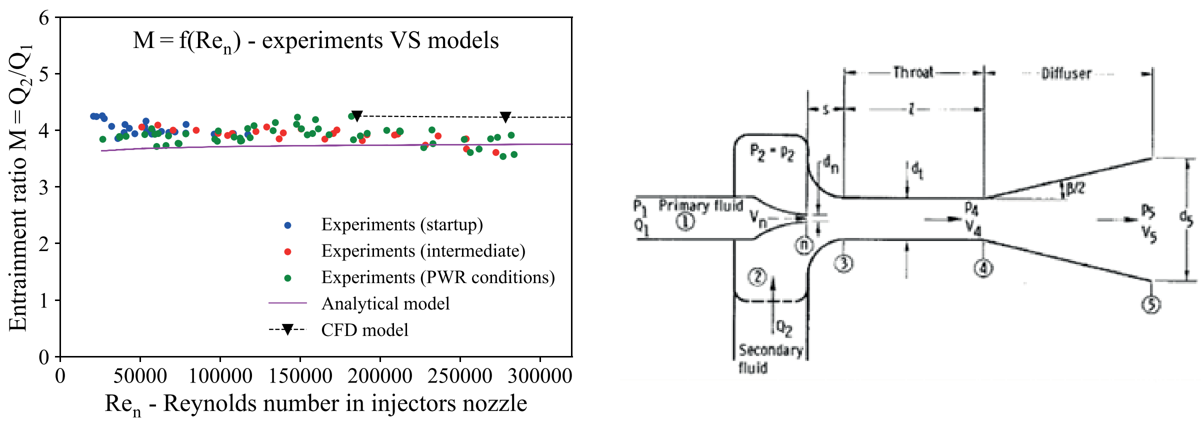

Figure 1. Comparison of entrainment factors (left) - schematic of a jet pump [3] (right)

Acknowledgements

This research was performed in the framework of JHR consortium activities (Technology Working Group) in a collaboration between CEA-DES-IRESNE (France), IAEC-NRCN and BGU (Israel).

References

[1] R.G. Cunningham, *Jet pump theory*, Pump Handbook 3rd Edition, Chapter 4, 2001.

[2] I.E. Idel'cik, *Memento des pertes de charge*, Eyrolles, Paris 1999.

[3] N.L. Sanger, *Non cavitating performance of two low-area-ratio water jet pumps having throat lengths of 7.25 diameters*, National Aeronautics and Space Administration, 1968.

INFLUENCE OF HUMIDITY ON SELF-EXCITED SHOCK WAVE OSCILLATIONS IN TRANSONIC PLANAR NOZZLES

M. Majkut[1], S. Dykas[1], K. Smołka[1], A. Bogusławski[2], K. Skoczylas[2]

[1] *Silesian University of Technology, Department of Power Engineering and Turbomachinery, 2A Akademicka St., 44–100 Gliwice, Poland*

[2] *Faculty of Mechanical Engineering, Czestochowa University of Technology, 42–201 Czestochowa, Poland*

E-mail: miroslaw.majkut@polsl.pl

Abstract. The paper summarizes an experimental investigation of how inlet air humidity modifies self-excited shock wave oscillations in planar convergent–divergent nozzles operating under transonic, over-expanded conditions. The focus is placed on changes in dominant oscillation frequency, shock and condensation wave dynamics and the underlying feedback mechanism linking humidity-driven condensation with shock wave-boundary layer interaction.

Keywords: Humidity, transonic nozzle, shock wave oscillations, condensation wave.

1. Introduction

Shock wave-boundary layer interaction in internal transonic flows can generate strong, self-sustained oscillations that adversely affect aerodynamic performance, noise and structural loading in propulsion and turbomachinery components. While this phenomenon has been widely characterized for dry air, much less is known about how realistic atmospheric humidity and associated non-equilibrium condensation alter the unsteady shock system in nozzles and ducts. Recent works have shown that moist transonic flows can undergo additional instabilities when condensation couples with inviscid pressure waves, suggesting that humidity may significantly influence both the amplitude and frequency of shock motion [1, 2]. The present study addresses this gap by systematically varying inlet relative humidity and characterizing the resulting changes in shock wave oscillations and condensation wave behavior in planar convergent-divergent nozzles.

Experiments were performed in an open-loop test stand drawing atmospheric air through three planar half-nozzles (N1–N3) with identical throat height but different expansion rates, corresponding to varying exit area ratios and exit Mach numbers. Nozzles were operated for nozzle pressure ratios NPR = 1.4, 1.6, and 1.8, and for three inlet air conditions representative of dry, moderate and humid atmospheres, characterized by relative humidity levels of approximately 30, 50 and 70%. High-speed Schlieren imaging at 6000 fps was synchronized with high-frequency wall-pressure measurements at three axial positions, yielding time-resolved information on shock location, condensation structures and pressure oscillations.

2. Experimental results

The measurements confirm that nozzle geometry and NPR are the primary factors controlling the base frequency of shock oscillations but humidity introduces a systematic secondary modulation of unsteady dynamics. For each nozzle and fixed NPR, increasing relative humidity from 30 to 70% produces a measurable rise in the dominant shock oscillation frequency, typically of the order of a few percent, indicating that condensation effects slightly stiffen the feedback loop linking separated boundary layer, subsonic recirculation region and upstream shock motion (Fig. 1).

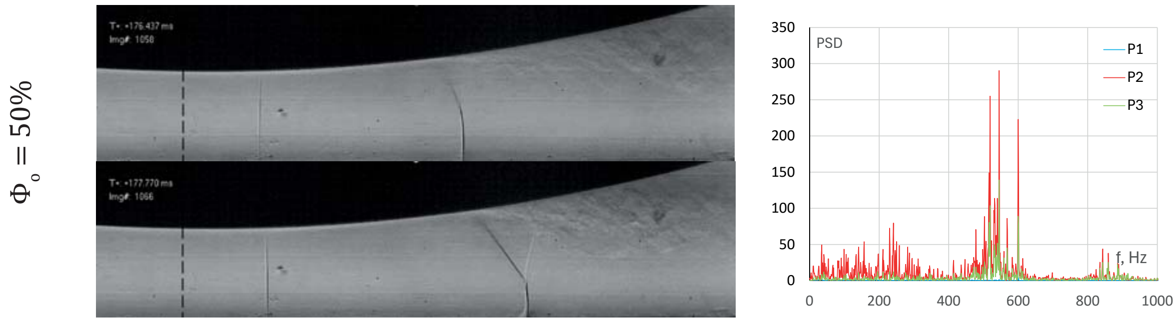

Figure 1. The coexistence of a condensation wave and a normal shock wave (min and max position) occur in the wet air flow through the nozzle N1 for NPR = 1.6

The condensation wave oscillates at a frequency roughly twice that of the downstream normal shock, revealing a coupled two-frequency system where phase-change structures modulate but do not fully lock, the primary shock motion. Static wall-pressure measurements with low-frequency transducers capture the average streamwise position of both shock and condensation waves, while numerical results reproduce the rapid pressure rise across the condensation front that is experimentally under-resolved, confirming the adequacy of the implemented condensation model for engineering-level prediction.

3. Conclusions

The study demonstrates that inlet air humidity, though less influential than nozzle geometry and NPR, exerts a clear and repeatable impact on the frequency and structure of self-excited shock wave oscillations in transonic planar nozzles. Increasing relative humidity consistently shifts the dominant shock oscillation frequency upward by several percent and introduces a strongly non-stationary condensation wave whose oscillation frequency is approximately double that of the main shock.

Acknowledgements

This research was funded by the National Science Centre, Poland, under project No. 2023/49/B/ST8/00773, and supported by statutory research funds from the Silesian University of Technology.

References

[1] Majkut M., Dykas S., Smołka K., *Analysis of normal shock wave instability in transonic moist air flows within convergent-divergent nozzles using experimental and numerical approaches*, THMT-25 Turbulence, Heat and Mass Transfer 11, 21–25 July 2025, Tokyo.

[2] Majkut M., Dykas S., Smołka K., Zhang G., *Study of shock wave and boundary layer interactions in converging–diverging nozzles with varying inlet air humidity levels*, 'Experiments in Fluids' 2025, vol. 66, no. 223.

[3] Tripathi M., Dykas S., Majkut M., Smołka K., Skoczylas K., Boguslawski A., *Spectral Energy of High-Speed Over-Expanded Nozzle Flows at Different Pressure Ratios*, 'Energies' 2025, vol. 18, no. 21.

THE EFFECT OF ELECTRIC FIELD ON THE COLLISION EFFICIENCY BETWEEN TWO UNCHARGED SETTLING CLOUD DROPLETS

M. Manna[1], **B. Rosa**[1,2], **A. Ababaei**[1]

[1] *Institute of Meteorology and Water Management – National Research Institute, Podleśna 61, 01–673 Warsaw, Poland*

[2] *Department of Applied Mathematics, Warsaw University of Life Sciences (SGGW), Nowoursynowska 166, 02–776 Warsaw, Poland*

E-mail: bogdan_rosa@sggw.edu.pl

Abstract. Collision efficiency between settling cloud droplets is strongly influenced by aerodynamic and electrostatic interactions, especially in the presence of electric fields. Using analytical models for hydrodynamic lubrication and electrostatic polarization, we numerically investigate collisions of uncharged droplets over a wide parameter space. The results show that strong electric fields can significantly enhance collision efficiency, highlighting its importance in cloud microphysical simulations.

Keywords: Atmospheric Science, Collision Efficiency, Electric Field, Charged Cloud Droplets.

1. Introduction

The growth of small water droplets with radii of 1–30 µm to precipitation sizes in warm (ice-free) clouds is governed primarily by their collision and subsequent coalescence rather than by condensation or evaporation. Collisions between settling droplets therefore play a central role in rain initiation. Droplet-droplet collisions are influenced not only by gravity and inertia, but also by mutual aerodynamic and electrostatic interactions; when present, external electric fields further modify the forces acting on the droplets. The interplay among these mechanisms leads to complex collision dynamics that are difficult to isolate experimentally and the associated technical challenges further limit laboratory investigations [1].

Numerical simulations offer the flexibility to study such processes under controlled conditions and several studies have examined charged cloud droplets settling in air under electric fields. However, collisions of uncharged droplets have received comparatively little attention [1–3] and existing studies often rely on approximate hydrodynamic descriptions. Moreover, only Plumlee and Semonin [3] employed a rigorous model for electrostatic interaction [4], with results restricted to a limited set of droplet sizes, field strengths and field orientations. The present study addresses these limitations by employing exact analytical models for both electrostatic and aerodynamic interactions, enabling simulations over a substantially broader parameter space. This approach allows a systematic assessment of how electric fields, droplet size disparity and short-range interactions jointly influence collision efficiency, providing improved physical insight into the microphysical processes governing warm-rain initiation.

2. Results and discussion

The left panel of Fig. 1 shows the electrostatic force component acting along the line of centres for an uncharged 10–5 µm pair of water droplets in a uniform electric field of 10^3 V/cm. The left vertical axis presents this parallel force as a function of the inter-droplet gap (lower axis) for horizontal (green) and vertical (blue) field orientations. The right vertical axis shows the same force as the field orientation angle ψ (upper axis) varies from 0 to $\pi/2$. For two neutral conducting droplets in a uniform electric field, the electrostatic interaction can be either attractive or repulsive depending on orientation: the force is attractive when the field is mostly aligned with the line of centres and becomes repulsive as the orientation approaches a perpendicular configuration.

A transverse force component (not shown) acts to rotate the pair into alignment with the field, where attraction dominates. The right panel of Fig. 1 presents the collision efficiency, E_{12}, for four uncharged droplet pairs settling in still air under vertical electric fields with intensities ranging from 10^{-1} to 10^{4} V/cm. The results indicate that weak electric fields ($E_0 \leq 10$ V/cm) do not appreciably affect collision efficiency. In contrast, stronger fields substantially enhance E_{12}, in some cases to values well above unity. The influence of the collected (smaller) droplet size becomes increasingly pronounced as field strength increases, with larger collected droplets leading to a stronger enhancement of E_{12} (note the logarithmic scale of the vertical axis).

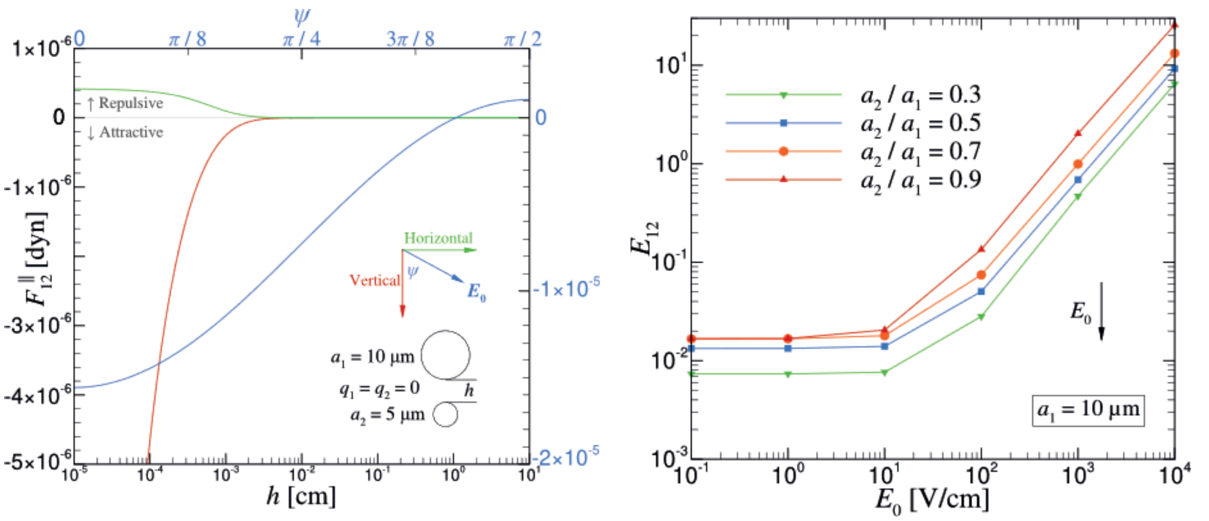

Figure 1. Left panel: the parallel component of F_{12} versus the size of the gap between the pair (lower axis) as well as the orientation of the electric field (upper axis). Right panel: E_{12} vs. the intensity of a vertical electric field for uncharged settling droplet pairs of sizes: 10–3 μm (green), 10–5 μm (blue), 10–7 μm (orange), and 10–9 μm (red)

References

[1] Telford J.W., Thorndike N.S.C., *Observation of small drop collisions*, 'Journal of Meteorology' 1961, vol. 18, p. 382.

[2] Lindblad N.R., Semonin R.G., *Collision efficiency of cloud droplets in electric* fields 'Journal of Geophysical Research' 1963, vol. 68, no. 4, pp. 1051–1057.

[3] Plumlee H.R., Semonin R.G., *Cloud droplet collision efficiency in electric fields*, 'Tellus' 1965, vol. 17, p. 356.

[4] Davis M.H., *Two Charged Spherical Conductors in a Uniform Electric Field: Forces and Field Strength*, 'The Quaterly Journal of Mechanics and Applied Mathematics' 1964 vol. 17, no. 4, pp. 499–511.

CFD SIMULATIONS OF MULTIPHASE FLOW AND RADIOMETRIC PROBE RESPONSE

P. Marczak, M. Jaszczur

AGH University of Krakow, Faculty of Energy and Fuels, Al. Mickiewicza 30, 30–059 Kraków, Poland

E-mail: jaszczur@agh.edu.pl, pmarczak@agh.edu.pl

Abstract. Multiphase flow measurement remains a significant challenge due to complex fluid dynamics, often limiting the effectiveness of conventional techniques. This paper focuses on modelling multiphase flow and radiometric probe response using Computational Fluid Dynamics and User-Defined Function. This approach facilitates probe calibration and performance assessment across various flow regimes without the need for extensive physical experiments. The generated signals allow for the determination of void fraction and void velocity, serving as a dataset for training Machine Learning models, leading to improved prediction accuracy.

Keywords: Multiphase Flows, CFD, VOF, Radiometric measurement, Gamma-ray absorption.

1. Introduction

Multiphase flows occur across diverse industrial sectors, from mining to the chemical industry appearing in distillation columns, reactors or pipelines transporting oil, gas or other mixtures. A common denominator connecting these industries is accurate flow measurement and regime prediction.

Advances in numerical simulations and computational power have provided tools to predict the behavior of mixture flow. Ranging from the Volume of Fluid (VOF) method to computationally demanding Eulerian models, Computational Fluid Dynamics (CFD) is now widely employed in both industry and academia. However, numerical models require validation against experimental data to ensure solution accuracy or to tune the models to reflect the real, measured values.

Multiphase flow measurement remains challenging. Available techniques range from positive displacement in-line meters to ultrasonic, electromagnetic, and separation-type meters [1]. Another category includes gamma-ray spectroscopy meters. Beyond basic flow characteristics such as a velocity, integrating these with Machine Learning (ML) yields information regarding the average flow of the secondary phase, flow regime, or even the fluid type [2].

The primary objective of this study is to develop a numerical model of the flow and radiometric probe setup. Air-water flow simulations are performed, using the VOF model, specifically for plug and plug-bubbly flows. A custom UDF code model the radiometric probe's response, allowing comparison of synthetic signals, and derived velocities against experimental data. To the best of our knowledge, the simulation of a radiometric probe's behaviour has not been previously reported in the literature.

The simulation capability enhances understanding of the radiometric measurement technique. It allows for the investigation of various parameters, including the distance between detectors, signal intensity and temporal resolution across different flow regimes or fluid types without extensive physical experiments. Furthermore, CFD-generated signals can serve as datasets for ML training, limiting the number of physical experiments solely to the final validation of the overall phenomenon. The datasets produced by this simulation make it possible to gather information about the behavior of various flows, for example oil and gas, for which laboratory tests are difficult to perform. Additionally, a greater variety of boundary conditions can be applied, such as velocities that are impossible to achieve in the current experimental rig. Based on these, datasets, the quality of the prediction of ML models can be compared to models trained on experimental data for air and water.

2. Experimental Facility and Numerical Methods

The radiometric flow measurement setup consists of a gamma-ray source (Am-241), scintillation probes and a channel transporting the air-water mixture. The operating principle relies on the differential absorption of gamma radiation which is higher for water than for air. Consequently, when air bubbles pass through the measurement section, an increase in the signal intensity is observed. Based on signal analysis, it is possible to calculate the secondary phase velocity, void fraction or identify flow regime. Details regarding the experimental setup and the measurement procedure are described in reference [2].

Numerical simulations model the air-water flow in a horizontal channel. Various flow regimes, including plug and plug-bubbly flow are evaluated using the VOF model. The VOF model can account for two or more phases by solving a single set of momentum equations and tracking the volume fraction of individual phases through the domain.

The simulation geometry consists of a horizontal pipe with a diameter of 50 mm and a length of 3500 mm. Calculations are performed in 3D using a transient solver to reproduce the dynamic phenomena occurring in the experimental setup. The probe response is modelled using a developed UDF code. The radiometric signal is analyzed to obtain essential multiphase flow parameters.

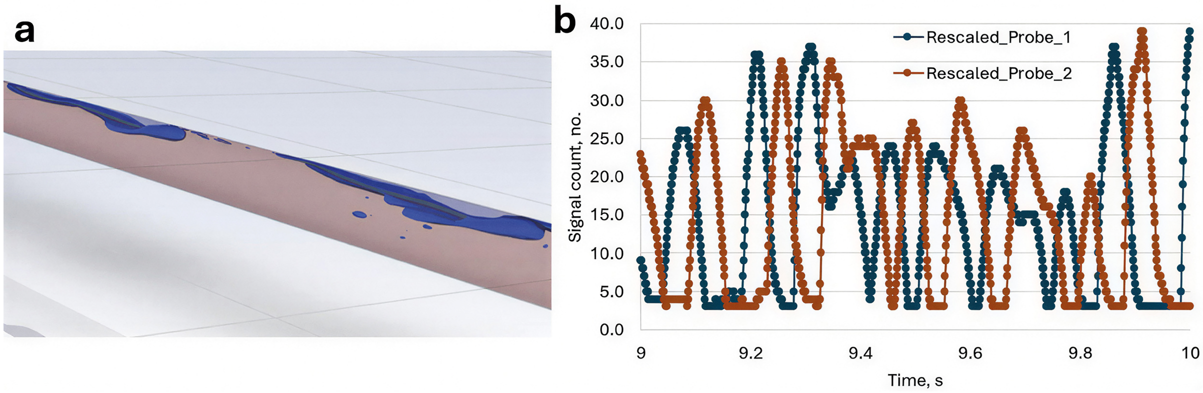

Figure 1. a – Simulation results, isosurface of air fraction, b – simulated radiometric probe response

Figure 1(a) shows an isosurface of the air fraction from transient calculations for a plug flow regime. In Figure 1(b), the synthetic radiometric probe response from two probes separated by 97 mm is presented for time interval 1 s of flow time (from 9 s to 10 s). The signal was post-processed to match the experimental measured data in terms of range, minimum and maximum with experimentally measured data.

Acknowledgements

This work was partly funded by the program “Excellence initiative – research university” for the AGH University of Krakow and Faculty of Energy and Fuels (Grant no. 500.00-210000-10000).

References

[1] Norwegian Society for Oil and Gas Measurement, The Norwegian Society of Chartered Technical and Scientific Professionals, *Handbook of Multiphase Flow Metering*, revision 2, Oslo 2005.

[2] Hanus R., Zych M., Mosorov V., Golijanek-Jędrzejczyk A., Jaszczur. M, Andruszkiewicz A., *Evaluation of liquid-gas flow in pipeline using gamma-ray absorption technique and advanced signal processing*, ‘Metrology and Measurement Systems’ 2021, vol. 28, no. 1, pp. 145–159.

FLUID FLOW THROUGH RANDOMLY PACKED PARTICLES

M. Marek, P. Niegodajew

Faculty of Mechanical Engineering, Częstochowa University of Technology, al. Armii Krajowej 21, 42–200 Częstochowa, Poland

E-mail: maciej.marek@pcz.pl

Abstract. For chemical reactors using random packed beds, flow maldistribution from particle layering is a key issue. This study employs a validated numerical model to demonstrate that introducing regular wall corrugation effectively disrupts layering and significantly improves flow uniformity, as quantified by entropy measures and averaged radial velocity profiles.

Keywords: Computational Fluid Dynamics, random packed bed, corrugated wall, gas flow.

1. Introduction

Randomly packed beds in cylindrical columns are commonly used in chemical reactors, for instance to support catalysts or to increase the interfacial contact area between reactants in absorbers. Process efficiency is highly dependent on the flow characteristics within the bed. In particular, a uniform flow distribution is generally required, as flow channeling can lead to undesirable hot-spots or underutilization of the packing material.

The geometry of the random packing itself is a primary cause of flow maldistribution, even with a uniform inlet. Particles packed against a smooth cylindrical wall tend to form ordered, layered structures which create long, continuous channels. These channels act as preferential flow paths, bypassing significant sections of the bed. Recent studies on spherical particles by Marek et al. [1, 2] have demonstrated that this layering can be effectively mitigated by applying a regular, periodic corrugation to the container wall, with a wavelength several times the particle diameter and an amplitude on the scale of the particle radius. These promising geometrical findings necessitate an analysis of the resulting fluid flow performance. The present work demonstrates that, firstly, the structure of a random packing within a corrugated-wall container can be accurately generated using a simplified numerical model and, secondly, that wall corrugation offers substantial benefits for flow distribution. This improvement occurs even in the near-wall region, where a significant void fraction peak persists – similar to the flat-wall case – yet the flow penetration into the corrugation troughs is limited.

2. Methods

The geometrical structure of the random packing is generated using a sequential algorithm. In this method, each particle introduced into the container is subjected to physical forces (gravity and contact forces) as well as an artificial radial force to increase the packing density. Detailed validation against experimental data [3] confirms that the algorithm accurately reproduces the global bed void fraction and the oscillatory radial void fraction profile characteristic of particle layering, while being computationally far less demanding than a full discrete element method (DEM) simulation.

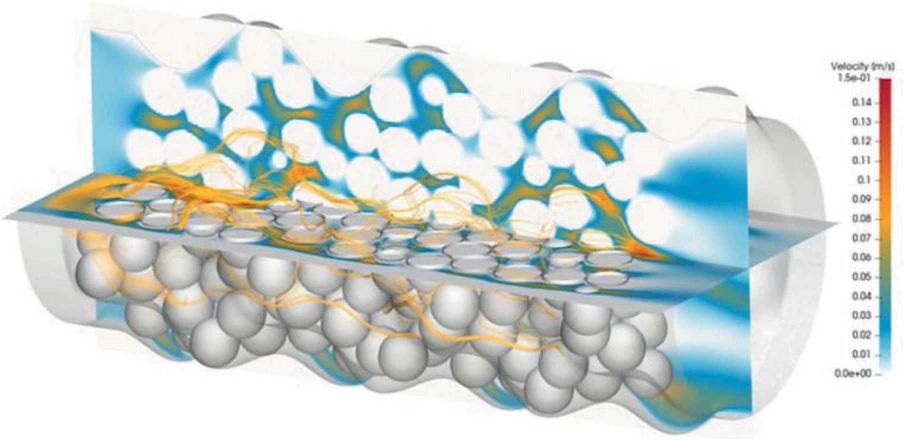

Figure 1. Fluid flow in a randomly packed bed of spheres confined by a corrugated cylindrical wall. Streamtraces are initiated at the inlet on a horizontal plane

Fluid flow in the low Reynolds number regime is simulated using an immersed boundary method, which allows the analysis of flow in complex geometries on a Cartesian grid. The solver is validated against experimental radial velocity profiles obtained by Magnetic Resonance Imaging (MRI) [4]. The close agreement between the simulated and measured flow velocity profiles, particularly in the near-wall region, confirms the adequacy of the numerical tools for analysing flow in random packings.

3. Sample results

Figure 1 shows the distribution of flow velocity magnitude in a sample packing with a corrugated wall, for a uniform inlet velocity profile (inlet plane on the left side of the structure). Direct numerical simulation enables the calculation of averaged radial velocity profiles which typically exhibit strong oscillations when particle layering is present. For selected wall corrugation parameters, these oscillations are shown to be significantly reduced. The characteristic velocity peak near the wall is also considerably diminished, despite the radial void fraction profile maintaining a large peak near the wall due to the corrugation troughs. However, these troughs are not easily penetrated by the flow.

Following the analysis of the bed's geometrical structure via configurational entropy in [1], the uniformity of the flow field can be similarly quantified using an entropy measure. It is shown that the Shannon entropy associated with the velocity field is higher in the corrugated container than in its flat-wall counterpart. Conversely, for certain corrugation parameters that enhance particle layering (geometric resonance [1]), the entropy decreases for both the packing geometry and the flow distribution.

Acknowledgments

The work funded by the Polish National Science Centre under Grant No. UMO-2023/51/B/ST8/01624.

References

[1] Marek M., Wilczynński M., Durajski A.P., Niegodajew P., *Preventing near-wall particles' ordering in narrow random packed beds of spheres*, 'Advanced Powder Technology' 2025, vol. 36, no. 11.

[2] Marek M., Wilczynński M., Durajski A.P., Niegodajew P., *Reducing wall effect in random packed beds of spheres through corrugation of the container's wall*, 'Powder Technology' 2026, vol. 467.

[3] von Seckendorff J., Achterhold K., Pfeiffer F., Fischer R., Hinrichsen O., *Experimental and numerical analysis of void structure in random packed beds of spheres*, 'Powder Technology' 2021, vol. 380, pp. 613–628.

[4] Eghbalmanesh A., Romijn N., Baltussen M.W., Peters E.A.J.F., Buist K.A., Kuipers J.A.M., *Hydrodynamics in a randomly packed bed of spheres: A comparison between PR-CFD simulations and MRI experiments*, 'AIChE Journal' 2024, vol. 70, no. 5.

FRACTAL FLOW-BASED COOLING SYSTEMS FOR SINGLE FUEL CELLS AND FUEL CELL STACKS

A. Merdjani, W. Olszewski, N. Kizilova

Warsaw University of Technology, Institute of Aeronautics and Applied Mechanics, 24 Nowowiejsta St., 00–665 Warsaw, Poland

E-mail: abdelhakim.merdjani.dokt@pw.edu.pl

Abstract. Fuel cells (FCs) is a promising green energy technology that widely used in cars, buses, airplanes, large and small portable units. Uniform operating temperature is an important condition of long efficient work of FCs. Existing cooling systems cannot provide uniform temperature distribution over the cell. Here an efficient cooling system as a fractal-type structure with a set of uniformly distributed outlets for the coolant outflow onto the working FC is proposed. Geometry of the fractal was optimized based on the minimum energy loss approach and validated by CFD computations. It was shown, the energy loss due to viscous and thermal dissipation was 8% lower while the flow and heat uniformity were 12% higher compared to the conventional cooling systems. Due to good scalability of the tree-like fractals, such systems can be used from macro- to micro- scales.

Keywords: Fluid Flow, Fuel Cell, Fractal Structures, Cooling, Computational Fluid Dynamics, Multicriteria Optimization.

1. Introduction

Proton Exchange Membrane Fuel Cells (PEMFCs) are widely recognized as efficient and clean energy conversion devices for transportation and stationary applications. However, thermal management remains a critical constraint for both single cells and FC stacks. During operation, a substantial portion of the electrochemical energy is converted into heat and insufficient heat removal leads to temperature gradients, membrane dehydration, catalyst degradation and reduced durability [1-2].

Conventional cooling plate configurations such as parallel and serpentine suffer from flow maldistribution and non-uniform temperature fields, particularly at higher current densities or larger active areas. These limitations increase entropy generation and pumping power requirements. Fractal tree-like flow design inspired by natural branching systems, provide improved fluid distribution with reduced hydraulic resistance. Based on the minimum energy loss principles, fractal geometries enable scalable and uniform coolant delivery at low pressure drop [3]. This study estimates a fractal flow-based cooling plate for single PEM FCs and stack configurations.

2. Materials and method

2.1. Fractal cooling design

A tree-like fractal cooling geometry was developed using branching laws derived from minimum energy dissipation principles [3]. The inlet channel bifurcates into successive branches to ensure uniform coolant distribution over the active area. Channel dimensions and branching ratios were selected to minimize total hydraulic resistance while maintaining equal outlet flow distribution. A conventional parallel channel cooling plate with identical external dimensions was used as a reference case.

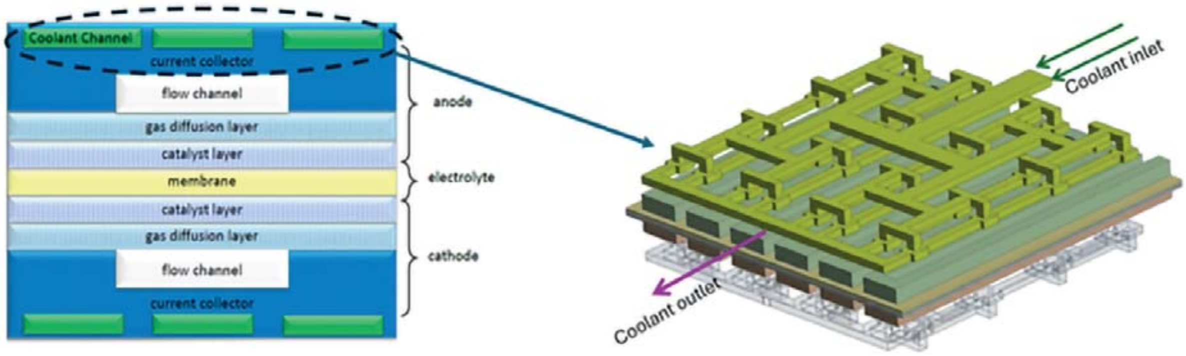

Figure 1. Schematic of the PEM fuel cell structure coupled with the proposed fractal cooling plate configuration

2.2. Numerical Model and Simulation Setup

A 3D PEM FC model coupled with the cooling plate was implemented. The computational domain included the cooling channel and solid layers responsible for heat conduction. Heat generation was introduced as a volumetric source term corresponding to nominal operating current density.

Numerical simulations were performed using ANSYS Fluent 2022 R2. The governing equations solved were [4]:

- Continuity equation,
- Momentum equation,
- Energy equation.

Assumptions included steady-state operation, coolant (Air), constant thermo-physical properties.

Boundary conditions were defined as follows:

- Coolant inlet:
  - specified velocity: 2 m/s,
  - temperature: 15°C.

3. Results and discussion

The fractal cooling configuration improved thermal uniformity and reduced hydraulic losses compared to the conventional parallel channel design:

- Temperature uniformity improved by 12%, with lower peak temperature and reduced hot spots,
- Total energy losses due to viscous dissipation decreased by 8%, indicating improved thermodynamic efficiency.

References

[1] Wang Y., Sun Z.Y., Yang L., *Optimizing temperature distribution in a PEMFC stack: A computational study on cooling plate and coolant dynamics*, ‘International Journal of Hydrogen Energy’ 2025, vol. 97, pp. 88–103.

[2] Merdjani A., Kizilova N., Awotwe T.W., Kostrzewski M., *Advancements and challenges in design of flow field plates in proton exchange membrane fuel cells: a comprehensive review*, ‘Frontiers in Energy Research’ 2025, vol. 13, art. no. 1506011.

[3] Kizilova N., Sauermoser M., Kjelstrup S., Pollet B.G., *Fractal-like flow-fields with minimum entropy production for polymer electrolyte membrane fuel cells*, ‘Entropy’ 2020, vol. 22, no. 2, p. 176.

[4] ANSYS, *ANSYS Fluent Fuel Cell Module Manual*, https://www.afs.enea.it/project/neptunius/docs/fluent/html/fuelcells/node3.htm (access: 31.03.2026).

TIME DEPENDENT TRANSITION ON VERTICAL HEATING PLATE

J. Muller[1], S. Rozborski[1], D. Boldo[2]

[1] *MFEE Department, EDF R&D, 6 Quai Watier, 78400 Chatou, France*

[2] *PRISME Department, EDF R&D, 6 Quai Watier, 78400 Chatou, France*

E-mail: jean.muller@edf.fr

Abstract. Many new nuclear power plants designs aim at relying on natural convection phenomena, seeking economic competitiveness. To improve RANS approaches in CFD and validate these new designs features, the transition from laminar to turbulent flow must be understood, and the influencing parameters studied. In this work, we investigate the time dependence of the transition position during relatively long experiments (4 hours). A clear change in transition altitude over time for several initial temperatures is observed.

Keywords: Experimental Fluid Mechanics, Measurement Techniques, Transition.

1. Introduction

The behavior of the transition from laminar to turbulent flow along a heated vertical plate is still in question in the literature, especially for Rayleigh number higher than 10^{14} [1]. The Rayleigh number is defined as follow, $Ra^* = g\beta q\, L^4/\nu\alpha$. With g the gravitational acceleration (m/s²), β the thermal expansion coefficient (1/K), q the thermal flux per unit area (W/m²), L the characteristic length (m), ν the kinematic viscosity (m²/s) and α: thermal diffusivity (m²/s).

The transition on a vertical plate has been experimentally studied by Vliet [2] and exhibits different behavior function of the heating power. In our study, we impose the heating power to investigate the effect of time and initial water temperature on the transition. In comparison with previous CFD studies in which the timescale is under 1 hour, such as [1]. The duration of the performed tests was 4 hours to match the timescale studied in [3]. The theoretical Ra* is of the order of 10^{15} in our experimental setup (function of the initial temperature).

2. Experimental method

The experiment consists of a tank with internal dimensions of 2 m × 1 m × 0.5 m filled with distilled water. The dimensions are shown in Figure 8-(a). The tank is insulated with three layers of insulating material on the side. This gives a theoretical thermal resistance of 6.9 m²·K/W on the side. On the upper face, a perforated layer of insulation limits thermal exchange while allowing instrumentation to pass through. At the bottom, no specific insulation is applied.

The heating plate, shown in red on Figure 1-(a) is 1650 mm high. It's composed of two zones: a heating zone of 1490 mm in height and a non-heating zone of 160 mm. The heating power per unit of surface is 7.23 kW/m² which corresponds to a total power of 5.2 kW.

The heating plate is instrumented with 26 Type-T thermocouples, mounted on the surface at a distance of less than 1.5 mm from the wall. 20 of these thermocouples are placed on a vertical line in the middle of the heating plate starting at 140 mm of the heating plate lower edge and separated of 60 mm each. 6 thermocouples are placed on the side of this vertical line to evaluate the three-dimensional aspect of the natural convection taking place in the experiment. The thermocouples have a (measured) response time of 0.3 s. They were connected to an acquisition system operating at 10 Hz and thermally isolated in a specific box to minimize temporal drift (measured).

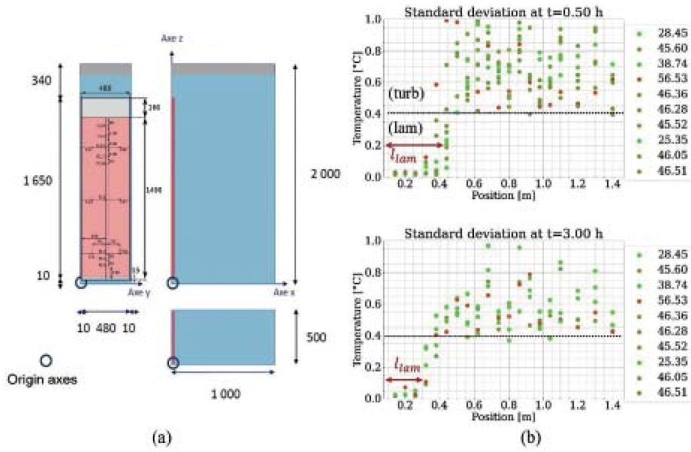

Figure 1: (a) Test section dimension filled with water. (b) Transition position displacement

3. Results and discussion

Figure 1-(b) shows the standard deviation of thermocouple readings after 30 minutes (top) and 3 hours (bottom) of the test. The use of the standard deviation to detect the transition from laminar to turbulent behavior is based on the recognition of changes in flow around the sensor in these two regions. In the laminar region, a small standard deviation is expected, whereas in the turbulent region, a high standard deviation is expected. This change in standard deviation is observed in all tests, regardless of the homogeneous initial temperature (indicated by the color of the dots), and at different instant during the test. The size of the laminar region, denoted as l_{lam}, decreases with time, implying that the transition occurs lower down the heating plate. This conclusion is consistent across all tests.

These findings raise questions about the timescale of the tests performed and the temporal behavior of the laminar-to-turbulent transition. An analysis of the displacement velocity of the transition and the influence of the bulk temperature will be the subject of future work and are intended to be presented at the conference.

Acknowledgements

The authors would like to thank the technical staff and the engineers involved in planning and executing of this experimental study conducted at EDF Lab Chatou.

References

[1] Yang S., Bieder U., Studer E., *LES of natural convection along a side-heated vertical wall in a water cavity applied for the scale of Small Modular Reactor*, 'Nuclear Engineering and Design' 2023, vol. 414.

[2] Vliet G.C., Liu C.K., *An experimental study of turbulent natural convection boundary layers*, 'Journal of Heat Transfer' 1969, vol. 91, no. 4, pp. 517–531.

[3] Morente A., Uribe J., Benhammadouche S., et al., *Towards New Experiments for Natural Convection at High Rayleigh Numbers: Definition, Sizing and Analysis using CFD*, NURETH-21, 2025.

FRACTAL BIOMIMETIC FINS FOR OPTIMAL FLOW-BASED SYSTEMS FOR INTERNAL/EXTERNAL COOLING/HEATING

S. Naqvi[1], N. Kizilova[2]

[1] *Warsaw University of Technology, Institute of Aeronautics and Applied Mechanics, 24 Nowowiejsta St., 00–665 Warsaw, Poland*

[2] *Warsaw University of Technology, Institute of Aeronautics and Applied Mechanics, 24 Nowowiejsta St., 00–665 Warsaw, Poland*

E-mail: nataliya.kizilova@pw.edu.pl
E-mail: saiyadhasan.naqvi.dokt@pw.edu.pl

Abstract. An optimal design of flow-based systems for heating or cooling a given area are essential for industry, transportation, electronics and domestic use. The target design is considered here as a multicriteria optimization problem allowing minimal viscous Z_h and thermal Z_{th} dissipation, and maximum flow and temperature uniformity at a given volume of the system. Geometry of fractal-type fins in the nasal ducts of Arctic animals is used as primary evolutionary optimal structure for further CFD-based improvements. Optimal scaling for the lengths and wid ths of the fractal fins and the number of generations have been determined. It was shown, both $Z_h \rightarrow$min& $Z_{th} \rightarrow$min and minimum entropy production criteria produce similar optimal designs. As it was shown by CFD computations with AnSys Fluent, the optimized design is more efficient (>10%) and scalable from micro/nano- heaters and coolers to large industrial systems.

Keywords: Fluid Flow, Biomimetics, Fractal Structures, Heating, Cooling, Computational Fluid Dynamics, Multicriteria Optimization.

1. Introduction

Efficient cooling of engines, reactors and other heat-producing equipment as well as heating of the air inside the buildings or fluids in the tanks needs specific geometry of the fluid-flow systems (tubes, channels) with higher surface/volume ratios. Surface-filling and volume-filling fractal systems have higher surface area per unit length compared to regular structures. Fractal structures are defined here as complex, geometric patterns exhibiting self-similarity across different scales, from nano/micro to macro. The T-type fractal fins can be found in the nasal ducts of different Arctic animals [1], which demonstrate efficient heating of the inhaled air from low (up to -30°C) to body (~40°C) temperatures [2] thanks to the principle 'split&mix' in the fractal structures of the total length L~5–8 cm only [3]. This design was chosen for heating fins inside the tube/channel as nature-inspired solution for fast and efficient heating of the cold fluid flow through the tube. It is also promising for implementation in the face masks for safe inhalation in cold climate and other breathing apparatus with low hydraulic Z_h and thermal Z_{th} resistivity based on the multicriteria optimization problem $Z_h \rightarrow$min & $Z_{th} \rightarrow$min [4].

2. Materials and method

A set of T-type fractals with n = 4–6 generations were designed as a fin inside a long circular tube of a radius R = 3.5 cm and L = 5 cm. The cross-sections of the fins of different widths (w_i) and lengths (l_i), i = 1 - n, are presented in Fig. 1. In total, 27 different geometries were considered, with both acute and smoothed corners. The total volume of the fins was taken constant V_s = 45% of the tube's volume, in accordance to biological design of Arctic animals [1-3]. Such structures produce sufficient 'heating via splitting & mixing' at a relative low hydraulic resistivity of the fractal fins with n > 6 generations.

Numerical computations were carried out with AnSys Fluent 2025 R1. Laminar and turbulent momentum equations with heat equation were solved at a wide range of Reynolds numbers Re = 10^2 - 10^4. The inlet velocity and temperature of the fluid (air) were taken as v_f = 1m/s and T_f = -20 °C. The wall temperature along the tube's wall and the fractal fin was taken constant T_w = 90 °C. The flow and temperature parameters were computed, and the thermal inlet length L_{th}, hydraulic resistivity $Z_h = \Delta p/Q_f$, thermal resistivity $Z_{th} = \Delta T/Q_h$, where Δp and ΔT are the pressure and temperature drop along the tube, Q_f is the fluid flow rate, Q_h is the heat flux and the total entropy S_{tot} generated by the viscous and thermal dissipation were computed. All the pairs of the values (Z_h, Z_{th}, L_{th}, S_{tot}) were taken as optimization criteria for Pareto-based multicriteria design optimization at the constrain V_s=const.

3. Results and conclusions

In the nasal ducts of Arctic animals, the fractal fins presented in Fig.1 heat the incoming cold air to comfortable breathing temperature of ~22–25 °C within a quite short length of the tube L ≤ 5 cm. The T-type bifurcations of the fins split the flow into uniformly thin layers which are efficiently and fast heated between the branches of the i = 2–4 generations. Higher numbers n > 4 produce solid structures with higher hydraulic resistivity and, thus, higher viscous dissipation and entropy production. Therefore, the fins with smoothed branches produce smaller viscous and thermal dissipation. Since, optimization problem has no unique solution with Pareto frontier approach, a set of best designs with similar entropy productions were selected.

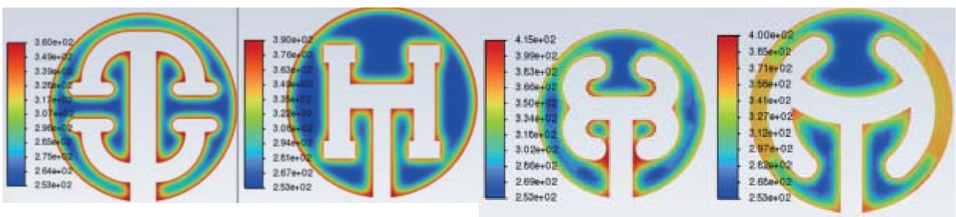

Figure 1. Temperature distribution inside the fluid flow with different fins

Therefore, the fractal fins allow maximisation of the heat transfer at the fluid-solid interface at very law viscous and thermal resistance, high flow and temperature uniformity that is important for different applications from micro/nanofluidics systems for large industrial heaters/coolers.

References

[1] Solberg S., Kjelstrup S., Magnanelli E., Kizilova N., Casado Barroso I.L., Acquarone M., Folkow L.P., *Energy efficiency of respiration in mature and newborn reindeer*, 'Journal of Comparative Physiology B' 2020, vol. 190, pp. 509–520.

[2] Cheon H., Kjelstrup S., Kizilova N., Flekkøy E.G., Mason M.J., Folkow L.P., *Structure-function relationships in the nasal cavity of Arctic and subtropical seals*, 'Biophysical Journal' 2023, vol. 122, pp. 4686–4698.

[3] Cheon H., Kizilova N., Flekkoy E., Mason M.J., Folkow L.P., Kjelstrup S., *The nasal cavity of the bearded seal: An effective and robust organ for retaining body heat and water*, 'Journal of Theoretical Biology' 2024, vol. 595, art. no. 111933.

[4] Write J., Copeland R.J., Srinivas G., Gebhard S.C., Karpuk M.E., Breathing apparatus, and method for controlling temperature fluctuations, 2017, USA Patent No. US 9597532 B2.

DEEP-LEARNING-BASED DESIGN OPTIMIZATION AND AERODYNAMIC PERFORMANCE VALIDATION OF A NATURAL LAMINAR FLOW AIRFOIL

M.A. Nasr*, B.Y.J. Wong, C.M.J. Tay

National University of Singapore, Singapore 117575, Republic of Singapore

*E-mail: m_nasr@nus.edu.sg

Abstract. This study presents a machine-learning-driven approach for the design optimization of a high-performance natural laminar flow (NLF) airfoil for specific flow conditions. By employing deep-learning-based tailored airfoil modes within a surrogate optimization framework, we developed an airfoil for intermediate Reynolds number applications. This design meets geometric and aerodynamic constraints while maximizing aerodynamic efficiency. Performance was validated across two design points $\mathrm{Re} = 2 \times 10^6$, and 4×10^6, and $\mathrm{M} = 0.1$ and 0.2, respectively, using medium-fidelity CFD. The results confirm the effective delay of transition onset and the achievement of extended laminar runs resulting in aerodynamic efficiency improvement.

Keywords: Aerodynamics, Deep Learning, surrogate optimization, Natural Laminar Flow, Airfoil Optimization, Computational Fluid Dynamics.

1. Introduction

Natural Laminar Flow airfoils are crucial for enhancing aerodynamic efficiency by minimizing drag, particularly in the context of intermediate Reynolds number applications. Achieving extended laminar flow over a significant portion of the airfoil surface directly translates to reduced fuel consumption and increased endurance. The design of such airfoils, however, presents a complex optimization challenge due to the sensitive nature of laminar-to-turbulent transition and the need to maintain performance across a range of flight conditions and geometric constraints. This study addresses these challenges by developing a robust NLF airfoil using the Efficient Global Optimization (EGO) framework, integrating a Kriging-based Gaussian Process Regression (GPR) surrogate model with XFOIL evaluations. To enhance optimization efficiency, the design space is defined by tailored airfoil modes extracted via Deep Learning. Specifically, a Generative Adversarial Network (GAN) is employed to generate realistic airfoil samples, while a Convolutional Neural Network (CNN) acts as a geometric filter to ensure all candidates remain physically consistent and manufacturable. Comprehensive CFD analysis has been performed to ensure the reliability and robustness of the resulting design.

2. Optimization Methodology

The objective of this study is to develop a multi-point natural laminar flow (NLF) airfoil design that outperforms a baseline airfoil, FX63-137m, for the desired flight conditions envelop. The design space encompasses 25 design points (DP) defined by Reynolds numbers $Re \in \{2e6, 2.5e6, \dots, 4e6\}$ and Mach numbers $Ma \in \{0.1, 0.125, \dots, 0.2\}$. The optimization is conducted for an angle-of-attack range of $\alpha \in \{0, 0.25, \dots, 5\}$, ensuring all solutions satisfy prescribed geometric and aerodynamic constraints.

The NLF airfoil optimization utilizes an Efficient Global Optimization (EGO) framework which iteratively refines a Kriging surrogate model by maximizing the Expected Improvement (EI) function. To ensure a physically consistent design space, the airfoil is parameterized using tailored modes extracted via a Wasserstein GAN (WGAN) trained on the UIUC database. The core of this methodology, as detailed in previous work [1], is a surrogate-based optimization approach where costly numerical simulations are replaced by computationally inexpensive approximation models, such as Kriging model coupled with XFOIL as the aerodynamic solver. This allows for effective exploration of high-dimensional design spaces, mitigating the risk of getting trapped in local minima which is often a concern with gradient-based optimization methods.

2.1. Optimization Problem Statement

This is a multi-point design optimization that can be defined as follows:

- Objective: Maximize the average value of lift/drag (L/D) for the flight conditions envelop;
- Variables: Coefficients of airfoil modes (x_{shape}) (15 modes), Re, Ma and α;
- Constraints: Maximum thickness > 18%, trailing edge thickness $t = 0.005c$ (c is the chord length), airfoil thickness > 0.07c @ $x = 0.75c$, transition location on suction side > 0.54c @ $DP1 = (Re, Ma) = (2 \times 10^6, 0.1)$ and > 0.5c @ DP2 = $(Re, Ma) = (4 \times 10^6, 0.2)$, and maximum lift coefficient ≥ 1.25 @ $Dp1$&$DP2$.

3. Aerodynamic Performance and Flow Analysis

To ensure the reliability of the XFOIL-based optimization process and aerodynamic performance improvement, extensive CFD validation was performed. The CFD framework was validated against the natural laminar airfoil developed by NASA, NLF-0416, where it showed a good match with their experimental results [2], before it was applied to the baseline and optimized airfoils. The RANS simulations were performed using the $k - \omega - SST\ 4 - eqn$ transition model in ANSYS FLUENT with hyperbolic O-mesh and $y^+ < 1$ to properly capture the transition region. The simulations were performed for the first and last design points ($DP1$&$DP2$) for the baseline and optimized airfoils.

3.1. Aerodynamic Performance

The optimized airfoil exhibits its maximum thickness further downstream relative to the baseline design which promotes a downstream shift of the transition location. This modification extends the laminar flow region, thereby reducing drag. Although there is a negligible improvement in the lift coefficient, the transition delay achieved on the optimized airfoil resulted in a significant change in drag which in turn improved the lift-to-drag by around 10–30% in the angle of attack range of interest, α = [0:5], as shown in Figure 1 for $DP1$.

a) b)

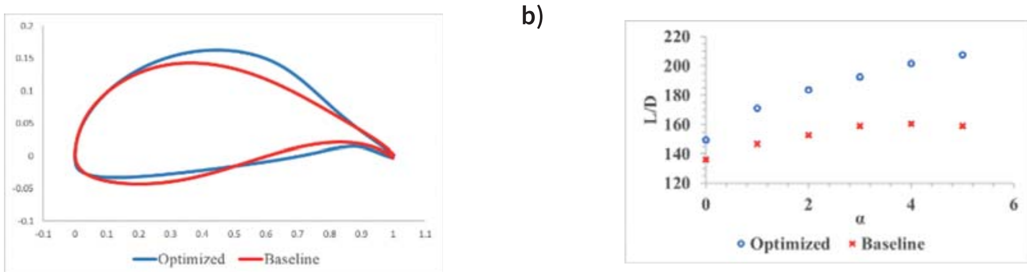

Figure 1. (a) Optimized airfoil profile compared to the baseline airfoil (b) Aerodynamic performance comparison between the baseline and optimized airfoils at *DP1* in terms of L/D

Acknowledgements

Computational resources for this work were provided by the High-Performance Computing Facility of National University of Singapore (NUS-HPC).

References

[1] Li J., Zhang M., Tay C.M.J., , Liu N., Cui Y., Chew S.Ch., Khoo B.Ch., *Low-Reynolds-number airfoil design optimization using deep-learning-based tailored airfoil modes*, 'Aerospace Science and Technology' 2022, vol. 121.

[2] Somers D.M., *Design and experimental results for a flapped natural-laminar-flow airfoil for general aviation applications*, National Aeronautics and Space Administration, Scientific and Technical Information Branch, 1981.

EFFECT OF COLUMN WALL CORRUGATION ON LIQUID TRANSPORT IN RANDOM PACKED BEDS OF SPHERICAL PARTICLES

P. Niegodajew[1], M. Wilczyński[1], A. Durajski[2], M. Marek[1]

[1] *Department of Thermal Machinery, Częstochowa University of Technology, al. Armii Krajowej 21, 42–201 Częstochowa, Poland*

[2] *Faculty of Electrical Engineering, Częstochowa University of Technology, Al. Armii Krajowej 17, Częstochowa, 42–200, Poland*

E-mail: pawel.niegodajew@pcz.pl

Abstract. This work experimentally investigates gravity-driven liquid flow in a random packed bed of smooth spheres confined in a cylindrical column, with emphasis on near-wall behavior under localized point injection. Spatially resolved outlet measurements are used to assess the influence of sinusoidal wall corrugation on liquid redistribution away from the wall.

Keywords: Experimental Fluid Mechanics, Trickle Bed Reactor, Corrugated Wall, Liquid Spreading.

1. Introduction

In random packed beds confined in cylindrical columns, the container wall promotes structural ordering of particles in the near-wall region. This confinement-induced layering, particularly pronounced in beds of spheres, leads to oscillations of the local void fraction and preferential flow paths adjacent to the wall, resulting in flow maldistribution in packed-bed devices.

Recent systematic studies by Marek et al. [1, 2] demonstrated that sinusoidal corrugation of the container wall can substantially suppress near-wall particle ordering and reduce void-fraction oscillations across a range of column-to-particle diameter ratios D_c/D_p. However, these works focused on the packing structure itself and the corresponding impact on fluid flow has not yet been addressed.

In the present work, we experimentally investigate gravity-driven liquid flow in a random packed bed of smooth spheres bounded by a sinusoidally corrugated wall. The study focuses on the near-wall region under localized, near-wall point injection, aiming to quantify the ability of wall corrugation to promote liquid migration away from the wall.

2. Experiment

The research was conducted using the experimental stand shown in Fig. 1a. The core of the setup consisted of a *vertical cylindrical column* filled with a random packing of smooth, monodisperse glass spheres. The column-to-particle diameter ratio was fixed at $D_c/D_p \approx 10$, while the packed bed height H was varied between $1D_c$ and $4D_c$. Liquid flow was driven gravitationally and supplied at the top of the bed through a single capillary, positioned in the near-wall region to probe the ability of the liquid to redistribute away from the column wall, providing a localised point source of injection. The liquid flow rate was fixed at 50 L/h, corresponding to a superficial velocity of about 0.8 mm/s.

To investigate wall effects, measurements were performed in columns differing only in the inner wall geometry (Fig. 1b): a reference column with a flat wall and a column with *sinusoidal wall corrugation*.

The corrugation was characterised by a wavelength of the order of $4D_p$, applied identically in both the axial and circumferential directions, and by an amplitude of approximately $1.1D_p$, corresponding to geometrical scales previously shown to disrupt near-wall particle ordering [1,2].

After percolating through the packed bed, the liquid exited the column and was collected using a custom-designed outlet collector (Fig. 1c). The collector discretised the column cross-section into 32 azimuthal sectors, each connected to an individual vertical measurement tank. This configuration enabled simultaneous, time-integrated quantification of the spatial distribution of the liquid flow at the column outlet. The sector numbering is indicated directly in the contour maps in Fig. 1d, while the grouping into outlet regions (I–VIII) used for regional analysis is illustrated in Fig. 1e.

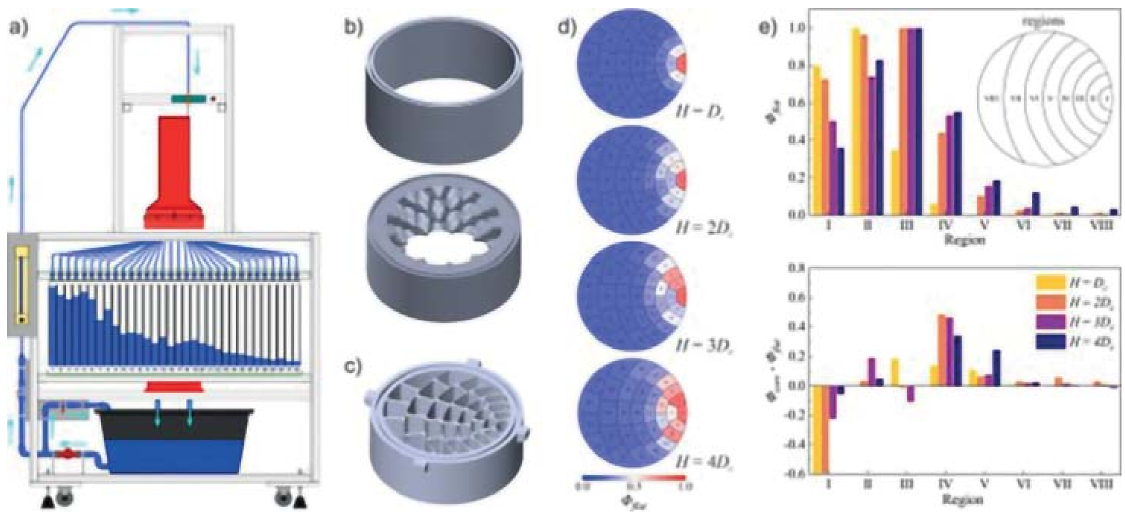

Figure 1. Schematic of the experimental stand (a), column wall geometries: flat and sinusoidally corrugated (b), sectorized outlet collector (c), contour maps of Φ for increasing bed height H/D_c in the smooth-wall column (d), and analysis of Φ in eight outlet regions (I–VIII) (e)

3. Preliminary results

Figure 1d shows the evolution of the normalized liquid throughput $\Phi = (V/A)/(V/A)_{\max}$ with increasing bed height H for the smooth-wall column, where V is the liquid volume collected in a given outlet sector and A is the corresponding collector pocket area. At low bed heights, the liquid throughput is strongly concentrated in sectors adjacent to the near-wall injection location, whereas increasing H leads to progressive radial spreading and attenuation of the near-wall dominance.

To facilitate quantitative comparison, the outlet cross-section was further subdivided into eight spatial regions (I–VIII), as illustrated in Fig. 1e. The upper plot presents regionally averaged values Φ_{flat} for the smooth-wall (flat) column, while the lower plot highlights the effect of wall corrugation through the difference $\Phi_{corr} - \Phi_{flat}$, where Φ_{corr} corresponds to the corrugated-wall column.

The regional representation reveals that, for the smooth-wall column, the liquid throughput remains strongly biased toward regions adjacent to the wall over a wide range of bed heights. Introducing wall corrugation systematically reduces this near-wall dominance and enhances liquid transport in regions farther from the wall, as reflected by positive values of $\Phi_{corr} - \Phi_{flat}$ in the inner regions. This trend indicates that the corrugation promotes radial redistribution of the liquid already at moderate bed heights.

Acknowledgments

The work funded by the Polish National Science Centre under Grant No. UMO-2023/51/B/ST8/01624.

References

[1] Marek M., Wilczyński M., Durajski A.P., Niegodajew P., *Preventing near-wall particles' ordering in narrow random packed beds of spheres*, 'Advanced Powder Technology' 2025, vol. 36, no. 11.

[2] Marek M., Wilczyński M., Durajski A.P., Niegodajew P., *Reducing wall effect in random packed beds of spheres through corrugation of the container's wall*, 'Powder Technology' 2026, vol. 467.

POROUS MEDIA LAYER MODEL TO ACCOUNT FOR ROUGHNESS IN THE MINI-CHANNEL FLOWS

B. Okonokhua, M. Pahlavanzadeh, K. Rusin, W. Wróblewski

Silesian University of Technology, Department of Power Engineering and Turbomachinery, Konarskiego 18, 44–100 Gliwice, Poland

E-mail: bethel.okonokhua@polsl.pl

Abstract. The Porous Media Layer (PML) model in the numerical solver is implemented to simulate the effects of roughness in the mini-channel flow. The parameters of the porous material are adjusted to the geometry of roughness given in the reference. The distributions of the flow parameters are compared with the DNS results to assess the simulation of the interaction of the roughness sublayer and the outer layer. The results provide insight into the limitations of the PML model.

Keywords: Computational Fluid Dynamics, Mini-channel flows, Roughness, Friction.

1. Introduction

Roughness affects many technical applications and modelling the real geometry of roughness is challenging due to the scale differences between the roughness, and the flow domain. Various approaches exist to model surface roughness. Yuan and Piomelli [1] studied the roughness sublayer using DNS of a channel flow. The symmetry at the top wall makes the case like the flow between two parallel plates. Periodic boundary conditions were applied on the side walls and a constant pressure gradient between the front and back surfaces was used to drive the flow through cyclic transfer of parameters until convergence. Li et al. [2] simulated the same case using LES and compared their results with [1].

Fully resolved roughness provides high accuracy but is computationally expensive, while empirical wall-function approaches offer efficiency at the cost of limited generality. Alternatively, the porous medium layer (PML) roughness model represents the rough surface as a thin homogenised porous layer adjacent to the wall, introducing the effects of roughness through momentum source terms rather than explicit geometric resolution. Pahlavanzadeh et al. [3] applied the PML roughness model to the analysis of Tesla turbines, demonstrating that it captures the effect of roughness height on flow parameters and turbine efficiency.

2. Simulation case

The case study is adopted from the DNS simulation performed in [1]. The domain with dimensions of *6h x 1h x 3h*, where *h* is half of the channel height respectively in the *x, y, z*, was discretised. The schematic showing how the different roughness layer approaches are defined is depicted in Fig. 1. The developed flow is driven by the pressure gradient adjusted for the constant mass flow. The Reynolds number, defined with half of the channel height and friction velocity, was close to $Re_\tau = 1000$. The channels with smooth walls and with two values of roughness were considered.

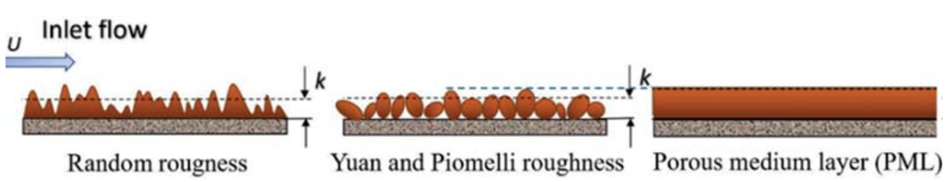

Figure 1. Schematics of random roughness, Yuan and Piomelli roughness, and porous layer

3. Numerical model and scope of the study

Numerical simulations employed the finite volume method to solve the discretised Reynolds-averaged Navier-Stokes (RANS) equations. The simulations presented in this study were performed using the k–ω SST turbulence model. In the PML method, a porous layer modifies the resistance to fluid flow, and the momentum term should be amended with respect to porous parameters.

Inside the porous layer, the porosity may vary, $0 \leq \alpha < 1$, and the resistance term, assuming steady fully developed 2-D flow in an isotropic porous medium, can be calculated from the Brinkman-Forchheimer-extended Darcy equation:

$$R = \frac{\mu}{K} U_i + \frac{\rho C_f}{K^{1/2}} {U_i}^2 \tag{1}$$

where K is the permeability, assuming $C_f = 0.55$

The study begins with the validation of the proposed approach against the results of [1] and [2]. The analysis continues with the presentation of different distributions of porous parameters along the porous layer to evaluate the performance of the model. The main objective was to evaluate the limitations of the PML model in reflecting the interaction between the roughness structures and the outer layer.

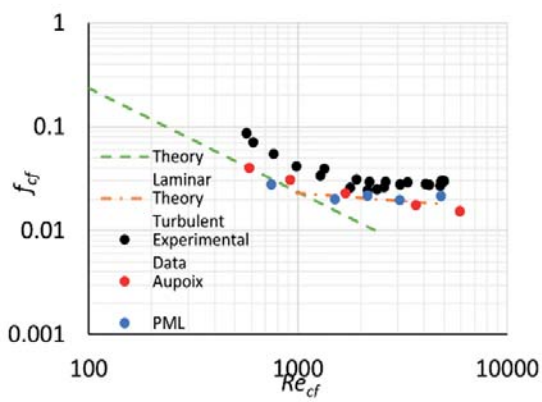

Figure 2. Figure shows the Fanning friction factor as a function of Constricted Reynolds number

Acknowledgements

The research presented was carried out within the UMO-2025/57/B/ST8/00179 research project financed by the Polish National Science Centre.

References

[1] Yuan J., Piomelli U., *Roughness effects on the Reynolds stress budgets in near-wall turbulence*, 'Journal of Fluid Mechanics' 2014, vol. 760.

[2] Li S., Yang X., Jin G., He G., *Wall-resolved large-eddy simulation of turbulent channel flows with rough walls*, 'Theoretical and Applied Mechanics Letters' 2021, vol. 11, no. 1.

[3] Pahlavanzadeh M., Rusin K., Wróblewski W., Rulik S., *Roughness effects on flow in Tesla turbine with parametric adjustment of porous layer model*, 'Physics of Fluids' 2025, vol. 37, no. 1.

NUMERICAL AND EXPERIMENTAL ANALYSIS OF FLOW UNIFORMITY IN A STAR-TYPE MANIFOLD

A. Olczyk, K. Sobczak, K. Kantyka, G. Liśkiewicz[1], B. Miller, M. Tomecka, P. Rusinow[2]

[1] *Lodz University of Technology, Institute of Turbomachinery, 217/221 Wolczanska St., 93–005 Lodz, Poland*

[2] *uFraction8 PL SP z o.o. Trzebińska 6, 60–003, Poznań, Poland, EU*

E-mail: grzegorz.liskiewicz@p.lodz.pl

Abstract. This paper presents a numerical and experimental analysis of flow uniformity in a star-type manifold designed for liquid distribution. The study compares CFD simulations performed in Ansys CFX with experimental measurements on a 20-outlet test rig. The results indicate that the manifold exhibits a neutral characteristic, with flow distribution primarily determined by the hydraulic resistance of the connected modules rather than the manifold geometry itself.

Keywords: Computational Fluid Dynamics, Experimental Fluid Mechanics, flow uniformity, star-type manifold.

1. Introduction

The objective of this study was to analyze the flow uniformity in a star-type manifold in a Segmented/Cave configuration, designed to distribute fluid into 20 outlets arranged in multiple levels. The research involved both CFD simulations and experimental validation. The study progressed from idealized simulations without throttling to analysis including hydraulic resistances of the filtering modules.

Flow distribution in manifold systems is important in heat exchangers, fuel cells and chemical reactors [1]. Star-type manifolds are promising due to their radial symmetry, though practical implementations often reveal discrepancies attributed to manufacturing tolerances [2, 3].

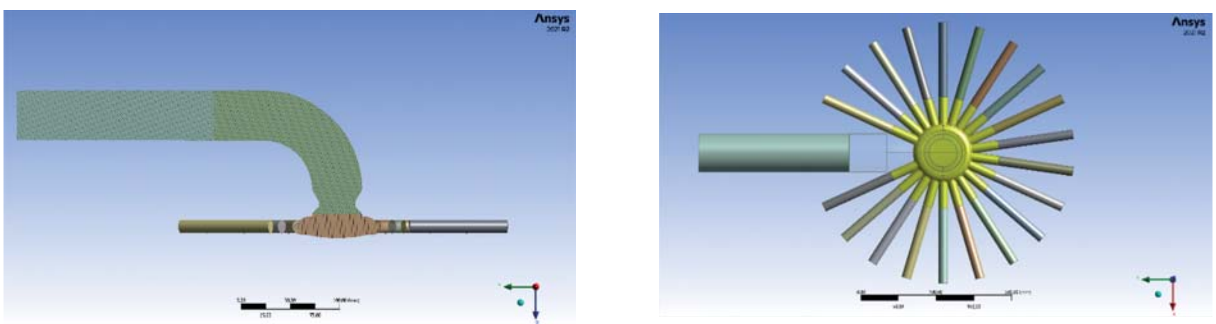

Figure 1: Schematic of the star-type manifold with 20 outlets

2. Methods

The numerical analysis was performed using Ansys CFX with an unstructured mesh of tetrahedral and prismatic elements. A mesh independence study (19.9, 34.5, 58.7M elements) led to selection of the 34.5 M grid. The k-epsilon RNG turbulence model was chosen for better stability. Water flow at 25°C was simulated with mass flow rate at the inlet and atmospheric pressure at the outlets. Module resistance was modeled via a porous media approach (permeability $3.50 \cdot 10^{-10}$ m²).

3. Experimental setup

The test rig comprised the star-manifold feeding 20 throttling modules, powered by a Seepex BN 5-6L pump. Flow was measured by weighing at each outlet, inlet pressure was monitored with an Aplisens AS transducer.

4. Results

4.1 CFD results

Preliminary CFD simulations without throttling showed near-perfect uniformity across all 20 outlets. With module resistances included, mass flow variations remained below 1%, while the manifold pressure drop (~55 Pa) was negligible compared to module resistance (~2 bar).

4.2 Experimental results and module-tolerance effect

Experimental results showed flow rate variations of 12.6–20.6%. A module-swap test (Module #6 vs. #12) confirmed that non-uniformity was caused by manufacturing tolerances, not manifold geometry. Tests with blocked outlets showed the system adapts with a slight inlet pressure increase.

5. Conclusions

The star-type manifold has a neutral hydraulic characteristic; observed experimental variations were caused by individual module resistances. The numerical model correctly predicts flow behavior when accounting for these resistances.

References

[1] Bajura R.A., Jones E.H., *Flow distribution manifolds*, 'Journal of Fluids Engineering' 1976, vol. 98, no. 4, pp. 654–666.

[2] Tong J.C.K., Sparrow E.M., Abraham J.P., *Geometric strategies for attainment of identical outflows through all of the exit ports of a distribution manifold*, 'Journal of Fluids Engineering' 2007, vol. 129, no. 9, pp. 1132–1140.

[3] Shen S., Ding Y., Chen J., Sun B., *Effect of manufacturing tolerances on flow distribution in fuel cell stacks*, 'International Journal of Hydrogen Energy' 2019, vol. 44, no. 59, pp. 31519–31529.

NUMERICAL AND EXPERIMENTAL ANALYSIS OF DRAG COEFFICIENT OF A DISC-GAP-BAND PARACHUTE

A. Olszewska, Z. Peter[1]

[1] *Wroclaw University of Science and Technology, Faculty of Mechanical and Power Engineering, Wybrzeże Wyspiańskiego 27, 50–370 Wrocław, Poland*

E-mail: aleksandraolszewska2006@gmail.com, zosiapeter18@gmail.com

Abstract This paper investigates the influence of gap configurations – specifically the number, size and spatial positions – on the aerodynamic performance of a disc-gap-band (DGB) parachute. Computational Fluid Dynamics (CFD) simulations were performed to analyse flow structures and drag coefficient variations. Complementary wind tunnel experiments assessed both drag coefficient and stability, with stability quantified by return-to-axis time. The study highlights a trade-off between drag and stability, showing that the mid-position gap configuration provides the best compromise – minimizing C_d reduction while ensuring faster stabilization than more extreme arrangements.

Keywords: Computational Fluid Dynamics (CFD), Experimental Fluid Mechanics, Aerodynamic optimalization, Drag coefficient, Disc-gap-band (DGB) parachute, Parachute aerodynamics, Wind tunnel testing, Canopy geometry.

1. Introduction

Disc-gap-band (DGB) parachutes are widely used in aerospace due to their stability and high drag coefficient (C_d) [1]. Their performance is sensitive to geometric modifications affecting flow separation and wake structure [2]. This study evaluates the effect of gap number, size and distribution on C_d using CFD simulations complemented by wind tunnel experiments to provide much-needed quantitative data for hybrid numerical-experimental approaches.

2. Geometry of the Disc-Gap-Band (DGB) Parachute and Test Configurations

2.1. Disc-Gap-Band Parachute Geometry

The DGB parachute consists of a central disc, an annular gap, and an outer band (Fig. 1). Seven configurations were derived from a baseline geometry [3] to systematically analyze gap effects on flow dynamics. Table 1 summarizes the investigated arrangements.

2.2. Gap Definition and Investigated Configurations

The influence of the number, size and position of gaps is investigated for seven parachute configurations, each differing in gap arrangement while maintaining identical reference dimensions. This allows a systematic comparison of gap configuration effects on flow dynamics and drag generation. Table 1 summarizes the investigated arrangements.

Table 1. Investigated disc-gap-band parachute configurations

Configuration ID	Number of Gaps	Gap position	Gap Width	Description
DBG-1	1	Upper	Standard	Baseline configuration
DGB-2	1	Middle	Standard	Single gap – mid position
DGB-3	1	Lower	Standard	Single gap – lower position
DGB-4	1	Middle	Narrow	Single gap – reduced width

DGB-5	1	Middle	Wide	Single gap – increased width
DGB-6	2	Upper + Lower	Standard	Double-gap configuration
DGB-7	3	Upper + Middle + Lower	Standard	Triple-gap configuration

3. Numerical Methodology

Numerical simulations were performed in a domain extending 20 diameters upstream and 50 downstream to ensure a fully developed wake [4]. Turbulence was modeled using the k–ω model, chosen for its ability to capture flow separation and complex wakes. The fluid was assumed Newtonian with constant viscosity at ambient conditions (T = 300 K, p = 1 bar). Velocity inlet and outflow boundaries were applied, with no-slip on parachute surfaces. A mesh independence study confirmed converged drag coefficient results.

4. Experimental Methodology

Wind tunnel tests were performed on rigid models of the DGB parachute to correlate numerical predictions with physical flow behavior. The models were tested in a low-speed wind tunnel and the aerodynamic drag force was measured using a calibrated force balance across a range of Reynolds numbers. Experimental observations show that variations in gap configuration significantly affect force fluctuations and drag levels. Specifically, the mid-position gap configuration (DGB-2) exhibited satisfactory stable behavior – quantified by a reduced return-to-axis time – while maintaining high aerodynamic resistance compared to extreme venting arrangements.

References

[1] Moog R.D., Bendura R.J., Timmons J.D., Lau R.A., *Qualification Flight Tests of the Viking Decelerator System*, NASA Technical Report, https://ntrs.nasa.gov/citations/19730046641 (access: 2.04.2026).

[2] Reichenau D.E.A., *Aerodynamic Characteristics of Disk-Gap-Band Parachutes*, ARO Report, https://apps.dtic.mil/sti/tr/pdf/AD0746291.pdf, (access: 2.04.2026).

[3] Knacke T.W., *Parachute Recovery Systems Design Manual*, https://apps.dtic.mil/sti/tr/pdf/ADA247666.pdf (access: 2.04.2026).

[4] Izadi M.J., Dawoodian M., *Numerical Simulation of Flow over a Disk-Gap-Band Parachute*, Proccedings of ASME 2009 Fluids Engineering Division Summer Meeting, Vail 2009, Paper No. FEDSM2009-78125.

ACTIVE SUPPRESSION OF VORTEX-INDUCED VIBRATIONS: COMPARATIVE STUDY BETWEEN PID AND SMC CONTROLLERS

M. Pilecki[1], **J. Płuziński**[2]

[1] *PWr In Space, Faculty of Information and Communication Technology, 27 Wybrzeże Wyspiańskiego St., 50-370 Wrocław, Poland*

[2] *PWr In Space, Faculty of Fundamental Problems of Technology, 27 Wybrzeże Wyspiańskiego St., 50-370 Wrocław, Poland*

E-mail: 1279994@student.pwr.edu.pl, 2278641@student.pwr.edu.pl

Abstract. This research investigates the active suppression of vortex-induced vibrations (VIV) in a circular cylinder using a coupled wake-oscillator model. We compare the performance of classical PID control with Sliding Mode Control (SMC) to address the inherent nonlinearities of the fluid-structure interaction. The study evaluates controller efficacy across varying flow regimes, focusing on the stabilization of the wake-oscillator limit cycle and the minimization of control effort.

Keywords: General Fluid Dynamics, Vortex-Induced Vibrations, Sliding Mode Control, PID Control, Nonlinear Dynamics, Active Flow Control.

1. Introduction

This work aims to develop a numerical framework for the real-time suppression of Vortex-Induced Vibrations (VIV) in cylindrical objects. Because VIV significantly degrades system performance and complicates bluff-body wake stabilization, it remains the subject of extensive ongoing research [1]. By investigating the nonlinear coupling between fluid wake dynamics and an oscillating body's response, this study utilizes a reduced-order model to streamline the design of feedback control laws.

2. Model Equations

2.1. Physical Model

The dynamics of cross-flow VIV for a 1-DOF rigid cylinder is modelled using a semi-empirical wake-oscillator framework of the following form [2]:
Structural and fluid equations

$$s = \ddot{y} + \left(2\xi\delta + \frac{\gamma}{\mu}\right)\dot{y} + \delta^2 y, \qquad f = \ddot{q} + \varepsilon(q^2 - 1)\dot{q} + q \tag{1}$$

Where $y = \frac{Y}{D}$ is the dimensionless cross-flow displacement of cylinder with Y being the dimensional displacement and D the diameter of the cylinder, q is the dimensionless wake variable, ξ is the reduced damping term, δ is the reduced angular frequency of the structure, γ is the stall parameter, μ is the dimensionless mass ratio, ε is the Van der Pol coefficient. The acceleration coupling model will be used due to its accuracy leading to the following form of the coupling terms: $s \sim q$ and $f \sim \ddot{y}$. All empirical coefficients will have values assigned in consistency with established literature [2].

2.2. Control Algorithms

2.2.1 PID Control

The Proportional-Integral-Derivative (PID) Controller [3] is applied to the displacement error $e(t) = y_{eq} - y$ and it's control input u is defined as:

$$u(t) = K_p e(t) + K_i \int_0^t e(\tau) d\tau + K_d \frac{de(t)}{dt} \tag{2}$$

Control objective is to design a control input *u(t)* such that:

$$\lim_{t\to\infty} e(t) = 0, \qquad \lim_{t\to\infty} \dot{e}(t) = 0 \tag{3}$$

u(t) is introduced as an external forcing term in the structural equation:

$$u(t) + s = \ddot{y} + \left(2\xi\delta + \frac{\gamma}{\mu}\right)\dot{y} + \delta^2 y \tag{4}$$

Oscillator remains unchanged and is affected indirectly through the structural acceleration coupling.

2.2.2. SMC Control

Sliding Mode Control [4] addresses the nonlinearities of the wake dynamics defining a sliding surface s in the state space:
where λ is a positive convergence gain. The control objective is satisfied system state reaches and stays on the sliding manifold $s = 0$.

$$s = \dot{e} + \lambda e \tag{5}$$

3. Simulation Methodology

Initial controller prototyping is performed in MATLAB and Simulink using the coupled systems. The controllers are first tuned using a fixed-step Runge-Kutta integrator. Controller parameters are optimized to minimize the vibrations. The secondary phase consists of results verification by comparing the model results with Ansys Fluent simulations done using URANS k-ω SST turbulence model [5]. The analysed Reynolds number are in range from 10 to 10^4.

References

[1] Li H., Ekici K., *Vortex-Induced Vibration Predictions of a Circular Cylinder Using an Efficient Pseudo-Time Code-Coupling Approach*, 'Fluids' 2025, vol. 10, no. 7, p. 182.

[2] Facchinetti M., de Langre E., Biolley F., *Coupling of structure and wake oscillators in vortexinduced vibrations*, 'Journal of Fluids and Structures' 2004, vol. 19, pp. 123–140.

[3] Song J., Du J., Gao, *Applying PID control to 2-dof vortex induced vibration of a cylinder*, 'Ocean Engineering' 2024, vol. 300.

[4] Utkin V., *Variable structure systems with sliding modes*, 'IEEE Transactions on Automatic Control' 1977, vol. 22, no. 2, pp. 212–222.

[5] Rosetti G.F., Vaz G., Fujarra A.L.C., *URANS Calculations for Smooth Circular Cylinder Flow in a Wide Range of Reynolds Numbers: Solution Verification and Validation,* 'Journal of Fluids Engineering' 2012, vol. 134, no. 12.

EFFECT OF INFLOW CONDITIONS ON SHOCK-INDUCED SEPARATION ON A COMPRESSOR STATOR PROFILE

M. Piotrowicz, M. Kurowski, A. Hanfy, P. Doerffer, M. Śleszyński, P. Flaszyński

Institute of Fluid-Flow Machinery, Polish Academy of Sciences, ul. Fiszera 14, 80–231 Gdańsk, Poland

E-mail: mpiotrowicz@imp.gda.pl

Abstract. This paper focuses on the influence of Reynolds number (5.9×10^5, 2.3×10^5) on a flow structure, an isentropic Mach number distribution, a shock wave position and a boundary layer development on the suction side of a compressor stator profile. The effects of a shock-boundary layer interaction (SBLI) are investigated using numerical and experimental methods. For this purpose, a linear three-profile test section based on a cascade configuration was designed to reproduce the flow representative for a suction side of the profile in cascade.

Keywords: Aerodynamics, Transonic flow, Reynolds number effects, (SBLI) Shock-boundary layer interaction, Compressor cascades, CFD simulation, Experimental validation.

1. Introduction

The development of advanced aero-engine technologies requires systematic increase in efficiency and emission reduction through the application of higher pressure ratio in transonic compressors. These designs generate complex flow structures induced by adverse pressure gradients resulting from shock-boundary layer interaction (SBLI) [1].

Particularly at low Reynolds numbers, laminar boundary layers upstream of the shock exhibit high susceptibility to separation, leading to intense turbulence, total pressure losses and may initiate unsteady shock oscillations [2], [3]. The influence of the Reynolds number on the Mach number distribution and a flow structure on a stator profile was the subject of numerical and experimental analyses [2]. For this purpose, a linear three-blade test section was designed for the IMP PAN transonic wind tunnel (Fig. 1). The cascade geometry, defined by Rolls-Royce Deutschland, was developed to reproduce flow structures characteristic of full-scale cascade simulations. The main objective of the research was a detailed analysis of SBLI mechanisms and their impact on boundary layer development and flow separation under varying Reynolds number conditions. The investigations were conducted for two Reynolds number values representing high-altitude cruise and take-off conditions.

2. Numerical results and comparison with experiment

Numerical simulations were performed for a compressor stator cascade using the FINE/Turbo Cadence solver with a two-equation BSL-EARSM turbulence model, coupled with a laminar-turbulent transition γ–Reθt model. Based on the authors experience, this model predicts with a high accuracy the shock-boundary layer interaction and separation on the suction side of the stator profile. A multi-block structured grid with appropriate resolution in the near-wall region and in the shock wave area was generated in the IGG Cadence, comprising a total of 31.7×10^6 grid elements. Computations and experimental investigations were performed for two Reynolds numbers: 5.9×10^5 and 2.3×10^5, at transonic inlet conditions consistent with the parameters in the wind tunnel.

The Reynolds number was defined based on the profile chord and density which was controlled by the valve installed at the inlet to reduce the total pressure upstream the test section, whilst maintaining the target inlet Mach number. Numerical computations were validated against dedicated measurements. The isentropic Mach number distribution was compared with pressure measurements on the stator suction side as well as on the upper and lower test section walls.

Reynolds number effect on the flow structure and velocity at selected traverses was investigated and compared with measurements upstream and downstream of the three profiles (Laser Doppler Anemometry) and oil flow visualisation which provided qualitative information about flow structure patterns close to the suction side and separation regions.

The comparison between numerical and experimental results demonstrates correct prediction of the shock wave position, Mach number distribution, velocity profiles and size of separation zones, thereby confirming the reliability of the numerical model.

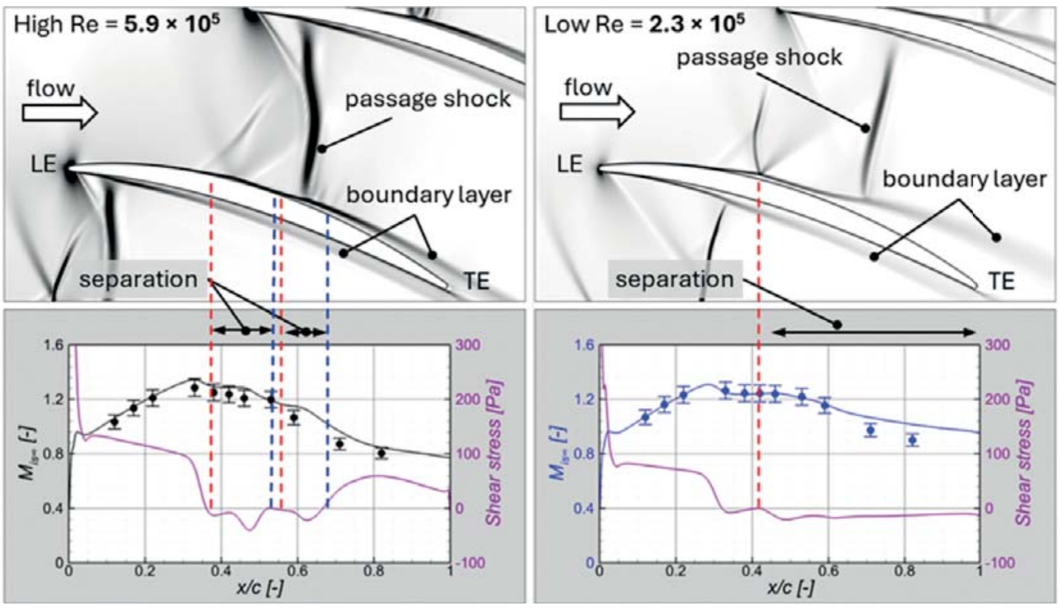

Figure 1. Shock-Boundary Layer Interaction (SBLI) at different Reynolds numbers

Acknowledgements

We gratefully acknowledge Polish high-performance computing infrastructure PLGrid (HPC Center: CI TASK) for providing computer facilities and support within computational grant no. PLG/2025/018509. Computations were carried out using the computers of the Centre of Informatics – Tricity Academic Supercomputer & Network (CI TASK).

References

[1] Piotrowicz M., *Oddziaływanie fali uderzeniowej z warstwą przyścienną na profilu sprężarki lotniczej*, Wydawnictwo IMP PAN, Gdańsk 2025.

[2] Flaszyński P., Babinsky H., Doerffer P., *Towards Effective Flow Control and Mitigation of Shock Effects in Aeronautical Applications*, Springer Nature, Cham 2025.

[3] Munoz Lopez E.J., Hergt A., Klinner J., Klose B., Willert C., Gümmer V., *The Unsteady Shock-Boundary Layer Interaction in a Compressor Cascade – Part III: Mechanisms of Shock Oscillation*, 'Journal of Turbomachinery' 2025, vol. 147, no. 9.

PEDESTRIAN COMFORT AND VENTILATION – NUMERICAL ANALYSIS OF AIRFLOW IN A BUILDING QUARTER

M. Pisula[1], M. Poćwierz[2], J. Szumbarski[3]

[1,2,3] *Warsaw University of Technology, Faculty of Power and Aeronautical Engineering, ul. Nowowiejska 24, 00–665 Warszawa, Poland*

[1] E-mail: maciej.pisula.dokt@pw.edu.pl
[2] E-mail: marta.pocwierz@pw.edu.pl
[3] E-mail: jacek.szumbarski@pw.edu.pl

Abstract. The work concerns the aerodynamic analysis of a building quarter in the context of pedestrian comfort and urban space ventilation. Numerical studies were performed using the RANS k–epsilon method in the ANSYS Fluent environment. A significant impact of the geometric parameters of the buildings on wind speeds and average air age was demonstrated, indicating directions for optimising the urban layout.

Keywords: Aerodynamics, Computational Fluid Dynamics, Air Pollution, Pedestrian Comfort.

1. Introduction

Contemporary cities require building designs that minimize the risk of stagnation zones conducive to the accumulation of pollutants, counteract the intensification of the urban heat island effect and at the same time do not generate dangerously high wind speeds at pedestrian level[1]. Appropriate urban design therefore requires a precise analysis of air flow, conducted from the perspective of both user comfort and ventilation. Geometric parameters can be used to describe the geometry of a building layout[2]. In cooperation with architects, a building quarter was developed which is a representative model for this type of construction in Poland. The aim of the work was to assess wind conditions and identify possible ways to optimize the initial quarter.

2. The subject of the research

The proposed building layout was developed after taking into account geometric parameters such as the ratio of street width to building height (W/H), floor area ratio (FAR), and plot coverage ratio (BCR), which determine the local characteristics of air flow and the level of ventilation in urban spaces. At the same time, it takes into account the legal conditions for design in Poland and was created using software that automatically generates and analyzes various design solutions based on input data such as plot boundaries, building boundaries, area and building height. The scale of the analyzed geometry corresponds to real-scale buildings of height equal to 24 meters.

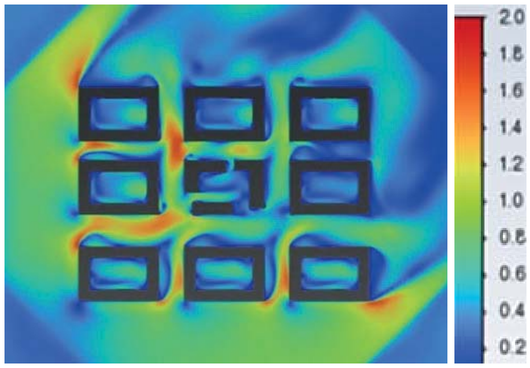

Figure 1. Contours of amplification factor at pedestrian level for air inflow from the southwest. Colors correspond to 'alpha' coefficient

3. Research method and results

Numerical calculations were performed in the ANSYS Fluent environment using the RANS k–epsilon Realizable turbulence model. Particular attention was paid to boundary conditions–velocity profiles, turbulent kinetic energy and kinetic energy dissipation–as well as roughness, which minimizes the degradation of specified profiles along the domain[3]. The calculations were supplemented with validation based on wind tunnel measurement data provided by the Architectural Institute of Japan which allowed for the assessment of the reliability of the results obtained for the analyzed type of development. Two variables were used to assess wind conditions. The first is the wind speed amplification factor (α), shown of the Figure 1, used mainly to assess the risk of excessive gusts which is the ratio of the wind speed at the analyzed height near buildings to the wind speed at the same location for undisturbed flow. The second parameter is the mean age of air (τ), which is a measure of the efficiency of ventilation and removal of pollutants from the analyzed urban structure. It provides information on how long a given air particle 'lives' in the analyzed area. In addition, regulations and guidelines concerning pedestrian comfort and ventilation used in various countries were analyzed which allowed the results to be placed in an international regulatory context. The next stage of the research involves changes to the geometry of the initial block: varying the height of buildings, manipulating distances from neighboring blocks and attempting to plan a so-called ventilation path.

4. Conclusions

The research focused on analyzing aerodynamic conditions in a building block designed based on geometric parameters characteristic of selected urban structures in large cities in Poland. The results confirm the need to consider aerodynamic issues already at the urban design stage. The results of the research can serve as a basis for formulating design recommendations concerning the geometry of buildings and the distances between them, allowing for the reconciliation of development intensity with the requirements for urban environmental quality.

References

[1] Wankhade R., Pernigotto G., Larcher M., *A Literature Review on Methods and Metrics for the Analysis of Outdoor Air Displacement Conditions in the Urban Environment,* 'Energies' 2023, vol. 16, no. 6.

[2] Palusci O., Monti P., Cecere C., Montazer H., Blocken B., Impact of morphological parameters on urban ventilation in compact cities: the case of the Tuscolano-Dondistrict In Rome, 'Science of the Total Environment' 2022, vol. 807.

[3] Blocken B., Stathopoulos T. and Carmeliet J., *CFD simulation of the atmospheric boundary layer: wall function problems*, 'Atmospheric Environment' 2007, vol. 41, no. 2, pp. 238–252.

UNDERSTANDING OF THE FLOW COMPLEXITY OF MOTORCYCLE WHILE CORNERING

B. Potęga, E. Cieślikowski, K. Walicki, M. Remer[1]

[1] *Warsaw University of Technology, Institute of Aeronautics and Applied Mechanics, Nowowiejska St. 24, 00–665 Warsaw, Poland*

E-mail: michal.remer@pw.edu.pl

Abstract. The work addresses the understanding of flow complexity around a racing motorcycle while cornering, combining telemetry-based boundary conditions, wind tunnel tests and CFD simulations. The study highlights strong three-dimensionality, asymmetry and curvature effects that significantly modify aerodynamic forces and moments compared to straight-line motion. Advanced URANS and hybrid LES approaches are developed to resolve unsteady flow structures and capture mesoscopic vortex dynamics that emerge during cornering manoeuvres.

Keywords: Vehicle aerodynamics, Experimental Fluid Mechanics, Computational Fluid Dynamics, Cornering flows, Telemetry data analysis.

1. Introduction

Cornering maneuvers radically change the incoming flow direction and effective incidence angle along the motorcycle length, leading to substantial modifications of drag, side force and aerodynamic moments compared to straight-line operation. For high-performance racing motorcycles this has a direct impact on stability, balance and tire utilization, making three-dimensional, unsteady flow understanding a design-critical issue [2, 3, 4]. The present contribution builds upon comprehensive experimental and numerical work devoted to the analysis of aerodynamic characteristic variations of a racing motorcycle during steady cornering and cross-wind conditions [1]. Here we focus on the flow-physics perspective: how curvature, lean angle and rider posture jointly control the wake structure, pressure distribution and the resulting force-moment system.

2. Methodology

Investigated scenarios cover straight-line motion, steady cross-wind and steady cornering with varying curvature, referenced to the racing motorcycle Perun with realistic rider geometry. Track telemetry from Poznań and Motorland Aragon determines representative combinations of speed, lean angle (approximately 50°) and curvature for three cornering radii. From lateral acceleration and GPS data, real path radii and curvatures are reconstructed and used to define boundary conditions for simulations. Numerical simulations employ a rectangular computational domain with a rotating reference frame to reproduce steady cornering. The geometry includes three rider-motorcycle configurations: upright ($\varphi = 0°$), leaned 50° in aerodynamic position and leaned 50° with the rider hanging off and the inner leg extended. Wind-tunnel experiments are performed on a 25%-scale simplified model with a six-component balance for straight-line and cross-wind cases at Reynolds numbers from 3·10^5 to 1.4·10^6 (full-scale reference).

3. Results and analysis

Simulation and measurement data confirm that cornering produces strongly three-dimensional and asymmetric flow structures with significant wake reorganization compared to straight-line motion. For cross-wind at 30° yaw, drag coefficient rises by approximately a factor of three, while side force and overturning moment increase markedly. In contrast, for steady cornering with a rotating reference frame, a non-intuitive trend is observed: drag coefficient decreases as curvature increases, whereas lateral forces and yaw moments tend to push the motorcycle out of the turn. Rider position plays a key role in controlling aerodynamic moments. Hanging off with the inner leg extended approximately doubles the yawing moment available for cornering initiation compared with the aerodynamic tucked position. Experimental investigation and steady CFD simulations of racing motorcycle aerodynamics during cornering reveal rich three-dimensional flow physics absent from simplified models. The counter-intuitive drag reduction with increasing curvature and strong dependence of aerodynamic moments on rider position demonstrates the necessity of resolving the complete three-dimensional flow field. The extended URANS employ k–ω SST–SAS formulation, while the hybrid RANS–LES simulations use SBES k–ω SST, both capturing mesoscopic-scale vortex dynamics and unsteady force fluctuations emerging during aggressive cornering. A mesh-sensitivity study was performed with grids of approximately 50, 100, and 150 million cells, with the highest refinement concentrated around the motorcycle–rider system. Near-wall resolution was enforced at $y^+ \approx 1$ on surfaces using prism cells. A fixed time step was used such that CFL < 20 for ~60% of the cells [5,6]. When combined with validated experimental reference data from wind tunnels and real-world telemetry, these advanced numerical tools will enable physics-based design optimization of racing motorcycles and support rider-aerodynamic interaction analysis.

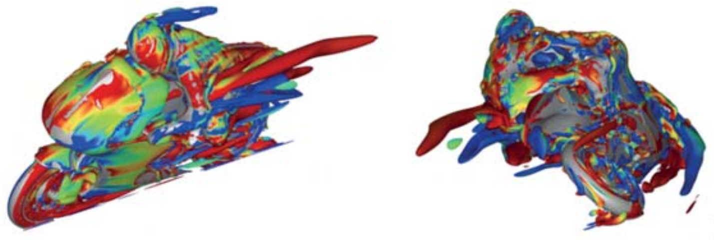

Figure 1. Isosurfaces of Q-criterion (Q = 25) by vorticity (Ωx) along (x)

4. Acknowledgments

Projekt realizowany w ramach przedsięwzięcia Ministra Nauki i Szkolnictwa Wyższego pt. 'Wsparcie studentów w zakresie podniesienia ich kompetencji i umiejętności' – nabór II, Działanie 01.05 Umiejętności w szkolnictwie wyższym, Program Fundusze Europejskie dla Rozwoju Społecznego 2021–2027, współfinansowany ze środków Unii Europejskiej.

References

[1] Potęga B., *Analysis of aerodynamic characteristics variations during cornering on example of racing motorcycle*, M.Sc. Thesis, Warsaw University of Technology, Warsaw 2025.
[2] McBeath S., *Competition Car Aerodynamics*, Haynes Publishing, Sparkford 1994.
[3] Katz J., *Race Car Aerodynamics: Designing for Speed*, Robert Bentley Inc, Cambridge 1995.
[4] Cossalter V., *Motorcycle Dynamics*, LULU Press Morrisville, 2006.
[5] Ekman P., Larsson T., Virdung T., Karlsson M., *Accuracy and Speed for Scale-Resolving Simulations of the DrivAer Reference Model*, Technical Paper SAE Mobilus, SAE International, Warrendale 2019.
[6] Ekman P., *Important factors for accurate Scale-Resolving simulations of automotive aerodynamics*, PhD Thesis, Linköping University Electronic Press, Linköping 2020.

AERODYNAMIC CHARACTERISTICS OF A LEANING RACING MOTORCYCLE UNDER COMBINED SLIP AND LEAN ANGLES: EXPERIMENTAL STUDY

B. Potęga, J. Lepiarz, K. Skalska, M. Remer[1]

[1] *Warsaw University of Technology, Institute of Aeronautics and Applied Mechanics, Nowowiejska St. 24, 00–665 Warsaw, Poland*

E-mail: michal.remer@pw.edu.pl

Abstract. This study presents an experimental investigation of the aerodynamic behavior of a racing motorcycle subjected to combined lean angles and small yaw angles, representative of steady-state cornering. Building upon previous tests performed in an upright configuration, the current work focuses exclusively on wind tunnel measurements using a 1:4 scale model equipped with a detailed rider representation. Aerodynamic forces, moments and flow structures were examined across a range of roll and slip angles. The goal was to quantify how lean angle influences drag, side force and aerodynamic stability under realistic cornering conditions.

Keywords: motorcycle aerodynamics, aerodynamics, aerodynamics performance, wind tunnel testing, scale models.

1. Introduction

Aerodynamic loads during motorcycle cornering differ substantially from straight-line operation because the vehicle operates at significant lean angles and experiences small but non-zero yaw angles arising from track curvature and tire slip. These conditions change the effective projection of the motorcycle–rider system and introduce strong flow asymmetries. Building on earlier upright-configuration measurements, the present experimental program focuses on leaned configurations combined with small yaw, using a consistent, repeatable protocol suited to low-speed wind-tunnel testing of scaled models. Only a small number of experimental studies address motorcycle aerodynamics in leaned and yawed configurations, with one of the few examples being the wind-tunnel validation work on a scaled speedway motorcycle model [1], whereas a far richer body of yaw-focused experiments exists for cars – e.g., Rijns studies on the DRIVAER model [2].

2. Model

The test article is a 1:4 scale model of an electric racing motorcycle developed within Student Association for Vehicle Aerodynamics. The highly detailed full-scale geometry was adapted for additive manufacturing, with simplifications limited to fairing thickness, internal components and assembly features. The wheels are non-rotating in the current campaign. Because the rider's shape critically affects motorcycle aerodynamics, a 3D scan of the rider in a racing (tucked) posture was used to produce a high-fidelity human model integrated with the motorcycle. External surfaces in critical regions (windscreen, upper fairing, shoulder area, tail) were smoothed and finished to achieve uniform surface quality consistent with scaled testing. Figure 1 shows the described model geometry at neutral lean angle.

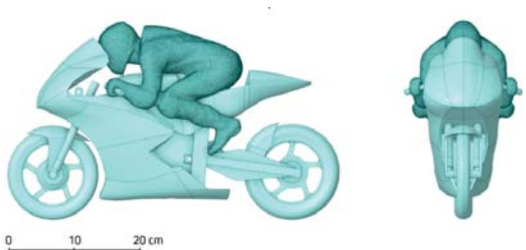

Figure 1. Geometry of the tested model

3. Methodology

3.1. Wind tunnel and operating conditions

Experiments are conducted in a low-speed wind tunnel at the Faculty of Power and Aeronautical Engineering, Warsaw University of Technology. The facility features a closed-return circuit with an open test section. The maximum air speed is 50 m/s, yielding a model Reynolds number of approximately 1×10^6 for the selected reference length. The blockage ratio of the motorcycle–rider assembly is about 4%, below the commonly recommended 5% threshold for low-speed testing [3]. Ambient conditions (temperature, pressure, humidity) are monitored for density correction.

3.2. Test rig

The model is mounted on a six-component internal balance located near the model centre of gravity. The balance was connected to the NI DAQ and LabView environment. A custom angle-setting fixture enables precise and repeatable adjustment of lean (roll) angle and yaw (slip) angle. The nominal angle set is: Lean (roll): 10°, 20°, 30°, 40°, 50°; Yaw: 0°, 2°, 4°, 6°. The ground plane is stationary (no moving belt) in this phase of testing. The fork/handlebar assembly is fixed at neutral steer for all runs.

3.3. Test matrix and sequence

For each lean setting, a yaw sweep is performed at selected tunnel speeds (up to 50 m/s). Additional velocity points (e.g., 20/30/40/50 m/s) are included for sensitivity to Reynolds number at representative lean–yaw combinations. The order of testing is arranged to minimize hysteresis and to maintain stable thermal conditions of the balance.

4. Scope of results

The full results will present:
- Aerodynamic force and moment coefficients as functions of lean and yaw (drag, side force, lift/downforce; roll/pitch/yaw moments);
- Uncertainty and repeatability analysis, including sensitivity to Reynolds number within the available tunnel envelope.

5. Acknowledgments

Projekt realizowany w ramach przedsięwzięcia Ministra Nauki i Szkolnictwa Wyższego pt. ‘Wsparcie studentów w zakresie podniesienia ich kompetencji i umiejętności’ – nabór II, Działanie 01.05 Umiejętności w szkolnictwie wyższym, Program Fundusze Europejskie dla Rozwoju Społecznego 2021–2027, współfinansowany ze środków Unii Europejskiej.

References

[1] Pujol Vidal I., *Numerical simulations of the aerodynamics of a speedway motorcycle*, Master’s thesis, Danmarks Tekniske Universitet, Kongens Lyngby 2025.

[2] Rijns S., Teschner T.R., Blackburn K., Brighton J., *Performance analyses of active aerodynamic load balancing designs on high-performance vehicles in cornering conditions*, ‘Physics of Fluids’ 2024, vol. 36.

[3] Barlow J.B., Rae W.H., Pope A., *Low-Speed Wind Tunnel Testing*, Wiley, New York 1999.

HIGH-FIDELITY PSEUDO-SPECTRAL SIMULATION OF SINGLE-PHASE AND DISPERSED TWO-PHASE ISOTROPIC TURBULENCE

M. Rajek[1, 2]**, J. Pozorski**[2]

[1] *Łukasiewicz Research Network, Institute of Aviation, Aleja Krakowska 110/114, 02–256, Warsaw, Poland*

[2] *Institute of Fluid Flow Machinery, Polish Academy of Sciences, Fiszera 14, 80–231 Gdańsk, Poland*

E-mail: michal.rajek@ilot.lukasiewicz.gov.pl

Abstract. In the present work, the authors develop a computational framework for high-fidelity direct numerical simulations (DNS) and large eddy simulations (LES) of both single-phase and particle-laden isotropic turbulence. A new deterministic forcing is developed to control the resolution of both large and small flow scales, yielding results in excellent agreement with the Kolmogorov theory. To model the unresolved turbulence in LES, the authors propose a new spectral eddy-viscosity based on a simple differential regulator. Unlike the well-established closure which assumes the existence of an infinite $k^{-5/3}$ energy spectrum, the new model accounts for the finite resolution of the simulation and promotes the development of the inertial subrange. The authors extend their pseudo-spectral code to simulate the motion of small, heavy inertial particles and demonstrate that the proposed framework significantly enhances the predictive capabilities of point-particle LES over a wide range of Stokes and Reynolds numbers.

Keywords: isotropic turbulence, inertial particles, DNS, LES, spectral closure.

1. Introduction

Dispersed two-phase flows with a particulate phase in the form of solid particles, droplets or bubbles constitute a broad class of flows relevant to many environmental phenomena and industrial processes. However, the turbulent transport of inertial particles remains a major theoretical and computational challenge [1]. This difficulty stems from the intrinsic non-linearity of the problem and from the wide range of spatial and temporal scales associated with turbulence and the particulate phase itself. One of the most powerful tools for exploring the physics of particle-laden flows are direct numerical simulations (DNS), in which the full Navier-Stokes equations are solved.

However, the computational cost of DNS still precludes its application to turbulent flows at high Reynolds numbers. An important alternative are large eddy simulations (LES), where only the large, energy-containing flow scales are resolved, whereas the effect of the unresolved turbulence is often accounted for statistically, leading to substantial computational savings. On the other hand, while in single-phase flows the consequences of spatial filtering can be compensated relatively easily, in dispersed two-phase flows the absence of small-scale turbulence affects inertial particle dynamics and may therefore require more advanced modeling.

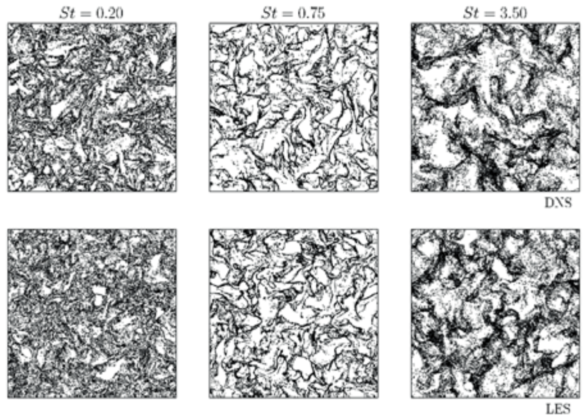

Figure 1. Instantaneous particle locations at $Re_\lambda \sim 100$ without gravitational effects; $St = \tau_p/\tau_\eta$ is the Stokes number and τ_η is the Kolmogorov time scale; total number of particles $N_p = 10^7$

2. Numerical methods

The authors consider an incompressible homogeneous and isotropic turbulence in a triply-periodic cubic box of size $L_B = 2\pi$. The filtered Navier-Stokes equations are expressed in Fourier space as in [2] to give

$$\left\{\frac{\partial}{\partial t} + [\nu + \nu_e(k,t;k_c)]k^2\right\}\hat{\bar{u}}_\alpha(k,t) = P_{\alpha\beta}(k)\left[\hat{\bar{N}}_\beta(k,t) + \hat{f}_\beta(k,t)\right], \tag{1}$$

where the overline denotes the filtered quantity and ν_e $(k,\ t;\ k_c)$ is the spectral eddy-viscosity; k_c is the cutoff wavenumber; $P_{\alpha\beta}(k) = \delta_{\alpha\beta} - k_\alpha k_\beta/k^2$ is the projection tensor; $\delta_{\alpha\beta}$ is the Kronecker delta and $k = |k|$. The non-linear term in physical space is given by $N(x, t) = u(x,t) \times \omega(x,t)$ where $\omega(x,t)$ is the vorticity field; ν is the kinematic viscosity of the fluid; $\hat{\boldsymbol{f}}(\boldsymbol{k},t)$ is an artificial force term used to sustain turbulence; $\hat{u}$ is used to distinguish between Fourier and physical space representations. To solve the above equations we use the pseudo-spectral approximation with the largest wavenumber limited to $k_{\max} = (2\pi/L_B)\lfloor\sqrt{2}N/3 + 0.5\rfloor$; $\lfloor\cdot\rfloor$ is the floor function. For particles much denser than the fluid, $\rho_p/\rho_f \gg 1$, their motion is governed by

$$\frac{\mathrm{d}\boldsymbol{V}(t)}{\mathrm{d}t} = -\frac{\boldsymbol{V}(t) - \bar{\boldsymbol{u}}\left[\boldsymbol{x}_p(t),t\right]}{\tau_p} + \boldsymbol{g}, \qquad \frac{\mathrm{d}\boldsymbol{x}_p(t)}{\mathrm{d}t} = \boldsymbol{V}(t) \tag{2}$$

where $\tau_p = 2\rho_p a^2/9\mu$ is the particle response time; V and a are respectively the particle velocity and radius, μ is the dynamic viscosity of the fluid; g is the gravity.

3. Results

The authors investigated the dynamics of inertial particles in LES at the Taylor-scale Reynolds number $Re_\lambda \sim 100$. As shown on Fig. 1 the instantaneous particle locations in LES (bottom panels) closely correspond to those from DNS (top panels). The authors argue that the proposed LES can predict certain large-scale phenomena, e.g., the clustering at length scales larger than η [3].

References

[1] Marchioli C., Bourgoin M., Coletti F., Fox R., Magnaudet J., Reeks M., Simonin O., Sommerfeld M., Toschi F., Wang L.-P., Balachandar S. , *Particle-laden flows*, 'International Journal of Multiphase Flow' 2025, vol. 191.

[2] Rajek M. Pozorski J., *High-fidelity pseudo-spectral simulations of isotropic turbulence: Large eddy simulations with semi-adaptive parametrization of residual flow scales*, 'Physics of Fluids' 2026, vol. 38.

[3] Rajek M., Pozorski J., *Adaptively reconstructed spectral eddy-viscosity in large eddy simulations of particle-laden isotropic turbulence, Part I: Particle statistics at low Reynolds number*, 'International Journal of Multiphase Flow' 2026, vol. 197.

EFFECT OF CHEVRON-INDUCED JET MIXING ON ENTRAINMENT CHARACTERISTICS OF A SUPERSONIC EJECTOR

R. Ramadas, S. Advaith

Department of Mechanical Engineering, Indian Institute of Technology Madras, Chennai, India

E-mail: advaith@iitm.ac.in

Abstract. The performance parameters of supersonic ejectors are strongly influenced by the mixing behaviour of the primary stream and the entrained secondary stream. Introducing chevrons at the nozzle exit is a passive method for enhancing mixing in a free jet by generating axial vortices. The present study investigates the effect of chevrons and their geometry on the performance of a supersonic ejector, particularly its entrainment ratio. The influence of chevrons on jet development and mixing in the free jet is studied using visualisation techniques. Parametric studies on ejectors with chevron nozzles are conducted to obtain performance parameters. Full experimental results will be presented at the conference.

Keywords: Experimental Fluid Mechanics, Ejectors, Chevron Nozzles, Supersonic Jets, Flow Visualisation.

1. Introduction

Supersonic ejectors are simple mechanical devices that operate on the principle of momentum and energy exchange between a driving fluid (primary stream) and a driven fluid (secondary stream). High-pressure primary fluid is allowed to expand through a supersonic nozzle. The expanded stream facilitates the entrainment of the secondary stream through momentum exchange. This entrainment process is controlled by shear-layer growth, jet spreading and mixing of the expanded jet, and shock interaction in the mixing chamber. Therefore, any modifications that improve jet mixing can enhance ejector performance.

Chevrons are V-shaped elements used in designs. Introducing chevrons at the trailing edge of the nozzles generates streamwise vortices at the exit plane, increasing the effective jet diameter and thereby promoting mixing. While extensively studied in acoustics noise reduction [1,2], their impact on influencing the entrainment behaviour in ejectors has been underexplored, except for a few recent numerical studies [3,4].

The present study primarily aims to explore this gap in the research by focusing on conducting experimental investigations to understand how modified nozzles with chevrons influence free-jet mixing and the entrainment behaviour of an ejector when a chevron nozzle is employed as its primary nozzle.

2. Experimental Methodology

Convergent-divergent nozzles with a throat diameter of 2 mm and an exit diameter of 3 mm are used as the primary nozzle, yielding an NPR of approximately 8. Chevrons are introduced at the nozzle exit, with chevron counts ranging from 3 to 5. The length of the chevron, l, is varied so that the ratio (l/d_e) takes the value of 1 and 1.5, where d_e represents the exit diameter of the nozzle. Two penetration angles of 0º and 2.5° are considered to investigate the influence of penetration angle on ejector entrainment and jet mixing.

The expanded supersonic free jet is visually studied using the schlieren visualisation technique. The density gradients in the supersonic flow are captured, yielding insights into shear layer development and shock structures.

The ejector experiments are carried out using the same chevron nozzles. The primary stagnation pressure is maintained between 2 bar and 5 bar, and a vacuum is maintained in the secondary stream using a vacuum chamber. The ejector back pressure is regulated to determine the ejector's operating range. The primary and secondary mass flow rates are measured using calibrated rotameters and pressure measurements.

3. Governing Equations

The entrainment ratio (ω) for an ejector is defined as

$$\omega = \frac{\dot{m}_s}{\dot{m}_p} \tag{1}$$

where, $\dot{m}_s$ and $\dot{m}_p$ refers to the secondary and primary flow rates respectively.

The introduction of chevron geometries at the nozzle exit generates streamwise vortices along the expanded jet, increasing the effective jet perimeter and thereby accelerating shear-layer growth and entrainment. These observations of chevrons in free jets, when applied to ejectors, are expected to increase the entrainment of the secondary fluid without causing excessive pressure losses.

4. Preliminary Observations and Discussion

Preliminary observations from the experimental trials suggest an enhancement of the entrainment ratio for the ejectors with their primary nozzles having chevrons similar to the conclusions reported in [3] and [4]. This enhancement in the entrainment ratio can be attributed to improved jet mixing resulting from the higher shear-layer growth rate. Further experiments are needed to study the effect of the chevron geometry on the ejector entrainment ratio.

The flow visualisation study is expected to reveal the increased jet spreading and an earlier breakdown of the potential core of the expanding jet by the vortices generated by the chevrons. Simultaneous analysis of these data, along with observations of ejector performance, can provide deeper insight into the physics underlying ejector entrainment.

5. Conclusions

An experimental study of chevron-induced mixing and its influence on ejector entrainment performance has been outlined. The experimental study involves measuring the entrainment performance of ejectors and visualising the free-jet expansion from conventional and modified nozzles. A qualitative and quantitative relationship between shear-layer growth and entrainment enhancement in the free-expanded jet and the ejector is developed from these experiments. The results and observations of the experiments on the entrainment ratio and mixing enhancement will be presented at the XXVII Fluid Mechanics Conference (FMC 2026).

Acknowledgements

The authors acknowledge funding support from the Government of India under the Institute of Eminence scheme for the Domestic Compact Solar Desalination and Cold Storage System Project at IIT Madras (Ref. SB/22-23/1236/MEE/TWO/002994).

References

[1] Tide P., Babu V., *Numerical predictions of noise due to subsonic jets from nozzles with and without chevrons*, 'Applied Acoustics' 2009, vol. 70, no. 2, pp. 321–332.

[2] Tide P., Srinivasan K., *Effect of chevron count and penetration on the acoustic characteristics of chevron nozzles*, 'Applied Acoustics' 2010, vol. 71, no. 3, pp. 201–220.

[3] Gokhul K., Sundaram S., *Simulation analysis on ejector performance with inclusion of chevrons in primary nozzle*, 'International Journal of Refrigeration' 2025, vol. 170, p. 113–123.

[4] Gokhul K., Sundaram S., *Numerical analysis on ejector performance with varying geometric parameters of chevrons*, 'International Journal of Refrigeration' 2025, vol. 178, p. 180–191.

MESOSCOPIC OSCILLATIONS OF TRIPLE LINE IN CAPILLARY FLOWS

M. Remer, T. Bobiński

Warsaw University of Technology, Institute of Aeronautics and Applied Mechanics, Nowowiejska St. 24, 00–665 Warsaw, Poland

E-mail: michal.remer@pw.edu.pl

Abstract. This work focuses on mesoscopic oscillations of the triple line in capillary tubes, bridging microscopic and macroscopic scales. Dynamic contact angle measurements reveal stick-slip behavior and interface oscillations at high contact line velocities. Advanced interface tracking enables detection of macro- and mesoscopic boundary transitions. The study validates and extends the Kistler model for water-air-glass systems, showing discontinuities at Re > 400 and demonstrating the necessity of replacing static contact angles with advancing angles in velocity-dependent contact angle models.

Keywords: Multi-phase Flows, Contact angle, Micro-flows, Experimental Fluid Mechanics.

1. Introduction

Understanding triple line dynamics remains critical for accurate numerical modeling of wetting phenomena in technological applications from microfluidics to coating processes. Current dynamic contact angle models, such as Kistler's and Shikhmurzaev's equations, rely on capillary number Ca dependencies and assume quasi-static conditions [2,3,5]. However, at elevated velocities in highly inertial flows, these models become insufficient [1]. This work addresses gaps in describing contact angle behavior at high Reynolds numbers and in time-dependent flow regimes, focusing on mesoscopic oscillations of the triple line in capillary tubes. Triple line dynamics span molecular (~50 nm), mesoscopic and macroscopic (~1 mm) scales. Viscous forces induce interface bending, causing apparent dynamic contact angle Θ_d changes differing from static values Θ_0. At high velocities, inertial effects become comparable to surface tension forces. Stick-slip behavior and contact line oscillations emerge at specific conditions, indicating transitions between wetting regimes [4,5].

2. Experimental methodology

High-speed imaging with optical magnification up to 8× captures interface dynamics at spatial resolutions of $\sim 0.5\ \mu$m per pixel. Glass capillary tubes with water and glycerol enable systematic variation of capillary number ($Ca = \mu U/\gamma$ from 10^{-5} to 10^{-2}) and Reynolds number ($Re = Ul/\nu$ from 1 to 500). Four contact angle measurement methods are employed: (1) polynomial fitting, (2) wall extrapolation, (3) fixed-distance measurement and (4) Hoffman method based on curvature fitting (Fig. 1).

3. Results and analysis

Experimental results reveal distinct oscillatory patterns at intermediate contact line velocities. For glycerol flow with $Ca \sim 5 * 10^{-4}$, stick-slip behavior manifests as periodic jumps and halts accompanied by dynamic contact angle fluctuations (Fig. 1). Oscillations are most pronounced in wall-proximate measurements (Methods 1–2), while the Hoffman method exhibits relative stability. This suggests mesoscopic interfacial deformations temporarily overcome adhesion forces, allowing rapid contact line advancement until surface tension restores equilibrium, a critical transition regime where neither purely viscous nor inertial descriptions suffice. Surface roughness influence: The observed stick-slip may be influenced by glass surface roughness at nanometer-micrometer scales. Surface heterogeneities act as pinning sites, creating energy barriers during triple line motion. While present capillaries exhibit optical-grade smoothness (RMS < 10 nm), local defects may contribute to periodic transitions at $Ca \sim 5 * 10^{-4}$.

Contact angle measurements at different magnifications reveal significant discrepancies between macroscopic apparent angle (Θ_{ap}) and microscopic values (Θ_m) measured within 3% of tube diameter from the wall. High-resolution recordings confirm that proper spatial resolution is essential for capturing oscillatory behavior $Ca \lesssim 10^{-2}$. Water flow analysis reveals exponential contact angle dependence on Re number, with notable discontinuity near $Re \approx 10$ and flow instability at $Re > 10$ where the interface becomes severely blurred. This is the first experimental confirmation of instability predicted numerically by Spelt [6] for capillary flows at elevated inertial conditions. For $Re > 400$ accurate contact angle determination becomes impossible due to interface fragmentation, suggesting mesoscopic oscillations evolve into larger-scale instabilities at very high velocities.

Experimental validation of the Kistler model for water-air-glass interfaces reveals reasonable predictions at low-to-intermediate Ca numbers but systematic deviations emerge at higher velocities. Model performance improves when static equilibrium contact angle is replaced by advancing angle Θ_{adv} rather than receding angle. The observed stick-slip behavior and mesoscopic oscillations are not described by existing continuum-level models, indicating the necessity for theoretical development incorporating time-dependent and oscillatory components.

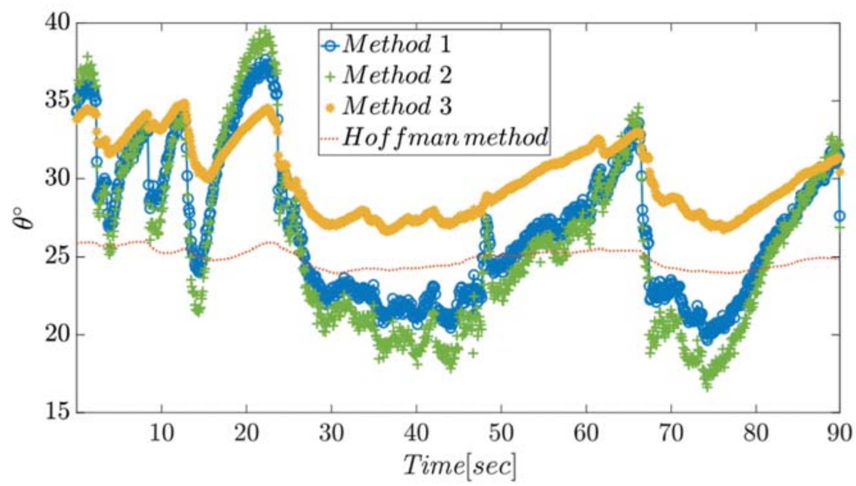

Figure 1. Changes of contact angle in time. $Ca \sim 5 * 10^{-4}$ (glycerol)

References

[1] Remer M., Szumbarski J., Bobiński T., *Triple line dynamics for droplet impingement and capillary flows* Ph.D. Thesis, Warsaw University of Technology, Warsaw 2022.

[2] Kistler S.F., *Hydrodynamics of wetting* in *Wettability*, Dekker, New York 1993.

[3] Shikhmurzaev Y.D., *Capillary Flows with Forming Interfaces*, Chapman & Hall/CRC, New York 2007.

[4] Blake T.D., *The physics of moving wetting lines*, 'Journal of Colloid and Interface Science' 2006, vol. 299, pp. 1–13.

[5] Snoeijer J.H., Andreotti B., *Moving Contact Lines: Scales, Regimes, and Dynamical Transitions*, 'Annual Review of Fluid Mechanics' 2013, vol. 45, pp. 269–292.

[6] Spelt P.D.M., *A level-set approach for simulations of flows with multiple moving contact lines with hysteresis*, 'Journal of Computational Physics' 2005, vol. 205, no. 2, pp. 389–404.

PRE-, NEAR-, AND POST-RESONANCE REGIMES OF SHEAR-THICKENING FLUIDS: DISTINCT DYNAMIC RESPONSES

M.P. Rezaei, G. Kudra, K. Witkowski, J. Awrejcewicz

Department of Automation, Biomechanics and Mechatronics, Lodz University of Technology, Stefanowski St 1/15, 90–924 Łódź, Poland

E-mail: mohammad-parsa.rezaei@dokt.p.lodz.pl

Abstract. Shear-thickening fluids (STFs) can strongly increase viscosity and generate resistance under dynamic loading. We investigate an STF in a mass–spring oscillator excited by an unbalanced rotor with a continuously increasing frequency. Measured displacement, rotor speed and STF force reveal three regimes: negligible action in pre-resonance, strong damping near resonance, and intermittent impact-like peaks in post-resonance.

Keywords: Experimental Fluid Mechanics, shear-thickening fluid, harmonic excitation, frequency.

1. Introduction

Shear-thickening fluids (STFs) become more viscous under shear stress [1], which makes them useful for many engineering and scientific applications, including passive damping concepts [2]. However, their normal-force responses during excitation frequency sweeps is still unclear. Therefore, a STF-filled oscillator under harmonic excitation with continuously increasing frequency is studied and compared with an STF-free baseline. The analysis follows the experimental methodology and parameter identification reported in [3], with emphasis on the transient regime transitions during a single sweep.

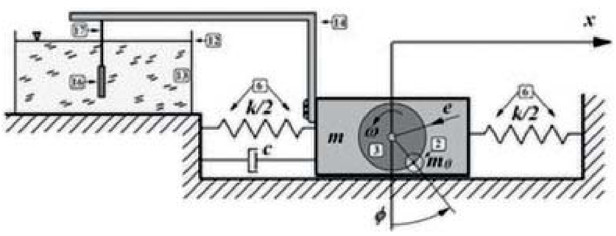

Figure 1. Schematic of the oscillator test rig

2. Experimental setup and procedure

An unbalanced rotor excites a vibrating plate submerged in an STF container, forming an effective mass-spring oscillator (Figure 1). Rotor speed is obtained from the motor encoder, displacement is measured on the moving trolley by a Hall sensor, and the STF reaction force is recorded by strain-gauge sensors mounted under the container base. The baseline oscillator parameters are identified from STF-free tests (empty container, no fluid). In this study one STF formulation is used.

3. Results

The sweep response shows three regimes. In pre-resonance, the STF force is negligible; near resonance, the STF strongly damps the motion and reduces amplitudes; in post-resonance, intermittent impact-like force peaks appear. This observation can be interpreted, for example, as a combination of low excitation and a liquid-like STF response at low shear (before the liquid-solid transition), but this is only an interpretation. Figure 2 illustrates representative measurements.

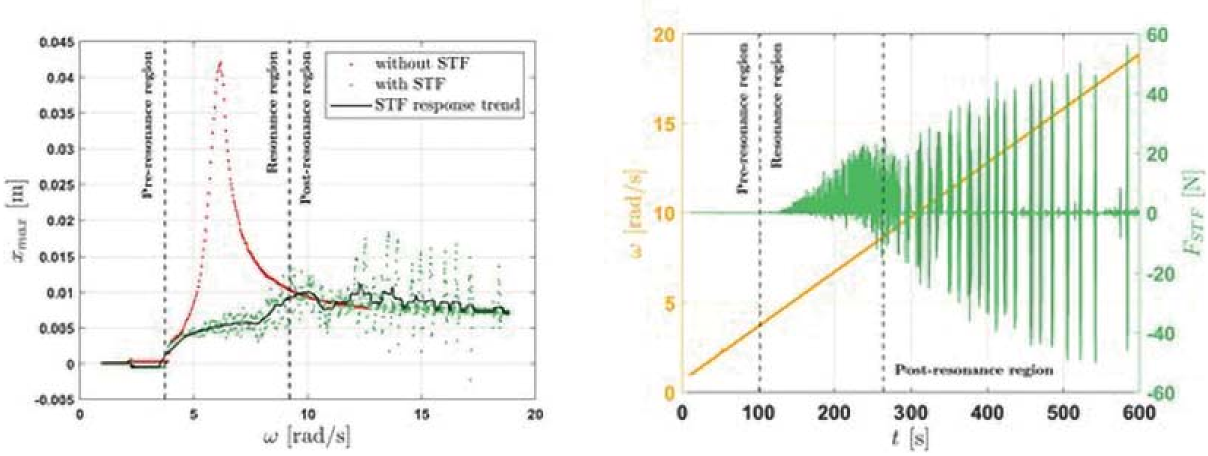

Figure 2. Representative sweep results: (left) maximum displacement versus excitation frequency, (right) excitation frequency and STF reaction force during the sweep

4. Discussion and implications

The force history shows that STF engagement is negligible in pre-resonance, becomes significant near resonance, and turns intermittent in post-resonance, producing large bursts. This behaviour explains why displacement suppression is most pronounced around the critical band; in representative sweeps the peak drops from about 0.04 m without STF to about 0.01 m with STF. The intermittent post-resonance bursts indicate a potential increase in irregular force transmission outside resonance.

5. Conclusions

STFs can effectively suppress resonance during a frequency sweep, but may introduce irregular post-resonance force peaks. These regimes should be considered when designing STF-based structures. These findings summarise and extend the sweep-based observations reported in [3]. Further procedure details, additional results, and extended discussion will be presented during the conference talk.

Acknowledgements

This abstract was created as part of participation in the project entitled "IMPROVE – International Mission for the Promotion of Research and Optimal Values in Education" under the National Agency for Academic Exchange STER programme – Internationalisation of Doctoral Schools – Call for Applications 2024.

References

[1] Hoffman R.L., *Discontinuous and dilatant viscosity behavior in concentrated suspensions. I. Observation of a flow instability,* 'Transactions of the Society of Rheology' 1972, vol. 16, no. 1, pp. 155–173.

[2] Zhang X.Z., Li W.H., Gong X.L., *The rheology of shear thickening fluid (STF) and the dynamic performance of an STF-filled damper*, 'Smart Materials and Structures' 2008, vol. 17, no. 3, art no. 035027.

[3] Rezaei M.P., Kudra G., Witkowski K., Wasilewski G., Awrejcewicz J., D*ynamic behavior of shear-thickening fluids under harmonic excitation: An experimental investigation*, 'Mechanical Systems and Signal Processing' 2025, vol. 237, art no. 113025.

EXPERIMENTAL STUDY OF LEFT-TILTED WAVY WALL FOR TURBULENT SEPARATION CONTROL

M. Romańczyk, A. Dróżdż, W. Elsner

Czestochowa University of Technology, Department of Thermal Machinery, Armii Krajowej 21, 42–200 Czestochowa, Poland

E-mail: mathias.romanczyk@pcz.pl

Abstract. The study presents the results of an experimental analysis of the impact of tilted-wavy-wall geometry on near wall flow subjected to an adverse pressure gradient (APG). It has been confirmed that the use of such geometry reduces the separation of the turbulent boundary layer, thereby reducing flow losses.

Keywords: Aerodynamics, Flow control, Separation, Turbulent flow.

1. Introduction

The energy efficiency of aerodynamic systems, such as an airplane wing, is fundamentally determined by the behavior of the near-wall flow, where an adverse pressure gradient (APG) on the suction side of a profile promotes turbulent boundary layer (TBL) separation.

Early experiments by Dróżdż et al. [1] at a friction Reynolds number $Re\tau \approx 4000$ demonstrated that carefully tuning the amplitude (A) and wavelength (λ) of a two-dimensional sinusoidal waviness (WW) on a wall surface increases small-scale sweeping motions, in a mechanism similar to amplitude modulation which is responsible for increasing τ_w downstream of the corrugation and delaying separation. Subsequent Large Eddy Simulation (LES) work by Kamiński et al. [2] showed that tilting the sinusoid shape to the left causes a substantial increase in τ_w compared to the non-tilted case.

The primary objective of this experimental study is to quantify the influence of this tilted geometry on τ_w, thereby evaluating its true potential for energy-saving flow control under strong APG conditions.

2. Experimental methodology

The research was conducted in a modular wind tunnel at Czestochowa University of Technology, designed for wind-turbine blade surfaces studies under realistic atmospheric conditions. Constant-temperature anemometry (CTA) was employed to characterize the turbulent boundary layer using a DANTEC StreamlinePro hot-wire system operated at an overheating ratio of 0.8. Mean velocity profiles and turbulence fluctuations were measured with single hot-wire probes of nondimensional length $l^+<15$. Inlet conditions were maintained at $U_{e,in} \approx 14.5$ m/s, corresponding to a friction Reynolds number $Re\tau \approx 3100$, that is higher than in the numerical studies by Kamiński et al. [2].

In the present work, maintaining a constant A/δ ratio and $\lambda = 0.135$ m three surface configurations were tested, i.e. smooth wall (Case A), serving as the baseline and simulating the original NACA 4412 suction-side contour, the original symmetric sinusoidal wavy wall section 540 mm long, four periods of λ = 0.135 m (Case B) and the left-tilted wavy wall with the same amplitude and wavelength as the symmetric case, inclined according to the geometry used by Kamiński et al. in their Large Eddy Simulation [2] (Case C).

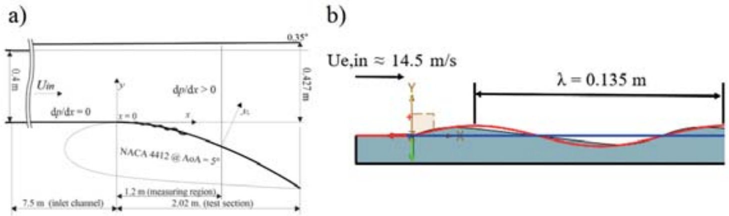

Figure 1. Visualization of experimental facility – a) and analyzed waviness geometries – b) smooth wall (original NACA 4412 suction-side contour) – blue line color (Case A); symmetric sinusoidal wavy wall – red line color (Case B) and the left tilted wavy wall geometry – full grey color (Case C)

3. Results and discussion

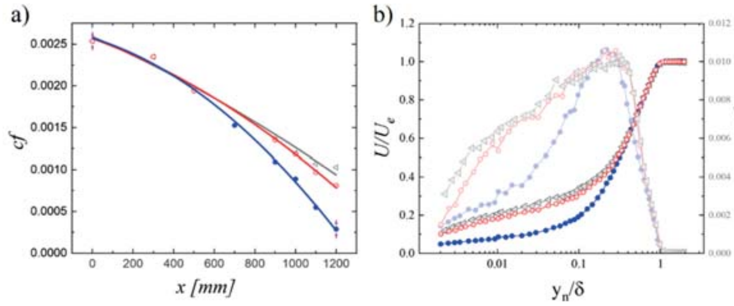

Figure 2. Local skin friction coefficient distribution – a) and Mean velocity and velocity variance components – b) at location from the inlet x = 1200 mm – Case A (closed dots), Case B (opened dots) and Case C (opened triangles)

It was demonstrated that wavy surface geometries can substantially enhance the near-wall velocity which shifts the separation point downstream and counteract turbulent boundary-layer separation. Among the configurations examined, i.e. Cases A, B, and C, the left-tilted wavy wall (Case C) exhibits the strongest effect (the highest increase of the local skin friction coefficient) which is in clear agreement with LES predictions previously obtained by Kamiński et al.[2].

Figure 2.a) illustrates the distribution of the local skin-friction coefficient (cf) along the entire measurement section. A consistent increase in (cf) for the left-tilted wavy wall (opened triangles), relative to the sinusoidal configuration, is observed as the distance from the inlet increases. The most pronounced difference occurs at the final measurement location, i.e., x = 1200 mm. For this reason, the detailed velocity and the velocity variance profiles are shown in Figure 2.b). The data indicates that the increase in shear stress is caused by a sharp jump in energy near the wall.

At the upcoming conference, the authors will present additional results and a more detailed discussion covering traverses from x = 900 mm to 1200 mm to verify conclusively whether the left-tilted waviness indeed represents the optimal geometry.

Acknowledgements

The investigation was supported by National Science Centre under Grant No. DEC-2020/39/B/ST8/01449.

References

[1] Dróżdż A., Sokolenko V., Elsner W., *Performance analysis of novel wavy-wall-based flow control method for wind turbine blade*, 'Experimental Thermal of Fluid Science' 2025, vol. 169.

[2] Kamiński P., Tyliszczak A., Elsner W., Niegodajew P., *Turbulent separation control with a tilted wavy wall: A promising approach for energy savings in aerodynamic systems*, 'Energy' 2025, vol. 324, 135758.

MULTIPHASE MODELLING OF VACUUM INSULATED TES CHARGING PROCESS

A. Rożek, S. Rulik

Silesian University of Technology, Department of Power Engineering and Turbomachinery, 18 Konarskiego st., 44–100 Gliwice, Poland

E-mail: aleksander.rozek@polsl.pl

Abstract. The research presented herein consists of an experimentally validated numerical model utilising the multiphase Volume of Fluid method. The model facilitates the quantification of transport phenomena and fluid-thermal coupling variables. Furthermore, the efficacy of the proposed model is substantiated through comparison with a model that does not employ the VoF method.

Keywords: Computational Fluid Dynamics, Phase-Change Materials, Multi-Phase Modelling, Heat Transfer.

1. Introduction

The European energy system is undergoing rapid transformation, bringing with it a number of critical challenges. Among the most pressing are the intermittency associated with renewable energy generation and limitations in power grid capacity. Electrical energy storage systems are often proposed as a remedy; however, they address only part of the problem. Combined heat and power production remains a cornerstone of national energy infrastructures. A fully electrified energy system would necessitate the electrification of all heat generation, which in turn would demand an unprecedented expansion of the electricity grid. Such an undertaking is currently impractical. Consequently, the energy transition calls for a balanced and carefully considered adjustment of current strategies. One such adjustment is the integration of thermal energy storage technologies. In particular, latent heat storage based on phase-change materials (PCM) represents a promising solution, especially for urban environments.

Numerical analyses have been validated against experimental results so as to quantify transport phenomena and thermal coupling variables. These simulations were performed using two otherwise identical models, differing only in the employment of the VoF method.

2. Vacuum chamber efficacy

In addition to the multiphase investigation, the presented research also aims to quantify the efficacy of vacuum insulation by way of conducting separate simulations for different pressure values. This information will be presented alongside the experimental data which quantifies the energy supplied to the vacuum pump. Analyses of insulation methods and configurations are essential for optimizing TES systems, as they directly govern heat losses and therefore overall efficiency. Minimising dissipation and extending storage duration is crucial for this type of system.

This aims to determine the energy efficiency, and therefore commercial viability of utilising vacuum insulation. The numerical model will elucidate the underlying thermodynamic and physical mechanisms governing fluid flow within the vacuum chamber as well as the liquid PCM. This will also allow the delineation of any discrepancies between the numerical and experimental evaluations.

Experimental investigations were conducted for a low-temperature PCM (melting point circa 335K), which was validated by way of a simple numerical model. This was later appended to accommodate for an air-filled section at the top, due to the thermal expansion of the PCM. This measure was implemented to alleviate the pressure that would otherwise accumulate in this domain. The numerical calculations were subsequently carried out for materials with more favourable thermal parameters, as well as a high-temperature PCM, in order to ascertain the moment in which vacuum insulation began being economically viable. The model was designed as shown below in figure 1:

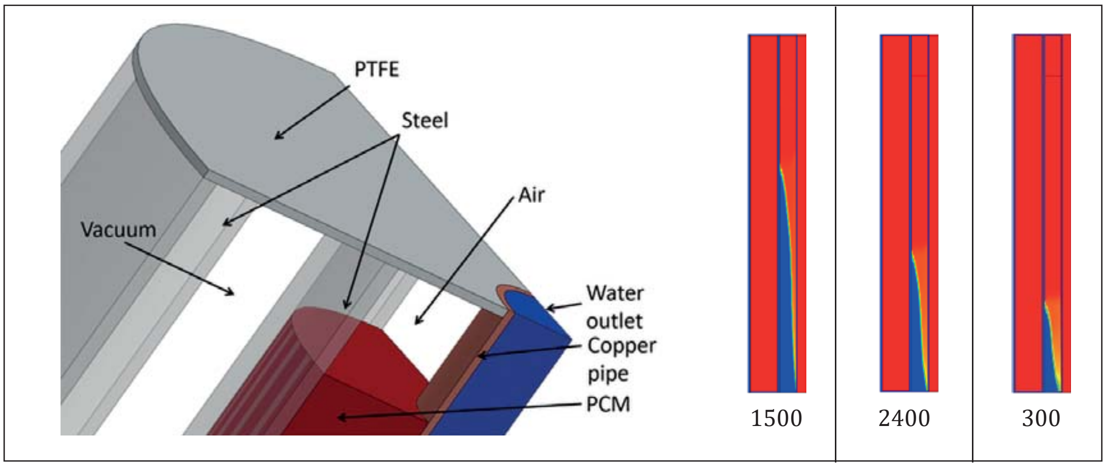

Figure 1. Design of numerical model and mass fraction contours (preliminary results)

3. Equations and mathematics

The model was based on a study by Rożek [1]. The governing equations consist of energy (1) and momentum (2) conservation. A key difference in the PCM/air domain is the appending of these equations to average the volumetric proportions within its domain.

$$\frac{\delta}{\delta t}(\rho E)+\nabla\cdot(\boldsymbol{v}\,(\,\rho E+p))=\nabla(k_{eff}\nabla T-\sum_q\sum_j h_{j,q}\,\boldsymbol{J_{i,q}}+(\bar{\bar{\tau}}_{eff}\cdot\boldsymbol{v})) \tag{1}$$

$$\frac{\delta}{\delta t}(\rho\boldsymbol{v})+\nabla\cdot(\rho\boldsymbol{v}\boldsymbol{v})=-\nabla p+\nabla\cdot\mu\left[(\nabla\boldsymbol{v}+\boldsymbol{v}^T)-\frac{2}{3}\nabla\cdot\boldsymbol{v}I\right]+\rho\boldsymbol{g}+\boldsymbol{F} \tag{2}$$

The numerical model was configured with a periodic boundary oscillating every ninety degrees. The interior radius of the PCM module was 14 mm, and the exterior radius was 34 mm. The heat transfer fluid flow was oriented counter to the gravitational vector as a means of inducing buoyancy -driven convection, thereby accelerating the melting rate.

This configuration allowed the model to capture the coupled effects of natural convection and phase change within the PCM domain, while also allowing for thermal expansion to occur. This allowed the influence of temperature-dependent thermal expansion on the system's thermal behaviour to be examined and compared across the different modelling approaches.

References

[1] Rożek A., *Numerical Analysis of the Utilization of Magnesium Chloride Hexahydrate As A Heat Storage Medium in an Adiabatic Environment*, 'Architecture, Civil Engineering, Environment' 2025, vol. 18, no. 4, pp. 87–94.

INFLUENCE OF TURBULENCE ON THE FLOW BEHAVIOR OF PROPELLER BLADE GEOMETRIES

F.U. Rückert, D. Hübner, S. Grün, B. Allweyer, C. Sassen

University of Applied Science Saarbrücken, Business Faculty, Waldhausweg 14, 66123, Saarbrücken, Germany

E-mail: frank.rueckert@htwsaar.de

Abstract. The study examines how turbulence affects the aerodynamic performance of a high-performance rotor designed to increase thrust and load capacity in UAVs. Turbulence-induced stall reduces rotor efficiency at high Reynolds numbers, yet propeller design is still largely empirical and based on simplified models. Conventional two-equation turbulence models often lack accuracy for rotating flows. To address this, a *Smagorinsky* LES approach was implemented in ANSYS CFX to vary operating conditions and capture turbulence and stall behavior along the blade in detail. The virtual test bench also integrates a UAV model to assess flight performance relative to rotor geometry. This method enables more efficient and sustainable UAV propulsion development and provides a fully digital workflow for future rotor and UAV design research.

Keywords: turbulence model, propeller, drone design, fluid flow, blade design, optimization, UAV, Large Eddy Simulation, Smagorinsky model, stall effect.

1. Introduction

Selecting the right turbulence model is crucial for CFD-based propeller optimization. Two-equation RANS models can misrepresent flow physics and overestimate accuracy by up to 60%. They smooth transient fluctuations into a steady eddy-viscosity field effectively thickening the flow without direction. In contrast, LES resolves unsteady turbulent structures instead of averaging them and provide a more physically representation and detachment along a blade. [1] The *Smagorinsky* LES resolves large, energy-containing turbulent eddies in space and time, allowing it to capture flow separation, vortex shedding, and shear-layer instabilities as transient phenomena. [2] This yields to more realistic predictions especially in wake-dominated regions and swirling flows around blades. It also explains stall and reduced thrust or lift force for UAV. We present results to be compared with further experimental studies. [3]

2. Model Equations for Large Eddy Simulation (LES)

Transient effects are central to the problem the temporal evolution of turbulent structures. The time-resolved nature of LES allows the simulation to produce turbulence fields that represent averages over time rather than instantaneous flow states. LES provides not only more realistic instantaneous fields but also more accurate transient statistics such as time histories, fluctuations of velocities and energy spectra. [2] An additional sub-grid scale stress tensor τ_{ij}^{SGS} is added to the Navier-Stokes-Equations and the *Boussinesq* hypothesis [4] leads to the solution of the sub-grid tensor

$$\frac{\partial \overline{u}_i}{\partial t} + \overline{u}_j \cdot \frac{\partial \overline{u}_i}{\partial x_j} = -\frac{1}{\rho} \cdot \frac{\partial \overline{p}}{\partial x_i} + \nu \cdot \frac{\partial^2 \overline{u}_i}{\partial x_j^2} - \frac{\partial \tau_{ij}^{SGS}}{\partial x_j} \tag{1}$$

$$\tau_{ij}^{SGS} - \frac{1}{3}\tau_{kk}^{SGS}\delta_{ij} = -2\nu_t^{SGS} \cdot \frac{1}{2} \cdot \left(\frac{\partial \overline{u}_i}{\partial x_j} + \frac{\partial \overline{u}_j}{\partial x_i}\right) \tag{2}$$

The *Smagorinsky* model defines the SGS eddy-viscosity ν_t^{SGS} [1]. Based on this, the model is often considered as more accurate in resolution of unsteady turbulence. It requires finer spatial and temporal resolution.

It uses a subgrid-scale viscosity spatially filtered incompressible formulation. [5] Here the model is a wall-resolved LES approach, not a wall-modeled LES, so SGS viscosity must drop to zero near the walls.

3. Interpretation of LES Simulation Results

Here we use tetrahedral meshes with approx. 1,000,000 cells for the blade as in *Chang*. [6] Figure 1 shows vortex core region and pressure fields. Boundary velocity is 25 [m/s] lead to Re = 13653.74 [-] as recommended by *Zhang*. [7] Results can be seen for different time-steps (dt=0.0003 [s] and 0.0009 [s]; C_s = 0.1). A swirl at the end can be visualized. Higher pressure zones at the blade lead to lower lift-forces (approx. 35 [N]). Vortex cores offer a consistent way to analyze vortex-dominated flows by large, energy-carrying turbulent structures.

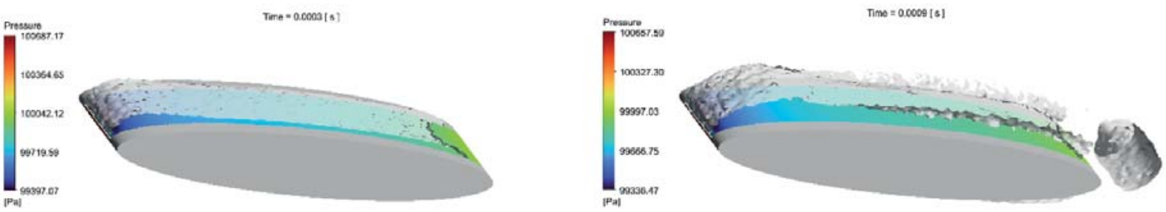

Figure 1. Vortex core region around a test blade at Reynolds number Re = 13653.74 and pressure distribution for different timesteps

With LES, a wide range of flow quantities such as vorticity, Q- and λ_2-criteria, helicity, turbulent kinetic energy, strain rate, pressure fluctuations, and the vortex core can be described. Together, these metrics enable precise characterization of tip vortices, separation-driven structures, vortex shedding, shear-layer instabilities, and wake topology. They improve understanding of aerodynamic limits, stall, and unsteady effects at rotors of UAV.

References

[1] Smagorinsky J., *General circulation experiments with primitive equations*, 'Monthly Weather Review' 1963, vol. 91, no. 3, pp. 99–164.

[2] Menter F.R., *Two-Equation Eddy-Viscosity Turbulence Models for Engineering Applications*, 'AIAA Journal' 1994, vol. 32, no. 8, pp. 1598–1605.

[3] Allweyer B., Grün S., DiBenedetto F., Bulduk G., Hübner D., Rückert F.U.. *Heat Transfer and Flow Behavior on the DYNOTIS ST-51 Propeller Testbench for Unmanned Aerial Vehicles*, [in:] Cetin B., Dursunkaya Z., Günay A.A., Gözükara A.C. (eds.), *Advances in Computational Heat and Mass Transfer II. ICCHMT 2025. Lecture Notes in Mechanical Engineering*, Springer, Cham, 2026.

[4] Boussinesq J., *Théorie de l'écoulement tourbillonnant et tumultueux des liquides dans les lits rectilignes a grande section*, vol. 1, Gauthier-Villars, Paris 1897.

[5] Benim A.C., Nahavandi A., Syed K.J., *URANS and LES analysis of turbulent swirling flows*, 'Progress in Computational Fluid Dynamics, an International Journal' 2005, vol. 5, no. 8, pp. 444–454.

[6] Chang, C.-L., Venkatachari B. , *Dynamic Smagorinsky Modeled Large-Eddy Simulations of Turbulence Using T etrahedral Meshes*, NASA Technical Report, 2019.

[7] Zhang D., *Comparison of Various Turbulence Models for Unsteady Flow around a Finite Circular Cylinder at Re = 20000*, 'Journal of Physics: Conference Series' 2017, vol. 910.

INVESTIGATION OF FLUID FLOW IN THE EJECTOR NOZZLE DURING EJECTOR DEEP HOLE DRILLING USING MESH-FREE METHODS

N. Rupasinghe[1], **S. Michel**[2], **A. Baumann**[1], **S. Gülde**[2], **D. Biermann**[2], **P. Eberhard**[1]

[1] *Institute of Engineering and Computational Mechanics, University of Stuttgart, Pfaffenwaldring 9, 70–569 Stuttgart, Germany*

[2] *Institute of Machining Technology, Technical University of Dortmund, Baroper Street 303, 44–227 Dortmund, Germany*

E-mail: nuwan.rupasinghe@itm.uni-stuttgart.de

Abstract. Ejector deep hole drilling utilizes the Venturi principle for machining high quality bores in resource efficient manner. Metal working fluid (MWF) flow characteristics in the ejector nozzle of the system strongly influence the process efficiency. In this work, the application of the Smoothed Particle Hydrodynamics (SPH) method to investigate the MWF flow in the ejector nozzle is presented. The applied SPH method which is highly suitable for transient flows with moving boundaries, is then validated using experimental tests.

Keywords: Computational Fluid Dynamics, Smoothed Particle Hydrodynamics (SPH), Ejector Deep Hole Drilling, Ejector Nozzle.

1. Introduction

Ejector deep hole drilling (EDHD) is used for machining high quality bore holes with large length-to-diameter ratios [1]. Metal working fluid (MWF) supply in the system significantly determines the chip evacuation from the cutting zone and process reliability [2]. As depicted in Figure 1, MWF supplied in EDHD is divided into two parts at the supply inlet. Although the volume flow distribution depends exclusively on the tool design, it is discharged according to a fixed ratio. Here, 38.1% of the necessary total supplied flow $\dot{V}_\Sigma$ is guided through the annular channel between the two bars up to the drill head where it emerges through bores. The MWF then flows around the cutting zone and flushes away the chips formed during drilling via the inner tube. The remaining 61.9% of $\dot{V}_\Sigma$ flows through the slits in the inner tube, also known as ejector nozzles and is discharged straight out of the system. This generates a reduction in the pressure in the inner tube and the chip mouth based on the Venturi principle. This phenomenon, which is known as the ejector effect, supports the chip-lubricant mixture flow in the inner tube and prevents the MWF leakage to the outside of the borehole, thus, enabling a stable drilling process.

Supply of MWF under high pressure to remove the generated metal chips from the cutting zone often demands higher energy consumption in the industrial machining centers. The energy demand of EDHD can be reduced through improved hydraulic efficiency of the ejector nozzle [3]. Therefore, understanding the flow conditions in the ejector nozzle using numerical methods such as the Smoothed Particle Hydrodynamics (SPH) approach is vital to improve the process efficiency.

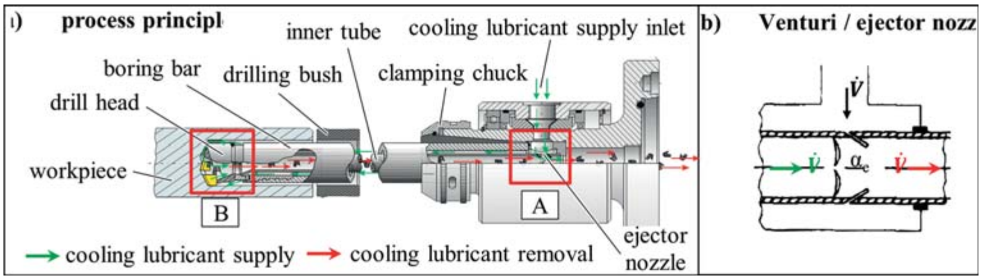

Figure 1. a) Process principle schematic of EDHD system. b) Ejector nozzle cross section

2. Numerical method and simulation model

The meshless Lagrangian SPH method is used to evaluate the fluid flow conditions around the ejector nozzle. Here, an approximation of the Navier-Stokes equation is obtained by discretizing the continuum medium with a set of interpolation points, called particles, that move along with the fluid flow. Due to the Lagrangian nature, SPH can be coupled with the Discrete Element Method which is used to model and discretize the solid tool structures. Because of the transient nature of the simulation, the simulation domain contains open free surfaces and moving structures. These numerical problems are successfully handled by the mesh-free SPH method with the additional advantage of the ability to extend the simulation as a liquid-gas multiphase flow problem.

As shown in Figure 2, the simulation work is focused on the fluid flow in the ejector nozzle and its interaction with the internal tube flow transported from the cutting zone. An in-house developed numerical solver 'Pasimodo' is employed to simulate the problem using the weakly compressible SPH approach in which pressure is computed directly from density through an equation of state [4]. In addition, only the Dirichlet velocity boundary condition is applied for the fluid inlets.

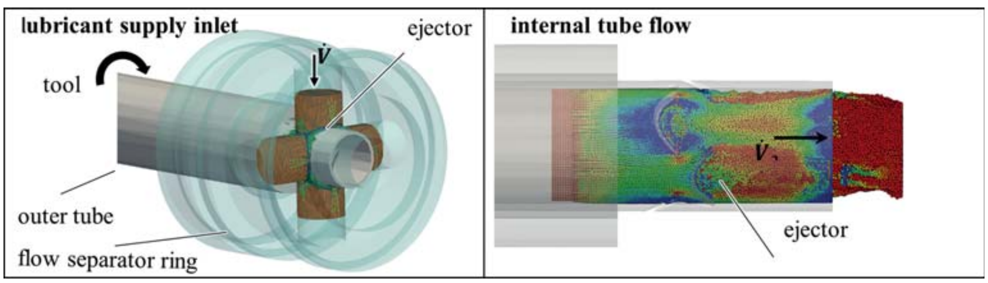

Figure 2. MWF flow around ejector nozzle at initial time steps

Acknowledgements

This research was funded and supported by the Deutsche Forschungsgemeinschaft (DFG) under grant numbers 439917965 and 405605200.

References

[1] Biermann D., Bleicher F., Heisel U., Klocke F., Möhring C., Shih A., *Deep hole drilling*, 'CIRP Annals' 2018, vol. 67, no. 2, p. 673–694.

[2] Baumann A., Oezkaya E., Schnabel D., Biermann D., Eberhard P., *Cutting-fluid flow with chip evacuation during deep-hole drilling with twist drills*, 'European Journal of Mechanics – B/Fluids' 2021, vol. 89, p. 473–484.

[3] Astakhov V.P., Subramanya P.S., Osman M., *On the design of ejectors for deep hole machining*, 'International Journal of Machine Tools and Manufacture' 1996, vol. 36, no. 2, p. 155–171.

[4] Schnabel D., Özkaya E., Biermann D., Eberhard P., *Modeling the Motion of the Cooling Lubricant in Drilling Processes using the Finite Volume and the Smoothed Particle Hydrodynamics Methods*, 'Computer Methods in Applied Mechanics and Engineering' 2018, vol. 329, p. 369–395.

SEMI-ANALYTICAL FLOW MODEL OF LOW-BOILING MEDIUM IN TESLA TURBINE

K. Rusin, W. Wróblewski

Silesian University of Technology, Department of Power Engineering and Turbomachinery, Konarskiego 18, 44–100 Gliwice, Poland

E-mail: krzysztof.rusin@polsl.pl

Abstract. Semi-analytical model of 2D flow in a Tesla turbine for the low-boiling media is presented. The model predicts distributions of kinematic and thermodynamic parameters with consideration of the real gas equation of state. The model enables optimisation of selected parameters. The highest obtained isentropic efficiency for the analysed range of parameters was 70%.

Keywords: Flow Machinery, Tesla turbine, ORC systems, semi-analytical modelling.

1. Introduction

The shift towards a carbon-free economy will largely rely on the utilisation of renewable energy sources, such as wind turbines or photovoltaics. However, smaller power systems, which may make use of low-temperature heat sources, can play a key role in filling in areas in which large power systems are not economically or technically viable. For this reason, systems based on Organic Rankine Cycle (ORC) can be an interesting option in this regard. In these systems, low-boiling media are often used as the working fluid. The key component of such a system is the expander which converts the enthalpy of a working medium into mechanical power. The selection of the turbine is of great importance.

On the one hand, the turbine must be selected with consideration of the fluid's properties and the processes it is intended to perform. On the other hand, an expander must be economically viable. One of the possible choices is a Tesla turbine. It is a bladeless which rotor comprises thin disks set apart by a sub-millimetre distance. The working fluid expands in the set of nozzles placed above the outer perimeter of the rotor and flows into the space between the disks. The Tesla turbine has multiple advantages that could be beneficial to the ORC systems, e.g. high resistance to erosion or low manufacturing costs. However, the selection of geometrical features of the turbine adjusted to a given heat source and working medium poses a great challenge. For this reason, a mathematical model was proposed within the framework of this paper to assess the working conditions of the turbine.

2. Mathematical model

The model was based on the paper by Rusin et al. [1]. The continuity equation (Eq.1), momentum equations in radial (Eq.2) and circumferential (Eq.3) directions and rothalpy equation (Eq.4) constituted the set of governing equations. Real gas equation of state was employed based on the RefProp Library to calculate physical properties and thermodynamic parameters of real gases. The average values are obtained after integrating the equations over the gap size. Therefore, the local velocities in the equations (1-4) are substituted with the product of the velocity averaged across the gap for a given radius and the normalised velocity profile.

$$\frac{1}{r}\frac{\partial(\rho r w_r)}{\partial r} = 0 \tag{1}$$

$$w_r\frac{\partial w_r}{\partial r} - \omega^2 r - 2\omega w_\theta - \frac{w_\theta^2}{r} = -\frac{1}{\rho}\frac{dp}{dr} + \nu\frac{\partial^2 w_r}{\partial z^2} \tag{2}$$

$$w_r\frac{\partial w_\theta}{\partial r} + \frac{w_r w_\theta}{r} + 2\omega w_r = \nu\frac{\partial^2 w_\theta}{\partial z^2} \tag{3}$$

$$I = h + 0.5\left(w_\theta^2 + w_r^2 - u^2\right) \tag{4}$$

The outer and inner radii in the reference geometry were 0.08 m and 0.04 m, respectively. The gap size was 0.12mm.

The temperatures of the heat source and heat sink were T_1 = 95 °C and T_2 = 40 °C, respectively, and the fluid temperature at the inlet was superheated by at least 5 K. The fluids under investigation were R1234yf, Toluene, R245fa and n-Hexane. The optimisation aiming at increasing the isentropic efficiency was conducted. The optimised parameters included the inlet pressure, rotational speed and the outer radius.

3. Results

The highest efficiency, equal to 39.7%, was obtained for n-Hexane. It was achieved for rotational speed n = 18650 rpm, outer radius r = 0.0592 m and inlet pressure p = 1.26 bar. The efficiency characteristic as a function of rotational speed is shown in Figure 1. It can be seen that after the peak, a sharp decline in efficiency is observed.

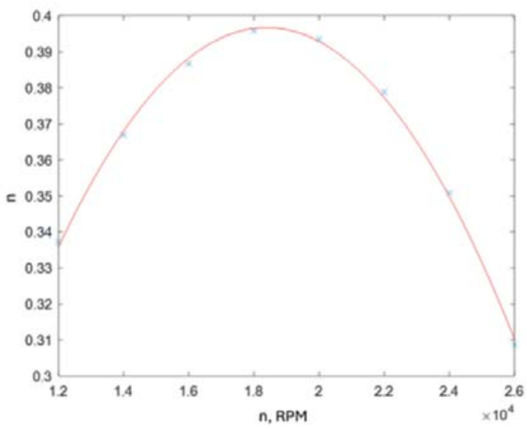

Figure 1. Efficiency characteristics for n-Hexane

Acknowledgements

The research presented was carried out within the UMO-2019/35/B/ST8/01871research project financed by the Polish National Science Centre and Statutory Research Funds of Silesian University of Technology

References

[1] Rusin K., Wróblewski W., Hasani E., Pahlavanzadeh M., Rulik S., *Extended analytical model of Tesla turbine with advanced modelling of velocity profile in minichannel between corotating disks with consideration of surface roughness*, 'Energy' 2024, vol. 307.

PRE-CLINICALLY VALIDATED LUMPED PARAMETER LIVER MODEL TO GUIDE PRE-OPERATIVE RESECTION

H. Saini[1], K. Gyoten[2], P. Friend[2], T. Pruett[3], J. Sushil Rao[3], J. Tithof[1]

[1] *Department of Mechanical Engineering, University of Minnesota, 111 Church St SE, Minneapolis, MN 55455, USA*

[2] *Nuffield Department of Surgical Sciences, John Radcliffe Hospital, Oxford, OX3 9DU*

[3] *Division of Solid Organ Transplantation, Department of Surgery, University of Minnesota, 516 Delaware St SE, Minneapolis, MN 55455, USA*

E-mail: saini056@umn.edu

Abstract. The article presents a pre-clinically validated lumped-parameter model to quantify altered sinusoidal wall shear stress (WSS) and pressure in resected porcine liver, then extend this model to living donor liver transplantation. Methods used to estimate unknown parameters are outlined. It will be used to test the hypothesis that WSS exceeding a critical threshold impairs regeneration, leading to liver failure. This patient-specific pre-operative tool can be extended to improve resection outcomes by predicting WSS levels that promote regeneration and reduce liver failure risk.

Keywords: Bio-flows, hydraulic network model, liver resection, wall shear stress.

1. Introduction

The liver receives dual blood supply from the hepatic artery (HA) and portal vein (PV), which branch through multiple generations before converging at the portal triad, located at the corners of hexagonal liver lobules. Blood then flows through the sinusoids and drains into the hepatic vein (HV) at the centre of each lobule. Endothelial cells lining the sinusoids sense hemodynamic changes and transmit signals to neighboring cells, triggering liver regeneration after resections. However, the liver's regenerative capacity is finite; excessive tissue removal can lead to complications such as small-for-size syndrome (SFSS). Studies indicate that SFSS is associated with high portal pressure and sinusoidal wall shear stress (WSS), potentially resulting in endothelial cell injury and cell death [1-3]. This highlights the importance of studying variation in WSS that plays an essential role in initiating and terminating liver regeneration. In this work, we use a lumped parameter model [4] for liver blood flow to include patient-specific anatomy. We validated the model against perfusion data of resected porcine livers and extended it to model living donor liver transplantation (LDLT). We aim to quantitatively analyze WSS that plays a significant role in liver regeneration.

2. Methodology

A lumped parameter hydraulic network model of blood flow through the entire human liver is used [4] due to its computational efficiency enabling simulations of the entire human liver. The model employs a structure of 'edges' representing blood-carrying vessels and 'nodes' denoting points where vessels branch or merge (illustrated in Figure 1). An important feature of this model is that it incorporates the Couinaud segmentation, which is a common clinical scheme which labels nine different regions of the liver. Each vascular segment has hydraulic conductance, based on Poiseuille flow, given by:

$$c_{ij} = \frac{\pi d^4}{128\mu L} \tag{1}$$

where d is the vessel diameter, μ is the dynamic viscosity, and L is the vessel segment length. The details of the associated linear algebra problem are given in [4].

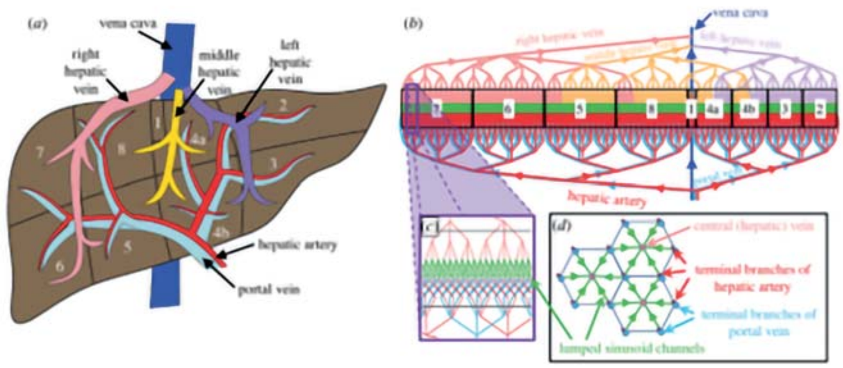

Figure 1. Schematic of the realistic model of human liver blood flow [4]

The model using normothermic machine perfusion data of 15 resected porcine livers is validated. Time series measurements of pressure and hematocrits were used as model inputs and corresponding volume flow rates are compared against the experiments. Morover, measured HA, PV, and HV diameters were used, as well as total and graft weights for organ-specific input parameters. The terminal vessels and lumped sinusoid diameters are not directly measurable but significantly control resistance and WSS. For each liver, we calibrate terminal HA, PV, HV and sinusoid diameters at one time point using Bayesian optimization to match measured flow at that time point, constrained by physiological diameter and perfusion ranges [5]. The calibrated parameters are then fixed for each liver and used to simulate the full time series to predict WSS. We extended our model to perform a retrospective study of LDLT patients. Because the measurement of major vessel and terminal diameters is difficult and collateral conductance is challenging to determine, we used Bayesian optimization to estimate these parameters across patients using the same parameter estimation approach.

3. Discussion and Conclusions

The simulated PV and HV volume flow rates for each liver demonstrate close agreement with measured flow rates. With the validated model, the sinusoidal pressure and WSS throughout the perfusion duration which are central to regeneration but not directly measurable were predicted. It was planned to correlate these predictions with regenerative markers and identify WSS thresholds that promote regeneration or cause damage. Simulations of LDLT also show good agreement with clinical measurements. We will test whether predicted WSS is related to surgical outcomes, including early allograft dysfunction, to support future studies linking elevated WSS to regeneration and to develop tools for resection planning and post-operative assessment.

References

[1] Schoen J., Wang H., Minuk G., Lautt W., Shear stress-induced nitric oxide release triggers the liver regeneration cascade, 'Nitric Oxide: Biology and Chemistry' 2001, vol. 5, no. 5, pp. 453–464.

[2] Poisson J., Lemoinne S., Boulanger Ch., Durand F., Moreau R., Valla D., Rautou P.-E., *Liver sinusoidal endothelial cells: Physiology and role in liver diseases*, 'Journal of Hepatology' 2017, vol. 66, no. 1, pp. 212–227.

[3] Ishikawa J, Takeo M., Iwadate A., Koya J., Kihira M., Oshima M., Suzuki Y., Taniguchi K., Kobayashi A., Tsuji T. , *Mechanical homeostasis of liver sinusoid is involved in the initiation and termination of liver regeneration*, 'Communications Biology' 2021, vol. 4, no. 1.

[4] Tithof J., Pruett T., Rao J., *Lumped parameter liver simulation to predict acute haemodynamic alterations following partial resections*, 'Journal of the Royal Society Interface' 2023, vol. 20, no. 207.

[5] Crawford A., Lin X., Crawford J., *The normal adult human liver biopsy: a quantitative reference standard*, 'Hepatology' 1998, vol. 28, no. 2, pp. 323–331.

CRITICAL ASSESSMENT OF THE BUOYANT FLOW DYNAMICS FOR ENHANCING THE PERFORMANCE OF A SOLAR UPDRAFT TOWER

S. Sengupta

Department of Mechanical Engineering, NIT Durgapur, Durgapur-713209, West Bengal, India

E-mail: ssengupta.me@nitdgp.ac.in

Abstract. At present, the power conversion efficiency of a solar updraft tower (SUT) is relatively low compared to other solar technologies. We enhance system efficiency by utilizing a well-designed collector with artificial roughness elements, optimizing their topology, positioning and size, and employing a strategic ground injection method. We also implement a throat-bottom chimney and a well-designed turbine. These modifications are borne from a fluid dynamic understanding aimed at minimising parasitic and energy conversion losses within the system.

Keywords: Computational fluid dynamics, Turbulent free convection, Artificial roughness, Solar Chimney, Performance.

1. Introduction

The solar updraft tower (SUT) [1] is a prominent example of a non-concentrated thermal system that may find applications in agricultural greenhouses, water desalination, humidity harvesting, waste heat recovery and urban heat island mitigation. We conduct a computational study to investigate the thermo-fluid-dynamics of a small-scale system (chimney height = 3 m and collector diameter = 3 m) for an SUT. The solar-heated collector ground builds a low-density air column inside the central chimney. A free convective suction arising from the density difference between the chimney and the outside atmosphere pushes the air radially inward. The velocity of radial inflow increases as it approaches through the converging collector passage towards the turbine location at the chimney center. The overall efficiency of the conventional SCPP is typically low (less than 1%), as mentioned by previous researchers [2,3]. One way to improve performance is to utilize a hybrid system, e.g., an SUT integrated with a solar still and an air HDH unit [4], yielding 21–39% efficiency. On the other hand, a remarkable increase in collector efficiency by optimizing the ground topology and employing a ground-injection method is achieved (Figure 1). The improvement of the thermal efficiency of the modified SUT addresses the challenges of sustainable development from a global perspective.

2. Methodology

A pressure-based finite volume method is employed to solve the continuity, momentum, energy and turbulence transport equations. The pressure-velocity coupling is done by the SIMPLE algorithm. Second-order accurate discretization schemes are employed, with a scaled residual of 10^{-6} as the convergence criterion for all flow variables in the simulations. A systematic grid independence test determines the ideal mesh size (~6.5 million), yielding reasonable accuracy. The reliability of the computational method and the appropriateness of various turbulence models are verified with the benchmark experimental data [5] available in the literature.

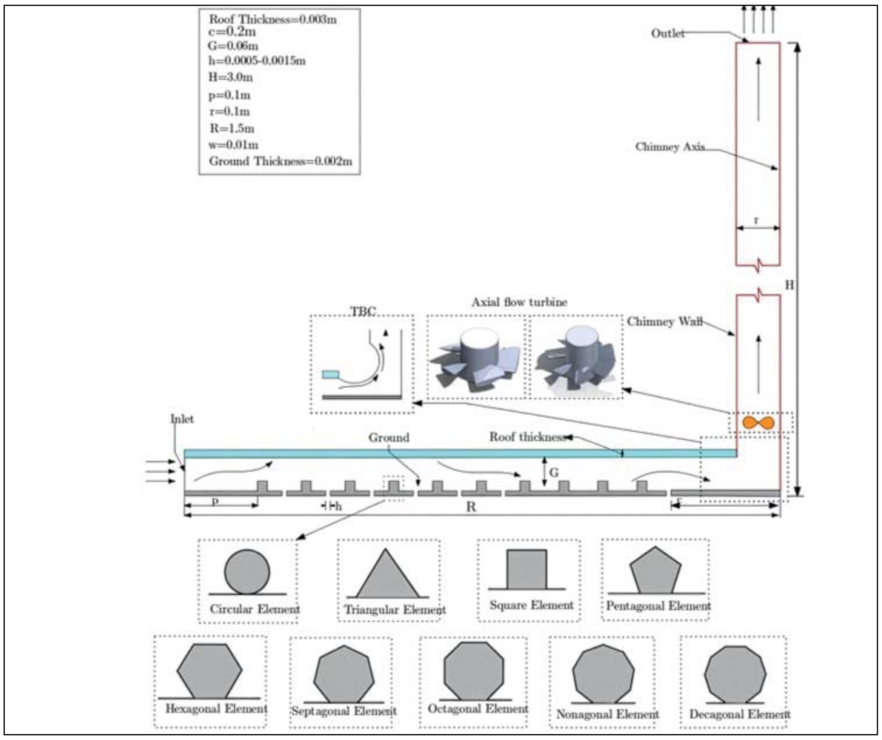

Figure 1. Schematic of a small scale SUT with proposed modifications

3. Major outcomes of a set of numerical experiments

This study systematically improves SUT performance through five design interventions. Ground-based artificial roughness is shown to outperform roof roughness by enhancing thermal mixing. Optimal collector performance is achieved using square ground elements of 0.01 m height arranged as non-axisymmetric, discontinuous structures with an azimuthal spacing of 4°. The introduction of optimized suction and blowing slots (~1 mm width) further improves performance by thinning the thermal boundary layer and enhancing turbulent mixing, with overall efficiency governed by their strategic placement. A throat-bottom chimney eliminates recirculation at the collector-chimney junction, yielding a 47% performance improvement over the baseline of 25.5% obtained from a conventional SUT [5]. Finally, an optimized axial-flow turbine, designed using a reduced numerical framework, effectively extracts buoyant-flow enthalpy, while future extensions may incorporate advanced fluid-dynamic concepts and hybrid smart-grid-integrated systems.

Acknowledgements

The author is grateful to his PhD scholar, Mr. Avishek Mukherjee, for generating CFD data.

References

[1] Harte R., Höffer R., Krätzig W.B., Mark P., Niemann H.J., *Solar updraft power plants: Engineering structures for sustainable energy generation*, 'Engineering Structures' 2013, vol. 56, pp. 1698–1706.

[2] Saleh M.J., Atallah F.S., Algburi S., Ahmed O.K., *Enhancement methods of the performance of a solar chimney power plant*, 'Results in Engineering' 2023, vol. 19, no. 5.

[3] Toghraie D., Karami A., Afrand M., Karimipour A., *Effects of geometric parameters on the performance of solar chimney power plants*, 'Energy' 2018, vol. 162, pp. 1052–1061.

[4] Kabeel A.E., El-Said E.M., *Experimental study on a modified solar power driven hybrid desalination system*, 'Desalination' 2018, vol. 443, pp. 1–10.

[5] Kasaeian A., Ghalamchi M., Ghalamchi M., *Simulation and optimization of geometric parameters of a solar chimney in Tehran*, 'Energy Conversion and Management' 2014, vol. 83, pp. 28–34.

HYDRODYNAMIC ORIENTING OF RIGID PARTICLES SETTLING UNDER GRAVITY IN A VISCOUS FLUID AT LOW REYNOLDS NUMBER

Ch. Shekhar, H.N. Mirajkar, P. Zdybel, Y. Melikhov, M.L. Ekiel-Jeżewska

Institute of Fundamental Technological Research, Polish Academy of Sciences, ul. Pawińskiego 5B, 02–106 Warsaw, Poland

E-mail: mekiel@ippt.pan.pl

Abstract. We study experimentally and numerically sedimentation of rigid particles with two perpendicular symmetry planes for Reynolds numbers much smaller than one. We demonstrate that a certain class of shapes tends to a stable stationary orientation. These shapes have the opposite signs of the two rotational-translational mobility coefficients, evaluated in the symmetric frame of reference relative to the center of mass. We present experimental and numerical methods to determine these coefficients.

Keywords: general fluid dynamics, low Reynolds number, experiments, theory and numerical computation, Stokes equations, rigid particle with two symmetry planes, stable stationary orientation.

1. Introduction

Recently, it has been shown theoretically [1] that rigid particles with two orthogonal symmetry planes, settling under gravity in the Stokes fluid, in general do not only move vertically. In addition to translating downwards, they perform a complex motion that belongs to one of three classes. Drifters tend to move sideways in a fixed direction and speed while keeping a constant inclination with respect to gravity (similarly as the rigid rods). Flutterers [2] all the time change their orientation and direction of their translation sideways, in general quasi-periodically. Settlers [3,4] approach a stable stationary orientation, with the intersection of the symmetry planes parallel to gravity.

The classification of shapes to one these three classes hinges on their rotational-translational mobility coefficients, μ_{42} and μ_{51}, evaluated in the symmetric frame of reference relative to the center of mass. The product of μ_{42} and μ_{51} vanishes for drifters, is positive for flutterers and negative for settlers. However, looking at the particle shape, it is not evident to which class it belongs. This work provides experimental and numerical methods to determine it.

2. Experimental, theoretical & numerical methods and results [5]

Our experimental setup consists of a glass tank 20 × 20 × 50 cm filled with the silicon oil of kinematic viscosity $5 \times 10^{-3}\ \mathrm{m^2\ s^{-1}}$, and two cameras with perpendicular lines of sight, lamps and millimetre-sized particles of different shapes: cones, arrowheads, crescent moons and open rings with different sizes of the opening. The shapes were chosen similar to the trumb-bells that were shown numerically to reorient to a stable orientation [4].

In the experiments, it was demonstrated that the chosen particles approach a stationary orientation and stay there for a long time. A special symmetric initial conditions was chosen, for which equations of motion simplify (in particular, the center of mass moves in a plane and the rotation takes place only along the horizontal axis perpendicular to one of the symmetry planes). The solutions of these simplified equations were fitted to the measured time-dependent angles, determine both μ_{42} and μ_{51}, and show that their product is negative. From the stability proof in [1], it was determined that the stationary orientation is indeed stable.

Numerically, the shapes of the particles used in the experiments were reconstructed as rigid conglomerates made of thousands of touching spherical beads. For such rigid objects, the theoretical method was applied, based on the multipole expansion of the Stokes equations, to evaluate the mobility coefficients, implemented in the numerical program Hydromultipole [6], and a reasonable agreement with the experimental values was obtained, with the same conclusion that all the particles are the settlers, and that they reorient rather quickly.

3. Conclusion

It was shown how to determine experimentally and numerically the rotational-translational mobility coefficients μ_{42} and μ_{51} of a rigid body with two perpendicular symmetry planes. Their signs allow to predict the type of the motion – is it a drifter, a flutterer or a settler. The character of the dynamics is important for studies of sedimenting flocs in aquatic media, marine snow, plastic microparticles translating in air, chiral fluids, ordered anisotropic suspensions and swimming microorganisms.

Acknowledgements

This work was supported in part by the National Science Centre under grant UMO-2021/41/B/ST8/04474.

References

[1] Joshi H., Govindarajan R., *Sedimentation dynamics of bodies with two planes of symmetry*, 'Physical Review Letters' 2025, , vol. 134, art. no. 014002.

[2] Miara T., Vaquero-Stainer C., Pihler-Puzović D., Heil M., Juel A., *Dynamics of inertialess sedimentation of a rigid U-shaped disk*, 'Communications Physics' 2024, vol. 7, art. no. 47.

[3] Ekiel-Jeżewska M.L., Wajnryb E., *Hydrodynamic orienting of asymmetric microobjects under gravity*, 'Journal of Physics: Condensed Matter' 2009, vol. 21, art. no. 204102.

[4] Candelier F., Gustavsson K., Sharma P., Sundberg L., Pumir A., Bagheri G., Mehlig B., *Torques on curved atmospheric fibers*, 'Physical Review Research' 2025, vol. 7, art. no. 013179.

[5] Shekhar C., Mirajkar H.N., Zdybel P., Melikhov Y., Ekiel-Jeżewska M.L., *Experimental and numerical study of rigid particles with two planes of symmetry approaching a stable, stationary orientation while sedimenting*, 'Journal of Fluid Mechanics' 2026, in press.

[6] Cichocki B., Ekiel-Jeżewska M.L., Wajnryb E., *Lubrication corrections for three-particle contribution to short-time self-diffusion coefficients in colloidal dispersions*, 'The Journal of Chemical Physics' 1999, vol. 111, pp. 3265–3273.

MULTIPHYSICS MODELING AND EXPERIMENTAL CHARACTERIZATION OF A COMMERCIAL HIGH-PRESSURE RECIPROCATING COMPRESSOR

A.B. Şimşek[1], B. Erdoğan[2], N.B. Üner[1,*]

[1] *Middle East Technical University, Department of Chemical Engineering, 06800 Ankara, Türkiye, https://che.metu.edu.tr*

[2] *Logos Kimya LLC, 06374 Ankara, Türkiye, https://www.logoskimya.com*

E-mail: nuner@metu.edu.tr

Abstract. The authors present a multidimensional modelling investigation on high-pressure reciprocating compressors through a 3-D CFD model as well as a macroscopic 0-D model. Reduced models of check valve dynamics and ambient heat dissipation were developed through dedicated experiments. Comparison with results obtained on a commercial 70 MPa booster confirms that the framework accurately predicts discharge pressures and flow rates, hence enabling rapid prototyping, as well as detailed design and optimization.

Keywords: Experimental Fluid Mechanics, Flow Machinery, Computational Fluid Dynamics, Compressible Flow, Booster Pump, High-Pressure.

1. Introduction

The capability to provide high-pressure compressed gas streams is a critical requirement in a diverse range of industrial processes, particularly those related to energy storage, green transportation, propulsion systems and the petrochemical sector. To meet these demands, oil-free electric driven reciprocating piston compressors are commonly employed as booster pumps. Their widespread adoption across various platforms is driven by their inherent safety, portability, small form factor and flexible design. Nonetheless, modeling and design of such reciprocating compressors become increasingly crucial and challenging as delivery pressures rise.

The design space for high-pressure boosters is exceptionally wide and governed by numerous interdependent parameters. These include suction and discharge gas temperatures, rotating shaft mechanics, compression ratios, gas composition and the material properties of pistons and seals. Due to this complexity, the development of new compressors has traditionally relied on expensive and time-consuming trial-and-error methodologies. Moreover, comprehensive numerical studies that are experimentally validated for high-pressure applications are notably rare in the existing literature [1-2]. Consequently, there is a distinct need for robust modelling approaches that can rationalize development and unravel key design constraints.

In this study, a comprehensive multidimensional modelling framework was developed to predict the effects of operation and design parameters on compressor performance. The framework integrates two complementary components: Computational Fluid Dynamics (CFD) multiphysics model and a 0-D mathematical model.

2. Modeling Framework

2.1. Dynamic compression models

A 3-D CFD model, utilizing a deforming mesh through commercial software, ANSYS Fluent, was built to simulate complex fluid flow, compression and heat transfer inside the piston-barrel assembly. A macroscopic 0-D model was developed to predict the main design parameters, mass flow rate and pressure inside the barrel, with significantly lower computational resources than the 3-D model. It was recognized that the accuracy of both models relies extensively on two sub-physics, check valve dynamics and external heat transfer [3-4], therefore additional effort was spent to model these phenomena.

2.2. Check valve dynamics

Compressor performance is heavily dependent on transient valve dynamics, as well as common check valve properties such as cracking pressure and conductance. To capture dynamic valve operation at high-pressure gas flow, a semi-empirical macroscopic model was developed where flow coefficients were determined through separate experiments and CFD analysis.

2.3. Heat transfer analysis

As external heat exchange plays a vital role in performance and efficiency, heat dissipation into the ambient was investigated separately as a distinct sub-physics component. Steady-state and transient experiments were conducted to measure accurate overall heat transfer coefficients describing the heat loss from the barrel to ambient which were then cross-checked with computational thermal analysis.

3. Validation Studies

For validation, mass flow rates were measured using a setup with geometry identical to the model. Gas was supplied at 4 MPa, while transducers monitored upstream and downstream pressures. Outlet pressure was maintained at 14 MPa via a backpressure regulator directing outflow into a sealed cylinder. Mass flow rate was calculated based on the real-time pressure rise within the collection cylinder.

4. Conclusions

While the CFD model offers details of internal pressure and temperature fields in high-resolution, the macroscopic mathematical model was found to successfully capture the trends in main operating parameters with much less computational resources. Details related to validation and model comparison will be presented and various scenarios of model-based exploration will be discussed.

Acknowledgements

The authors would like to thank LOGOS Kimya LLC Engineers; Onur Ulutaş, Furkan Turgut, and Ecem Dönmez for their support on experimental setup.

References

[1] Farzaneh-Gord M., Niazmand A., Deymi-Dashtebayaz M., Rahbari H. R., *Thermodynamic analysis of natural gas reciprocating compressors based on real and ideal gas models*, 'International Journal of Refrigeration' 2015, vol. 56, pp. 186–197.

[2] Elhaj M., Gu F., Ball A.D., Albarbar A., Al-Qattan M., Naid A., *Numerical simulation and experimental study of a two-stage reciprocating compressor for condition monitoring*, 'Mechanical Systems and Signal Processing' 2008, vol. 22, no. 2, pp. 374–389.

[3] Kim J., Wang S., Ryu K., La J., Park S., *Valve Dynamic Analysis of a Hermetic Reciprocating Compressor*, 2006, available online: https://docs.lib.purdue.edu/icec (access: 02.04.2026).

[4] Dutra T., Deschamps C.J., *Experimental characterization of heat transfer in the components of a small hermetic reciprocating compressor*, 'Applied Thermal Engineering' 2013, vol. 58, no. 1–2, pp. 499–510.

NUMERICAL AND EXPERIMENTAL STUDY OF EXTERNAL HEAT LOSS ON THE PISTON-BARREL ASSEMBLY OF A HIGH-PRESSURE RECIPROCATING COMPRESSOR

A.B. Şimşek[1], B. Erdoğan[2], N.B. Üner[1]

[1] *Middle East Technical University, Department of Chemical Engineering, 06800 Ankara, Türkiye*

[2] *Logos Kimya LLC, 06374 Ankara, Türkiye*

E-mail: nuner@metu.edu.tr

Abstract. This study analyzes external heat losses in high-pressure compressor housings surrounded by annular fins. Three approaches were used to find the heat transfer coefficient: steady-state experiments, transient experiments with an analytical model and CFD validation via ANSYS. Results, demonstrate strong agreement between all three methods and reveal that radiation contributes significantly to total heat loss. The integrated approach ensures robust thermo-fluidic characterization of the system.

Keywords: Interdisciplinary Areas in Heat and Fluid Flow, Heat Transfer, Computational Fluid Dynamics, Overall Heat Transfer Coefficient, Reciprocating Compressor.

1. Introduction

The overall performance of a compressor is mainly dictated by the management of heat generated during gas compression. Excessive internal heat accumulation negatively impacts the thermodynamic and volumetric efficiency by reducing the discharge mass flow rate [1-2]. Furthermore, the operational longevity of critical sealant materials, most notably polytetrafluoroethylene (PTFE) and polyether ether ketone (PEEK) is strictly governed by the thermal environment within the compressor assembly. To date, research focused on internal heat transfer has been instrumental in predicting temperature distributions across the fundamental stages of compression, discharge, expansion and suction [3]. However, investigations into the external heat dissipation of reciprocating compressors remain scarce in the literature. Characterizing these external losses is inherently challenging, often necessitating the application of complex experimental techniques, such as the integration of thin-film heat flux sensors or the implementation of rigorous calorimetric approaches which are difficult to employ for high-pressure (>10 MPa) compressors [4-5]. This study addresses this gap by developing accessible methodologies for evaluating external thermal characteristics. The authors demonstrate two simple experimental approaches to determine the overall heat transfer coefficient (U) for a forced convection-cooled annular fin housing manufactured for a commercial 70 MPa booster, with and without radiation included. Results were further corroborated with computational fluid dynamics (CFD) that resolve the flow around the finned housing.

2. Methodology

2.1. Steady-state Measurements

The determination of U under steady-state conditions was predicated on the equilibrium between constant internal heat generation in the piston barrel and peripheral heat dissipation. To establish this steady-state temperature profile, a regulated heat source was employed, with input power adjusted using a variable transformer to modulate voltage and a clamp-type ammeter to monitor current. Temperature was recorded via a K-type thermocouple positioned at the cylindrical axis of the heat source. Experimental observations revealed a proportional relationship between heater power and magnitude of U. This result indicates that the enhancement of the overall heat transfer coefficient is primarily driven by the intensified contribution of radiative heat loss from the fin housing surfaces as operating temperatures increase, which is a difficult contribution to calculate directly.

2.2. Transient Measurements

To isolate convection and conduction heat transfer from radiative effects, an asymptotic approach was developed to monitor heat loss under vanishing temperature difference between the fin housing and the ambient. Through the use of an analytical solution for 1D unsteady heat conduction in cylindrical geometry, the authors show that Biot number can be estimated from temperature vs. time data. Custom-manufactured cylinders that match the compressor's internal dimensions were pre-heated in an oven and then placed immediately within the housing. The resulting temperature decay data were processed, and the bounds of thef linear tail of the logarithmic cooling region was identified based on the R^2 value. By extracting the slope and intercept from that region, the model enables the estimation of the Biot number and the corresponding U.

2.3. CFD Calculations

Steady-state conjugated heat transfer simulations were performed in ANSYS Fluent to support the results obtained with the radiation-free, transient measurements. Since air flow over the fins was turbulent, the realizable $k\text{−}\epsilon$ turbulence model coupled with a second order coupled solver was preferred. The moving reference frame method was implemented to simulate the rotation of the cooling fan. The CFD model enabled us to investigate local temperatures and heat transfer coefficients which were seen to differ only slightly across the entire fin housing.

3. Conclusions

Where simple steady-state experiments that characterize extended surface heat losses are always coupled with radiation losses, transient heat loss experiments can be conducted at vanishing temperature differences to minimize the effect of radiation, thereby allowing insight into purely convective losses. CFD simulations verify the results obtained from transient measurements. The authors will detail the measurements, present practical advantages and difficulties, and elaborate on the simplifications made when compared to a full CFD analysis.

References

[1] J. Tuhovcak, J. Hejcik, and M. Jicha, "Comparison of heat transfer models for reciprocating compressor," *Appl Therm Eng*, vol. 103, pp. 607–615, Jun. 2016, doi: 10.1016/j.applthermaleng.2016.04.120.

[2] W. H. Hsieh and T. T. Wu, "Experimental investigation of heat transfer in a high-pressure reciprocating gas compressor," *Exp Therm Fluid Sci*, vol. 13, no. 1, pp. 44–54, Jul. 1996, doi: 10.1016/0894-1777(96)00013-1.

[3] F. P. Disconzi, E. L. L. Pereira, and C. J. Deschamps, "Development of an In-Cylinder Heat Transfer Correlation for Reciprocating Compressors," *In: Proc. Int. Compressor Eng. Conf.*, 2012.

[4] T. Dutra and C. J. Deschamps, "Experimental characterization of heat transfer in the components of a small hermetic reciprocating compressor," *Appl Therm Eng*, vol. 58, no. 1–2, 2013, doi: 10.1016/j.applthermaleng.2013.04.039.

[5] A. Morriesen and C. J. Deschamps, "Experimental investigation of transient fluid flow and superheating in the suction chamber of a refrigeration reciprocating compressor," in *Applied Thermal Engineering*, 2012. doi: 10.1016/j.applthermaleng.2011.12.011.

EXPERIMENTAL AND NUMERICAL STUDY OF THE BIOMIMETIC CATALYTIC CARRIER BASED ON FISH GILLS

K. Sindera

Institute of Chemical Engineering, Polish Academy of Sciences, Bałtycka 5, 44–100 Gliwice

E-mail: katarzyna.sindera@iich.gliwice.pl

Abstract. Presented research focuses on innovative catalytic carrier inspired by fish gills. These natural structures have been chosen due to their excellent heat and mass transfer properties, coupled with a large specific surface area which are desirable features of catalytic support. The geometry, called 'Gill-like Structured Carrier' (GSC), was analyzed through experimental methods and Computational Fluid Dynamics (CFD) modeling. Results demonstrate significant heat transfer intensity and acceptable flow resistance, highlighting the potential of GSCs as catalytic carriers.

Keywords: Computational Fluid Dynamics, catalytic carriers, gill-like structured carriers, heat transfer, flow resistance.

1. Introduction

Currently, the Earth atmosphere is contaminated with many hazardous substances (like: methane, volatile organic compounds, nitrogen oxides and sulfur oxides) that pose risks to both the environment and living organisms. Catalytic afterburning in structured reactors may be used for neutralizing these pollutants. However, due to increasing air quality requirements, new ways to enhance the transport and flow properties of these devices are needed. One possibility is to modify the geometry of the catalytic support, that is responsible for transporting reagents to and from the catalytic active sites, thus influencing the overall rate of the catalytic process. During these studies, a new type of catalytic support was introduced. The basis for its developing was the gills (the fish respiratory organ) – structures with high transport intensity and a large specific surface area, that are also desirable features for catalytic carrier. The developed geometry is called Gill-like Structured Carrier (GSC). It is inspired by the shape of the filaments and lamellae found in fish gills, as shown in Fig. 1.

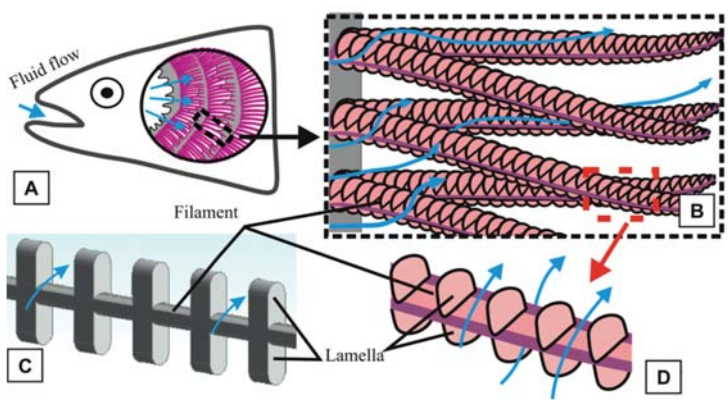

Figure 1. Flow through: natural fish gills (A, B, D) and GSC (C)

2. Results and discussion

Various GSCs types were examined both experimentally and with the use of CFD (Computational Fluid Dynamics) modelling. Results for exemplary GSC are presented in Fig. 2. The agreement between experimental and numerical results for both the heat transfer coefficient and the Fanning friction factor is high (the average relative error was 23 and 11%, respectively). GSC is characterised by high heat transfer coefficients. Fanning friction factors are high as well, however it is acceptable considering intense heat transfer properties. The conducted research indicate that GSC has the potential to be used as a catalytic support.

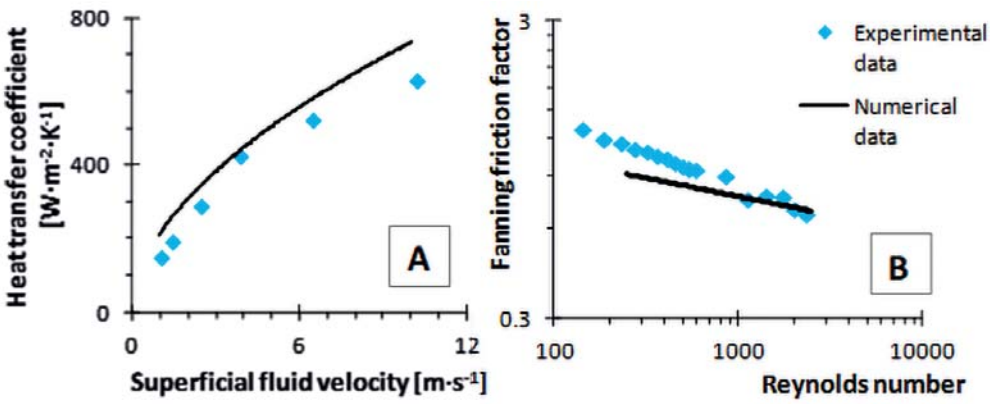

Figure 2. Transport (A) and flow (B) propertie of GSC

Acknowledgements

This work was supported by the research grants from Polish National Science Centre (Project No. 2023/49/N/ST8/00819).

NUMERICAL AND EXPERIMENTAL STUDIES OF LOW-FREQUENCY UNSTEADINESS IN SHOCK WAVE BOUNDARY LAYER INTERACTION

K. Skoczylas[1], A. Bogusławski[1], S. Dykas[2], M. Majkut[2], K. Smołka[2]

[1] *Faculty of Mechanical Engineering, Czestochowa University of Technology, ul. J.H. Dabrowskiego 69, 42–201, Czestochowa, Poland*

[2] *Department of Power Engineering and Turbomachinery, Faculty of Energy and Environmental Engineeering, Silesian University of Technology, ul. Akademicka 2A, 44–100 Gliwice, Poland*

E-mail: kamil.skoczylas@pcz.pl

Abstract. Time-resolved experiments and URANS simulations are combined to investigate unsteady shock-boundary layer interactions in an asymmetric convergent-divergent nozzle. Schlieren imaging and pressure measurements reveal downstream shock migration and three dominant frequency bands linked to shock motion and shear-layer instabilities. Numerical results reproduce the experimental shock topology and spectral trends, providing a validated framework for predictive SBLI analysis.

Keywords: Experimental Fluid Mechanics, Computational Fluid Dynamics, Shock Waves, Transonic, Low-Frequency Unsteadiness, de Laval Nozzle.

1. Introduction

This work addresses the occurring of Shock-wave Boundary Layer Interactions (SBLIs) by combining time-resolved experiments with URANS simulations to investigate unsteady shock motion in an asymmetric convergent–divergent nozzle during supersonic flow. The study characterizes dynamic shock behavior through spectral analysis and examines the influence of pressure ratio, providing a validated framework for improved predictive understanding of nozzle SBLIs.

Experiments were performed at the Air Test Rig of the Department of Power Engineering and Turbomachinery, Silesian University of Technology, using a planar asymmetric convergent–divergent (de Laval) nozzle with one straight and one curved wall downstream of the throat. The channel expansion is characterized by a ratio of maximum channel height to throat height of 4:1, while the throat itself has a square cross-section, with a width-to-height ratio of 1:1. The nozzle was operated in a blowdown facility providing controlled and repeatable pressure ratio, temperature and humidity conditions. Time-resolved Schlieren imaging at 6000 fps and high-frequency wall-mounted pressure transducers were used to capture shock motion and flow unsteadiness. Shock positions were extracted using edge detection and pixel tracking, and analyzed using FFT and CWT to obtain spectral and temporal characteristics. Complementary URANS simulations were performed in ANSYS Fluent 2024 using the SST k-ω model and a structured, multi-block hexahedral mesh with local refinement near the throat and Mach disk. Boundary conditions were prescribed from experimental measurements to ensure direct comparability.

2. Experimental and numerical results

Static pressure and Mach number distributions showed downstream migration and increasing complexity of the shock system with rising pressure ratio (PR = 1.44, 1.6, 1.81), transitioning from a stable normal shock to a broadband λ-foot structure with enhanced separation and turbulence. Schlieren imaging (Fig. 1) revealed shock motion, separation bubbles, shear-layer instabilities and reflected shocks, and these experimental visualizations were directly compared with numerical Schlieren reconstructions, which exhibited similar shock topology and unsteady features, providing time-resolved shock positions for subsequent spectral analysis.

The λ-foot is formed on both walls, but in the present case, the structure on the rectilinear wall is much weaker and associated with a very thin separation region, making it difficult to detect in Schlieren images but still visible in the numerical results.

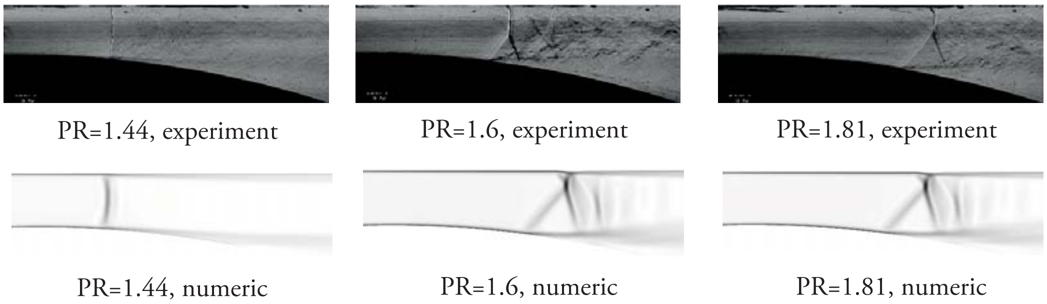

Figure 1. Comparison of Schlieren images: experimental visualizations and corresponding numerical reconstructions obtained with a preliminary coarse mesh

Spectral decomposition of Schlieren-derived shock motion and pressure transducer signals revealed three dominant frequency bands, centered near 250 Hz, 500–600 Hz and 800–900 Hz. Representative spectra are shown in Fig. 2. The lowest band corresponded to large-scale shock oscillations, while the higher bands were associated with shear-layer flapping and small-scale instabilities. As PR increased, the dominant oscillation frequency rose while the displacement amplitude of the shock decreased, reflecting the stabilizing influence of λ-foot structures relative to normal shocks. Numerical Schlieren reconstructions reproduced the downstream migration of the shock system, the development of λ-foot structures and the overall shock topology observed experimentally. Spectral analysis of simulated pressure signals revealed the same three frequency bands and consistent frequency shifts and amplitude trends across all PRs.

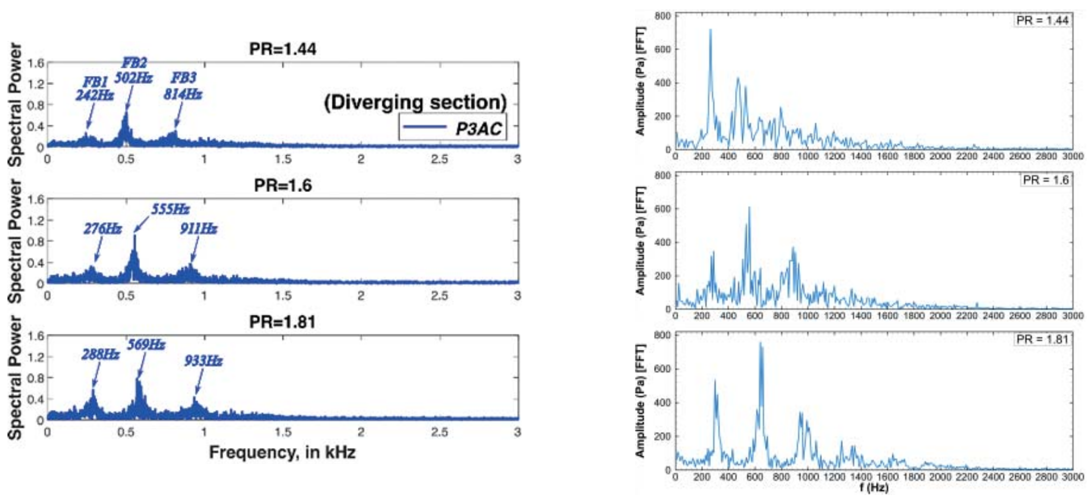

Figure 2. Fast Fourier Transform (FFT) of static pressure signals in the nozzle diverging section: (left) experimental measurement shown as spectral power and (right) numerical prediction shown as amplitude spectrum at the corresponding location

Acknowledgements

The authors acknowledge the National Science Centre of Poland (Grant No. 2023/49/B/ST8/00773) and the Silesian University of Technology for financial and logistical support. Computational resources were supplemented by the PLGrid infrastructure (ACK Cyfronet AGH) under Grant No. PLG/2025/018453.

ON THE USE OF ENTROPY GENERATION TO QUANTIFY FLOW CONDITIONING

E. Smyk

Bydgoszcz University of Science and Technology, Institute of Mechanics and Computer Methods, Al. prof. S. Kaliskiego 7, 85–796 Bydgoszcz, Poland

E-mail: emil.smyk@pbs.edu.pl

Abstract. This study proposes using entropy generation to assess flow conditions and flow conditioners. A simplified 1D model suitable for hot-wire anemometry is derived and validated against Prandtl's profiles and experimental data. A new criterion for stream straightener performance is introduced: the ratio of flow entropy reduction to the entropy generated by the device itself. This approach offers a novel metric for evaluating conditioning and relaminarization efficiency in engineering applications.

Keywords: Channels, Inner Flow, Straightener, Entropy, Prandtl's Power Law.

1. Introduction

Laminar and conditioned flows are widely used in technology and science, ranging from wind tunnel experiments to high-precision metrology and biomedical engineering. In these applications, the quality of the flow directly impacts the reliability of measurements and the efficiency of processes. Despite this importance, the literature still lacks comprehensive studies on this topic, particularly those focusing on the possibility of flow relaminarization and a holistic assessment of flow character. Although the definition of laminar flow is relatively simple and intuitive, in practice, it is often difficult to determine whether a given flow is strictly laminar, transitional, or turbulent, or to quantitatively assess the level of turbulence structure beyond simple fluctuation metrics.

Flow assessment is particularly critical in flow conditioning, where the goal is to reduce turbulence and straighten the velocity profile. Conventional methods often rely on measuring the turbulence intensity (Tu), which quantifies velocity fluctuations but does not account for the energy dissipation mechanisms inherent in the flow. Consequently, relying solely on Tu can be misleading when evaluating the efficiency of stream straighteners. Flow assessment is, therefore, crucial to verify whether a conditioner is operating properly and efficiently. This topic is significant from both scientific/cognitive and engineering perspectives, as it bridges the gap between theoretical fluid dynamics and practical flow control.

There are a number of methods for assessing flow, described among others in [1, 2]. However, there is still a lack of methods that would allow for the evaluation of stream straighteners and conditioners in a way other than comparing basic flow parameters for a specific case. A robust metric should account for the thermodynamic irreversibility of the process. The solution seems to be to measure the entropy generated by the flow. It is well established that entropy generation is directly linked to viscous dissipation and heat transfer, making it a powerful tool for identifying losses and flow irregularities.

It is known that for a fluid flow, the local entropy generation rate per unit volume can be represented as [3]:

$$\begin{aligned}\dot{s}_{gen} = \frac{\Phi}{T} = \frac{\mu}{T}\Bigg[& 2\left\{\left(\frac{\partial \bar{u}}{\partial x}\right)^2 + \left(\frac{\partial \bar{v}}{\partial y}\right)^2 + \left(\frac{\partial \bar{w}}{\partial z}\right)^2\right\} \\ & + \left(\frac{\partial \bar{u}}{\partial y} + \frac{\partial \bar{v}}{\partial x}\right)^2 + \left(\frac{\partial \bar{u}}{\partial y} + \frac{\partial \bar{w}}{\partial x}\right)^2 + \left(\frac{\partial \bar{v}}{\partial y} + \frac{\partial \bar{w}}{\partial x}\right)^2\Bigg] \\ & + \frac{\mu}{T}\Bigg[2\left\{\overline{\left(\frac{\partial u`}{\partial x}\right)^2} + \overline{\left(\frac{\partial v`}{\partial y}\right)^2} + \overline{\left(\frac{\partial w`}{\partial z}\right)^2}\right\} \\ & + \overline{\left(\frac{\partial u`}{\partial y} + \frac{\partial v`}{\partial x}\right)^2} + \overline{\left(\frac{\partial u`}{\partial z} + \frac{\partial w`}{\partial x}\right)^2} + \overline{\left(\frac{\partial v`}{\partial z} + \frac{\partial w`}{\partial y}\right)^2}\Bigg]\end{aligned} \tag{1}$$

where Φ is the viscous dissipation function dependent on the strain tensor [Pa/s], T is the absolute temperature of the flowing fluid [K], μ is the dynamic viscosity [Pa·s], u,v and, w are the velocity components in x, y, z directions [m/s], respectively. The symbol $\overline{\square}$ denotes the time-averaged value, while ` represents the fluctuating component.

It should be noted that the analysis of the total flow velocity field is very rarely used. One- or two-dimensional flows are much more common, and for flows through circular pipes, the velocity profile is most often measured in only one axis, treating them as axisymmetric [1, 2, 4]. In such a case, it is necessary to calculate the mean square of the gradients of velocity fluctuations in the radial direction. However, this is not always possible, for example, for single hot-wire anemometer (HWA) measurements. Therefore, a simplified approach can be adopted, in which the entropy generated by turbulent dissipation is ignored, or the following simplification can be adopted:

$$\dot{s}_{gen} = \frac{\Phi}{T} = 2\frac{\mu}{T}\left[\left(\frac{\partial \bar{u}}{\partial r}\right)^2 + \overline{\left(\frac{\partial u`}{\partial r}\right)^2}\right] \tag{2}$$

or if it is impossible to calculate the average of the squared gradients of velocity fluctuations in the radial direction:

$$\dot{s}_{gen} = \frac{\Phi}{T} = 2\frac{\mu}{T}\left[\left(\frac{\partial \bar{u}}{\partial r}\right)^2 + \left(\frac{\overline{u`}}{L}\right)^2\right] \tag{3}$$

where r is the radial coordinate of the pipe [m], and L is the characteristic size of turbulence (e.g. diameter of the stream straightener mesh) [m].

This paper aims to demonstrate that the measurement of generated entropy expressed by Eq. (3) can be used to evaluate the flow after conditioning and to evaluate the performance of stream straighteners. For this purpose, theoretical velocity distributions based on Prandtl's power law were analyzed. Next, the measurements presented in [1] were used for experimental analysis, and based on experimental measurements using HWA, the flow assessment using the proposed method was presented. Finally, the stream straighteners were evaluated, and their performance was compared based on the ratio of the reduction of the entropy generated by the flow to the entropy generated by the straighteners.

Acknowledgements

This research was fully or partially funded by the National Science Centre under project number 2023/49/N/ST8/03737.

References

[1] Kühnen J., Scarselli D., Hof B., *Relaminarization of Pipe Flow by Means of 3D-Printed Shaped Honeycombs*, 'Journal of Fluids Engineering-Transactions of the Asme' 2019, vol. 141, no 11.

[2] Smyk E., Stopel M., Rachwalski A., *Impact of honeycomb straightener parameters on operation in a straight duct,* 'Journal of Theoretical and Applied Mechanics' 2025, vol. 63, no. 4, pp. 781–794.

[3] Kock F., Herwig H., *Local entropy production in turbulent shear flows: A high-Reynolds number model with wall functions*, 'International Journal of Heat and Mass Transfer' 2004, vol. 47, no. 10, pp. 2205–2215.

[4] Majdalani J., Shelton C.M., *On Prandtl's turbulent flow expressions for arbitrary power-law and shear-stress exponents*, 'Physics of Fluids' 2025, vol. 37, no. 8.

MULTISCALE ANALYSIS OF TURBULENT FLUXES FOR REYNOLDS AVERAGING IN ATMOSPHERIC FLOWS

J. Spała[1], **M. Wacławczyk**[1], **J-I. Yano**[2]

[1] *University of Warsaw, Faculty of Physics, Ludwika Pasteura 5, 02–093 Warsaw, Poland*

[2] *Centre National de Recherches Météorologiques, Toulouse, France*

E-mail: j.spala@student.uw.edu.pl

Abstract. Turbulence in stable Atmospheric Boundary Layer (ABL) is studied. Unlike the controlled laboratory conditions, the flows in ABL are inherently non-stationary and intermittent. This brings many fundamental questions related to their statistical analyses, particularly, how the Reynolds decomposition into the mean and eddy parts should be performed. We investigate this problem using the multiscale analyses based on wavelets and show that the answer strongly depends on the local stability of the flow.

Keywords: Atmospheric Science, Turbulence, Monin-Obukhov Theory.

1. Introduction

Reynolds decomposition, which separates a variable into a mean and a fluctuation, $x = \overline{x} + x'$, is widely used in fluid mechanics. In atmospheric studies, it is commonly applied to estimate turbulent fluxes, such as momentum $\langle u'w' \rangle$ or heat $\langle w'T' \rangle$, which are required for assessing energy transfer and atmospheric stability.

In its classical definition, the Reynolds mean is obtained as an ensemble average over an infinite number of realizations [1], which can be approximated in laboratory experiments through repeated measurements under identical conditions. In atmospheric flows, which are inherently transient, this approach is not feasible, and time averaging over a finite window of length τ is therefore commonly used, but the choice of τ strongly influences estimated fluxes. Typically used values are 30–60 minutes, but it lacks strong physical justification.

Identification of turbulent and mesoscale regimes using multiscale analysis provides a more physically grounded basis for selecting the averaging time. In this study, wavelet methods are used, although a simple moving average can also be applied. The results suggest that τ depends strongly on the local stratification parameter.

2. Multiscale analysis and concept of a gap scale

The wavelet method is classically used for multiscale analysis, as it ensures an orthogonal and energy-conserving decomposition across scales [2]. The resulting cospectra the scale-wise covariances show that flux contributions increase from the smallest scales, reach a turbulent peak, and then decrease. Beyond the zero crossing, the cospectrum exhibits more irregular behavior (see Figure 1, left). Hence, the zero crossing scale separates the flow into two regions, the first one commonly associated with the inertial subrange and small-scale turbulences and the second with larger-scale mesoscale motions.

With this physical interpretation, the zero crossing of the cospectrum can be adopted as a practical definition of the gap scale [3]. Automatic detection of this scale enables analysis of larger datasets and facilitates further investigations, which is the point of this study.

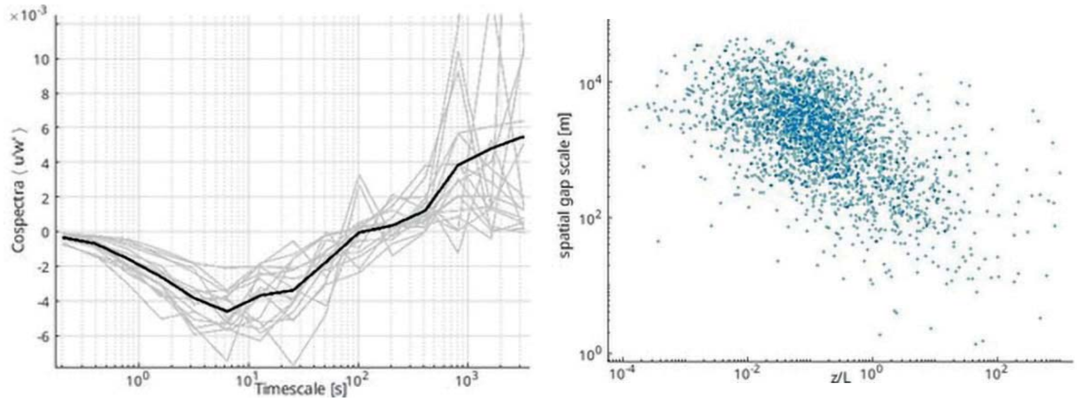

Figure 1. left: Examples of <u'w'> cospectra; right: Scatter of z/L and gap scale

3. Data and illustrative results

The dataset used in this study was collected during the MOSAiC campaign conducted in 2019–2020 [4]. The measurement mast drifted with the sea ice for almost a year, collecting data from sonic anemometers and other instruments. Velocity measurements at 10 Hz under stable atmospheric conditions are well suited for the purpose of this analysis.

Both panels in Figure 1 present results from the MOSAiC data. The left panel shows cospectra computed at different times. Although these spectra do not always closely resemble the idealized form, their physical interpretation remains possible in most cases.

The right panel shows a scatter plot of the detected gap scale versus the stability parameter z/L. On a logarithmic scale, a clear trend is observed. For smaller values of z/L, corresponding to near-neutral conditions, the gap scale tends to be larger, which is consistent with a well-developed inertial range. For higher values of z/L representing strongly stable conditions, the gap scale decreases, indicating suppression of turbulence at larger scales.

4. Discussion

Multiscale analysis can provide valuable insight in atmospheric flows and the gap scale concept can help in physical justification of the averaging time τ. While the scatter in the data is undeniable, a relationship between the gap scale and the Obukhov parameter is visible.

Moreover, in addition to automatic detection, which enables quantitative studies on large datasets, qualitative inspection of individual cospectra can also improve understanding of local flow conditions and the structure of turbulence.

Acknowledgements

This research was funded by the National Science Centre, Poland grant number 2020/37/B/ST10/03695, through the OPUS 19 program.

References

[1] Randall D. *Reynolds Averaging Lecture Notes,* University of Colorado, 2018.

[2] Mallat S., *Wavelet Tour of Signal Processing*, Academic Press, 1998.

[3] Vickers D., Mahrt L., *The Cospectral Gap and Turbulent Flux Calculations*, 'Journal of Atmospheric and Oceanic Technology' 2003, vol. 20, no. 5, pp. 660–672.

[4] Shupe M.D., Rex M., Dethloff K., Damm E., Fong A.A., Gradinger R., Heuzé C., Loose B., Makarov A., Maslowski W., Nicolaus M., Perovich D., Rabe B., Rinke A., Sokolov V., Sommerfeld A., *The MOSAiC Expedition: A Year Drifting with the Arctic Sea Ice*, NOAA Report, 2020.

A COMPARATIVE STUDY OF PHYSICS-BASED, SPARSE, AND BLACK-BOX REDUCED ORDER MODELS OF TANDEM CYLINDER WAKE DYNAMICS

W. Stankiewicz, T. Krakowski

Poznan University of Technology, Institute of Applied Mechanics, Jana Pawla II 24 st., 60–965 Poznan, Poland

E-mail: witold.stankiewicz@put.poznan.pl

Abstract. Laminar flow past tandem cylinders of unequal diameters is simulated using high-resolution DNS of the Navier-Stokes equations, revealing rich wake dynamics with strong vortex-wake interactions. Proper Orthogonal Decomposition is used to extract dominant modes, which are employed to build physics-based, sparse, and black-box reduced-order models. All ROMs are compared against high-fidelity data to assess their predictive capability for the observed dynamics.

Keywords: Computational Fluid Dynamics, Reduced-order modelling, Proper Orthogonal Decomposition, Galerkin projection, SINDy, machine learning, tandem cylinders, wake dynamics.

1. Introduction

Reduced-order modeling (ROM) provides efficient, low-dimensional representations of complex fluid flows, enabling analysis, control, and prediction beyond the reach of full-order simulations. While most ROM studies focus on flows around single bluff bodies or fully developed periodic regimes, tandem cylinders of unequal diameters generate significantly richer wake dynamics due to vortex–wake interference. The upstream cylinder excites and modulates the downstream wake, leading to multi-scale interactions and amplitude modulation that challenge low-dimensional modeling assumptions.

In such interacting-wake configurations, preserving long-term stability and accurately reproducing the limit-cycle attractor becomes nontrivial, particularly when different modeling paradigms are employed. Despite extensive work on POD-based ROMs, systematic comparisons of modeling strategies for interacting tandem wakes remain limited.

This work compares three fundamentally different ROM paradigms: physics-based Galerkin projection [1], sparse identification via SINDy [2], and black-box supervised machine learning models. To ensure a consistent and fair assessment, all models are constructed in the same POD state space derived from high-fidelity DNS data. The comparison therefore focuses on differences in dynamical modeling rather than on reduction strategies.

2. Flow configuration for Direct Numerical Simulation

The laminar flow past two tandem cylinders of unequal diameters is simulated at Reynolds number Re = 100 using the incompressible Navier–Stokes equations. The computational domain is discretized with a high-resolution finite-element mesh of second-order elements (Fig. 1), en-suring accurate representation of vortex shedding. Uniform inflow is prescribed at the inlet, no-slip conditions are applied on the cylinder surfaces, and a zero-pressure boundary is imposed at the outflow. Time-resolved simulations capture the fully developed wake dynamics and vortex–wake interactions between the upstream and downstream cylinders (Fig. 2).

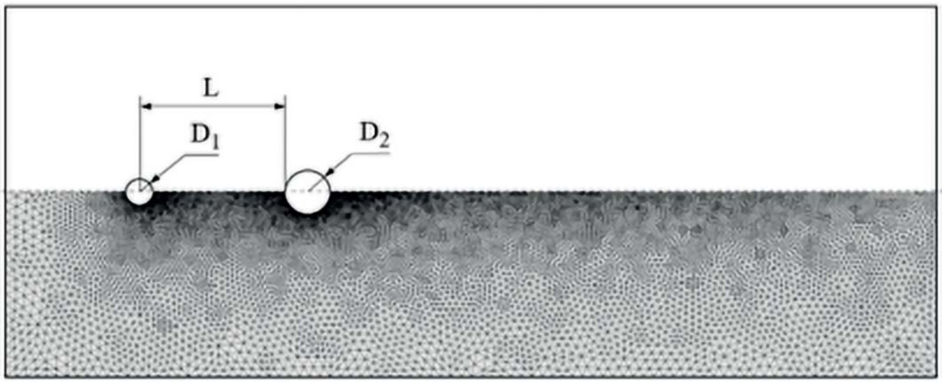

Figure 1. Computational domain and its finite-element discretization

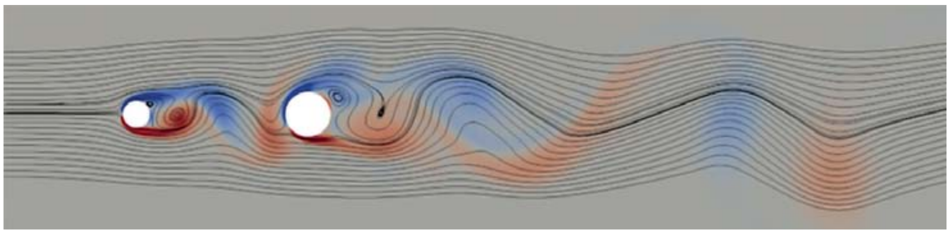

Figure 2. Instantaneous velocity field visualized with streamlines and vorticity

3. Modal Decomposition and Reduced-Order Models

Proper Orthogonal Decomposition (POD) is applied to the time-resolved velocity fields from the fully developed wake to extract the dominant coherent structures. A small number of modes captures the majority of kinetic energy associated with vortex shedding and wake interaction.

These modes form the basis for constructing three classes of reduced-order models (ROMs): physics-based Galerkin projection, which evolves the modal amplitudes according to the projected Navier–Stokes dynamics, sparse identification via SINDy, which selects the most significant interactions among modal amplitudes through LASSO regularization, and black-box supervised machine-learning models, trained to predict the time evolution of the modal amplitudes without explicit physical constraints.

All ROMs are built using the same dataset and evaluated in terms of their ability to reproduce the observed limit-cycle wake dynamics, modal energy distribution, and long-term stability. This unified framework enables a direct assessment of how physical structure, sparsity constraints, and data-driven learning influence wake modelling in interacting bluff-body flows.

Acknowledgements

Supported by grant 0612/SBAD/3640 of the Polish Ministry of Science and Higher Education.

References

[1] Noack B.R., Papas P., Monkewitz P.A., 2005, *The need for a pressure-term representation in empirical Galerkin models of incompressible shear flows*, 'Journal of Fluid Mechanics', vol. 523, pp. 339–365.

[2] Brunton S.L., Proctor J.L., Kutz J.N., *Sparse identification of nonlinear dynamics with control (SINDYc)*, 'IFAC-PapersOnLine' 2016, vol. 49, no. 18, pp. 710–715.

[3] Holmes P., Lumley J.L., Berkooz G., *Turbulence, Coherent Structures, Dynamical Systems and Symmetry*, Cambridge University Press, Cambridge 1998.

APPLICATION OF HELIUM FILLED SOAP BUBBLES FOR 3D PIV INVESTIGATIONS OF LARGE SCALE PASSIVE FLOW CONTROL DEVICES

W. Stryczniewicz

Łukasiewicz Research Network – Institute of Aviation, Warsaw, Poland, 110/114 Krakowska Av., 02–256 Warsaw, Poland

E-mail: wit.stryczniewicz@ilot.lukasiewicz.gov.pl

Abstract. The paper deals with application of large scale PIV for investigation of flow field over structured surfaces used for flow control. The aim of the work was to demonstrate the feasibility of Helium Filled Soap Bubbles for investigation passive flow control in wind tunnel at real-world scale and flow speeds. The flow control strategy relies on creating vortex formations in the boundary layer with use of dimples. In order to match the Reynolds number representative for automotive and general aviation aerodynamics the measurements were performed in low speed wind tunnel with test section diameter of 5 m at flow speeds of 20 m·s^{-1} and 30 m·s^{-1}. Application of HFSB enabled for 3D PIV measurements in large volume of O(0.5) m^3 and revealed change in flow topology over structured surface.

Keywords: Aerodynamics, Measurement Techniques, Flow control, Large scale PIV, Helium Filled Soap Bubbles, STB.

1. Introduction

Passive flow control with use of structured dimples might prevent turbulent separation, intensify heat transfer and reduce drag. Visualization of flow topology near the wall surface is beneficial to understand the influence of geometrical parameters of this flow control devices. Recent advances in effective generation of sub-millimeter size naturally buoyant seeding in form of Helium Filled Soap Bubbles [1] volume self-calibration together with advanced particle tracing algorithms such as Shake-the-Box [2] allowed for performing volumetric PIV measurements in large volumes. In this study we investigate the feasibility of large scale PIV for investigation of flow topology above flat plate for case of flat smooth and structured surface at Reynolds numbers representative for automotive and general aviation aerodynamics.

2. Materials and methods

The test were performed in Łukasiewicz Research Network – Institute of Aviation T-3 wind tunnel in open test section of 5 m diameter. The test object was a flat plate (400 mm × 500 mm) with a row of dimples (40 mm × 10 mm) with -35° and 35° alternating skew angle (see Figure 2 left). The HFSB injector in form of 8 Linear Nozzle Array from LaVision was positioned at the exit of the wind tunnel nozzle. The test object was placed downstream of WT/HFSB flow at the test section end as depicted in Figure 1. The test where performed at flow speeds of 20 m·s^{-1} and 30 m·s^{-1}.

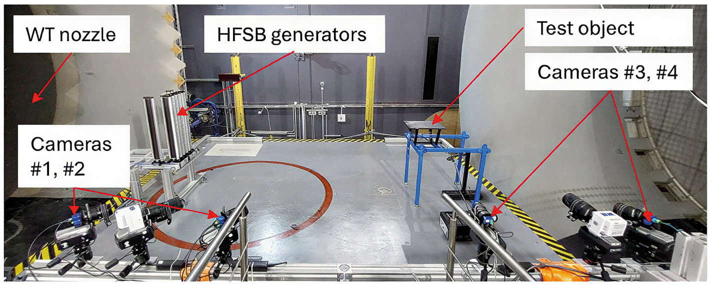

Figure 1. HFSB 3D PIV STB system in T-3 test section

2.1. Velocity measurements

The PIV system consisted of a Nd:YAG laser (400 mJ at 15 Hz) with volumetric optics and four cameras with 16 Mpx COMS sensors with high quality lenses (f ca 24 mm). The volume of 0.6 × 1.2 × 0.8 m^3 was calibrated with use of flat dotted calibration target. The particle positions and displacement was detected in domain 1200 × 200 × 450 mm with double pulse particle tracking algorithm (Shake the Box). The particle tracks averaged from 1000 measurements were interpolated on cartesian grid with binning procedure with 3.439 mm grid spacing giving Dynamic Spatial Range (DSR) of 63. The Dynamic Velocity Range calculated for ensemble PTV measurement is DVR = 125.

3. Results

Figure 2 shows the 3D velocity field over test object in configuration with and without dimples. The test show capabilities for large scale volumetric measurements at industrial scale in Łukasiewicz – Institute of Aviation T-3 wind tunnel.

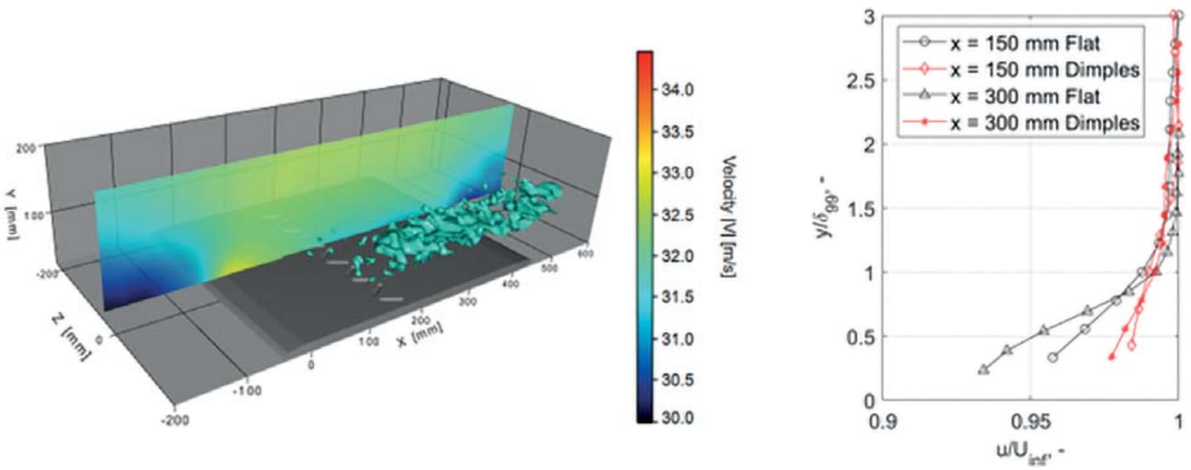

Figure 2. *(left)* 2D cross-sections of 3D velocity field. The isosurfaces shows constant value of vorticity ω_z. *(right)* Mean streamwise velocity profiles measured with HFSB

Acknowledgements

This work was subsidized by the National Recovery Plan (NRP) under the project entitled "CeBRINS - Centrum Badawczo-Rozwojowe Innowacyjnych Napędów i Struktur Lotniczych" under grant KPOD.01.18-IW.03-0008/23.

References

[1] Engler Faleiros D., Tuinstra M., van Rooijen B.D., Scarano F., Sciacchitano A., *Soap bubbles for large-scale PIV in industrial wind tunnels*, 13th International Symposium on Particle Image Velocimetry (ISPIV 2019), Munich, Germany, July 22–24, 2019.

[2] Schanz D., Gesemann S., Schröder A., *Shake-The-Box: Lagrangian particle tracking at high particle image densities*, 'Experiments in Fluids' 2016, vol. 57, no. 5, pp. 1–27.

AEROACOUSTIC INVESTIGATION OF TRAVELLING WAVE AS FLOW CONTROL FOR AIRFOIL DRAG REDUCTION

T. Suresh[1], N. Maynard[2], J.A. Khalil[2], R. El Akoury[2], M. Braza[2], O. Szulc[1], P. Flaszyński[1]

[1] *Institute of Fluid-Flow Machinery, Polish Academy of Sciences, Fiszera 14, 80–231 Gdansk*

[2] *Institut de Mécanique des Fluides de Toulouse - IMFT, 31400, Toulouse, France*

E-mail: thanu@imp.gda.pl

Abstract. Electroactive morphing is implemented on an airfoil through a sinusoidal travelling wave actuation. The impact of this on the aerodynamic performance of the airfoil (drag reduction) in the subsonic regime, is conducted through numerical simulations and the consequent impact on the noise emission is also presented.

Keywords: piezo-ceramic actuator, Arbitrary Lagrangian-Eulerian method, FW-H analogy.

1. Introduction

Taking inspiration from birds, some of which can alter their wing properties to produce small deformations and vibrations, to increase their aerodynamic performance while simultaneously decreasing sound (owls), an innovative concept called the morphing is applied to an airfoil. The morphing concept is implemented by a sinusoidal travelling wave actuation (TW) on an airfoil in the low subsonic regime. The travelling wave actuation has a strong capability to interact with turbulent structures and reshape wake dynamics, thereby increasing the lift-to-drag ratio [1]. Numerical flow and acoustic investigations are presented for a static and morphing airfoil.

2. Theoretical background

The pressure distribution obtained from the flow simulations described in [2] acts as input to the aeroacoustic code [3]. The travelling wave actuation implemented in the morphing airfoil causes variation of the loading forces on the airfoil surface that consequently influences the noise emitted. This is captured by the pressure fluctuations on the airfoil surface which is encapsulated in the dipole term of the solution derived by Farassat [4] for the Ffowcs-Williams and Hawkings acoustic analogy (FW-H) [5].

3. Methodology and preliminary results

Two-dimensional numerical simulations are conducted for a prototype with a chord of 70 cm length at a Reynolds number of 1×10^6, in a subsonic regime (Mach = 0.063). Results show that the upper and lower shear layers formed upstream of the separation area and downstream of the trailing edge, respectively, develop Kelvin-Helmholtz vortices. The two shear layers interact farther downstream and form the von Kármán vortex street (Figure 1).

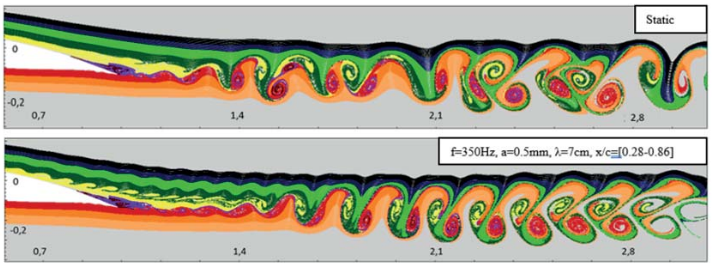

Figure 1. Streaklines visualisation of the wake in static and TW actuation cases. The colour of each particle represents its initial position. In the morphing case, a decrease in the drag coefficient of 7.86% is obtained, associated with a lift-to-drag ratio increase of 8.67%

Acoustic pressure emitted by the morphing airfoil is compared against the static airfoil in both time and frequency domains to assess their relative acoustic impact for two microphone locations (representing listeners) - in-plane of the airfoil, M4 microphone at ($5c$, 0, 0) and one out-of-plane microphone, M5 at (c, 0, $5c$) with c being the airfoil chord, to demonstrate the sound directivity pattern of the wing. The time domain results depict that the M5 microphone (Figure 2b) emits more sound than M4 microphone (Figure 2a). At both microphone locations, the morphing wing reduces noise at low frequencies, while showing varying trends at higher frequencies, compared to the static wing. The Overall Sound Pressure Level (OASPL) values are also reduced by the morphing airfoil by ≈ 3 dB. Preliminary results show a promising trend in the noise reduction potential of the morphing airfoil relative to the static airfoil.

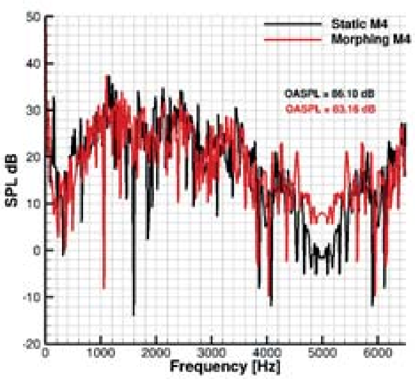

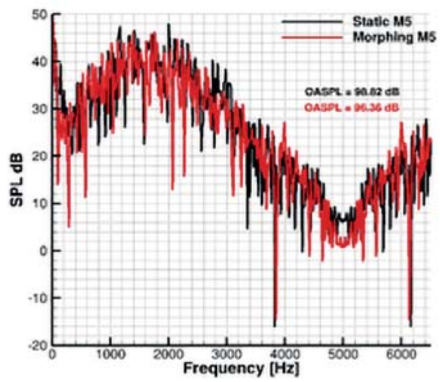

Figure 2. Comparison of loading noise for the static/morphing airfoil for selected microphones. Left: In-plane microphone, right: Out-of-plane microphone

Acknowledgements

This research work is supported by the HORIZON 2023-2027 Pathfinder Open Project No 101129952 - BEALIVE (Bioinspired Electroactive multiscale Aeronautical Live skin) and by the HPC center CI TASK in Gdansk (Poland).

References

[1] Kang W., Pengfei L., Zhang J.-Z., Xu M, *Effects of local oscillation of airfoil surface on lift enhancement at low Reynolds number*, 'Journal of Fluids and Structures' 2015, vol. 57, pp. 49–65.

[2] Khalil J.A., Navarro C.J., El Jeaid R., Marouf A., El Akoury R., Hoarau Y., Rouchon J.-F., Braza M. , *Aerodynamic performance increase over an A320 morphing wing in transonic regime by numerical simulation at high Reynolds number*, 'International Journal of Numerical Methods for Heat & Fluid Flow' 2024, vol. 34, no. **7**, pp. 2709–2747.

[3] Suresh T., Szulc O., Flaszynski P., *Aeroacoustic analysis based on FW–H analogy to predict low-frequency in-plane harmonic noise of a helicopter rotor in hover*, 'Archives of Mechanics' 2022, vol. 74, no. 2–3 pp. 201–246.

[4] Farassat F., *Derivation of Formulations 1 and 1A of Farassat*, 'NASA Technical Reports' 2007, pp. 1–25.

[5] Ffowcs-Williams J.E., Hawkings D.L., *Sound generation by turbulence and surfaces in arbitrary motion*, 'Philosophical Transactions of the Royal Society of London Series A' 1969, vol. 264, pp. 321–342.

HIGH-FIDELITY ANALYSIS OF LOW-NOISE UAV ROTOR DESIGNS

O. Szulc[1], T. Suresh[1], A. Sieradzki[2], P. Flaszyński[1]

[1] *Institute of Fluid-Flow Machinery, Fiszera 14, 80–231 Gdańsk, Poland*

[2] *Łukasiewicz Research Network - Institute of Aviation, Al. Krakowska 110/114, 02–256 Warszawa, Poland*

E-mail: Oskar.Szulc@imp.gda.pl
E-mail: Adam.Sieradzki@ilot.lukasiewicz.gov.pl

Abstract. The paper presents the application of an in-house aeroacoustic solver for predicting both harmonic and broadband noise generated by Unmanned Aerial Vehicle (UAV) propellers that were designed, manufactured and experimentally tested at the Łukasiewicz Institute of Aviation. The flow around small-scale propellers is simulated using the block-structured FLOWer solver, employing RANS and DES transitional approaches to turbulence and a fourth-order accurate numerical scheme, while the acoustic modeling is based on Farassat's solution to the FW-H equation (formulation 1A).

Keywords: Aerodynamics, Aeroacoustics, Computational Fluid Dynamics.

1. Introduction

Unmanned aerial vehicles (UAVs), while invaluable for tasks such as aerial imaging, infrastructure inspection, surveillance, goods delivery and medical transport, generate significant noise that adversely affects communities, wildlife and environmental comfort. Moreover, drones are increasingly deployed across civilian, commercial and military applications. The scale and rapid growth of both the global fleet (2.8M commercial units in 2024) and the market, projected to exceed $164B by 2030, underscore the critical need for advancing research into UAV aerodynamics, noise generation and mitigation to improve public acceptance.

The primary objective of this paper is to numerically analyse the flow-field and acoustic emissions (both tonal and broadband) of three two-bladed, small-scale propellers (radius R = 0.15 m) designed, manufactured and experimentally tested at the Łukasiewicz Research Network – Institute of Aviation (Ł-ILOT) [1–3]. These propellers (designated as in4_11, in8_1 and in10_5) were optimized with respect to aerodynamic performance and noise generation (see Fig. 1). A benchmark two-bladed propeller of the same radius R = 0.15 m from the Technical University of Delft (TUD) was included for reference [4]. Initially, the reference propeller was investigated at 5000 RPM, corresponding to a tip Mach number of 0.23 and sectional Reynolds numbers below $100{\cdot}10^3$, i.e., within the transitional flow regime, to enable comparison with the benchmark experimental data from TUD. Subsequently, all four propellers were tested in an anechoic chamber under hover conditions at a constant thrust of 8N (Ł-ILOT). Rotor loading (thrust and torque) was measured simultaneously with acoustic emissions which were recorded using free-field microphones positioned 1.2 m (8R) from the rotation axis at in-plane and out-of-plane locations.

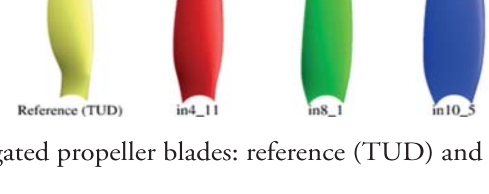

Figure 1. Investigated propeller blades: reference (TUD) and optimized (Ł-ILOT)

2. Physical and numerical modeling

The physical modelling of low-Reynolds-number flows requires accounting for the natural transition of the boundary layer from a laminar to a turbulent state which strongly affects surface pressure fluctuations induced by laminar separation and shear-layer instability. Such phenomena can be captured using high-fidelity numerical approaches, in particular hybrid RANS-LES methods, such as Delayed Detached Eddy Simulation (DDES) implemented in FLOWer (DLR) solver. These approaches are commonly based on the SA-type or k-ω SST formulations which act either as Reynolds-averaged turbulence models in RANS regions or as subgrid-scale models in the LES zones. Additionally, high-order numerical schemes are preferred, such as the fourth-order upwind SLAU2 scheme of Kitamura for spatial discretization and the optimized second-order backward difference scheme (BDF2OPT) for temporal integration, applied on dense structured grids (Fig. 2).

3. Initial acoustic results

As a result, the resolved surface pressure fluctuations associated with the flow phenomena are supplied to in-house acoustic solver as input for the noise analysis, which is based on Farassat's formulation 1A of the solution to the Ffowcs-Williams and Hawkings (FW-H) equation [5]. This approach enables the prediction of acoustic signals in both the time and frequency domains (exemplary in-plane microphone noise spectrum obtained for TUD propeller is presented in Fig. 3.).

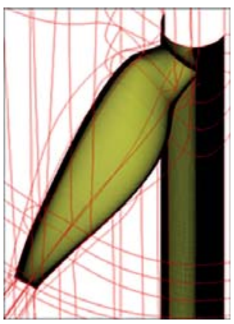

Figure 2. Single blade grid topology and surface mesh (reference propeller)

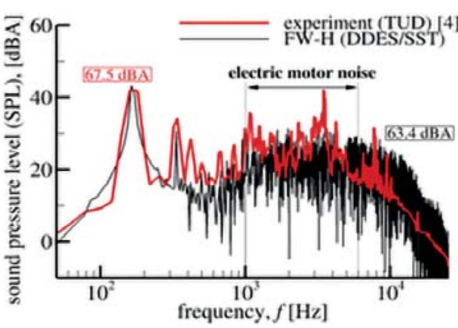

Figure 3. Exemplary A-weighted sound pressure level (SPL) spectra for reference propeller (TUD)

Acknowledgements

This research was supported by the CI TASK in Gdansk (Poland) and PLGrid Infrastructure.

References

[1] Sieradzki A., Kekus P., Klimczyk W., *Validation of a Surrogate-Based Methodology for Low-Noise UAV/UAM Rotor Design*, Proceedings 49th European Rotorcraft Forum, Bückeburg 2023.

[2] Klimczyk W., Sieradzki A., *RANS-Based Aeroacoustic Global Sensitivity Study and Optimization of UAV Propellers*, 'Aerospace' 2023, vol. 10, no. 3.

[3] Kekus-Kumor P., Sieradzki A., *A low-cost anechoic chamber for rotor aeroacoustics research: design and validation*, 'Transactions on Aerospace Research' 2025, vol. 279, no. 2, pp. 18–39.

[4] Casalino D., Grande E., Romani G., Ragni D., Avallone F. , *Definition of a benchmark for low Reynolds number propeller aeroacoustics*, 'Aerospace Science and Technology' 2021, vol. 113.

[5] Szulc O., Suresh T., Flaszyński P., 'Archives of Mechanics' 2025, vol. 77, no. 1, pp. 67–85.

FLOW INSTABILITY IN A CHANNEL WITH OBLIQUELY CORRUGATED WALLS

J. Szumbarski

Warsaw University of Technology, Faculty of Power and Aeronautical Engineering, ul. Nowowiejska 24, 00–665 Warszawa, Poland
E-mail: jacek.szumbarski@pw.edu.pl

Abstract. The paper presents an analysis of the linear stability of the flow of an incompressible Newtonian fluid in a channel with wavy walls. Generally, the angle between the direction of the wall waviness and the average pressure gradient driving the flow is arbitrary. However, the research focuses on the case of small deviations from a configuration called transverse orientation which is known to lead to destabilization of flows at very low Reynolds numbers. The main aim of the study is to determine the effect of a slight deviation from this 'ideal' orientation on stability characteristics, in particular the value of the critical Reynolds number and the form of unstable disturbances.

Keywords: flow instability, channel flow, wavy walls, critical Reynolds number.

1. Introduction

The study of instabilities in internal flows, especially in the context of the mixing enhancement at low Reynolds numbers, has remained an important research issue in fluid mechanics for at least half a century. In order to intensify mixing, passive methods are often used, which consist in introducing a properly selected system of obstacles into the flow area, thanks to which the flow obtains a complex, three-dimensional kinematic structure. However, this type of manipulation is typically accompanied by a significant increase in hydraulic resistance. An alternative approach without this disadvantage is the introduction of transverse periodic wall waviness of appropriately selected wavelength and amplitude. In the paper [1], it is shown that it is possible to reduce the critical Reynolds number below 60, i.e. by two orders of magnitude. Subsequent works, e.g. [2], proved that the flow obtained as a result of nonlinear saturation of the initial perturbation has promising kinematic properties, without the penalty of increased hydraulic losses. The subject of the current work is to check to what extent this result is sensitive to small inaccuracies of the ideal wave configuration. This question is important, as in practice small deviations are inevitable.

2. The subject of the research

The subject of the study is the flow in a channel with unidirectional and periodic corrugation of the walls, forced by a pressure gradient which is oriented at an arbitrary angle to the direction of the corrugation (Fig. 1, left). In the coordinate system aligned with the wave crests, the base flow has three velocity components depending on the two coordinates. Such flow kinematics is significantly more complex than in the case of ideally transversal case, where the base flow is unidirectional.

Consequently, the linear stability analysis is also much more difficult. The equations governing evolution of small disturbances have been derived in transformed to a convenient reduced form which reduces dimension of the resulting eigenvalue problem. The main goal is to identify the unstable normal mode (or modes) and to investigate its parametric variation, in particular to find settings that minimize the critical Reynold number. Finally, the main goal is to assess sensitivity of the stability thresholds to small deviations form ideally transversal orientation of the wall corrugation.

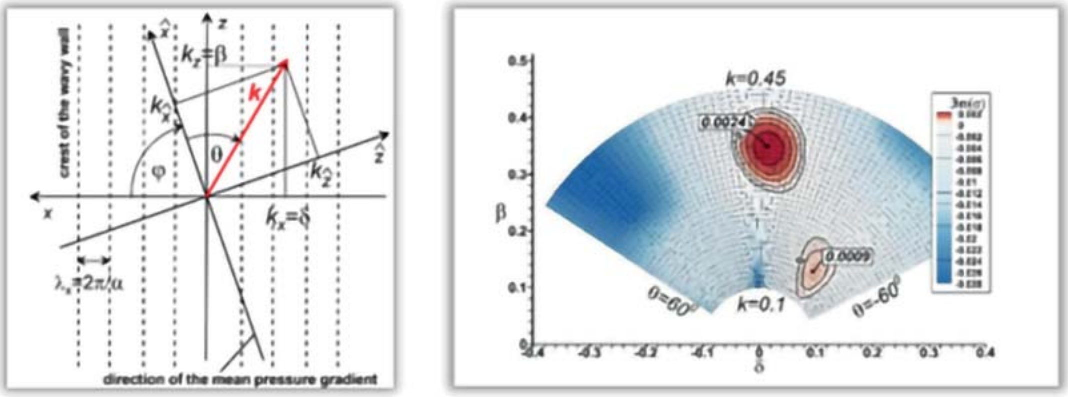

Figure 1. (left) Orientation of wall corrugation an mean pressure gradient, (right) the amplification rate plotted vs. wave numbers of the disturbance field; Re =100, φ = 87°, corrugation amplitude S = 0.3 and wave number α = 0.8

3. Research method

This base flow is determined numerically using the in-house spectral method using the concept of submerged boundaries, as in [3]. The resulting flow is subjected to linear stability analysis, again with spectral accuracy, as in [4]. The effect of such discretization is an large algebraic eigenvalue problem. Unstable normal modes are determined using procedures from the LAPACK library and their parametric variability is tracked using the inverse iteration method. Contour maps of the unstable mode's amplification rates have been created (see Fig. 1 right for a sample result). The critical Reynolds number and its variation as a function of the angle of deviation of the direction of the wall corrugation from the perfectly transverse configuration are also determined.

4. Conclusions

The calculations carried out lead to the conclusion that with increasing deviation from the ideally transverse orientation of the wave, the critical Reynolds number increases. Moreover, the unstable mode is an oblique traveling wave and the disturbed flow is quasi-periodic in space. Nevertheless, in the range of small deviations it still remains much smaller than in the case of a smooth channel. The reason for the increase in the critical Reynolds number is the rapid drop of the transverse modulation of the base flow velocity with increasing deviation angles.

References

[1] Szumbarski, J., *Instability of viscous incompressible flow in a channel with transversely corrugated walls*, 'Journal of Theoretical and Applied Mechanics' 2007, vol. 45, no. 3, pp. 659–683.

[2] Yadav N., Gepner S.W., Szumbarski J., *Instability in a channel with grooves parallel to the flow*, 'Physics of Fluids' 2017, vol. 29.

[3] Szumbarski J., Floryan J.M., *A direct spectral method for determination of flows over corrugated* boundaries, 'Journal of Computational Physics' 1999, vol.153, pp. 378–402.

[4] Szumbarski J., *Immerse boundary approach to stability equations for a spatially periodic viscous flow*, 'Archives of Mechanics' 2002, vol. 54, no. 3, pp. 199–222.

SIMULATION OF UNSTEADY INTERNAL FLOWS WITH NOVEL DISSIPATIVE INLET/OUTLET CONDITIONS

J. Szumbarski[1], **J. Gałecki**[2]

[1,2] *Warsaw University of Technology, Faculty of Power and Aeronautical Engineering, ul. Nowowiejska 24, 00–665 Warszawa, Poland*

E-mail: jacek.szumbarski@pw.edu.pl 1; jakub.galecki@pw.edu.pl 2

Abstract. This paper presents a numerical methodology for modeling unsteady flows of viscous incompressible fluids within internal domains containing multiple inlet and outlet sections. A new formulation of dissipative boundary conditions, incorporating unsteady and direction-sensitive nonlinear terms, is introduced. The approach enables the imposition of time-dependent flow rates and/or section-averaged pressures at the domain boundaries. Fluid motion unsteadiness is addressed by combining Backward Differentiation Formulae (BDF) schemes with Operator-Integration-Factor splitting to manage advective nonlinearity. Nonlinearity related to the boundary conditions are accounted for using a polynomial extrapolation. Numerical simulation results, generated using a spectral-element in-house solver applied to a two-dimensional test cases, are also detailed.

Keywords: Navier-Stokes equations, unsteady internal flows, dissipative boundary conditions, spectral element method, Operator-Integration-Factor splitting.

1. Introduction

Modeling unsteady flows in complex internal domains poses a challenge for both theoreticians and CFD practitioners. One of the main difficulties is the formulation of physically relevant and numerically tractable flow conditions at artificial boundaries of a computational domain. For internal flows, these boundaries usually include inlet and outlet sections that arise from trimming a large flow domain to a smaller computational one. Usually, some variant of the open boundary conditions is used, especially at the outlet sections. In particular, the so called 'do-nothing' conditions are commonly used. Their basic variant is easy to implement within spectral-h/p element methods and allows for using time-dependent section-averaged pressures and/or flowrates as inputs for flow simulations [1]. Nonlinear variants have been also proposed to alleviate tendency for numerical instability caused by the occurrence of backflow [2]. Yet another variants were design for better capturing specific flow features. The dissipative boundary conditions, originally proposed in [3], belong to this category. These are the open conditions supplemented with terms which simulate the presence of an external fluid reservoir connected to the flow domain through a porous structure obeying the linear Darcy law. Clearly, such modification is sound only for flows with small Reynolds numbers and slow time variations.

2. The subject of the research

The topic of the current study is to generalize the open dissipative conditions for flows with strong unsteadiness and with higher Reynolds numbers. To this aim, the unsteady term was added, i.e., the term which depends on the rate of change of the flow rate, and the inertial term which depends quadratically on the flow rate. Additionally, the nonlinear term is made direction-sensitive since, in general, the inertial part of the pressure loses in a (hypothetical) porous media attached to inlet/outlet sections might depend on the bulk-flow direction. Hence, the form of the inlet/outlet conditions is:

$$p\mathbf{n} - \mu\frac{\partial}{\partial\mathbf{n}}\mathbf{u} - \left[\eta_k\frac{d}{dt} + \lambda_k + \gamma_k|Q_k(t)|\right]Q_k(t)\mathbf{n} = S_k(t)\mathbf{n} \quad at \;\; \Gamma_k, k = 1, \dots, \mathrm{K} \tag{2}$$

where p, u and μ denote the pressure, velocity and fluid viscosity. The (signed) flow rate $Q_k(t)$ or the far-field reservoir pressure $S_k(t)$ is given at the inlet/outlet Γ_k. The coefficients γ_k can depend on the bulk-flow direction, i.e., on the sign of the flow rate.

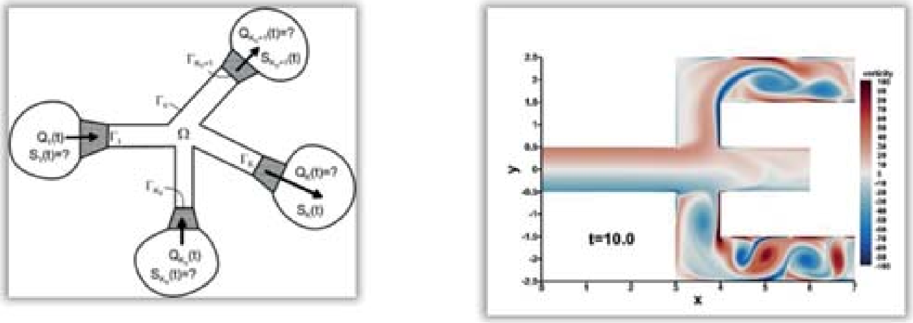

Figure 1. (left) The flow domain with K inlet/outlet sections. The flow rates are prescribed for first K_v sections, while section-averaged pressures are given for the remaining ones, (right) an instantaneous pattern of the vorticity field of the test flow

3. Research method

Novel boundary conditions have been included into the weak formulation of the governing equations. The 2nd-order backward-differentiation scheme has been used to deal with flow unsteadiness. The nonlinear advective terms have been integrated using the Operator-Integration-Factor Splitting (OIFS) technique. Nonlinearity incurred by the boundary conditions has been managed by means of the polynomial extrapolation. This way, the numerical problem solved at each time step is linear. To achieve the desired flow rates, a transient flow field is constructed as a superposition of solutions to specific Stokes problems. Only one such problem is solved in the course of the simulation. The test case has been solved with the use of the in-house 2D spectral-element solver with quadrilateral elements.

4. Conclusions

Novel formulation of the nonlinear dissipative conditions, applicable to unsteady viscous flows in duct networks, has been proposed, implemented and tested. The pros and cons have been discussed.

References

[1] Heywood J.G., Rannacher R., Turek S., *Artificial boundaries and flux and pressure conditions for the incompressible Navier-Stokes equations*, 'International Journal of Numerical Methods in Fluids' 1996, vol. 22, no. 5, pp. 325–352.

[2] Dong S., Karniadakis G.E., Chryssostomidis C., *A robust and accurate outflow boundary condition for incompressible flow simulations on severely-truncated unbounded domains*, 'Journal of Computational Physics' 2014, vol. 261, pp. 83–105.

[3] Maury B., Meunier N., Soualah A., Vial L., *Outlet dissipative conditions for air flow in the bronchial tree*, 'ESAIM Proceedings' 2005, vol.14, pp. 201–212.

EXPERIMENTAL INVESTIGATION OF A 3D-PRINTED HEAT PIPE WITH MATHEMATICALLY DETERMINED OPERATING LIMITS

M. Szydłowski, G. Górecki, A. Gutkowski

Lodz University of Technology, Institute of Turbomachinery, 217/221 Wolczanska St., 93–005 Lodz, Poland

E-mail: mateusz.szydlowski@dokt.p.lodz.pl

Abstract. Tests of a 3D-printed aluminium grooved heat pipe (HP) filled with propane have been conducted. Such geometries of the grooves have not been found in the literature. The main limits of HP operation have been specified and they will be mathematically described. The values corresponding to the investigated device will be assessed and the contour of the working region will be drawn. The results of this work will deliver unique conclusions in the field of HP designs and their novel manufacturing methods.

Keywords: Interdisciplinary Areas in Heat and Fluid Flow, Multi-phase Flows, Experiment, Mathematical Model, Thermal performance.

1. Introduction

A heat pipe (HP) is a sealed mechanical device that transfers heat from one end to another without requiring additional energy input. The hot part causes the fluid to evaporate and flow to the cold, condensation section. The fluid in the liquid phase flows back to the evaporator and the cycle continues. HPs are commonly used in electronics and aerospace cooling, heat recovery, solar thermal systems or nuclear systems.

One of the methods to enhance HP's performance is modifying its geometry. The external changes improve heat transfer between the HP and its environment, while the internal ones affect the operating limits. There have been theoretical and numerical studies on complex shapes that would be hard to produce with traditional methods. Additive manufacturing could be a solution for incorporating these designs into real-world testing [1]. Familiarity with operational limitations and, thus, heat transport capabilities is a helpful indicator for choosing reasonable production solutions.

The authors aim to expand knowledge regarding heat pipe design and its operating limitations. A test rig was constructed for conducting experiments over a 3D-printed heat pipe. The geometry of the device, namely the groove shape, has not been found in the literature. Thus, its thermal characteristics and the derived heat transfer limitations will ensure the uniqueness of the research.

2. Test stand description

The constructed test stand was equipped with a single heat pipe during operation, cooling and heating mechanisms, a filling mechanism, carefully selected sensors and National Instruments measurement cards. The data acquisition system was prepared in LabVIEW software.

A heat pipe of external diameter 25.4 mm was 3D-printed out of aluminium ($AlSi_{10}Mg$) in two separate parts due to the production limitations. The models and their printed versions are shown in Figure 1. Every part was connected to an additional aluminium ring that later allowed the connection of those parts with bolts. With such a construction, it will be easier to change the sections to ones with different geometry modifications. The evaporator section of the heat pipe was 250 mm and it was heated up by three electric heaters with a maximum power of 300 W each. The condenser section was cooled through a water jacket. The liquid was delivered at around 10°C, thanks to a chiller and a thermostat. Cold section's length was also 250 mm.

The whole heat pipe was 550 long, leaving 50 mm for the adiabatic section. Working fluid inside the heat pipe was pure propane (R290, C_3H_8).

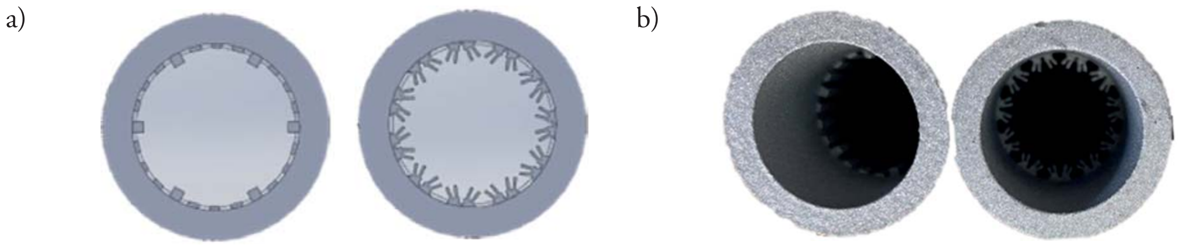

Figure 1. Modelled a) and 3D-printed b) heat pipes

3. Heat transfer limitations

Five main heat transport limitations strictly impact the HP's performance. Combining them all provides an operational range from which it is possible to predict the transferred heat. These limitations depend on the working fluid used, the heat pipe's geometry and the operating conditions. The vapour pressure limit occurs when the total vapour pressure is balanced by viscous forces, leading to low or no flow. Reaching the sonic level and velocity by vapour causes the vapour flow to choke. The entrainment limitation occurs when vapour, due to its high shear force, prevents the liquid from returning to the evaporator. The circulation or capillary limitation indicates that the capillary pressure is insufficient to deliver liquid from the condenser to the evaporator. The boiling limit is caused by bubbles in the wicks created through nucleate boiling, which prevent liquid flow [2]. However, in the investigated case there are no wicks, except the rough structure at the walls. Thus, it is predicted that the boiling limit will not occur. The limitations will be presented in a graph with the suggested working range marked. The experimental results obtained will be additionally plotted on this graph.

Acknowledgements

This extended abstract has been completed while the first author was the Doctoral Candidate in the Interdisciplinary Doctoral School at the Lodz University of Technology, Poland.

Work co-financed under the „FU²N – Fundusz Udoskonalania Umiejętności Młodych Naukowców" programme supporting the scientific excellence at the Lodz University of Technology – grant no. 4/FU²N/IMech/2025.

References

[1] Szymanski P., Mikielewicz D., 2022 *Additive Manufacturing as a Solution to Challenges Associated with Heat Pipe Production*, 'Materials' 2022, vol. 15, no. 4.

[2] Nemec P., Čaja A., Malcho M., *Mathematical model for heat transfer limitations of heat pipe* 'Mathematical and Computer Modelling' 2013, vol. 57, no. 1–2, pp. 126–136.

SOME ASPECTS OF MODELLING THE PROCESS OF ORGANIC WASTEWATERS REMOVAL IN BIOREACTORS AND INFLUENCE OF OXYGEN REGIME ON EFFICIENCY OF PURIFICATION

S. Telyma

Institute of Hydromechanics of National Academy of Sciences of Ukraine,03057 M.Kapnist St.,8/4, Kyiv, Ukraine

E-mail: sertelyma@gmail.com

Abstract. The mathematical model of oxygen supply at purification the wastewaters with organic pollutants in bioreactors with fixed biocenosis (biofilm) is presented. The features of modeling of the oxygen regime is cosidered. For the valuation of the influence of oxygen regime on efficiency of wastewater tratment the relation of oxygen to ammonium is proposed. This relation is the better alternative for control of nitrification process in bioreactors in comparison with determined concentration oxygen data. Using of proposed relation in practical calculations give the possibility to regulate the wastewater treatment processes and allows to improve the efficiency of bioreactors exploitation.

Keywords: model, purification, oxygen, organic pollutants nitrification, biofilm, bioreactor.

1. Introduction

In biological wastewater treatment reactors the removal of organic contaminants (OC) occurs in aerobic conditions that is when oxygen is consumed for bio-oxidation of OC and self-oxidation of cell material and also used in other processes that may occur at this time. Therefore the modeling and development of the aeration system consist in investigation of such an oxygen regimes when the rate of the biological treatment process should not be limited by the amount of oxygen contained in the reactor.

2. Aim of invesitgations

The aim of investigations was consisted in creation of the mathematical model for valuation and analyse of the oxygen regimes in bioreactors according to considered conditions on the base of corresponding equations of material balance recorded relative the concentration of oxygen C.

3. Methods and results

In the given paper the peculiarities that occur in modeling the oxygen regime at aerobic biological treatment of wastewaters in bioreactors with fixed biocenosis are considered. At this for evaluation of removal of OC the linear kinetics of reactions of the first and zero orders according to Monod were used. In general case the summary flow of oxygen entering into biofilm through its surface is determined by the next equation:

$$N_c = -D_c \frac{dC}{dz} = (1-\eta) K_C \left(C_a - C|_{z=0}\right) + \eta \alpha K_{Cn} \left(\beta C_p - C|_{z=0}\right). \tag{1}$$

where η – the ratio of the surface area of the biofilm when in contact with air bubbles to the total surface area of the biofilm, D_c – coefficient of diffusion in biofilm, α and β – parameters of kinetic equation relatively first and zero order. In other words, the equation (1) takes into account the possible additional flow of oxygen into a biofilm both from the volume of liquid in the form of dissolved oxygen and as a result of the so-called inter-surface transfer (IST) directly from the bubbles adhered to the biofilm. Note that the determination of the flow of oxygen through the surface of the biofilm, N_C , may be obtained in a result of solving the following equation which characterize the consumption of oxygen at the removal of OC by a fixed biocenose (biofilm):

$$\frac{\partial C}{\partial t} = D_C \frac{\partial^2 C}{\partial z^2} - R_C \tag{2}$$

For practical calculations the solution of equation (2) is sufficient to solve for stationary conditions that occur fairly quickly that is when $\frac{\partial C}{\partial t} = 0$. The solution of equation (2) is performed under the following boundary conditions, namely: $N_c = 0$ for $z = 0$ and $\frac{\partial C}{\partial t} = 0$ for $z = \delta$ which allows us to determine the change in the concentration of oxygen along the thickness of the biofilm, δ, and in subsequent calculations for determination of the concentration on the surface of the biofilm $C|_{z=0} = C\delta$.

In the above equations and dependencies $\tilde{N}$, C_δ, C_a, C_0 are respectively the concentration of oxygen in the biofilm, on the surface of the biofilm, in bioreactor and in the wastewaters at the entrance to it; C_p – concentration of saturation (soluble) oxygen in the liquid; R_c – the rate of reactions of using oxygen in a biofilm taking into account the oxidation velocity of the isolated substances during the death of microorganisms; K_{cn}, K_c – respectively the mass transfer coefficient for oxygen between the surface and biofilm and mass transfer coefficient of oxygen in liquid film [1-3]. Implementation of the proposed model allows with known r characteristics to evaluate the influence of oxygen regime on the processes of waste treatment in bioreactors.

4. Conclusions

At creation of the models of wastewaters treatment it is necessary at first to take into account the heterogeneous structure of biofilm, oxygen supply regimes and correspond balance equations of kinetic reactions. Evaluation of oxygen influence on the oxidation process ammonium to nitrate with using of the relation O_2/N-NH_4 is recommended. In practical calculations the proposed relation allows to regulate the purification processes and improve the efficiency of bioreactor exploitation.

References

[1] Kilich T., Babi E.B., *Biofilm control strategies in the light of biofilm – forming microorganisms*, 'World Journal of Microbiology and Biotechnology' 2023, vol. 39, pp. 1–22.

[2] Laspidou1 C.S., Kungolos A., Samaras P., *Advances in mathematical modelling of biofilm structures* 'Water Resources Management IV' 2007, vol. 103, pp. 231–240.

[3] Levandowski Z., Beynal H., *Fundamentals of biofilm research*, CRC Press, Boca Raton 2014.

EXPLICIT ALGEBRAIC REYNOLDS STRESS MODEL VALIDATION BASED ON SHOCK WAVE-BOUNDARY LAYER INTERACTION EXPERIMENT

F.D. Tomczak

Łukasiewicz Research Network, Institute of Aviation, al. Krakowska 110/114, 02–256 Warsaw, Poland

E-mail: Franciszek.Tomczak@ilot.lukasiewicz.gov.pl

Abstract. In the present study the explicit algebraic Reynolds stress model is validated for shock– boundary layer interaction at Mach 5 using the experimental wind tunnel data. Wall pressure measurements from and velocity profiles were compared against CFD results obtained using two RANS k-ω models: the SST and the EARSM WK-BSL. In contrast to the literature, the results indicate that the two models implemented in the Ansys Fluent software behave similarly; this is presumably due to the simplified implementation of the EARSM model.

Keywords: Computational Fluid Dynamics, Explicit Algebraic Reynolds Stress Model, Shock Wave-Boundary-Layer Interactions, Turbulence Modeling.

1. Introduction

Shock boundary layer interaction plays a crucial role in various engineering applications, such as supersonic inlets, wind tunnel facilities and aircraft pylons for dummy equipment. One notable example of this interaction is the NASA X-15, where a design issue caused the pylon to melt [1]. The phenomenon is currently better understood, however, Reynolds Averaged Navier-Stokes (RANS) CFD modelling is still burdened with various limitations that become apparent during strong interaction [2].

On the other hand, the Explicit Algebraic Reynolds Stress Model (EARSM) provides better agreement with both experimental measurements and Direct Numerical Simulations (DNS) when compared to other RANS models. This is especially the case when adverse pressure gradients are present, as occurs in shock wave-boundary layer interaction (SWBLI) cases [3].

In present study we aim to explore and validate such EARSM models in SWBLI cases due to their promise of better agreement with experimental results while preserving the low computational cost of RANS models. This models have been successfully applied to various cases, demonstrating far greater agreement with experiments than the standard SST model [4]. The study focuses on validating experimental data collected in a supersonic wind tunnel of a two-dimensional wedge generator of impinging shock on a flat plate at Mach 5 [5], using SST and EARSM models available in the commercial software Ansys Fluent. This software provides the Wallin and Johansson k-ω EARSM model [6] which is implemented with a simplified definition of eddy viscosity [7]. For this reason, the study focuses on the consequences of this simplification and aims to compare it with the approach recommended by the model authors for effective eddy viscosity.

2. Turbulence Models

Wallin and Johansson [6] stated that a formulation with an effective eddy viscosity allows for better capture of pressure gradients in the boundary layer by enabling asymptotic behaviour of the boundary layer edge. They proposed the following definition for eddy viscosity:

$$\mu_T = \left(\frac{C_\mu}{\beta^*}\right)\left(\frac{k}{\omega}\right) \tag{1}$$

In Equation 1, β^* is a constant, k is turbulence kinetic energy, ω is the specific rate of dissipation of the turbulence kinetic energy and C_μ is effective eddy viscosity defined as:

$$C_\mu = -\frac{1}{2}(\beta_1 + II_\Omega \beta_6) \tag{2}$$

In Equation 2, β coefficients are functions of the invariants and II_Ω is one of this invariants [6]. Ansys Fluent implementation of the model with standard eddy viscosity is presented as follows:

$$\mu_T = \frac{k}{\omega} \tag{3}$$

This solution clearly modifies the diffusion term. In this study, it is aimed to identify the consequences of such changes.

3. Experiment

The chosen experiment consists of two plates placed in a supersonic wind tunnel. The first plate acts as an impinging shock generator. The second plate is placed beneath it to create a boundary layer. The location of the first plate is determined so that the position of the impinging shock is 350 mm from the beginning of the bottom plate. Various angles of the first plate were tested, however, the 14° configuration was of primary interest since boundary layer separation occurs. Tests were conducted at the DLR Ludwig Tube Wind Tunnel Facility under the following flow conditions: Mach number M = 5; total temperature T_0 = 410 K; total pressure P_0= 21.2 bar and unit Reynolds number Re = 40 x 10^6 m^{-1}[5].

4. Results

The results will describe the wall pressure distribution along the plate, as well as the four velocity profiles distributed along the flow. Additional parameters, such as skin friction, may be used. The results will compare the SST and EARSM models to the tabulated results from the experiments.

References

[1] Watts J.D., *Flight Experience with Shock Impingement and Interference Heating on the X-15-2 Research Airplane* Flight Reaserch Center, Edwards 1968.

[2] Oliver A.B., Lillard R.P., Schwing A.M., Blaisdell G.A., Lyrintzis A.S., *Assessment of Turbulent Shock-Boundary Layer Interaction Computations Using the OVERFLOW Code*, 45th AIAA Aerospace Sciences Meeting and Exhibit, Reno 2007.

[3] Menter F.R., Garbaruk A.V., Egorov Y., *Explicit Algebraic Reynolds Stress Models For Anisotropic Wall Bounded Flows*, 'Progress in Flight Physics' 2012, vol. 3, pp. 89–104

[4] Raje P., Sinha K., *Anisotropic SST turbulence model for shock-boundary layer interaction*, 'Computers & Fluids' 2022, vol 228.

[5] Schülein E., Krogmann P., Stanewsky E., *Documentation of Two-Dimensional Impinging Shock/Turbulent Boundary Layer interaction Flow*, DLR, Göttingen 1996.

[6] Wallin S., Johansson A.V., *An explicit algebraic Reynolds stress model for incompressible and compressible turbulent flows*, 'Journal of fluid mechanics' 2000, vol. 403, pp. 89–132.

[7] ANSYS® Fluent, R2, *Theory Guide, Section 4.10 Explicit Algebraic Reynolds Stress Model (EARSM)*, ANSYS, Inc., Canonsburg 2024.

SUBCRITICAL TRANSITION TO TURBULENCE IN THE FLOW BETWEEN COUNTER-ROTATING CYLINDERS

E. Tuliszka-Sznitko

Poznan University of Technology, Institute of Thermal Energy, 3 Piotrowo St., 60–965 Poznan, Poland

E-mail: ewa.tuliszka-sznitko@put.poznan.pl

Abstract. The subcritical transitional flow in the strongly counter rotating Taylor-Couette configuration of radius ratio 0.9 is studied using DNS. The attention is focused on the characteristic features of the subcritical flows: interpenetrating spirals, turbulent spots, intermittency and hysteresis. Reynolds number of the inner cylinder Re_1 is increased (at fixed Reynolds number of outer cylinder Re_2) to reach the turbulent flow. Starting from this state Re_1 is reduced gradually to show the reverse transition out of turbulence to the laminar flow (Re_2 from -2400 to -1800).

Keywords: Turbulence, Subcritical Transition, Rotating Flows, DNS.

1. Introduction

In the presentation the subcritical laminar-turbulent transition is studied numerically (DNS) in the short Taylor-Couette (TC) configuration of radius ratio $\eta = R_1/R_2 = 0.9$ (the end-walls are attached to the inner cylinder). Generally, in the shear flows two types of the subcritical transition are observed: bypass and amplification [1, 2, 3]. The bypass means that the linear mechanism is bypassed in transition process – the flow becomes turbulent if the critical value of Reynolds number is reached. In the amplification scenario, the unstable flow acts as an intermediary flow which triggers the turbulence [2, 3]. The main goal of the research on the subcritical transition in the TC configurations is to deepen our knowledge on the transitional processes occurring in the other (more complex) shear flows. The most characteristic features of the subcritical transition (intermittency, hysteresis) can be observed in the simple TC configurations. In the TC flows, by varying the governing geometrical and physical parameters, i.e. aspect ratio $\Gamma = H/(R_2-R_1)$, radius ratio $\eta = R_1/R_2$, Reynolds number of the inner cylinder $Re_1 = \Omega_1 R_1(R_2-R_1)/\nu$, Reynolds number of the outer cylinder $Re_2 = \Omega_2 R_2(R_2-R_1)/\nu$, a rich variety of the flow patterns can be observed, [1, 2]. The classic subcritical transition occurs in the TC configurations with the rotating outer cylinder and steady inner one. But, the subcritical transition also can occur in the narrow counter-rotating configurations (η from 0.9 to 1.0) if the outer cylinder rotates faster than the inner one (the amplification scenario is observed). The investigations are mostly performed in very long cavities to avoid confinement in the axial direction, see [1, 2]. However, in contrast to most studies in [3] the authors have analyzed a subcritical transition in the short counter-rotating TC configuration of Γ=5.26, η=0.905, with the end-walls attached to the outer cylinder. The results showed strong stabilizing influence of such end-wall boundary conditions on the flow dynamics.

2. Research objective, results and discussion

The computations are performed in the counter-rotating configuration of Γ= 4.71, η = 0.9, with the end-walls attached to the inner cylinder. Such end-wall conditions result in the strong flow destabilization, in contrast to the results obtained in [3]. The aim of computations is to show that for an appropriately selected range of Re_2, the flows in short TC configurations have the same key characteristics, as those observed in the other shear flows (e.g. in the circular pipe flow). The investigations are carried out for Re_2 = -2400, -2200, -2000 and -1800. Starting from laminar flow, Re_1 is increased gradually(at fixed Re_2) to reach the turbulent flow – the state called in [1] 'featureless turbulence'. With increas ing Re_1 the interpenetrating spirals appear first (the obtained structures are identical to those described in [3]). With the further increase of Re_1 the turbulent spots appear very rapidly (the turbulent spots are surrounded by the interpenetrating spirals). Figures 1a-1f show the intermittent flow structure obtained for different values of the dimensionless time $t\Omega_1$ (the middle section of cavity, $t\Omega_1$ = 0.0, 0.5, 1, 1.5, 2, 2.5, Re_1 = 607, Re_2 = -2400). On the abscissa axis (circumferential direction) we have φ from 0.0 to 2π, on the ordinate axis (axial direction) we have z from 0.0 to H. Figures illustrate how the turbulent spots move in the circumferential direction. With further increase of Re_1, new turbulence spots appear which gradually (slowly) fill the entire space. Starting from this state the value of Re_1 is reduced gradually to show the reverse transition leading finally to laminar flow. In the presentation, a detailed analysis of the phenomena occurring in the vicinity of the end-walls is carried out and the analysis of the radial profiles of the statistical parameters. The used DNS method is based ona pseudo-spectral Chebyshev-Fourier-Galerkin collocation approximation.

a)
b)
c)
d)
e)
f)

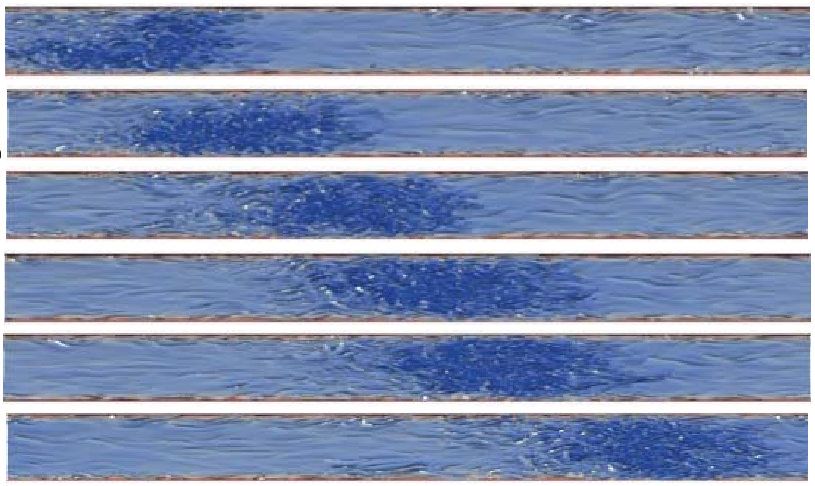

Figure 1. The λ_2 iso-surfaces in the (ϕ, z) the middle section of cavity (ϕ from 0.0 to 2π). The time section $t\Omega_1$ from 0.0 (a) to 2.5 (f) Re_1 = 607, Re_2 = –2400

Acknowledgements

The DNS computations have been performed in Poznan Supercomputing and Networking Centre which is gratefully acknowledge.

References

[1] Andereck C., Liu S., Swinney H., *Flow regimes in a circular Couette system with independently rotating cylinders*, 'Journal of Fluid Mechanics' 1986, vol. 164, pp. 155–183.

[2] Feldmann D., Borrero-Echeverry D., Burin M., Avila K., Avila M., *Routes to turbulence in Taylor–Couette flow*, 'Phylosophical Transactions of the Royal Society A' 2023, vol. 381.

[3] Crowley C., Krygier M., Borrero-Echeverry D., Grigoriev R., Schatz M., *A novel subcritical transition to turbulence in Taylor–Couette flow with counter-rotating cylinders*, 'Journal of Fluid Mechanics' 2020, vol. 892.

CONTROL OF INTERFACE OSCILLATIONS IN HANGING DROPLETS VIA LONG-RANGE INTERACTIONS

I.P. Ungureanu[1,2], M. Boni[1], I.R. Andrei[1], A. Staicu[1]

[1] *INFLPR – National Institute for Laser, Plasma and Radiation Physics, 409 Atomistilor street, Magurele, Ilfov, RO-077125, Romania*

[2] *The Faculty of Physics, University of Bucharest, 409 Atomistilor Street, Magurele, Ilfov, 077125, Romania*

E-mail: ionut.ungureanu@inflpr.ro

Abstract. This study investigates long-range interactions and interface oscillations of two hanging droplets. External factors such as evaporation and thermal gradients induce local variations in surface tension, causing oscillations in nearby droplets without direct contact. This work adds a novel aspect, within the context of interfacial phenomena and experimental fluid mechanics, by studying the long-range interactions between droplets, based on vapor-mediated motion. In particular, it focuses on the generation and control of the interface oscillations for hanging droplets. The oscillations are controlled by varying the distance between droplets through approach and retraction. Preliminary results show that the amplitude of droplet interface oscillations depends on droplet volume and inter-droplet distance.

Keywords: Experimental Fluid Mechanics, Long-range interactions, Vapor-mediated coupling.

1. Introduction

Droplet dynamics are strongly influenced by external factors such as evaporation, ambient vibrations, temperature fields and surface tension gradients [1,2]. These factors induce long-range interactions between two spatially separated droplets, resulting in motion driven by attractive and repulsive forces acting between them [3].

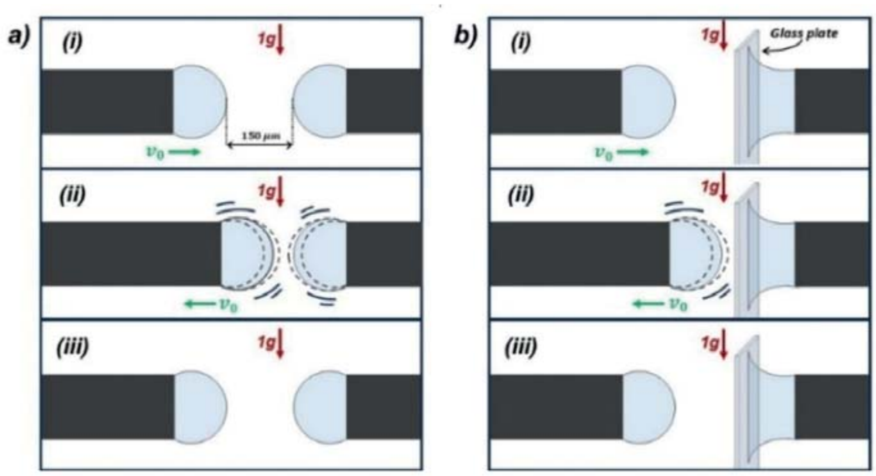

Figure 1. Experimental setup: a) two hanging droplets; b) droplets separated by a glass plate

This study focuses on the control of interface oscillations in hanging droplets through long-range interactions. External stimulation by vapor and thermal gradients induces local surface tension variations, causing droplets to oscillate without direct contact. The study also presents a new method to investigate long-range interactions via oscillations induced by thermal waves.

2. Experimental Approach

Long-range interactions were studied using two methods. *Method 1*: Two droplets (V~4μ*L*) were generated at the tips of vertically aligned needles without touching, with an initial inter-droplet distance of ~150 μ*m* [Figure 1a)]. One needle was moved with a stepper motor until the inter-droplet distance reached ~20 μ*m*, inducing oscillations in both droplets. Returning the needle stopped oscillations. Each experiment lasted ~3 min, with several approach-retraction sequences. *Method 2*: A similar motion was applied, with a transparent glass plate inserted between the droplets [Figure 1b)]. The plate was positioned so that the moving droplet did not touch it, while the fixed droplet adhered to it, forming a liquid bridge between the needle and the plate.

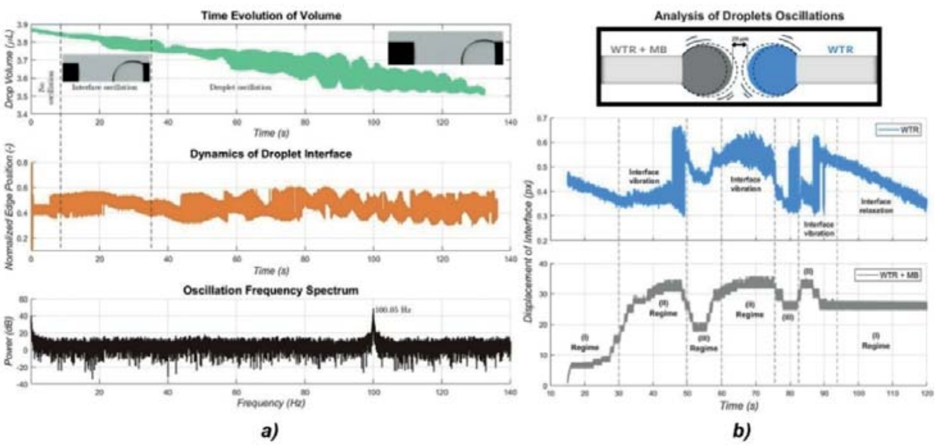

Figure 2. Oscillation analysis: a) single droplet reaching the critical volume; b) two droplets during approach and retraction, showing distance-dependent oscillations: *Region I* – initial position; *Region II* – approach to 20 μ*m*; *Region III* – retraction until oscillations stop

3. Results and Discussion

Preliminary results show that droplets oscillate when reaching a critical volume ($V = 3.8\ \mu L$) correlated with their resonance frequency if stimulated by external factors (background vibrations or temperature variations). Larger droplets oscillate only after evaporation reduces them to the critical volume [Figure 2a)]. A similar behaviour is observed when two droplets approach each other: droplets with volumes far from the critical value do not oscillate, whereas two droplets near the critical volume begin to oscillate as they come closer [Figure 2b)]. The results demonstrate that droplet oscillations can be controlled by approaching and retracting droplets relative to each other.

Acknowledgements

This work was supported by a grant from the Ministry of Education and Research, National Research Authority and UEFISCDI, project number PN-IV-P7-7.1-PED-2024-1995, within PNCDI IV, and Romanian National Nucleu Program LAPLAS VII, project number 30N/2023.

References

[1] Shen L., Ren J., Duan F., *Surface temperature transition of a controllable evaporating droplet*, 'Soft Matter' 2020, no. 41, pp. 9568–9577.

[2] Zhao H., Orejon D., Sefiane K., Shanahan M.E.R., *Long-Range Vapor-Mediated Interactions between Adjacent Droplets*, 'Langmuir' 2025, vol. 41, no. 6, pp. 3986–3994.

[3] Man X., Doi M., *Vapor-induced motion of liquid droplets on an inert substrate*, 'Physical Review Letters' 2017, vol. 119, art. no. 044502.

NUMERICAL STUDY OF A TWIN-FOIL SYSTEM FOR DIODE LASER HYGROMETER

T. Wacławczyk

Warsaw University of Technology, Institute of Aeronautics and Applied Mechanics, Nowowiejska 24, 00-665 Warszawa, Poland

E-mail: tomasz.waclawczyk@pw.edu.pl

Abstract. This paper presents an undergoing numerical study of turbulent flow around a twin-foil system housing components of a diode-laser hygrometer. The objective is to reduce turbulence-induced flow structures and to lay the groundwork for future investigations of polydisperse particle distributions and their impact on laser-light absorption along the hygrometer's optical path in flight deployment.

Keywords: Aerodynamics, Computational Fluid Dynamics, Multi-phase Flows.

1. Introduction

Accurate, fast water-vapor measurements underpin studies of convection, cloud microphysics, radiative transfer, and stratosphere–troposphere exchange yet are difficult where mixing ratios can fall below 10 ppm and instrument sampling artifacts (e.g. caused by the finite size water droplets or ice crystals) become comparable to the atmospheric signal. Optical hygrometers based on diode-laser absorption spectroscopy address this need by directly linking measured absorption to H_2O number density via well-characterized spectroscopy, enabling high precision and rapid time response in flight and ground deployments [1, 2]. Open-path airborne systems minimize sampling-line 'memory' by measuring absorption in the free stream and for this reason they are particularly suited for investigations from relatively small cost Unmanned Aerial Vehicles (UAVs) and/or full-scale planes. However, comparisons continue to show that even high-end hygrometers can disagree under challenging conditions, emphasizing that 'measurement physics' includes aerodynamics and thermodynamics of sampling as much as laser spectroscopy [1-3].

In the presented herein undergoing work, we use Computational Fluid Dynamics (CFD) to provide a quantitative way to design that sampling environment, so the optical path sees air that is representative, well-mixed and free of condensed-phase interference. As we plan to place fast infrared hygrometer [3] on the UAV platform, our study differs from previous investigations, where CFD was used to design closed-path hygrometers, and optimize inlets, tubing, and flow cells by minimizing recirculation and dead volumes [4]. However, as in the known works, we aim to predict spatial gradients of pressure, temperature, humidity along the laser beam that bias retrievals of the instruments. The main goal of this study is to address a particularly important design problem is the multiphase particle flow of small droplets or ice particles that may enter the measurement region. These droplets can scatter/attenuate the beam, contaminate windows or partially evaporate in heated sections, creating time-varying biases that affect as true vapor variability. Instruments that separate vapor and total-water channels explicitly rely on aerodynamic particle rejection or inertial enhancement; CFD coupled with Lagrangian particle tracking can predict size-dependent trajectories, impaction hot spots and evaporation timescales under realistic pressure, temperature and flow conditions.

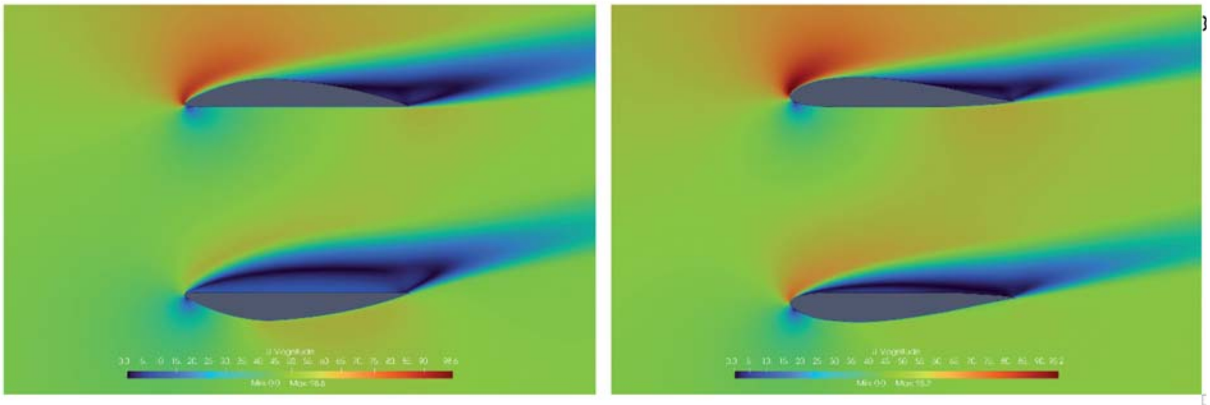

Figure 1. Twin-foil configuration at non-zero angle of attack in turbulent flow of air $Re = 5.5 \times 10^5$ Laser emitter and receiver (top foil), mirror (bottom foil). Modification (right) of the original (left) aerofoil shape reduces recirculation region and based on the levels of turbulence kinetic energy production of turbulent fluctuations (not in the figure)

2. Geometry, methodology and current results

The fast infrared hygrometer (FIRH [3]) will be integrated into a system of two foils, each with a chord length of 0.15 m. The set-up is intended to be mounted on a UAV or aircraft, outside the fuselage boundary layer. The FIRH diode-laser emitter and receiver are housed in the upper foil, while a mirror that reflects the laser beam is installed in the lower foil. The 0.25 m optical path length is twice the distance between the foils, as shown in Figure 1.

The results presented in this abstract are obtained using OpenFOAM free, open-source C++ library. At present, we use standard solver based on the RANS approach with $k - \varepsilon$ turbulence model and wall functions, coupled with the incompressible momentum and mass conservation equations. A computational grid of approximately $\sim 4 \times 10^5$ control volumes is used to discretize two-dimensional computational domain with freestream boundary conditions. The minimum non-dimensional distance from the wall is maintained at about $y^+ \sim 30$. The initial values of turbulent kinetic energy k and its dissipation rate ε are estimated assuming and upstream turbulence intensity of 3%.

A time-marching procedure is employed to obtain quasi-stationary velocity and pressure fields. The results shown in Figure 1 illustrate a modification of the originally proposed geometry (depicted on the left). The new geometry, based on the modified ClaryYH foil, reduces the size of the recirculation region leading to lower drag and decreased turbulent kinetic energy intensity which indicates mitigation of turbulent eddies.

References

[1] Diskin G., *Optical Science and Technology, SPIE's 48th Annual Meeting*, Proceedings of International Symposium on Optical Science and Technology, 2002, vol. 4817, p. 196.

[2] Buchholz B., Afchine A., Klein A., Schiller C., Krämer M., Ebert V., *HAI – A new, airborne, absolute, twin dual-channel, multi-phase TDLAS-hygrometer*, 'Atmospheric Measurments Techniques' 2017, vol. 10, p. 35.

[3] Stacewicz T., Winkowski M., Kuk N., *Reduction of Optical Noise in Near-Infrared Range Laser Hygrometry*, 'Metrology and Measurement Systems' 2023, vol. 30, no. 1, pp. 169–181.

IDENTIFICATION OF NOISE SOURCES IN HVAC END ELEMENTS USING ACOUSTIC CAMERA IN AN ANECHOIC ENVIRONMENT

D. Walisiak, J.M. Kopania, P. Gaj, K. Wójciak

Institute of Power Engineering - National Research Institute, Mory 8, 01–330 Warsaw, Poland

E-mail: damian.walisiak@itc.edu.pl

Abstract. This paper investigates the aeroacoustic noise generated by ceiling diffusers in HVAC systems using an acoustic camera and a single-microphone noise analyser. Measurements were conducted in an anechoic chamber at various flow velocities, taking into account the influence of the measuring stand. The results demonstrate that the acoustic camera effectively identifies noise source locations and structural tonal frequencies. This method is faster in terms of identifying noise sources in the facility and could be comparable to standardised single-microphone techniques for noise diagnostics and optimising.

Keywords: Experimental Fluid Mechanics, Measurement Techniques, Noise Camera, HVAC systems.

1. Introduction

Technology is developing quickly in the field of HVAC (Heating, Ventilation and Air Conditioning) inspection and maintenance. Acoustic imaging, a technique that enables specialists to truly 'see' sound, is among the most cutting-edge instruments entering the sector. Acoustic cameras show the intensity of sound, same as thermal cameras show variations in temperature. Noise camera with beamforming algorithm is a technique where a microphone array is used to visualise the location of a noise signal. Beamforming is a method for processing microphone array data to produce images that represent the distribution of the acoustic source. It is an imaging technique that applies to continuous or discrete source distributions. Nowadays, the technique has become an important tool to minimise the noise in the industry. For example, a comprehensive methodology for identifying and reducing noise emissions from an industrial plant situated near a residential area by using the primary tool for localisation, an acoustic camera which utilises an array of 112 microphones and the Beamforming Method to visualise sound sources, was tested by Fiebig and Dąbrowski [1]. Acoustic camera measurements can also be used to analyse occupational noise exposures. Noise mapping is becoming an effective tool for visualising noise pollution, supporting decision-making regarding occupational safety, creating hazard maps, assessing employee hearing risks and proposing Hearing Loss Prevention Programs [2].

The HVAC industry is only now starting to realise the potential of noise cameras because of the increased precision of problem diagnosis and the presentation of unambiguous visual proofs of noise leaks. In one of the noise studies, an acoustic camera was used to analyse the noise generated by a prototype HVAC unit and improve passenger comfort in vehicles. The primary goal was the early detection of annoying sounds during ventilation system operation which allowed for design modifications to be implemented early in product development [3].

This paper aims to demonstrate that the acoustic camera enables the fast and precise localisation of noise sources from end ventilation objects and can also assess the nature of aeroacoustic sources. The method was applied to an experimental HVAC system that utilised two different ceiling diffusers as the end elements. The measurements were done on the specially constructed test stand with an outlet to an anechoic chamber. The noise produced by the flow was analysed using a noise camera and compared with the standardised single microphone method.

2. Test procedure

The measurements were performed on the specially constructed test stand with the outlet to the anechoic room – Figure 1.

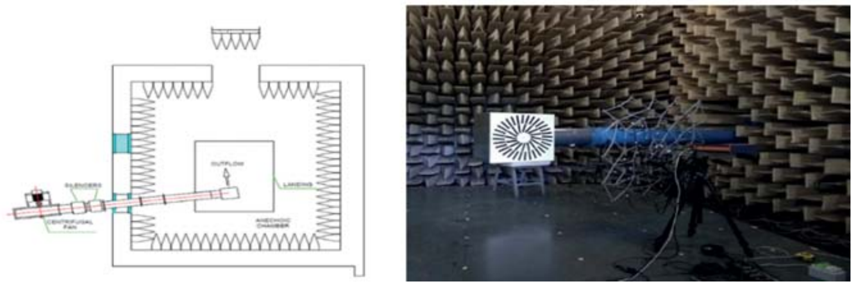

Figure 1. Scheme of test stand in the anechoic chamber

Airflow was induced by a fan mounted on the inlet of the stand and regulated by the power inverter. The stand test was equipped with a set of silencers to eliminate fan noise, according to the ISO7235 Standard. The outlet of the test stand was in the anechoic room at the Institute of Power Energy 'ITC' in Lodz. The anechoic test chamber is cubic, approximately 350 m^3 in size, and has walls that are acoustically treated with foam wedges, providing a reflection-free environment. The measurements were taken at four flow velocities. The measurement of the far-field noise was made by a sound pressure level analyser, located at a distance of 1 m from the front of the box and directed against the direction of the flow, and also by an acoustic camera, with 40 MEMS microphones and an HD camera and software that allows real-time sound imaging for quick results.

3. Conclusions

In this work, the aerodynamic noise generated by the end elements of HVAC systems – ceiling diffusers – was studied. The two types of ceiling diffusers with different controlled blades were tested. The measurements were made in an anechoic room at low to moderate Reynolds numbers using a specially constructed test stand. The 1/3 octave A-weighted equivalent continuous sound levels depend on the flow velocities at various flow velocities which were measured using an acoustic camera and sound pressure level analyser. Characteristic tonal frequencies were observed in the acoustic spectra for each of the diffusers which were assigned to their structural components. The sound distribution across the diffusers, obtained from an acoustic camera, allows for the identification of the locations where the highest noise is generated.

References

[1] Fiebig W., Dabrowski D., *Use of acoustic camera for noise sources localization and noise reduction in the industrial plant*, 'Archives of Acoustics' 2020, vol. 45, no. 1, pp. 111–117.

[2] Ahmed S.S., Gadelmoula A.M., *Industrial noise monitoring using noise mapping technique: a case study on a concrete block-making factory*, 'International Journal of Environmental Science and Technology' 2022, vol. 19, no. 2, pp. 851–862.

[3] Grigg S., Al-Shibaany Z.Y.A., Pearson M.R., Pullin R., Calderbank P., *Acoustic Sensing and Noise Identification of a Heating, Ventilation and Air Conditioning Unit: Industrial Case Study*, 'Applied Sciences' 2021, vol. 11, no. 21.

XDEM FOR MODELLING THERMAL CONVERSION PROCESSES IN GRANULAR MEDIA

I. Wardach-Święcicka

Institute of Fluid-Flow Machinery, Polish Academy of Sciences, 14 Fiszera St., 80-231 Gdańsk, Poland

E-mail: izabela.wardach@imp.gda.pl

Abstract. An in-house e-Xtended Discrete Element Method is presented. This uses a mixed Eulerian-Lagrangian framework to simulate the motion and conversion of multiple particles. Coupling Computational Fluid Dynamics with the Discrete Element Method enables the model to provide a detailed and reliable analysis of complex reactive multiphase flows involving heat and mass transfer. This tool provides particle-resolved data which would be difficult or impossible to obtain through high-temperature experiments.

Keywords: Interdisciplinary Areas in Heat and Fluid Flow, CFD, DEM, Particles, Porous Materials, Thermodynamics, Heat and Mass Transfer.

1. Introduction

Coupling Computational Fluid Dynamics (CFD) with the Discrete Element Method (DEM) provides a robust framework for simulating multiphase systems involving fluid flow and discrete particles. This approach is widely used in the study of porous media, fluidised beds and granular systems. However, representing particles as simple spheres provides fast solutions but limits the accurate prediction of complex, non-homogeneous materials, particularly when structural transformations under thermal or mechanical loading must be resolved. This work introduces the XDEM (eXtended DEM) method, which efficiently couples intra-particle physics with Lagrangian-Eulerian approaches. Unlike classical discrete methods, which treat particles as rigid bodies with lumped properties, the proposed solution adopts a reactive thermodynamic approach, resolving internal heat transfer, species transport, chemical reactions, phase changes and structural evolution at the particle level.

2. XDEM method

XDEM is advanced software for modelling the behaviour of granular materials subjected to various external factors, including different flow and thermal conditions [1]. The model's key advantage is that it considers the sequence of thermodynamic processes undergone by each particle as it moves in an external fluid field. This is mathematically governed by a set of transient one-dimensional balance equations. This approach thus extends the classical DEM widely used for predicting particle movement. XDEM is coupled with conventional CFD. While DEM predicts the position and orientation of each particle in space and time, XDEM also evaluates their thermophysical properties, such as internal temperature, density, composition and porosity [2]. The motion of a particle in the system is determined using the equations of classical mechanics:

$$m_p \frac{d\vec{v}_p}{dt} = \vec{\mathrm{F}}_\mathrm{c} + \vec{\mathrm{F}}_\mathrm{g} + \vec{\mathrm{F}}_\mathrm{b} + \vec{\mathrm{F}}_\mathrm{d}\,, \qquad I_p \frac{d\vec{\omega}_p}{dt} = \sum_j \vec{\mathrm{M}}_{\mathrm{p,j}} \tag{1}$$

where the subscripts appearing with the forces $\vec{\mathrm{F}}[N]$ denote their following types: c – contact, g – gravitational, b – buoyancy, d – drag. The equations describes Newton's Second Law for translational movement and for the rotation, where I_p [kg m^2] is the particle's moment of inertia, $\vec{\omega}_p$ [rad/s] is the particle's angular velocity, and $\overrightarrow{M}_{p,j}$ [N m] are the torques. The coupling with CFD is performed within the OpenFOAM code, considering its porous zone model. Heat and mass transfer from fluid to/from particles are performed via the source terms of the corresponding conservation equations. In the case of biomass particles, chemical reactions are also considered here.

3. Results and conclusions

Figure 1 illustrates the temperature of the surroundings and its influence on the structure of the cylindrical biomass particles after some exposure time in the laboratory reactor [3]. The analysed reactor has an unusual half-tube shape, designed to visualise flame propagation. Due to its particular shape, the acceleration of the gas flow at the external curved walls is observed and the thermochemical changes differ from those in commonly used cylindrical reactors. The hot fluid flows from the bottom, heating the particle bed. Due to heat transfer between phases, the particles' internal structure changes and the bed level decreases. The used software provides information on all the particles in the system, thus, is a powerful and advanced approach for simulating complex multiphase and multicomponent systems.

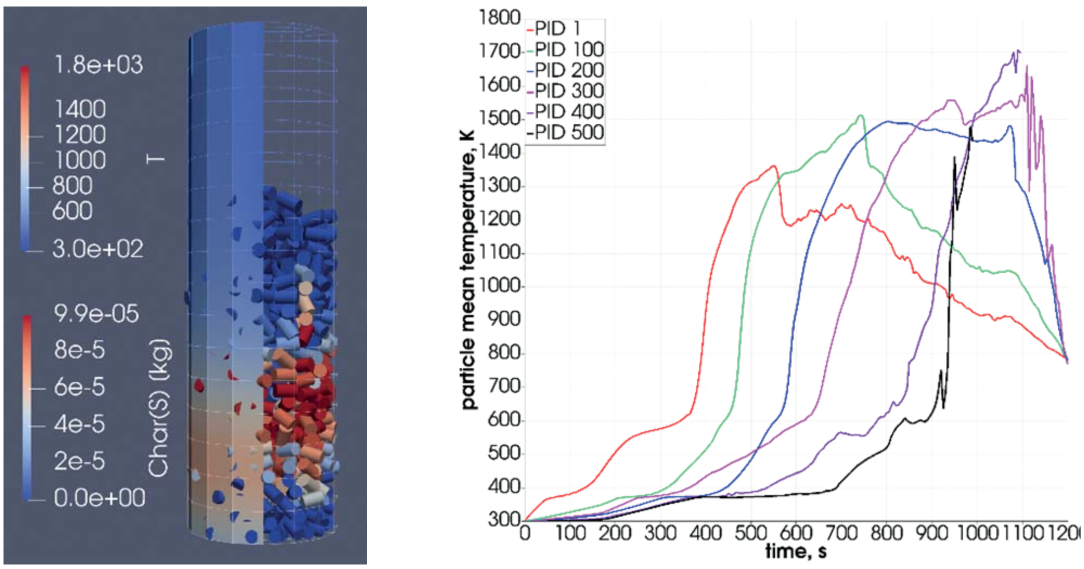

Figure 1. Temperature of the fluid and char content in the biomass particles after 600s (left), and temperature distribution in selected particles (right)

Acknowledgements

This research was supported by the computer centre CI TASK.

References

[1] Peters B et al. 2013 Univ. J. Eng. Sc. 1 139–145

[2] Peters B., Baniasadi M., Baniasadi M., Besseron X., Estupinan Donoso A., Mohseni M., Pozzetti G., *XDEM multi-physics and multi-scale simulation technology: Review of DEM–CFD coupling, methodology and engineering applications*, 'Particuology' 2019, vol. 44, pp. 176–193.

[3] Wardach-Święcicka I., Kardaś D., *Biomass Moving Bed Combustion Analysis via Two-Way Coupling of Solid–Fluid Interactions Using Discrete Element Method and Computational Fluid Dynamics Method*, 'Energies' 2024, vol. 17, no. 14, p. 3571.

ANALYSIS OF AERODYNAMIC DAMPING OF A WIND TURBINE BLADE OSCILLATING IN A COLD CHAMBER

F. Wasilczuk[1]*, P. Flaszyński[1], M. Piotrowicz[1], K. Gnebner[2], Y. Govers[2], B. Zima[3], M. Wojcik[3]

[1] *Institute of Fluid Flow Machinery, Polish Academy of Sciences, Gdańsk, Poland*

[2] *Institute of Aeroelasticity, German Aerospace Center (DLR), Göttingen, Germany*

[3] *Gdańsk University of Technology, Gdańsk, Poland*

* E-mail: fwasilczuk@imp.gda.pl

Abstract. This abstract describes numerical simulations of a wind turbine blade undergoing harmonic flapwise oscillations in a cold-chamber-sized domain, aimed at quantifying aerodynamic damping and assessing the influence of chamber walls on blade vibrations. An URANS model with mesh morphing as well as HAWC2 aeroelastic simulations are used to compute for analysis. Preliminary studies show that an increase in temperature causes a slight reduction (below 6%) in the amplitude of the blade root bending moments.

Keywords: Aerodynamics, aeroelasticity, wind energy, fluid-structure interaction.

1. Introduction

HYBRID WIND project (https://hybridwind.dtu.dk/) aims at reducing the cost of wind energy through the development of a fast digital twin of a wind turbine intended for monitoring for O&M cost reduction. The digital twin should be able to predict the characteristics of a wind turbine over a wide range of conditions, including weather effects (e.g. temperature) and its influence on the propagation of defects.

Measurements of vertically mounted blades undergoing cyclic loading can already be found in literature, even for long blades such as 52 m [1] and 60 m [2], including artificial de-bonding [3]. The present models and experiment expand on those studies by installing the blade with deliberate imperfection in a cold chamber. The process of debonding and its impact on blade characteristics will be observed.

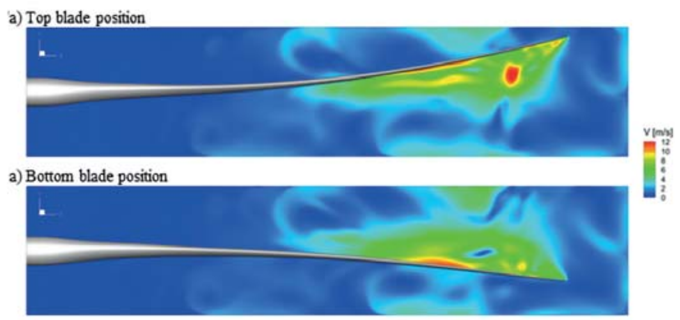

Figure 1. Distribution of the velocity magnitude for two example blade positions

2. Methods

Two modelling methods were used for the task: URANS STARCCM+ simulations and aeroelastic HAWC2 simulations. The former provides high-fidelity results, necessary for validation and flow structure analysis, while the latter offers higher computational speed, allowing the computation of a large number of cases.

The numerical model is based on the test section of a horizontally mounted 12.6 m wind turbine blade installed in a cold chamber. An exciter with rotating mass is installed to induce cyclic oscil lations of the blade in flapwise direction. The measurements in the test section are planned for the first half of the 2026 and validated results are expected to be presented at the FMC 2026 conference. The blade movement set for URANS simulations was created based on the HAWC2 model and preliminary measurements.

3. Results

At the current stage of the research the models were tested and sensitivity studies were performed. In CFD, a grid independence study was performed, the final grid is an unstructured, polyhedral grid, consisting of $9.7 \cdot 10^6$ elements. Various definitions of numerical methods were tested, to obtain the best convergence and numerical stability, for future comparison with experiment. The HAWC2 model was used to create a sensitivity study regarding the parameters of the exciter, such as mass, rotational velocity and the position of the center of rotation. Figure 1. shows preliminary velocity contours of the oscillating blade in the cold chamber.

Using the HAWC2 model the blade root bending moments as a function of temperature were determined. The aerodynamic model of HAWC2 is based on Blade Element Momentum theory, where temperature is not considered. Thus, density was used as a substitute, the limits were selected based on extreme values occurring in the atmosphere at sea level. Simulations were carried out for densities of 1.0, 1.2 and 1.4 kg/m³. Table 1 shows the amplitude of root bending moments for the three values of density. There is a slight effect of density on the amplitude, which increases with decreasing density, likely due to lower aerodynamic damping.

Table 1. Amplitude of blade root bending moments for density equal to 1.0, 1.2 and 1.4 kg/m³ and the relative change

	ρ=1.0 kg/m³ (a)	ρ=1.2 kg/m³ (b)	ρ=1.4 kg/m³ (c)	Change 100%·(c-a)/b
Mx [kNm]	54.75	53.75	53.05	-3.1%
My [kNm]	0.15	0.14	0.14	-5.5%
Mz [kNm]	10.53	10.38	10.23	-2.9%

Acknowledgements

The research was carried out within the project CETP/2022/49/HYBRID WIND/2024, financed by the National Centre for Research and Development, Poland.
Funded by the German Federal Ministry for Economic Affairs and Climate Action (FKZ 03EE3102A).

We gratefully acknowledge the Polish high-performance Infrastructure PLGrid CI TASK for providing computer facilities and support within computational grant no PLG/2025/018509.

References

[1] Fremmelev M.A., Ladpli P., Orlowitz E., Bernhammer L.O., McGugan M., Branner K., *Structural health monitoring of 52-meter wind turbine blade: Detection of damage propagation during fatigue testing*, 'Data-Centric Engineering' 2022, vol. 3.

[2] Post N., Burkner F., *Fatigue Test Design: Scenarios for Biaxial Fatigue Testing of a 60-Meter Wind Turbine Blade*, NREL report, 2016.

[3] Chen X., Semenov S., McGugan M., Madsen S.H., Yeniceli S.C., Berring P., Branner K., *Fatigue testing of a 14.3 m composite blade embedded with artificial defects – Damage growth and structural health monitoring*, 'Composites Part A: Applied Science and Manufacturing' 2021, vol. 140.

DYNAMICS OF LIFTED FLAME BASE INFLUENCED BY GLOBAL INSTABILITY

A. Wawrzak

Czestochowa University of Technology, Faculty of Mechanical Engineering, Al. Armii Krajowej 21, 42–201 Czestochowa, Poland

E-mail: agnieszka.wawrzak@pcz.pl

Abstract. Lifted hydrogen jet flames are investigated with emphasis on flame base dynamics using large eddy simulations performed with the SAILOR code. Global instability (GI) triggered by suction leads to the formation of coherent toroidal vortices that strongly enhance mixing upstream of the flame base. The ignition characteristics of stoichiometric mixture are obtained from Cantera. Combined LES and Cantera results enable assessment of the role of autoignition relative to GI in the flame stabilization mechanism.

Keywords: Combustion, Computational Fluid Dynamics, Lifted hydrogen Flame, Global Instability.

1. Introduction

Lifted jet flames play a crucial role in modern combustion systems, as they effectively protect burners components from exposure to hot combustion products. Their control, however, requires a detailed understanding of the stabilization mechanisms that anchor the flame at a finite distance from the fuel nozzle. These mechanisms depend on degree of premixedness and dominant physical processes such as autoignition in heated environments and interactions with large-scale flow structures. In particular, coherent vertical structures can strongly influence flame lifting and anchoring by governing fuel-oxidizer mixing upstream of the flame base.

A promising strategy for controlling lifted flames relies on exploiting the global instability (GI) phenomenon [1,2]. Unlike the convective Kelvin-Helmholtz (K-H) instability which produces vortex rings that are convected downstream with a limited impact on mixing, GI arises when a locally absolutely unstable flow region forms due to density stratification or the presence of an external flow. Disturbances generated in such a region grow both upstream and downstream, leading to a self-sustained oscillatory flow and the formation of strong, coherent vortices.

In the present study, an annular counter-current flow establishes an absolutely unstable region directly above the nozzle exit, triggering GI and generating coherent toroidal vortices. Building on previous studies, the focus is placed on the dynamics of the lifted flame base, with particular emphasis on the quantitative contribution of autoignition relative to GI in the flame stabilization mechanism. The analysis is performed using high-fidelity large eddy simulations (LES) carried out with the academic code SAILOR [3] and supported by Cantera [4] calculations.

2. Problem description

A nitrogen-diluted hydrogen jet issues into heated coflowing air under autoignitive conditions. A counter-current nozzle configuration, involving annular suction at the jet periphery, is employed to promote the onset of global instability. The flames are examined under both dry and humidified coflow conditions (1–5% H_2O by mass). Humidification is consistent with current trends in wet and low-emission combustion concepts and is used to promote conditions hindering autoignition. Autoignition characteristics are further analyzed using 0D batch reactor simulations, with initial mixture compositions corresponding to the stoichiometric mixture fraction ξ_{st} of 3D LES cases.

3. Results

The overall flame structure exhibits a corrugated flame base anchored several nozzle diameters downstream of the inlet plane, as shown in Fig. 1(a). The flow dynamics associated with GI governs the early formation of strong, coherent toroidal vortices, identified using the Q-criterion. These structures enhance mixing upstream of the flame base and control its mean lift-off position, indicated in Fig. 1 by the red dashed line.

Analysis of temperature evolution along the isoline $\xi = \xi_{st} \pm 0.02$ in a central axial plane (Fig. 1(b)) shows that, prior to ignition, mixture temperatures approach the minimum values required for autoignition and remain only slightly below the autoignition temperatures predicted by Cantera. At later times, significant temperature variations along this isoline arise due to the presence of the flame. Acounting for thermal diffusion effects, autoignition is therefore likely to contribute to flame stabilization. The addition of water vapor increases the ignition temperature and ignition delay time, which may further influence the flame stabilization process.

a)

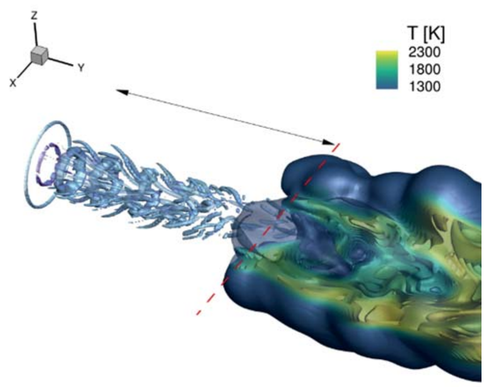

b)

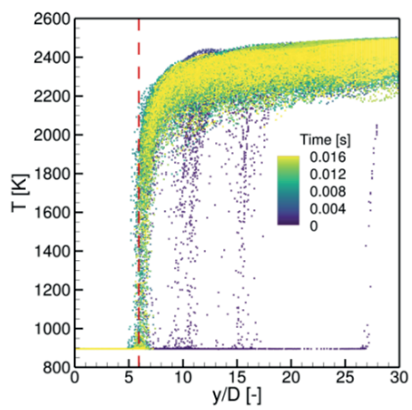

Figure 1. Lifted hydrogen jet flame (a); temperature evolution along the stoichiometric isoline extracted from a central flame cross-section over the simulation time (b)

Acknowledgements

This work was supported by the National Science Center (Grant No. 2022/47/D/ST8/01902). I gratefully acknowledge Polish HPC infrastructure PLGrid (Cyfronet AGH) for providing computer facilities (Grant No. PLG/2025/018542), and Prof. Artur Tyliszczak for providing the SAILOR code.

References

[1] Wawrzak A., Wawrzak K., Boguslawski A., Tyliszczak A., Geurts B.J., *Global instability phenomenon as a physical mechanism controlling dynamics of a nitrogen-diluted hydrogen flame*, 'International Journal of Heat and Mass Transfer' 2023, vol. 213, art. no. 124260.

[2] Wawrzak A., Tyliszczak A., *Reducing a lift-off distance of a nitrogen-diluted hydrogen flame evolving in a dry and humidified ambient flow through suction-driven global instability: Insights from LES*, 'International Journal of Heat and Mass Transfer' 2026, vol. 258, art. no. 128261.

[3] Tyliszczak A., *High-order compact difference algorithm on half-staggered meshes for low Mach number flows*, 'Computers & Fluids'2016, vol. 127, pp. 131–145.

[4] Goodwin D.G., Moffat H.K., Schoegl I., Speth R.L., Weber B.W., *Cantera: An Object-oriented Software Toolkit for Chemical Kinetics, Thermodynamics, and Transport Processes*, https://zenodo.org/records/17620923, (access: 1.04.2026).

INFLUENCE OF DIFFUSION MODELS ON LES/DNS OF HYDROGEN FLAMES

K. Wawrzak

Department of Thermal Machinery Czestochowa University of Technology, al. Armii Krajowej 21, 42–201 Czestochowa, Poland

E-mail: karol.wawrzak@pcz.pl

Abstract. The influence of species diffusion models on LES and DNS of hydrogen flames is analysed using a simplified canonical configuration based on the Taylor-Green vortex. Simulations are performed for a range of Reynolds numbers to assess how the effects of unity and constant Lewis number assumptions, as well as mixture-averaged diffusion, depend on the strength of vortical structures and their interaction with flame.

Keywords: Computational Fluid Dynamics, Turbulent Combustion, Hydrogen Flame, LES, DNS.

1. Introduction

Interactions between diffusion flames and vortical structures play a crucial role in many practical combustion applications. Coherent vortical structures strongly influence flame curvature and unsteady flame behaviour, thereby affecting local burning rates and flame stability. In addition, diffusion flames are susceptible to quenching processes when subjected to external disturbances such as heat losses or stretch. The interaction between flames and turbulence can further lead to combustion instabilities, which are highly undesirable in practical combustion devices [1]. Hydrogen combustion has attracted significant attention as a promising pathway toward low-carbon energy system, driven by the growing demand for alternative and sustainable energy sources. Therefore, investigating the interaction between hydrogen flames and vortical structures in turbulent flows is crucial for advancing the fundamental understanding of hydrogen combustion.

To investigate the fundamental mechanism governing turbulent combustion, high-fidelity numerical approaches such as Direct Numerical Simulation (DNS) and Large Eddy Simulation (LES) are particularly well suited. These methods enable detailed resolution of the interaction between flow structures and reactive processes, providing deep insight into flame dynamics, turbulence-chemistry coupling and transport phenomena. The Taylor-Green vortex (TGV) is a well-defined canonical flow that has been widely used to study vortex evolution and the laminar-turbulent transition [2]. The combination of TGV with a hydrogen flame provides a valuable benchmark for numerical codes [3] and serves as a simplified framework for investigating the fundamental physics underlying turbulence-flame interactions [1]. In the present work, a reactive TGV is analyzed using different diffusion models, including unity and constant Lewis number assumptions and a mixture-averaged diffusion formulation. Simulation are performed using both DNS and LES in order to assess how the diffusion models behave in fully resolved simulation and in LES, which is more accessible for practical applications, while a range of Reynolds numbers is considered to examine their performance under different levels of turbulence intensity.

2. Configuration

Following the work of Abdelsamie et al.[3] and Xu, and Chen [1], the computational domain is cubic box of size $[0, L_0]^3$, where $L_0 = 2\pi[\mathrm{mm}]$. The central region is initially filled with a H2/air mixture ($Y_{\mathrm{H}_2} = 0.0556, T = 300$ [K], where Y denotes the species mass fraction and T temperature, while the surrounding region contains air with $Y_{\mathrm{O}_2} = 0.233$. The equilibrium state is then computed locally using *lib-Cantera* and used to initialize the temperature and species mass fractions. The velocity field is initialized using TGV configuration. The initial fields of x – velocity (U), temperature T and hydrogen mass fraction Y_{H_2} are shown in Fig.1.

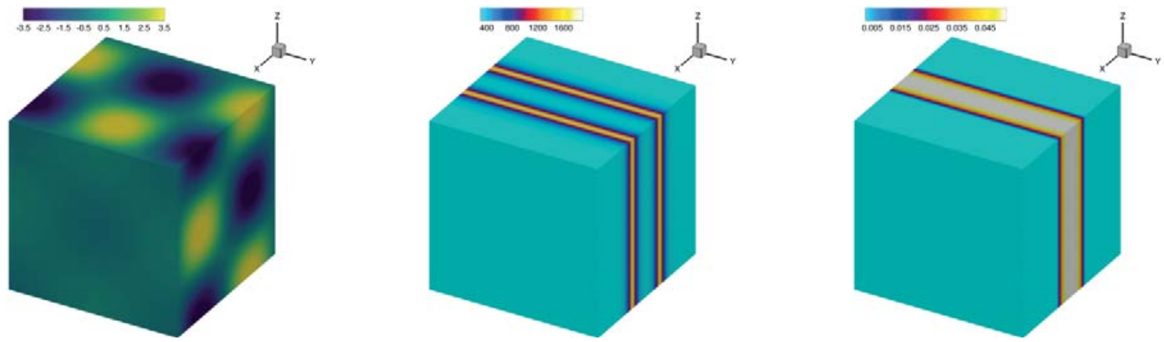

Figure 1. Initial conditions: U (left), T (middle), Y_{H_2} (right)

3. Preliminary results

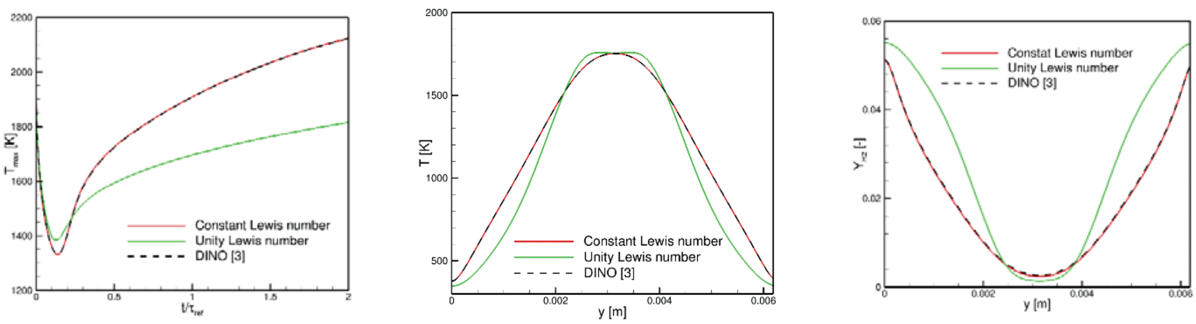

Figure 2. Maximum temperature over time (left); T (middle) and Y_{H_2} (right) at $x = 0.5L_0$

The comparison of the DNS results is performed for a flow characterized by Re = 250 with reference to data reported in [3]. Both the temporal evolution of the maximum temperature and the profiles of T and Y_{H_2} obtained for constant Lewis number model show excellent agreement with [3] and they significantly outperform the results obtained using the unity Lewis number assumption. In addition, several test cases at different Reynolds numbers, including simulations employing mixture-average diffusion model, are considered to enable a more quantitative assessment of diffusion effects.

Acknowledgements

This work is supported by the National Science Center in Poland (Grant 2024/53/B/ST8/02908) andPLGrid ACK Cyfronet AGH (Grant PLG/2025/018864).

References

[1] Xu Y., Chen Z.X., *Direct numerical simulations of the Taylor–Green vortex interacting with a hydrogen diffusion flame: Reynolds number and non-unity-Lewis number effects*, 'Physics of Fluids' 2023, vol. 35, no. 4, art. no. 045128.

[2] Taylor G.I., Green A.E., *Mechanism of the Production of Small Eddies from Large Ones*, 'Proceedings of The Royal Society A: Mathematical, Physical and Engineering Sciences' 1937, vol. 158, p. 499–521.

[3] Abdelsamie A., Lartigue G., Frouzakis C.E., Thevenin D., *The Taylor–Green vortex as a benchmark for high-fidelity combustion simulations using low-Mach solvers*, 'Computers & Fluids' 2021, vol. 223, art. no. 104935.

VAWT LOAD-LIMITING OPTIMIZATION USING HEIGHT-VARIABLE BLADE SKEW

J. Wiśniewski, J. Szumbarski

Warsaw University of Technology, The Faculty of Power and Engineering, Division of Aerodynamics, ul. Nowowiejska 24, 00–665 Warszawa, Poland

E-mail: jan.wisniewski@pw.edu.pl

Abstract. The current research is a follow-up to previous successful attempts at limiting fatigue loads on darrieus-type wind turbines, using a specifically divided, translated and rotated H-type rotor. The current purpose is to achieve a similar effect by optimizing the skew gradient along the length of a helical rotor, while maintaining its efficiency and other key performance parameters. A set of interesting geometrical scenarios, simulated using URANS will be presented within the full material.

Keywords: Computational Fluid Dynamics, Aerodynamics, VAWT, Vertical Axis Wind Turbine, Load-limiting, Aerodynamic Optimization.

1. Introduction

Both straight-bladed and helical Vertical Axis Wind Turbines (VAWTs) are subject to pulsating loads related to a cyclic variation in angles of attack occurring as part of each rotation [1][2]. Cyclic loading, depending on actual values can be the cause of fatigue based failure [3] or have no consequence on achieving an expected wind turbine operational lifetime.

Within prior research, the authors have presented an experimental and numerical validation of a load-limiting concept using VAWT H-rotors divided in two parts, by specific proportions along the length of the tower, rotated azimuthally and, in most scenarios also translated horizontally. This has yielded very significant results. When compared with a single-level test case of identical total rotor height, each verified experimental test case presented weighted average reduction values of bending moment amplitudes and maximum values at the bottom of the rotor shaft, understood as a shaft attachment height, of 80-84% and 40-42% respectively [4]. It was afterwards theorized that it could be very advantageous to use a modified application of the same general principles to further optimize helical VAWTs.

2. Description of the solution

Helical, skewed or spiral designs of darrieus rotors typically use heavier blades than their straight bladed counterparts which can be a limiting factor for industrial scale installations. In return, due to more smoothly covering the azimuth angle during rotation, they offer a reduction in base-relative spanwise bending moment leading to lower fatigue loads [5]. With additional shaping this process can be further optimized, combining fatigue load reduction with high energy production efficiency, no unnecessary material use and self-starting properties at any wind-relative position.

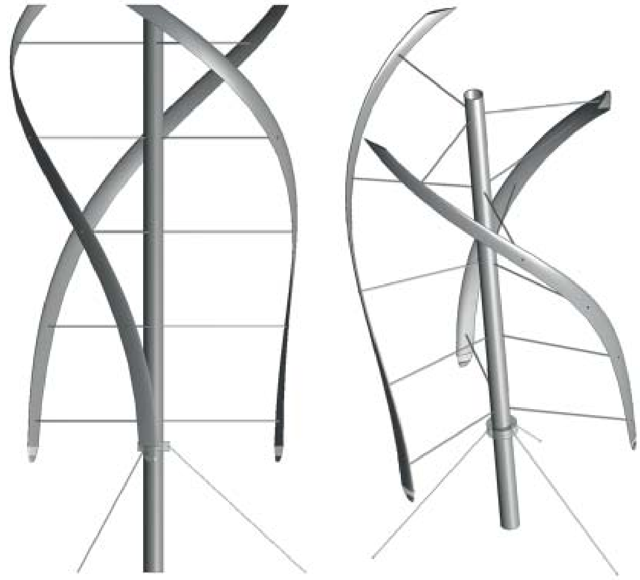

Figure 1. Variable-skew VAWT rotor example

The operation of the discussed version of a spiral turbine allows for limiting the bending moments in the mounting of the rotor shaft, in a critical element of the structure, by distributing the base-relative bending moments more evenly than in Gorlov rotors or similar ones, that have a twist that is either even or symmetrical with relation to half the height of the rotor blades. For a large number of blades within a rotor, it may be advantageous to have the longitudinal twist angle of the blades in the rotation axis of the rotor along the entire height of the rotor from 100% to 120% of the full angle divided by the number of blades in the rotor, to ensure the most accurate representation of moments from all attack angles relative to the incoming wind.

If fewer blades are used, the variant in which the longitudinal twist angle of the blades in the rotation axis of the rotor along the entire height of the rotor is not less than 90% of the half-full angle divided by the number of blades in the rotor may also be beneficial. This allows the construction of rotors with reduced skewness and reduced material consumption than the above-mentioned variant, with the most equal representation of moments from evenly spaced angles of attack relative to the incoming wind, more effective in reducing the amplitude of loads and maximum load values in the work cycle at the place of attachment of the rotor at the base than in a uniformly twisted rotor. Smaller total skew scenarios focusing on lower material use are also tested. The full material will show results of URANS simulations of most interesting scenarios of turbines having height variable skew.

References

[1] Kharade V. Jagtap K., *A Review Study on Vertical axis Wind Turbines(lift and drag type) for Optimizing the Aerodynamic and Structural Performance*, 'IOSR Journal of Engineering (IOSR JEN)' 2019, vol. 2019, p. 61–65.

[2] Galinos C., Larsena T.J., Madsena H.A., PaulsenU.S., , *Vertical axis wind turbine design load cases investigation and comparison with horizontal axis wind turbine*, 'Energy Procedia' 2016, no. 00 (2016) 000-000.

[3] Sutherland H.J., Berg D.E., Ashwill T.D., *A retrospective of VAWT technology*, SandiaReport SAND2012-0304, Sandia National Laboratories, Albuquerque 2012.

[4] Wisniewski J. Rogowski K., Gumowski K., Szumbarski J., 'Wind Energy Science' 2021, vol. 6, no. 1, pp. 287–294.

[5] Gharaati M., Wei N.J., Dabiri J.O., Martínez-Tossas L.A., Yang D.,*Large-eddy simulations of turbulent flows in arrays of helical- and straight-bladed vertical-axis wind turbines*, 'Journal of Renewable Sustainable Energy' 2023, vol. 15, art. no. 063309.

REAL-WORLD AERODYNAMIC AND ACOUSTIC PERFORMANCE OF MULTI-DISK RADIAL FANS

K. Wójciak[1], I. Czajka[2], J. Kopania[1]

[1] *Institute of Power Engineering - National Research Institute, Mory 8, 01–330 Warsaw, Poland*

[2] *AGH University of Science and Technology, Department of Power Systems and Environmental Protection Facilities, Mickiewicza 30, 30–059 Kraków, Poland*

E-mail: kamil.wojciak@itc.edu.pl

Abstract. This paper presents experimental aerodynamic and acoustic characteristics of three Tesla-type multi-disk radial fans. Pressure rise, power, efficiency and sound power level were measured for various volume flow rates and rotational speeds. The results quantify the low specific speed and low-noise features that have been reported qualitatively in earlier studies. The measurements were performed in standardised test rigs to provide reliable reference data for future modelling and design.

Keywords: Experimental Fluid Mechanics, Flow Machinery, Aerodynamic Noise, Multi-Disk Fan.

1. Introduction

Bladeless multi-disk machines, originally proposed in the early twentieth century by Nikola Tesla, employ tangential viscous shear and boundary-layer effects between closely spaced disks to transfer energy between a rotor and a working fluid [1]. In such devices, the flow is guided by smooth disk surfaces instead of conventional blades. Previous studies on disk-type radial fans have indicated a low specific speed, i.e. a high pressure rise at relatively low volume flow rates and have suggested potentially low noise emission [2]. However, the available publications focus mainly on theoretical performance estimates or limited aerodynamic measurements, while acoustic data remain scarce.

The present work provides an aerodynamic and acoustic characterisation of multi-disk radial fans derived from the Tesla fluid propulsion concept. The objective is to determine pressure-flow characteristics, shaft power demand, efficiency curves and sound power spectra of such fans for several impeller geometries and rotational speeds. The experimental results serve as a reference dataset for future modelling and support the development of design procedures for bladeless radial fans intended for ventilation applications.

2. Experimental setup, methods and results

Three radial fans with multi-disk impellers were manufactured according to the Tesla fluid propulsion concept. The impellers differ in outer and inner diameters while maintaining a constant number of disks and inter-disk spacing. The first impeller has an outer diameter d_2 = 250 mm and an inlet diameter d_1 = 105 mm, corresponding to a diameter ratio d_1/d_2 = 0.40. The second impeller has d_2 = 160 mm and d_1 = 64 mm (diameter ratio 0.40), whereas the third impeller has d_2 = 160 mm and d_1 = 96 mm (diameter ratio 0.60). All impellers consist of 16 parallel disks separated by a uniform axial gap of 1.5 mm and are mounted in a radial fan housing with an axial inlet and a tangential outlet, as illustrated in Figure 1.

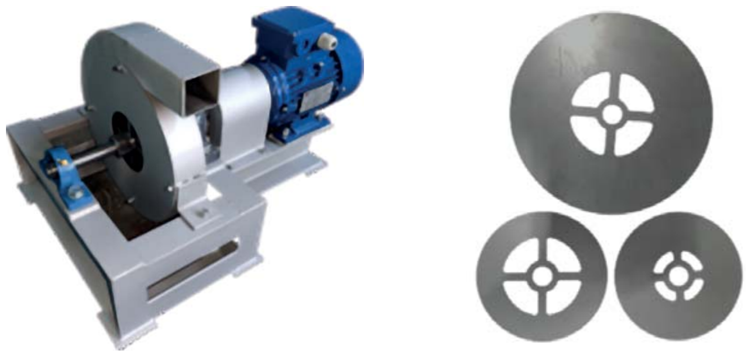

Figure 1. Photograph of the prototype fan equipped with a multi-disk rotor

Aerodynamic tests were carried out in a standardised test rig compliant with ISO 5801 [3]. The fans were driven by an electric motor with speed control and measurements were performed at four nominal rotational speeds: 725, 1450, 2175 and 2900 rpm. For each speed and impeller configuration, the pressure rise across the fan and the corresponding volume flow rate were determined by throttling the system. The data were processed to obtain pressure-flow, power-flow and efficiency-flow characteristics. Acoustic measurements were conducted in a reverberation chamber in accordance with ISO3741 [4]. The fan outlet was connected to a duct terminating in the reverberation chamber. Sound pressure levels were measured at multiple microphone positions and converted to sound power levels. Third-octave-band sound power spectra were determined for all tested rotational speeds and impeller geometries.

At the highest investigated rotational speed of 2900 rpm, the impeller with outer and inlet diameters of 250 mm and 105 mm achieved a maximum volume flow rate of 64 dm³/s, a maximum pressure increment of 815 Pa, a specific speed of σ = 0.17 at the optimum operating point and an A-weighted sound power level L_{WA} of 73 dB. For the impeller with diameters 160 mm and 64 mm, the corresponding maximum volume flow rate and pressure rise were 27 dm³/s and 292 Pa, with a specific speed of σ = 0.21 at the optimum operating point and L_{WA} = 66 dB. The impeller with diameters 160 mm and 96 mm reached a maximum volume flow rate of 27 dm³/s and a maximum pressure increment of 289 Pa, with a specific speed of σ = 0.24 at the optimum operating point and an A-weighted sound power level of 64 dB.

3. Conclusion

The experimental investigation provides a consistent set of aerodynamic and acoustic data for radial fans equipped with multi-disk impellers derived from the Tesla fluid propulsion concept. The measured characteristics confirm that these machines operate in a low specific speed regime, with a relatively high pressure rise at modest volume flow rates. The sound power spectra indicate predominantly broadband noise with a limited contribution from discrete tonal components, which is consistent with the bladeless nature of the impellers. The results fill the existing gap in experimental data for multi-disk radial fans and form a basis for the development of calculation methods and design guidelines for practical engineering applications.

References

[1] Tesla N., *Fluid Propulsion*, 1913, US Patent 1061142.

[2] Radwański J., *Analiza teoretyczna i doświadczalna wentylatora promieniowego z wirnikiem tarczowym*, "Zeszyty Naukowe Politechniki Śląskiej. Seria: Energetyka" 1993 vol. 118(1221), pp. 177–190.

[3] ISO 5801:2017. Fans – Performance testing using standardized airways.

[4] ISO 3741:2010. Acoustics – Determination of sound power levels and sound energy levels of noise sources using sound pressure – Precision methods for reverberation test rooms.

ANALYSIS OF A THERMAL VORTEX RING GENERATED IN THE LABORATORY: VORTEX DYNAMICS

J-I. Yano

CNRM, UMR3589, CNRS, Météo France, Toulouse, France.

E-mail: jun-ichi.yano@cnrs.fr

Abstract. A experimentally-generated thermal vortex ring is analyzed from a point of view of the vortex dynamics. The azimuthal vorticity is dominated by the filamentary structures, as expected from the vortex-sheet dynamics under an axisymmetric configuration. The spectrum-space budget analysis shows that the cascades of energy and enstrophy dominate, respectively, in the large and small scales in analogy with the two-dimensional turbulence: the energy cascades upscale as in two-dimensional turbulence, whereas the cascade direction of enstrophy oscillated both with time and wavenumber.

Keywords: Experimental Fluid Mechanics, General Fluid Dynamics, Thermal, Vortex, Turbulence, Energy and Enstrophy Cascades.

1. Experimental Setup

A series of laboratory experiments of the thermal vortex ring was performed over a period of 2010–2012 at Geophysical Institute, University of Warsaw by Anna Górska at her PhD project under the supervision of Szymon Malinowski. Here, a thermal vortex ring generated by this experiment is analyzed from a point of view of the vortex dynamics.

A thermal vortex ring is generated by a buoyancy anomaly released from below. Its evolution is measured on vertical section generated by a laser sheet. The analysis is performed on this section, adopting the cylindrical coordinates defined by assuming that the section contains the vertical axis of the vortex ring.

2. Analysis Results

The vorticity in the azimuthal direction is dominated by the filamentary structures, shown by the graphics below: the vorticity contours (right) closely follow those of tracer in the image (left), suggesting that vorticity is advected like a passive scalar. Those behaviors are best explained by assuming that the flow is dominated by the axisymmetric component, although the divergence is found just as comparable in magnitude as the vorticity in the azimuthal direction. The axisymmetric nature of the flow suggested here is consistent with Yano and Morrison [1], who found by analyzing a full numerical simulation that the budget of circulation and impulse is dominated by axisymmetric components and the non-axisymmetric contribution is negligible. It leads to a dynamics similar to the vortex-sheet dynamics under an axisymmetric configuration and as presented by the contour dynamics in Figure 1.

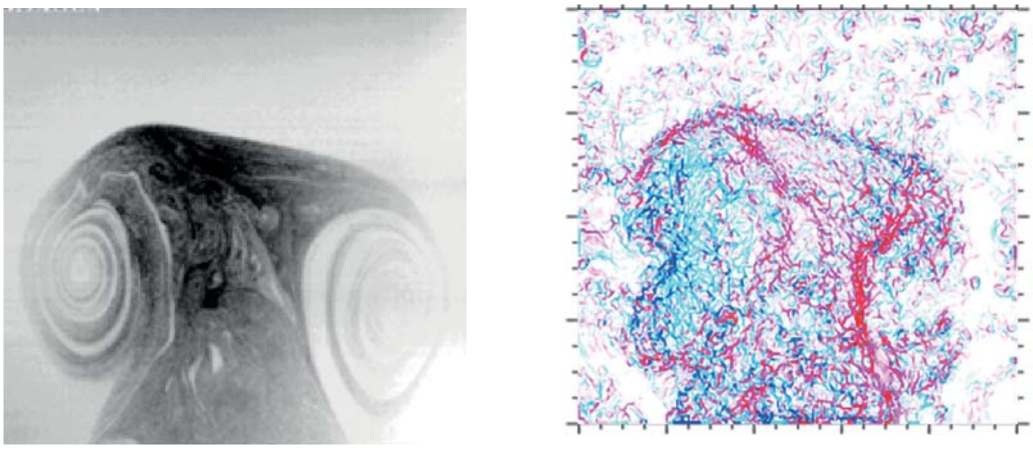

Figure 1. A snapshot of the laser section image obtained by the experiment [Left], and the corresponding vorticity field [Right]. Note that vorticity field closely follows the tracer contours seen in the image

Budget analyses further suggest the nonlinear dynamics of this thermal vortex ring somehow akin to that of the two-dimensional turbulence: the kinetic-energy budget is dominated by an upscale energy transfer by nonlinear advection over the smallest wavenumbers (the total wavenumber less than ten), likely as a consequence of the axisymmetric flow behaving like a two dimensional turbulence. Thus, the power-spectrum slope of -5/3 over this range is interpreted as a manifestation of forward energy-cascading inertial subrange. Here, the wavenumber is defined by taking the vortex-ring radius as the unit scale.

The enstrophy budget, on the other hand, is dominated by the nonlinearity at the higher wavenumbers, over the range of 1-10^2, suggesting a behavior akin to that of the enstrophy-cascading inertial subrange. This tendency is also supported by a steeper energy spectrum close to -3 at higher wavenumbers, although the power-law behavior is less well defined. Moreover, the direction of the enstrophy transfer over this wavenumber range is not well defined, either, and the sign oscillates over the wavenumbers as well as with time. Thus, the result suggests an enstrophy-dominant dynamics over this scale but without representing a well-defined cascade direction.

Acknowledgments

The original laboratory experiment is performed by Anna Górska as her PhD project under the supervision of Szymon Malinowski. Unfortunately, she tragically lost her life during her expedition in the Spitsbergen by an avalanche accident before she could complete her thesis. The author thanks Szymon Malinowski for arranging data for him as well as for discussions.

References

[1] Yano J.-I., Morrison H., *Thermal vortex ring: vortex-dynamics analysis of a high-resolution simulation*, ‘Journal of Fluid Mechanics’ 2024, vol. 991.

CRITICAL STROUHAL VELOCITY DURING FLOW OVER SEMI-FIXED INDUSTRIAL STEEL CHIMNEY

P.J. Ziółkowski, M. Bryk, T. Ochrymiuk, J. Badur*

Institute of Fluid Flow Machinery, Energy Conversion Department, 14 Fiszera St., 93–005 Gdańsk, Poland

E-Mail*: jb@imp.gda.pl

Abstract. Slender industrial structures often have a low mass-to-stiffness ratio which makes them highly susceptible to strongly unsteady and chaotic wind actions. The close proximity of adjacent buildings can change the wind dynamics acting on a slender structure by creating zones of turbulence and increasing wind pressure on the structure. Furthermore, climate change, which is causing an increase in the number of violent storms and gales, keeps the issues of structural safety and the proper selection of wind loads in the design process constantly relevant. Firstly, this paper presents a parametric CFD analysis, which has been examined the impact of wind speed, height and distance of surrounding structure on wind loads on a 100-meter steel industrial chimney [1] which allowed the Strouhal number and corresponding number to be determined. Next, using momentum-FSI , the critical Strouhal number and resonance area were determined. The results obtained were compared with the results of the standard Eurocode procedure for wind load assessment [2,3] and a comparative analysis was performed.

Keywords: momentum-FSI (CFD-CSD coupling by momentum exchange), Computational Solid Dynamics, the Strouhal number, Computational Fluid Dynamics, General Fluid Dynamics.

1. Research overview

The European wind norm allows a simplified procedure for calculating the forces, moments and displacements of a slender structure in a wind flow even at the critical Strouhal velocity. This is the wind speed in which the period of the detached von Karman vortices coincides with the period of eigenvalue vibrations of the structure: $f_v \approx f_n$. The dimensionless frequency of detaching of alternating vortices is called the Strouhal number, and knowing it we can determine the critical velocity of the wind as well as the range of lock-in phenomena.

However, as experience shows, determining the Strouhal number for a real construction is not a simple matter and requires time and expensive experiments. Therefore, the aim of the paper is to determine such a number – using the momentum-FSI as numerical tools instead of an experimental setup. The advantage of the momentum-FSI over the experiment is that the data for the condition $f_v \approx f_n$ are calculated simultaneously for f_v and f_n. Especially, it is important in the case of a semi-fixed cylinder (Fig. 1a), where Eurocode predictions fail and lead to serious failures [1].

The analysis refers to the failure of a 100-metre-high steel industrial chimney presented in [1]. The geometry of the chimney was recreated on the basis of this work using CAE tools (Figure 1a). Information on the distance from the adjacent building or its dimensions was not presented in [1], therefore, the authors decided to carry out a variant (parametric) analysis which provides a more general perspective on the case in question.

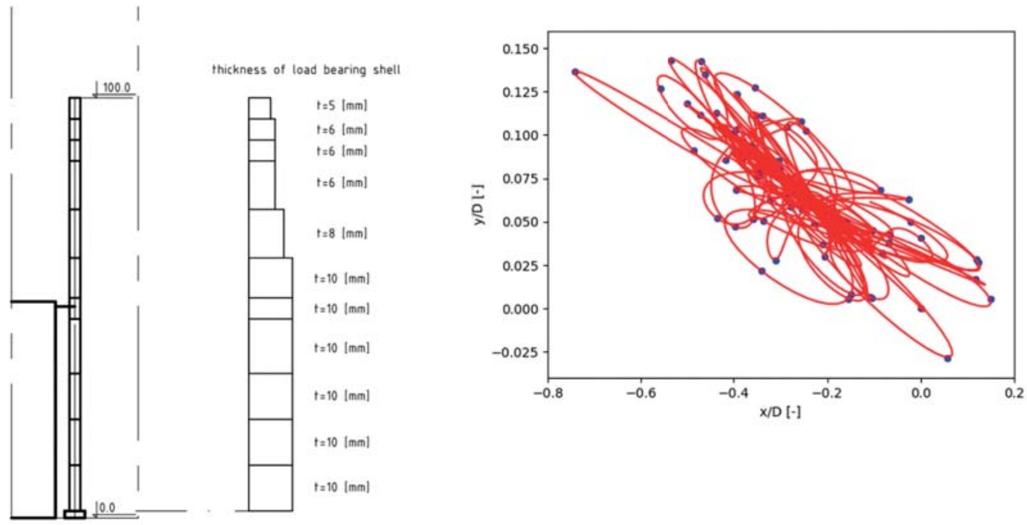

Figure 1. a) Chimney scheme b) an example of top moving at the range of lock-in

Using Strouhal's definition [4] and the experience from [5], we try to reproduce the Strouhal research methodology by performing a series of wind loads induced by a pressure profile generated according to the wind standard. According to the European norm, the characteristic speed is the speed at a height of 10 meters above the ground level, and it is for this that we determine the Strouhal number, they are aware of the fact that it changes with altitude.

Firstly, for determination of the Strouhal law a series of CFD analysis was performed for various wind speed and direction values, heights and distances of the surrounding structure. The obtained results were critically compared with the appointment of Strouhal number in the standard wind load assessment procedure, both at EN 1991-1-4:2008 Eurocode [2] and PN-77/B-02011 [3]. Next, removing rigidity assumption for whole chimney, and putting its real stiffness, the momentum-FSI has been performed for the environmental data nearly $f_v \approx f_n$. By analysing a motion of top of chimney (Fig. 1.b) the critical Strouhal number and lock-in range where determined. The shift of the lock-in region in the right $U_r < III$ has been discovered.

Another aspect of the work is the reference to the PN-77/B-02011 [2] and PN-EN-1991-1-4:2008 [3] standard algorithms. The authors refer to both algorithms for determining wind loads due to the period in which the chimney was built, i.e. 2003 which in Poland was a transitional period from Polish standards to European standards in the process of designing buildings.

References

[1] Kawecki J., Żurański J.A., *Cross-wind vibrations of steel chimneys – A new case history*, 'Journal of Wind Engineering and Industrial Aerodynamics' 2007, vol. 95, no. 9/11, pp. 1166–1175.

[2] PN-77/B-02011 Obciążenia budowli. Obciążenia wiatrem.

[3] PN-EN-1991-1-4:2008 Eurokod 1. Oddziaływania na konstrukcje. Część 1-4: Oddziaływanie ogólne. Oddziaływania wiatru.

[4] Strouhal V., *Über eine besondere Art der Tonerregung*, 'Annalen der Physik und Chemie' 1878, b. V,h. 10, pp. 216–251.

[5] Ziółkowski P.J., Ochrymiuk T., Eremeyev V., *Fluid–solid interaction on a thin platelet with high-velocity flow: vibration modelling and experiment,* 'Continuum Mechanics and Thermodynamics' 2023, vol. 35, no. 4,pp. 1495–1521.

TOWARDS PERFECT CLOAKING - COMBINING CLOAKS FOR ENHANCED INVISIBILITY IN WATER WAVEGUIDE SYSTEMS

D. Żyła-Jabłońska, T. Bobiński

Warsaw University of Technology, Faculty of Power and Aeronautical Engineering, ul. Nowowiejska 24, 00–665 Warszawa, Poland

E-mail: daria.zyla.dokt@pw.edu.pl

Abstract. We introduce a novel cloaking design surpassing prior work by integrating established techniques with explicit phase-shift control behind the cylinder. This achieves at least 25-fold scattered energy reduction versus the reference case, with near-perfect transmission $T \approx 1$ over a significant broadband frequency range.

Keywords: Surface water waves, Cloaking.

1. Introduction

Surface water waves interacting with an impermeable body scatter energy and induce hydrodynamic loads, making scattered-energy minimization a central problem in coastal and ocean engineering. Cloaking refers to eliminating this scattered field to reduce loading, achieved through metamaterial-inspired designs, that have advanced wave control in electromagnetism, acoustics, elastodynamics and water waves. Here, we study broadband cloaking of a surface-piercing impermeable cylinder on the channel centreline. Earlier approaches using variable bathymetry [1], floating plates [2], modified walls [3] or auxiliary cylinders [4] achieved perfect cloaking only at selected frequencies or minimized backscattering without accounting for phase shifts. This work explores a hybrid cloak combining optimized channel-wall geometry and bathymetry to minimize the total scattered field across a broad frequency range.

2. Methods

We consider linear surface water waves in the harmonic regime, restricted to the frequency range where only the plane mode propagates. The propagation of waves is modeled using the non-dispersive linear shallow-water equation under the long-wave approximation ($\frac{kL}{\pi} \ll 1$).

$$\nabla \cdot (h\nabla\eta) + \omega^2 g^{-1}\eta = 0 \tag{1}$$

A priori unknown bottom depths may yield locally significant kh, causing (SWE) to inaccurately describe water wave propagation, thus, we also consider the mild-slope equation under the assumption of a mild bed slope ($\left|\frac{\nabla h}{kh}\right| \ll 1$), which incorporates weak dispersion effects

$$\nabla \cdot \left(c_p c_g \nabla \eta\right) + k^2 c_p c_g \, \eta = 0 \tag{2}$$

Here η is the free-surface elevation, k the wavenumber, h the water depth and c_p, and c_g the phase and group velocities, related through $\omega^2 = gk\tanh(kh)$. In the reference case, waves propagate in a straight channel of width L with a flat bottom and a surface-piercing cylinder of diameter $D = 0.6L$ centered at the origin. We consider the objective function

$$\chi_{sc} = \frac{\int(|R|^2 + |T-1|^2)d\tilde{k}}{\int(|R_0|^2 + |T_0-1|^2)d\tilde{k}} \tag{3}$$

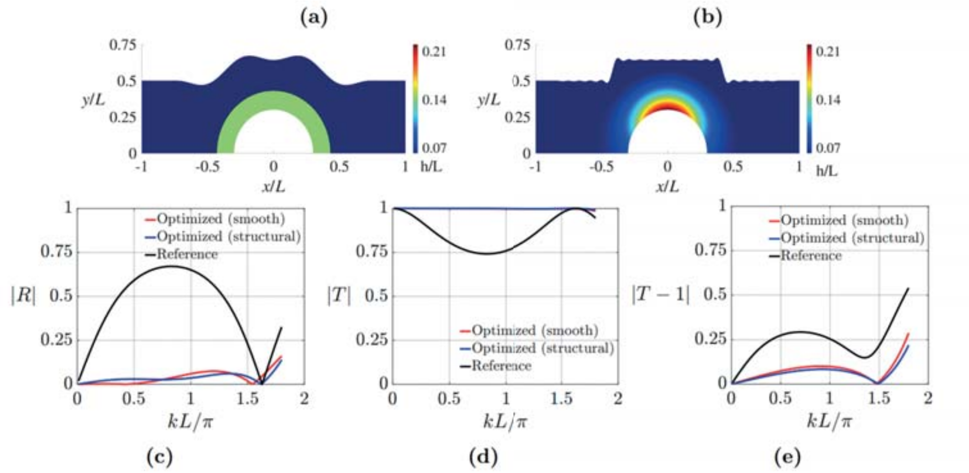

Figure 1. Figures a) and b) show optimized geometries; c), d), and e) show the dependence of reflection $|R|$, transmission coefficient $|T|$ and $|T-1|$ factor, on wavenumber $\tilde{k}$.

3. Results and discussion

Integrating two established cloaking methods reduced the scattering objective function χ_{sc} to 0.0348 (smooth bathymetry) and 0.0221 (structured), achieving at least 25-fold total scattered energy reduction vs. the reference case. Optimal hybrid geometries combining bottom profiles with wall deformations (presented in the Figure 1) ensure near-perfect transmission, minimal backscattering and outperform single-method cloaks [3] by at least 7-fold greater reduction across twice wider bandwidth.

Acknowledgements

This research was funded in whole by the National Science Centre Poland, under agreement UMO-2020/39/D/ST8/01.

References

[1] Bobinski T., Maurel A., Petitjeans P., Pagneux V., *Backscattering reduction for resonating obstacle in water-wave channel*, 'Journal of Fluid Mechanics' 2018, vol. 845, p. R4.

[2] Takahito I., Ahma Z., Mohammad-Reza A., *Water wave cloaking using a floating composite plate*, 'Journal of Fluid Mechanics' 2023, vol. 954, p. A4.

[3] Zyla D., Bobinski T., *Cloaking waveguide defects at low frequencies using local wall deformations*, 'Journal of Fluid Mechanics' 2025, vol. 1006, p. A26.

[4] Newman J.N., *Cloaking a circular cylinder in water waves*, 'European Journal of Mechanics B/Fluids' 2014, vol. 47, pp. 145–150.

INDEX OF AUTHORS

A

Ababaei, A. 37, 131
Advaith, S. 165
Ahizi, S. 59
Alavi, A. 39
Allweyer, B. 41, 43, 85, 175
Ambrose, S. 103
Amiri, M. 45
Andrei, I.R. 219
Awrejcewicz, J. 169
Ayats, R. 47

B

Badur, J. 239
Banaszkiewicz, T. 67
Banerjee, A. 49
Bartosik, A. 51
Baumann, A. 177
Biegowski, S. 53
Biermann, D. 177
Błaszczyk, M. 55
Bobiński, T. 65, 101, 167, 241
Bogusławski, A. 57, 129, 193
Boldo, D. 139
Boni, M. 219
Braza, M. 203
Bryk, M. 239
Bukowski, K. 59
Burns, C. 61

C

Caban, L. 63
Carnevale, L.H. 65
Che, Z. 65
Cieślikowski, E. 159
Ciorga, Ł. 67
Clément, S. 127
Czajka, I. 79, 235
Czarnecki, M. 69

D

De Maria, T. 59
Deuar, P. 65
Dimitrieva, N.F. 71
Doerffer, P. 155
Donizak, J. 115
Dorenda, M. 107
Dróżdż, A. 73, 171
Durajski, A. 145
Dykas, S. 129, 193
Dziuba, J. 75

E

Eastwick, C. 103
Eberhard, P. 177
Ekiel-Jeżewska, M.L. 185
El Akoury, R. 203
Ellis, C. 103
Elsner, W. 73, 171
Erdoğan, B. 187, 189

F

Fabisiak, J. 77
Fadhila, H. 103
Flaszyński, P. 155, 203, 205, 227
Friend, P. 181

G

Gaillot, S. 127
Gaj, P. 69, 79, 223
Gałecki, J. 81, 209
Gepner, S. 77, 83
Geurts, B.J. 57
Giesecke, A. 91
Gnatowska, R. 105
Gnebner, K. 227
Govers, Y. 227
Górecki, G. 211
Grün, S. 41, 43, 85, 175
Gülde, S. 177
Gundrum, T. 91
Gutkowski, A. 211
Gyoten, K. 181

H

Hanfy, A. 155
Hercel, P. 87
Hof, B. 47
Hokpunna, A. 89
Hübner, D. 41, 43, 85, 175

J

Jani, K.K. 91
Jankiewicz, J.A. 93
Jaszczur, M. 133
Jaworska-Jóźwiak, B. 51
Jaworski, A. 119
Jóźwiak, B. 95
Juszczak, K. 107

K

Kajzer, A. 97
Kamiński, P. 99
Kantyka, K. 149
Kardaś, D. 87
Katz, M. 127
Kawahara, G. 83
Khalil, J.A. 203
Kizilova, N. 137, 141
Klamka, M. 65, 101
Klepacz, J. 107
Klotz, L. 47
Knight, J. 103
Kocoń, A. 105
Kołata, A. 107
Kopania, J.M. 69, 79, 109, 223, 235
Kowalewski, T.A. 111
Krakowski, T. 113, 199
Kraszewska, A. 115
Król, S. 117
Kubacki, S. 119
Kudra, G. 169
Kulak, M. 61, 107
Kumar, D. 121
Kurec, K. 119
Kurowski, M. 155

L

Leonardi, C. 123
Lepiarz, J. 161
Lipian, M. 107
Liśkiewicz, G. 149
Li, Y. 125
Lo Pinto, E. 127

Ł

Łaniewski-Wołłk, Ł. 123

M

Maciejewski, J. 107
Majkut, M. 129, 193
Manna, M. 37, 131
Marczak, P. 133
Marek, M. 135, 145
Maynard, N. 203
Medina, H. 103
Melikhov, Y. 185
Mendez, M.A. 59
Merdjani, A. 137
Michel, S. 177
Miller, B. 149
Mirajkar, H.N. 185
Muller, J. 139

N

Naqvi, S. 141
Nasr, M.A. 143
Ng, K.L. 65
Niegodajew, P. 135, 145
Noack, B.R. 125

O

Ochrymiuk, T. 239
Okonokhua, B. 147
Olasek, K. 107
Olczyk, A. 149
Olszewska, A. 151
Olszewski, W. 137

P

Pahlavanzadeh, M. 147
Paprota, M. 53
Pasiarski, M. 51
Peter, Z. 151
Pilecki, M. 153
Piotrowicz, M. 155, 227
Pisula, M. 157
Płuziński, J. 153
Poćwierz, M. 157
Potęga, B. 159, 161
Pozorski, J. 163
Pruett, T. 181

R

Rajek, M. 163
Ramadas, R. 165
Remer, M. 159, 161, 167
Rezaei, M.P. 169
Romańczyk, M. 73, 171
Rosa, B. 37, 131
Rozbicki, K. 107
Rozborski, S. 139
Rożek, A. 173
Rückert, F. 41, 43, 85, 175
Rulik, S. 173
Rupasinghe, N. 177
Rusin, K. 147, 179
Rusinow, P. 149

S

Sadowski, M. 51
Saini, H. 181
Sassen, C. 175
Sengupta, S. 183
Shekhar, Ch. 185
Sieradzki, A. 205
Şimşek, A.B. 187, 189
Sindera, K. 191

Skalska, K. 161
Skoczylas, K. 129, 193
Smołka, K. 75, 129, 193
Smyk E. 195
Sobczak, K. 61, 149
Spała, J. 197
Staicu, A. 219
Stankiewicz, W. 113, 199
Stefani, F. 91
Stryczniewicz, W. 201
Suresh, T. 203, 205
Sushil Rao, J. 181
Szulc, O. 203, 205
Szumbarski, J. 81, 157, 207, 209, 233
Szydłowski, M. 211

Ś

Śleszyński, M. 155

T

Tay, C.M.J. 143
Telyma, S. 213
Theodorakis, P.E. 65
Tithof, J. 181
Tomczak, F.D. 215
Tomecka, M. 149
Tomecki, W. 107
Tuliszka-Sznitko, E. 217
Tyliszczak, A. 45, 57, 63, 99

U

Üner, N.B. 187, 189
Ungureanu, I.P. 219
Urbanowicz, K. 39

W

Wacławczyk, M. 117, 197
Wacławczyk, T. 221
Walicki, K. 159
Walisiak, D. 223
Wardach-Święcicka, I. 225
Wasilczuk, F. 227
Wawrzak, A. 63, 229
Wawrzak, K. 231
Weiss, Y. 127
Widerska, G. 107
Wielgosz, M. 119
Wilczyński, M. 145
Wiśniewski, J. 233
Witkowski, K. 169
Wojcik, M. 227
Wong, B.Y.J. 143
Wójciak, K. 69, 223, 235
Wróblewski, W. 147, 179

Y

Yano, J-I. 197, 237

Z

Zawadzki, K. 107
Zdybel, P. 185
Zima, B. 227
Ziółkowski, P.J. 239

Ż

Żyła-Jabłońska, D. 241

ISBN 978-83-67934-99-2